USAAMRDL TECHNICAL REPORT 71-61

CRITERIA FOR EXTERNALLY SUSPENDED HELICOPTER LOADS

By

S. J. Briczinski
G. R. Karas

November 1971

EUSTIS DIRECTORATE
U. S. ARMY AIR MOBILITY RESEARCH AND DEVELOPMENT LABORATORY
FORT EUSTIS, VIRGINIA

CONTRACT DAAJ02-70-C-0021
UNITED AIRCRAFT CORPORATION
SIKORSKY AIRCRAFT DIVISION
STRATFORD, CONNECTICUT

DISCLAIMERS

The findings in this report are not to be construed as an official Department of the Army position unless so designated by other authorized documents.

When Government drawings, specifications, or other data are used for any purpose other than in connection with a definitely related Government procurement operation, the United States Government thereby incurs no responsibility nor any obligation whatsoever; and the fact that the Government may have formulated, furnished, or in any way supplied the said drawings, specifications, or other data is not to be regarded by implication or otherwise as in any manner licensing the holder or any other person or corporation, or conveying any rights or permission, to manufacture, use, or sell any patented invention that may in any way be related thereto.

Trade names cited in this report do not constitute an official endorsement or approval of the use of such commercial hardware or software.

DISPOSITION INSTRUCTIONS

Destroy this report when no longer needed. Do not return it to the originator.

DEPARTMENT OF THE ARMY
U. S. ARMY AIR MOBILITY RESEARCH & DEVELOPMENT LABORATORY
EUSTIS DIRECTORATE
FORT EUSTIS, VIRGINIA 23604

This report was prepared by Sikorsky Aircraft, Division of United Aircraft Corporation, under the terms of Contract DAAJ02-70-C-0021. It consists of a discussion of the method used to simulate externally slung helicopter loads, a reduction to graph form of the data generated by this simulation, and a method for determining design criteria from these data for aircraft hardpoints, load lift points, and slings.

The object of this effort was to quantify the maximum load factors which are developed in hardpoints, lift points, and slings during various maneuvers to which the helicopter-slung load system could be subjected during any given flight, and to use these data to develop design criteria for this hardware.

In general, it can be stated that the method developed is a reasonable approach to formulating useful design criteria.

The conclusions contained herein are concurred in by this Directorate.

The technical monitor for this contract was J. Everette Forehand, Aircraft Subsystems and Equipment Division.

Unclassified

Security Classification

DOCUMENT CONTROL DATA - R & D

(Security classification of title, body of abstract and indexing annotation must be entered when the overall report is classified)

1. ORIGINATING ACTIVITY (Corporate author) Sikorsky Aircraft Division United Aircraft Corporation North Main St., Stratford, Connecticut	2a. REPORT SECURITY CLASSIFICATION Unclassified 2b. GROUP

3. REPORT TITLE

CRITERIA FOR EXTERNALLY SUSPENDED HELICOPTER LOADS

4. DESCRIPTIVE NOTES (Type of report and inclusive dates)

Final

5. AUTHOR(S) (First name, middle initial, last name)

Stanley J. Briczinski
George R. Karas

6. REPORT DATE	7a. TOTAL NO. OF PAGES	7b. NO. OF REFS
November 1971	209	0

8a. CONTRACT OR GRANT NO. DAAJ02-70-C-0021 b. PROJECT NO. c. Task 1F162203A43501 d.	9a. ORIGINATOR'S REPORT NUMBER(S) USAAMRDL Technical Report 71-61 9b. OTHER REPORT NO(S) (Any other numbers that may be assigned this report) Sikorsky Engineering Report 50731

10. DISTRIBUTION STATEMENT

Approved for public release; distribution unlimited.

11. SUPPLEMENTARY NOTES	12. SPONSORING MILITARY ACTIVITY Eustis Directorate U.S. Army Air Mobility R&D Laboratory Fort Eustis, Virginia

13. ABSTRACT

This study was conducted to determine the dynamic effects of a helicopter external load combination by simulating flight using a computer. Design criteria for sling members and hard points of the system were also established. A computerized hybrid simulation of the coupled motion of a CH-54 helicopter and selected external loads was conducted in real time with a pilot in the loop on both fixed-base and moving-base simulators. The results of the study indicate that the dynamic load factors produced in sling elements and at hard points during a maneuver often exceed the normal load factor developed by the helicopter. Data is included for the various loads and maneuvers.

Unclassified

Security Classification

14. KEY WORDS	LINK A		LINK B		LINK C	
	ROLE	WT	ROLE	WT	ROLE	WT
Helicopter-external load combination Design criteria Sling elements Load hardpoints CH-54A helicopter						

Unclassified

Security Classification

Task 1F162203A43501
Contract DAAJ02-70-C-0021
USAAMRDL Technical Report 71-61
November 1971

CRITERIA FOR EXTERNALLY SUSPENDED HELICOPTER LOADS

Final Report

By
S. J. Briczinski
G. R. Karas

Prepared by

United Aircraft Corporation
Sikorsky Aircraft
Stratford, Connecticut

for

EUSTIS DIRECTORATE
U.S. ARMY AIR MOBILITY RESEARCH AND DEVELOPMENT LABORATORY
FORT EUSTIS, VIRGINIA

ABSTRACT

The purposes of this study were to determine the dynamic effects of a helicopter-external load combination as the system is flown throughout a range of flight maneuvers, and to establish design criteria for sling members and hardpoints of the system. Typical slings and sling arrangements were selected, and representative external loads were established under the scope of the contract. A computerized hybrid simulation of the coupled motion of a CH-54A helicopter and the external loads was conducted in real time with a pilot in the loop on both a fixed-base simulator and a moving-base simulator. Load factors in the sling elements and at helicopter and load hardpoints relating to the dynamic effects of the combined system were determined and are presented in this report.

The results of this study indicate that the dynamic load factors produced in sling elements and at hardpoints during a maneuver often exceed the normal load factor developed by the helicopter during the maneuver. In some cases the load factors in the sling elements and at the hardpoints exceed the design limit load factor of the helicopter. It was also found that during a given maneuver, the peak values of sling and hardpoint load factors did not necessarily occur at the same time that the helicopter developed its peak normal load factor value.

The load factor data from the simulation were used in establishing sling and hardpoint design criteria. The design criteria are presented as functions of the helicopter design load factor for each of the various slung load types and sling configurations studied. The load factor data, and therefore the eventual design criteria, proved to be greatly influenced by the type of slinging configuration used and the density of the load. It was also found that the geometry of the sling is an important parameter in determining the maximum forces developed in sling members and at hardpoints. For this reason, the design criteria established in this study pertain directly to the specific slung load configurations which were modeled in the simulation. The design criteria must include a geometry effect calculation before they are used as universal criteria which would be applicable to any slinging arrangement.

TABLE OF CONTENTS

LIST OF ILLUSTRATIONS

Figure		Page

LIST OF TABLES

LIST OF SYMBOLS

A_{max}	maximum frontal area of load, ft^2
c_w	ratio of average downwash velocity on load over average downwash velocity at rotor disc
c_x, c_y	x and y components of distance between load hardpoints, ft
d	component of distance from pallet center to load cg in load x direction, ft
d_f, d_r	component along load body x-axis direction of distance from load cg to front and rear load slinging hardpoint, respectively, ft
d_h	component along load body x-axis direction of distance from load cg to cargo hook, ft
$d_{i_H}, b_{i_H}, h_{i_H}$	components of distance from helicopter cg to helicopter hardpoints, along x, y, and z helicopter body axis directions respectively, ft
$d_{i_L}, b_{i_L}, h_{i_L}$	components of distance from load cg to load hardpoints, along x, y, and z load axis directions respectively, ft
D_L, Y_L, L_L	aerodynamic drag, side force, and lift on load along load body axis directions, lb
$D_{L_{Sf}}, D_{L_{Sr}}$	sum total of static trim values of drag forces at all front and all rear load hardpoints, respectively, lb
D_w, Y_w, L_w	aerodynamic drag, side force, and lift on load along wind axis directions, lb
DT_1, DT_2, DT_3, DT_4	tensions in drag legs of Brooks and Perkins pallet, lb
$\Delta D/_q$	normalized drag contribution due to drogue chute, lb
f_w	equivalent flat plate area of load, viewed from above, ft^2
ΔF_j, ΔF_{jM}	tension components in nylon legs due to rolling and pitching moment balance, ft-ib
$\Delta F_{xH}, \Delta F_{yH}, \Delta F_{zH}$	additional forces on helicopter due to load, along helicopter body axis directions, lb
g	acceleration of gravity, ft/sec^2

h	component of distance from pallet center to load cg, along load z - direction, ft
h_f, h_r	components along load body z-axis direction of distance from load cg to front and rear load slinging hardpoints, respectively, ft
h_h	component along load body z-axis direction of distance from load cg to cargo hook, ft
I_{xx},I_{yy},I_{zz}	moments of inertia of combined helicopter and pallet load, slug-ft^2
I_{xx_L},I_{yy_L}, I_{zz_L},I_{xz_L}	load moments and product of inertia, slug-ft^2
i	subscript which denotes individual cables or helicopter hardpoints
j	subscript which denotes individual nylon legs
k	subscript which denotes individual load hardpoints
K_i	cable spring rate, lb/ft
K_j	nylon leg spring rate, lb/ft
K_{LL_j}	component of nylon leg spring rate in the direction of line LL, lb/ft
K_N	spring rate of the equivalent nylon spring in the direction of line LL, lb/ft
K_s	steel cable spring rate in the single-cable - multileg dynamic solution, lb/ft
K_T	spring rate of the total equivalent spring between the helicopter cg and load cg in the single-cable - multileg dynamic solution, lb/ft
ℓ_j,m_j,n_j	direction cosines of individual sling legs in space fixed axis directions
ℓ_L^L,m_j^L,n_j^L	direction cosines of individual sling legs in load axis directions
ℓ_{o_j}	unstretched nylon leg length, ft
L_i	cable length

L_1	steel cable length in the single cable - multileg dynamic solution, ft
L_{i_o}	unstretched cable length, ft
L_j	nylon leg length, ft
L_m	distance from helicopter cg and load cg in the single-cable - multileg dynamic solution, ft
L_{m_o}	unstretched value of L_m, ft
L_N	distance from hook to load cg, ft
L_{N_o}	unstretched value of L_N, ft
$\mathcal{L}_L, M_L, N_L$	aerodynamic rolling, pitching, and yawing moments of load about load body axis directions, ft-lb
$\mathcal{L}_p, M_p$	rolling and pitching moment contributions about load cg, ft-lb
$\mathcal{L}_w, M_w, N_w$	aerodynamic rolling, pitching, and yawing moments of load about wind axis directions, ft-lb
$\Delta\mathcal{L}_H, \Delta M_H, \Delta N_H$	change in rolling, pitching, and yawing moments of helicopter due to the load, ft-lb
ΔL_j	change in length of individual nylon legs from the no-load condition, ft
ΔL_m	change in L_m compared to unstretched value, ft
LFT_C	load factor form of cable tension
$LFT_{C_{max}}$	maximum cable tension load factor
LFT_L	load factor form of nylon leg tension
$LFT_{L_{max}}$	maximum nylon leg tension load factor
$LFV_H, LFD_H, LFS_H, LFP_H$	load factor form of vertical, drag, side, and inplane forces at helicopter hardpoints
$LFV_{H_{max}}, LFD_{H_{max}}, LFS_{H_{max}}$	maximum vertical, drag, and side force load factors at helicopter hardpoints
$LFV_L, LFD_L, LFS_L, LFP_L$	load factor form of vertical, drag, side, and inplane forces at load hardpoints

$LFV_{L_{max}}$, $LFD_{L_{max}}$, $LFS_{L_{max}}$	maximum vertical, drag, and side force load factors at load hardpoints
$M_{X_{LCG}}$, $M_{Y_{LCG}}$, $M_{Z_{LCG}}$	rolling, pitching, and yawing moments about pallet load cg, ft-lb
$M_{X_{LP}}$, $M_{Y_{LP}}$, $M_{Z_{LP}}$	rolling, pitching, and yawing moments about pallet center, ft-lb
m_L	mass of the load, slugs
N	number of nylon legs
N_p	number of plys per leg
N_s	parameter representing any general sling or hardpoint load factor
N_z	aircraft (helicopter) normal load factor
$N_{z_{max}}$	maximum helicopter load factor attained
$\Delta N/_q$	normalized yawing moment contribution due to drogue chute, ft-lb
P_j	load per ply in each nylon leg, lb
p_L, q_L, r_L	roll, pitch, and yaw rates of load about load body axis directions, rad/sec
$\overset{\circ}{p}, \overset{\circ}{q}, \overset{\circ}{r}$	components of angular acceleration of combined helicopter and pallet load, rad/sec^2
$\overset{\circ}{p}_L, \overset{\circ}{q}_L, \overset{\circ}{r}_L$	components of angular acceleration of load about load body axis directions, rad/sec^2
q	$1/2\ \rho\ V_{R_L}{}^2$; free stream dynamic pressure, lb-ft^2
S_{T_1}, S_{T_2}, S_{T_3}, S_{T_4}	tension in side legs of Brooks and Perkins pallet, lb
$T_{C_{max}}$	maximum dynamic value of cable tension, lb
T_{C_s}	static trim value of cable tension, lb
$T_{C_{sf}}$, $T_{C_{sr}}$	static trim value of cable tension
T_i	cable tension, lb
T_j	total tension in individual nylon legs, lb

T'_j	tension contribution in nylon legs due to external forces, lb
T_1	steel cable tension in the single cable dynamic solution, lb
T_1, T_2, T_3, T_4	tension in the vertical legs of the Brooks and Perkins pallet, lb
$T_{L_{max}}$	maximum dynamic value of nylon leg tension, lb
T_{L_s}	static trim value of nylon leg tension, lb
$T_{L_{s_f}}, T_{L_{s_r}}$	static trim value of nylon leg tension in front and rear legs, respectively, lb
$TX_{i_H}, TY_{i_H}, TZ_{i_H}$	components of cable tension along helicopter axis directions, lb
$TX_{i_L}, TY_{i_L}, TZ_{i_L}$	components of cable tension along load axis directions, lb
ΔT	duty cycle of digital solution, sec
u_H, v_H, w_H	components of linear velocity of helicopter cg along helicopter axis directions, ft/sec
u_L, v_L, w_L	components of linear velocity of load cg along load axis directions, ft/sec
$\bar{u}, \bar{v}, \bar{w}$	components of linear velocity of load cg relative to helicopter cg, ft/sec
$\mathring{u}_L, \mathring{v}_L, \mathring{w}_L$	components of linear acceleration of load cg, ft/sec^2
$\mathring{v}_x, \mathring{v}_y, \mathring{v}_z$	components of linear acceleration of combined helicopter and pallet load, ft/sec^2
$V_{H_{max}}, D_{H_{max}}, S_{H_{max}}, P_{H_{max}}$	maximum dynamic value of vertical, drag, side, and inplane forces at helicopter hardpoints, lb
$V_{H_S}, D_{H_S}, S_{H_S}, P_{H_S}$	static trim values of vertical, drag, side, and inplane forces at helicopter hardpoints, lb
V_i, S_i, D_i, P_i	vertical, side, drag, and inplane forces at helicopter hardpoints, lb
V_k, S_k, D_k, P_k	vertical, side, drag, and inplane forces at load hardpoints, lb

$V_{L_{max}}, D_{L_{max}}$ $S_{L_{max}}\ P_{L_{max}}$	maximum dynamic value of vertical, drag, side, and inplane forces at load hardpoints, lb
V_{L_s}, D_{L_s}, $S_{L_s}\ P_{L_s}$	static trim values of vertical, drag, side, and inplane forces at load hardpoints, lb
$V_{L_{s_f}}, V_{L_{s_r}}$	static trim value of vertical forces at front and rear load hardpoints, respectively, lb
$V'_{L_{s_f}}, V'_{L_{s_r}}$	sum total of static trim values of vertical forces at all front and all rear load hardpoints, respectively, lb
V_{LCG}, S_{LCG}, V_{LCG}	vertical, side, and drag forces at pallet load cg, lb
V_{LP}, S_{LP}, D_{LP}	vertical, side, and drag forces at pallet center, lb
V_{R_L}	resultant velocity of load, ft/sec
W_L	weight of the load, lb
W_Z	force on load in load z direction due to downwash, lb
w_o	average downwash velocity at the rotor disc, ft/sec
x_j, y_j, z_j	components of distance from load cg to load hardpoints along load body axis directions, ft
$\bar{x}, \bar{y}, \bar{z}$	components of distance from helicopter cg to load cg along space axis directions, ft
$x_{D_F}, y_{D_F}, z_{D_F}$	components of hook relative to helicopter hardpoint along space axis directions, ft
$\bar{x}_i, \bar{y}_i, \bar{z}_i$	components of distance from helicopter hardpoints to load hardpoints along space axis directions, ft
$x_{j_F}, y_{j_F}, z_{j_F}$	components of load hardpoints relative to the helicopter cg along space axis directions, ft
$\bar{x}_1, \bar{y}_1, \bar{z}_1$	components of distance from helicopter hardpoint to the hook along space axis directions, ft
$(x_L - x_{cg})$, $(y_L - y_{cg})$, $(z_L - z_{cg})$	components of distance between load cg and combined cg of the pallet load plus helicopter, ft
$x\ell_L, y\ell_L, z\ell_L$ xm_L, ym_L, zm_L xn_L, yn_L, zn_L	direction cosines of load axes in the space axis system

z_c	z component of distance from load cg to the top of the load, ft
α_L	angle of attack of load, rad
β_L	angle of sideslip of load, rad
γ_f,γ_r	true angle between the helicopter body y axis and the front or rear sling members, respectively, rad
γ_M	angle between load z axis and the projection of the steel cable in the xy plane of the load, rad
θ_f,θ_r	true angle between the load body z axis and the front or rear sling members, respectively, rad
$\theta_{f_{x_z}},\theta_{r_{x_z}}$	projection in the load body xz plane of the angle between the load body z axis and the front or rear sling members, respectively, rad
θ_h	angle between the load body z axis and the line of action of the load weight, rad
θ_j	angle between individual legs and load z direction, rad
λ,ζ,ν	direction angles of x-, y-, and z-load axes relative to line LL, rad
ρ	density of air, slug/ft^3
τ_j	direction angle of individual nylon legs relative to line LL, rad
ϕ,θ,ψ	roll, pitch, and yaw attitudes of helicopter and pallet load relative to space axis directions, rad
ϕ_H,θ_H,ψ_H	roll, pitch, and yaw attitudes of helicopter relative to space axis directions, rad
ϕ_L,θ_L,ψ_L	roll, pitch, and yaw attitudes of load relative to space axis directions, rad
$\mathring{\phi}_L,\mathring{\theta}_L,\mathring{\psi}_L$	components of angular velocity of load about space axis directions, rad/sec

BACKGROUND

In helicopter movement of cargo as an externally suspended load, problems have been encountered with suspension subsystems and their components that adversely affect the safety, efficiency and effectiveness of this mode of support mobility. Recognizing the importance of this problem, the U. S. Army held a meeting in 1968 at which service agencies and industry personnel met to set a standard for rating sling strengths. The discussions at this meeting emphasized the depth of the problem. At this meeting, Sikorsky Aircraft outlined a proposed program for the establishment of design criteria for slings, aircraft hardpoints, and load suspension points.

Such a program was undertaken by Eustis Directorate in three phases. The first phase, which constitutes the work of this contract, was to determine the load factors due to dynamic and aerodynamic forces in flight for various sling arrangements and slung loads. The second phase, being performed concurrently by the U. S. Army Air Mobility Research and Development Laboratory, was to investigate the functional factors that affect the properties of materials suitable for use in helicopter sling design. This program measures the effects of attachment methods, environmental conditions, repeated loadings, and other related parameters in order to establish design criteria. The third phase, which will be performed during 1971 by Sikorsky Aircraft under Contract DAAJ02-71-C-0015, is intended to combine the results of the first two efforts and produce a design guide for helicopter slings, load suspension points, and aircraft hardpoints. The design guide will contain design techniques and procedures for each of the system segments suitable for use by design engineers concerned with the design of external load suspension systems on helicopters.

In order to establish valid design criteria for helicopter slings, load suspension points and aircraft hardpoints, it is necessary to establish the load factors due to dynamic and aerodynamic forces in flight. Prior to this program, the flight load factors used in sling design were the same as the designed flight load factors of the aircraft. Thus, if a helicopter were designed to withstand 2.5g flight loads, then the slings were also designed with this factor. Repeated sling failures led to speculation that the actual load factors on the load were higher than those on the aircraft. This study determines the actual load factors on the aircraft and on the slung load due to dynamic and aerodynamic forces in flight. The study will show that the helicopter studied, designed for 2.5g flight loads, never develops g forces greater than 2 even in violent maneuvers and that the actual load factor on the slung load is in excess of the nominal 2.5g design load factor. The method of determining these actual load factors for a variety of loads and sling arrangements in a variety of maneuvers is described in detail in this report.

In September 1970 the contract was amended to cover an examination of a limited number of representative cases on the moving-base simulator. The significance of motion cues in performing these few maneuvers was assessed, and their importance on the design criteria has been investigated in this report.

TECHNICAL APPROACH

LOADS

Sikorsky Aircraft has established representative external loads and typical sling and sling arrangements used for the work performed under this contract. Slings and sling arrangements include both single and multipoint suspended loads. For each arrangement, various types of sling loads are considered to account for inertia variations and aerodynamic lift and drag effects on the slung bodies in flight.

Load Types

The load types investigated cover the range of loads which can be carried as external helicopter loads without creating or encountering severe stability problems. They are grouped into four basic types:

Type I: High density loads; $W_L/A_{max} > 250\ \text{lb/ft}^2$

Type II: Medium density loads; $250\ \text{lb/ft}^2 > W_L/A_{max} > 50\ \text{lb/ft}^2$

Type III: Low density loads; $W_L/A_{max} < 50\ \text{lb/ft}^2$

Type IV: Aircraft

W_L is the weight of the load and A_{max} represents the maximum frontal area the load can have in an attitude which might be expected during flight. Types I, II, and III represent relatively bluff bodies which are stable or can be stabilized easily by artificial means such as drogue chutes. Loads which are highly unstable or whose aerodynamic characteristics are very sensitive to orientation are not included in this study. Aircraft have been treated as a distinct type because of their inherent aerodynamic surfaces and because of the tactical and economic importance of aircraft recovery as a helicopter mission.

Suspension Systems

The suspension systems considered in this program are of two basic types: single point and multipoint. The true sling angle is the angle between the sling leg and a vertical line, and is measured in the plane defined by the sling leg and the vertical line. Since the views of the helicopter and loads shown on Figures 2 through 7 are not parallel to this plane, the true angles are not presented pictorially.

Single-Point Suspension

In a single-point suspension, the load is attached to the aircraft at one point only. This is generally the main cargo hook of the aircraft. The sling is the device that attaches the load to the main cargo hook of the aircraft. In this program, three basic sling types are considered: the single-legged sling, the three-legged bridle and the

four-legged bridle. The material chosen for single-point suspension slings is nylon webbing. The webbing is described in MIL-W-4088F, Table II, as Type XXVI, with a width of 1-3/4 + 1/16 inches and a thickness of .150 to .180 inches. The lengths of the three-legged and four-legged bridles were set at 19 feet because this length fits most external loads in military inventory and because it provides a spring rate for the total sling which prevents objectionable vertical bounce.

1. The Single-Legged Sling: The single-legged sling (pendant) is the simplest arrangement. One end of the single-legged sling has a loop or donut which engages the aircraft cargo hook; the other end usually has a swivelling hook which engages an eye or shackle on the load. In this program, a 15,000-pound solid concrete block is suspended from a single-legged sling (see Figure 1).

2. The Three-Legged Bridle: The three-legged bridle is generally used to carry aircraft or other loads which because of their shape and hardpoint locations are best suspended from three points. A four-legged sling may be used with two legs going to the same point, making it essentially a three-legged sling. The apex of the three legs is a donut or a shackle which engages the aircraft cargo hook or pendant. The ends of the three legs usually terminate in chains or hooks or other hardware which engages the three lifting points on the load. In this program, a fixed-wing aircraft weighing approximately 12,000 pounds is suspended from a three-legged sling (see Figure 2).

3. The Four-Legged Sling: The four-legged sling is the most common in current usage. It is used to carry containers, almost all vehicles, some aircraft and special equipment. The three-dimensional geometry of most loads is such that four lifting points are desirable. The apex of the four legs is a donut or shackle which engages the aircraft cargo hook or pendant. The four legs usually terminate in chains or hook other hardware which engages the lifting points on the load. In this program, five loads were suspended from a four-legged sling:

   a. An empty 8x8x20 foot container representing a Type III load, illustrated in Figure 3.

   b. An 8x8x20 foot container at 15,000 pounds gross weight with cg forward, aft, and at the center, representing a Type II load.

   c. An 8x8x20 foot container at 15,000 gross weight with a forward cg and one sling leg failed.

   d. A 15,000-pound solid concrete block, representing a Type I load, illustrated in Figure 4.

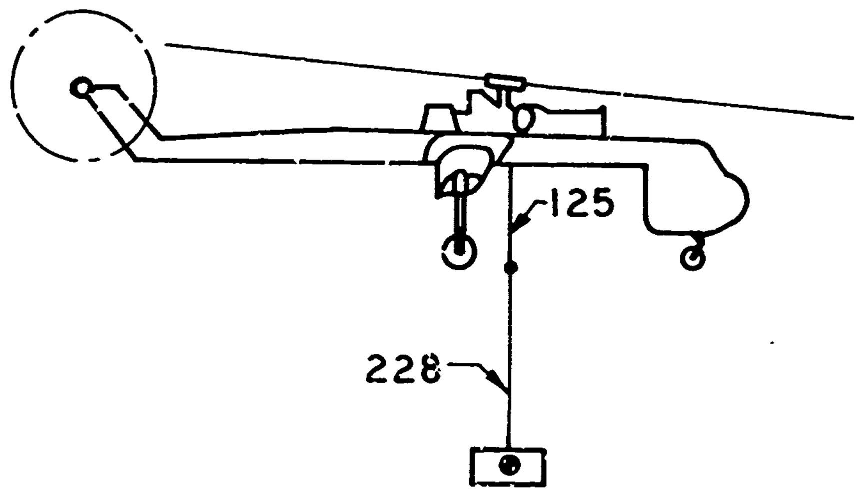

Figure 1. Single-Legged Sling Suspension of a 15,000-Pound Solid Concrete Block.

(Note: Dimensions in inches unless otherwise noted)

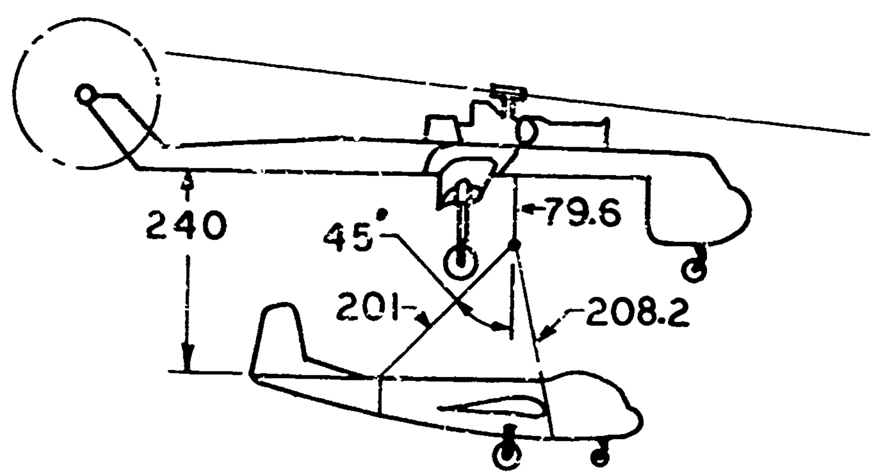

Figure 2. Three-Legged Bridle Suspension of a 12,000-Pound Fixed Wing Aircraft.

(Note: Dimensions in inches unless otherwise noted)

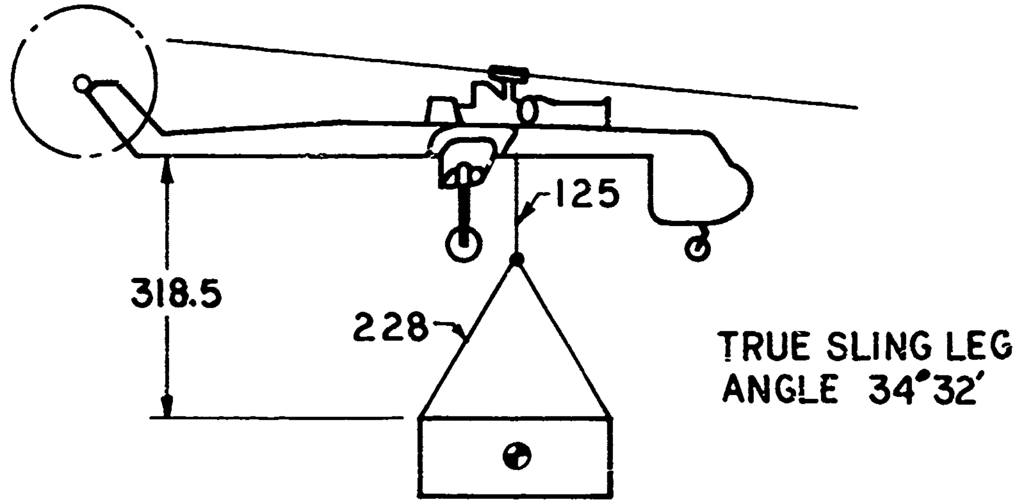

Figure 3. Single Point Suspension of 8x8x20 Foot Container From a Four-Legged Sling - 4000 Pound.

(Note: Dimensions in inches unless otherwise noted)

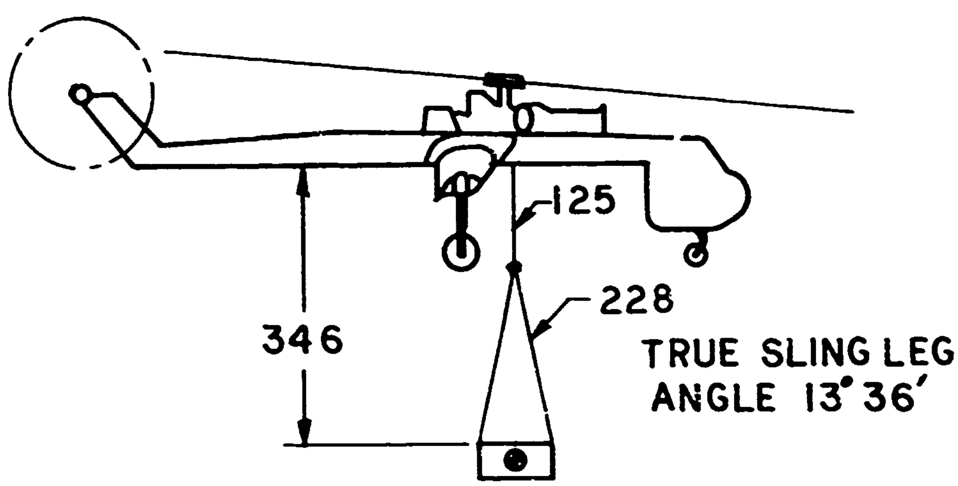

Figure 4. Single-Point Suspension of a 15,000-Pound Solid Concrete Block From a Four-Legged Sling.

(Note: Dimensions in inches unless otherwise noted)

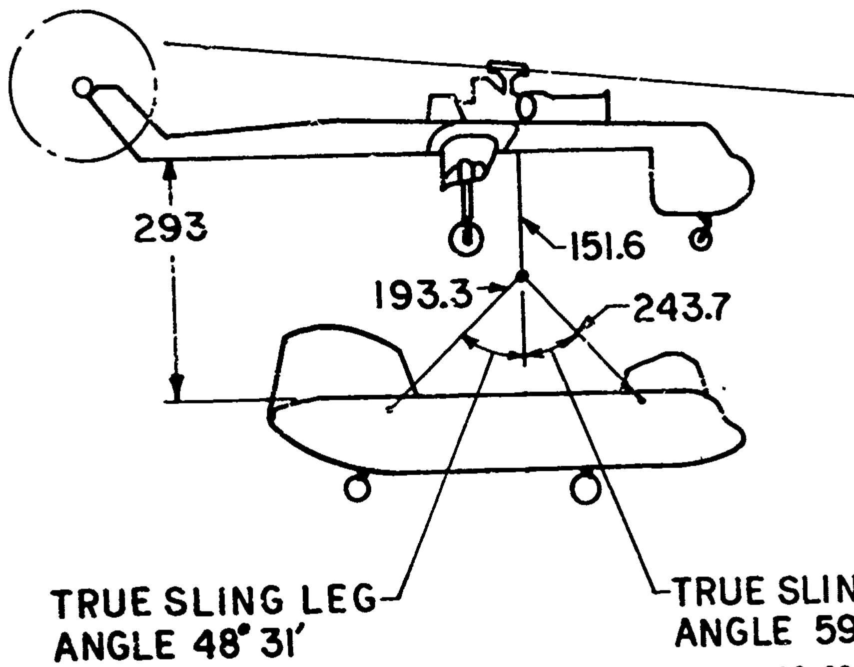

Figure 5. Single-Point Suspension of a 13,000-Pound Helicopter From a Four-Legged Sling

(Note: Dimensions in inches unless otherwise noted)

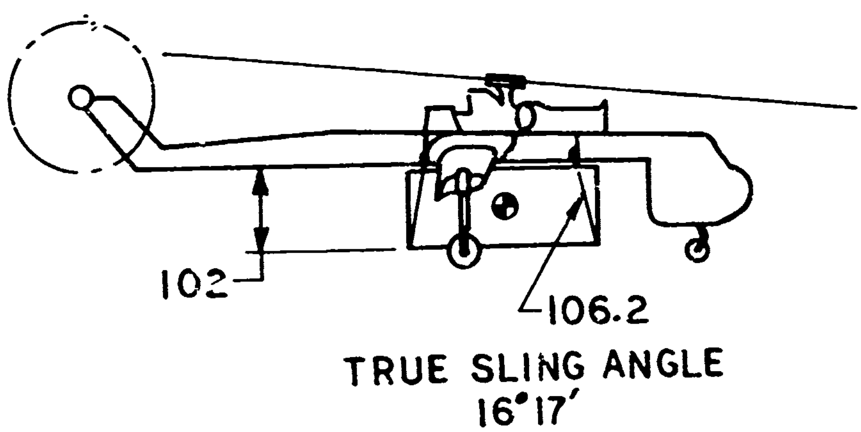

Figure 6. Multipoint Suspension of an 8x8x20 Foot Container.

(Note: Dimensions in inches unless otherwise noted)

e. A 13,000-pound helicopter representing a Type IV load, illustrated in Figure 5.

Multipoint Suspension

The four-point suspension system found on the CH-54A and the CH-54B aircraft is used to carry loads close to the aircraft and provides a greater degree of load restraint and stability than does the single-point system. In this program, two different loads are suspended by the four-point suspension system under a variety of conditions:

1. An 8x8x20 foot container at 15,000 pounds gross weight with the cg forward, on center, and aft representing a Type II load, illustrated in Figure 6.

2. An 8x8x20 foot container at 15,000 pounds gross weight with a forward cg and one failed cable.

3. A pallet load with six suspension points on the pallet at a gross weight of 15,000 pounds with cg forward, on center, and aft representing a Type II load, illustrated in Figure 7.

Load Classification

The loads described in the preceding paragraphs were used in this study for the determination of flight load factors and are representative of the many vehicles, pieces of equipment and supplies that constitute military external helicopter loads. Specific vehicles and items of equipment are classified by name, load type and weight and are grouped by general type for convenience. The list appears in Appendix I.

Vertical Bounce

For this study, it is assumed that the helicopter, together with its suspended load, is free from objectionable vertical bounce, and that the characteristics of the slings will not accentuate this phenomenon nor will the loads on the slings be significantly increased by it. This assumption is justified for the CH-54A and the CH-54B as load isolators (or decouplers) are used to effectively eliminate the problem. Included as Appendix II is a reprint of Appendix 4 entitled "Design Criteria and Analysis for the Prevention of Vertical Bounce" published as part of Technical Report 68-2, entitled Aerial Recovery Kit, Concept Formulation Study, U. S. Army Aviation Materiel Command, St. Louis, Missouri, June 1968, AD 673102.

The sling and bridle geometry was selected to achieve a spring constant which removes the natural frequency of the suspension/load system from the forcing frequencies found in helicopters.

METHOD OF SOLUTION

A computerized simulation of the coupled motion of the CH-54A helicopter

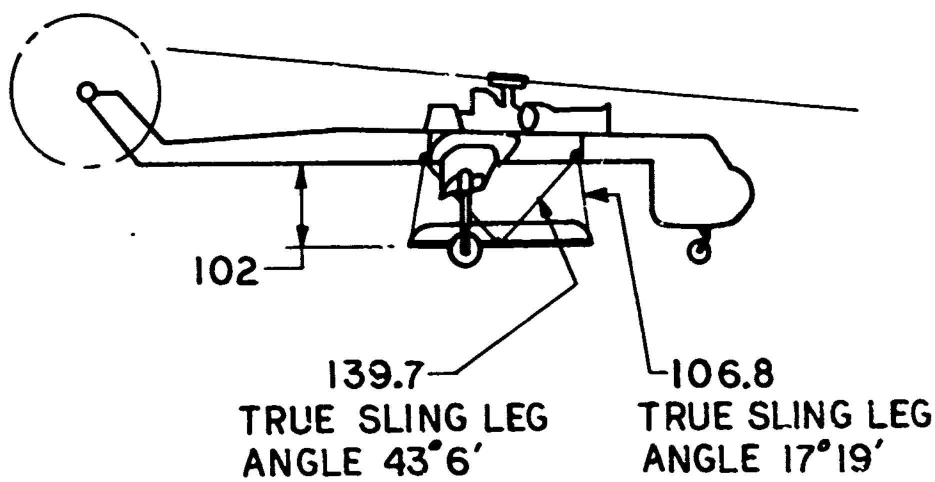

Figure 7. Multipoint Suspension of
a Pallet Load.

(Note: Dimensions in inches unless otherwise noted)

with each external load was conducted using a hybrid computer system to solve the coupled equations of motion for the helicopter and the slung load. The hybrid computer system consists of a general-purpose digital computer, the Digital Equipment Corporation PDP-6, with an interactive console for on-line computing and recording of data. For real time fixed-base runs, a full-scale Sikorsky S-61 helicopter cockpit with a Norden Contact Analog display system is also used. Digital-to-analog converters and analog-to-digital converters relay information back and forth between the cockpit (rig) and the PDP-6. If the motion system is employed, the same rig has moving-base capabilities, and the calculations which determine the motion cues which are to be relayed to the rig are carried out on an analog computer. See Figure 8.

The actual solution of the equations describing the motion of the helicopter and the external load is done by the PDP-6 computer. The simulation of the CH-54A used in this study was done by the General Helicopter Simulation Program (GHSP). This is a program developed at Sikorsky Aircraft for simulating continuous flight of a single-rotor helicopter. The degrees of freedom in GHSP include six spatial degrees of freedom, as well as blade flapping and variable rotor speed. There are no small angle limitations or small disturbance about a trim point restriction in GHSP. In the program, the rotor is not restricted to low advance ratios, small Mach numbers, or small blade angles of attack.

GHSP is arranged so that equations are solved repetitively, and the calculated data are updated at the end of every cycle. Effectively, the calculation cycle begins with initial or previously calculated values of velocity, attitude, and control position. The rotor forces and moments are calculated, followed by the calculation of the aerodynamic forces and moments on the fuselage. These values are then summed with the inertial forces to calculate the six accelerations. The accelerations are integrated, yielding the values of helicopter velocity and attitude. Instrument data for the rig is then updated, and any output data is collected. The cycle is then repeated.

Due to the length of the total helicopter-external load solution, including the load analysis and data scanning routines, a scheme for arriving at the total solution within computer time limits had to be devised. A real time solution with a pilot in the loop, whether using the fixed-base rig or the moving-base rig, must be completed within 0.060 sec. A duty cycle of 0.060 sec results in about sixteen passes through the entire solution per second. Therefore, the instruments and the display system in the cockpit simulator are updated at least sixteen times a second. If they were updated less frequently, the pilot could detect the discrete changes being supplied to the instruments and display, and a realistic response from the pilot would no longer be possible. To keep the simulation realistic without losing any accuracy in determining the various load factors developed in the sling members and at the hardpoints, the approach used was to first fly the helicopter-external load solution on the fixed-base rig in real time, saving only a record of control inputs from the pilot, and then to recreate the same maneuvers in nonreal time on only the PDP-6 by playing back the recorded pilot inputs into a more thorough analytic solution. See Figure 9.

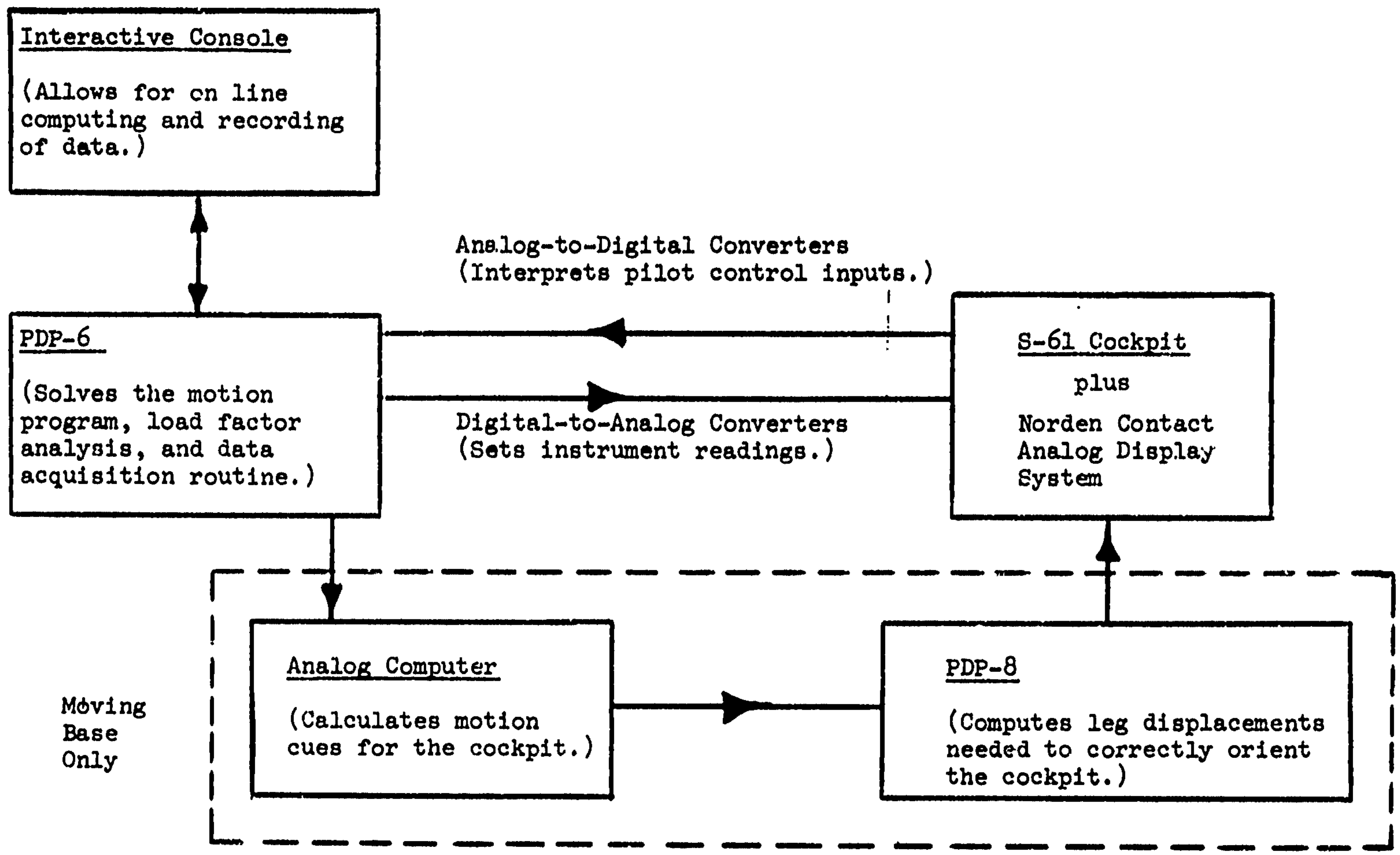

Figure 8. Facilities Used in the Helicopter - External Load Real Time Simulation.

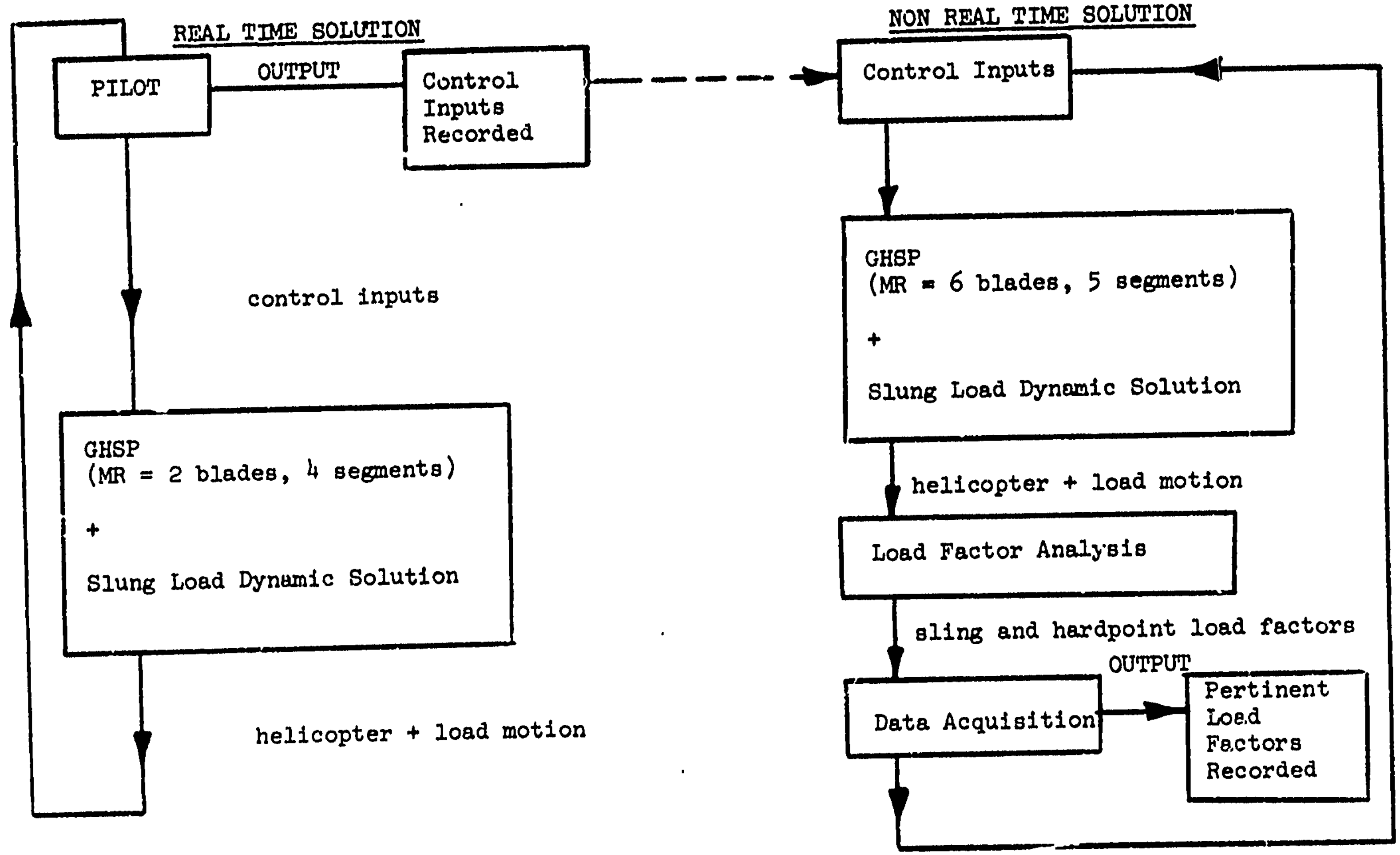

Figure 9. General Scheme for the Helicopter - External Load Simulation Plus Sling and Hardpoint Load Factor Analysis.

The nonreal time solution consisted of the helicopter-external load simulation plus the load analysis and data scanning routines, the combination of which was too lengthy for completion in real time. After both the real and nonreal time fixed-base maneuvers were finished, the same approach was used to do the moving-base maneuvers. Each of these steps is described in detail in the sections which follow.

A slung load simulation program has been developed which describes the motion of an external load. The method of solution of the load motion is similar to the method used to describe helicopter motion in GHSP. The slung load program has been interfaced with GHSP, and the resulting program is a simulation of a helicopter-external load combination. To fulfill the requirements of this contract, various sets of equations were derived and programmed to determine the loads within sling members and at helicopter and slung load hardpoints. Routines were also programmed for scanning all the load values calculated in the sling members and at the hardpoints during the solution of motion. The scanning routines were set up to select and save only data which would be pertinent in formulating design criteria.

Fixed-Base Real Time Runs

In order to include the effect of in-flight corrections by the pilot in response to the interaction between the load and helicopter, a pilot was inserted as an integral element in the control loop. Having a pilot in the loop called for a real time solution. Using the fixed-base rig, the pilot receives cues of the behavior of the helicopter from the flight instruments and the visual display in the cockpit. The externally slung load affects the helicopter overall motion and response, and this is reflected in the cockpit instrument readings and on the visual display. The existing version of GHSP is typically run in real time by simulating three main rotor blades and four segments along each blade. This is required to reduce the time needed for one complete pass through GHSP to less than 0.0600 sec. But when the slung load simulation was coupled with GHSP, the increase in length of the resultant program made it necessary to reduce the rotor simulation to two blades and four segments so that the solution could be accomplished in real time. The real time helicopter-external load simulation for all load and sling types used a rotor simulation consisting of two blades and four segments per blade.

All of the fixed-base real time runs were done with a duty cycle of 0.050 sec. This insured enough calculations per revolution of the main rotor to properly describe the sinusoidally varying main rotor forces and moments, thereby allowing for a proper description of the entire system. The duty cycle of 0.050 sec also guaranteed that the instrument reading and cockpit display in the simulator were updated frequently enough.

Four-Point Dynamic Solution

The slung load solution derived for use with GHSP uses an elastic cable approach for solving the tensions developed in the cables between helicopter hardpoints and hardpoints on the load. Basically, the helicopter and load motions can be solved separately, but the equations of the two

bodies are tied together by the cable tension solution. From the distance between the helicopter hardpoints and load hardpoints and from the original unstretched cable lengths, the change in length of each cable is determined. Multiplying this change in length by the spring rate allows the tension to be solved explicitly for each cable. Figure 10 outlines the general flow of the helicopter-external load solution.

The elastic cable approach used includes a number of benefits. If a solution using rigid cables were attempted, the four-point configuration would include four unknown cable tensions to solve for, thus resulting in an indeterminant system. The use of elastic cables overcomes this difficulty, since the tensions can be solved for explicitly. The use of elastic cables also allows for a more accurate description of the motion of the load, especially if the cables are very soft and can stretch some nonnegligible distance.

The general slung load configuration with a four-point suspension system is shown in Figure 11. Similar to the GHSP solution, the slung load equations of motion are solved repetitively and the calculated data are updated at the end of the cycle. At the beginning of the cycle, the load attitude and the load velocity are assumed to be known. Also known are the helicopter attitude and helicopter velocity, as well as the relative distance between load cg and helicopter cg.

The components of distance between hardpoints, along inertial axis directions, are given by

$$
\begin{aligned}
x_i = \; & x + d_{i_L} \cos\theta_L \cos\psi_L \\
& + b_{i_L} \cdot (\sin\phi_L \sin\theta_L \cos\psi_L - \cos\phi_L \sin\psi_L) \\
& + h_{i_L} (\cos\phi_L \sin\theta_L \cos\psi_L + \sin\phi_L \sin\psi_L) \\
& - d_{i_H} \cos\theta_H \cos\psi_H \\
& - b_{i_H} (\sin\phi_H \sin\theta_H \cdot \cos\psi_H - \cos\phi_H \sin\psi_H) \\
& - h_{i_h} (\cos\phi_H \sin\theta_H \cos\psi_H + \sin\phi_H \sin\psi_H) \qquad (1)
\end{aligned}
$$

$$
\begin{aligned}
y_i = \; & y + d_{i_L} \cos\theta_L \sin\psi_L \\
& + b_{i_L} (\sin\phi_L \sin\theta_L \cdot \sin\psi_L + \cos\phi_L \cos\psi_L) \\
& + h_{i_L} (\cos\phi_L \cdot \sin\theta_L \sin\psi_L - \sin\phi_L \cos\psi_L) \\
& - d_{i_H} \cos\theta_H \sin\psi_H \\
& - b_{i_H} (\sin\phi_H \sin\theta_H \sin\psi_H + \cos\phi_H \cdot \cos\psi_H) \\
& - h_{i_H} (\sin\phi_H \sin\theta_H \sin\psi_H - \sin\phi_H \cdot \cos\psi_H) \qquad (2)
\end{aligned}
$$

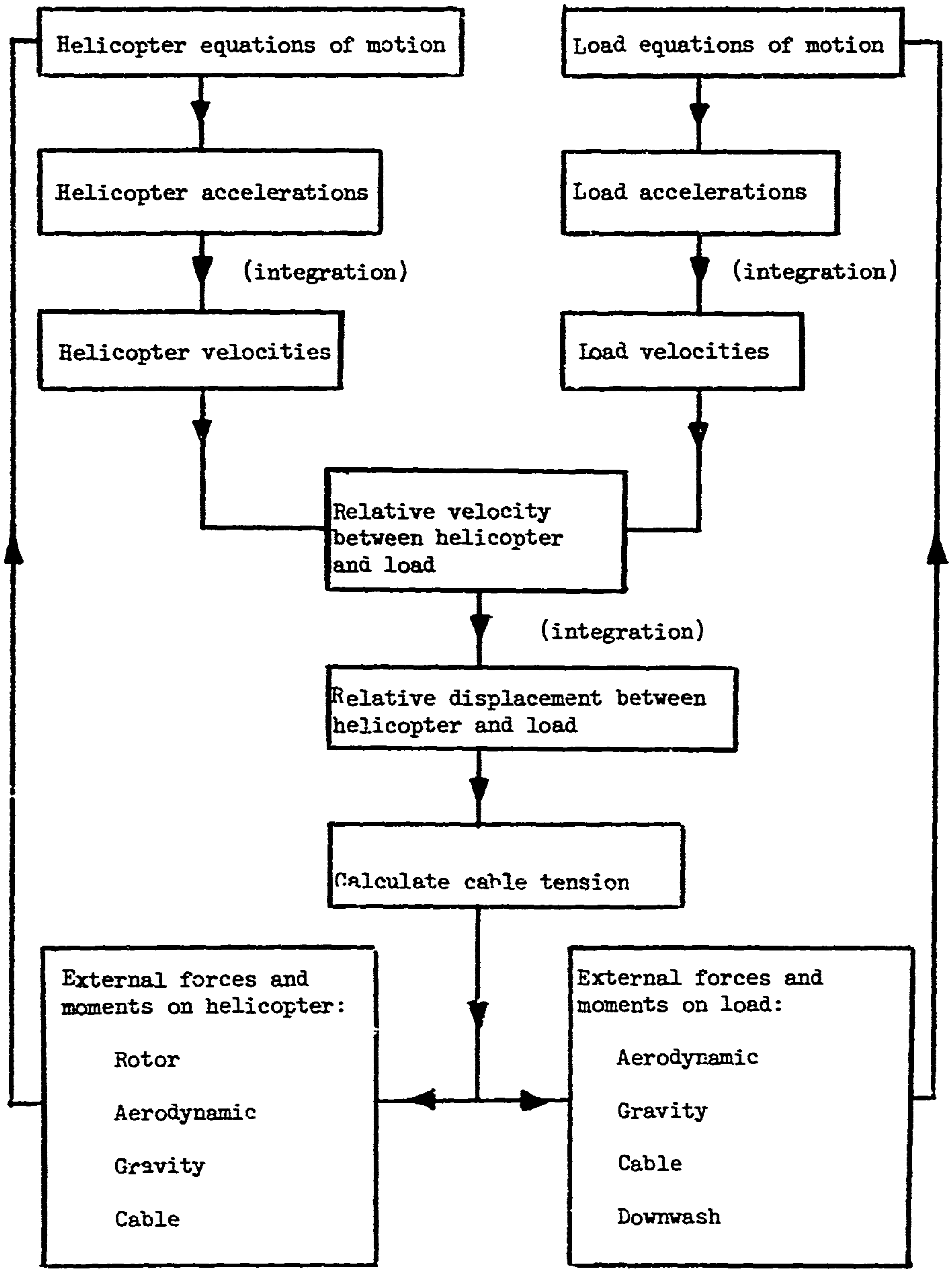

Figure 10. Flow Diagram of the Combined Helicopter and Slung Load Dynamic Solution

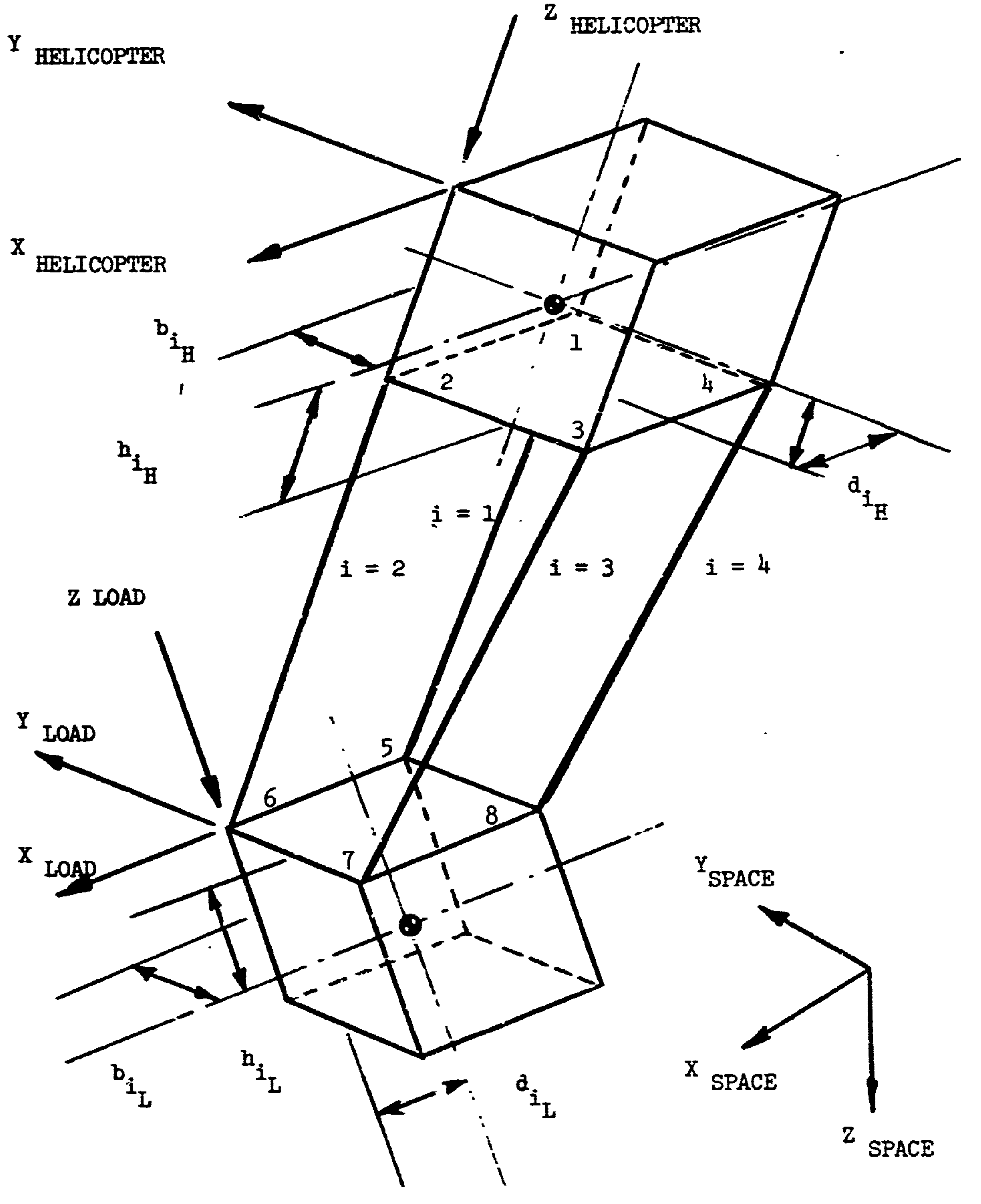

Figure 11. General Helicopter - Load Configuration for the Four-Point Sling Arrangement.

$$z_i = z - d_{i_L} \sin\theta_L + b_{i_L} \sin\phi_L \cos\theta_L + h_{i_L} \cos\phi_L \cdot \cos\theta_L + d_{i_H} \sin\theta_H - b_{i_H} \sin\phi_H \cos\theta_H - h_{i_H} \cos\phi_H \cdot \cos\theta_H \quad (3)$$

where

$\bar{x},\bar{y},\bar{z}$ = components of relative distance between helicopter cg and load cg , ft

$d_{i_L}, b_{i_L}, h_{i_L}$ = components of distance from load cg to load hardpoints, along load axes , ft

$d_{i_H}, b_{i_H}, h_{i_H}$ = components of distance from helicopter cg to helicopter hardpoints, along helicopter axes , ft

ϕ_L, θ_L, Ψ_L = load roll, pitch, and yaw attitudes , rad

ϕ_H, θ_H, Ψ_H = helicopter roll, pitch, and yaw attitudes, rad

i = 1 to 4; denotes individual cables

The length of each cable is given by

$$L_i = (\bar{x}_i^{\,2} + \bar{y}_i^{\,2} + \bar{z}_i^{\,2})^{1/2} \quad (4)$$

The solution assumes elastic cables; therefore, the tension in the cables is given by

$$T_i = K_i(L_i - L_{i_o}) \quad (5)$$

where

K_i = spring rate of the cables, lb/ft

L_{i_o} = unstretched cable lengths , ft

If the original length is greater than the present value, the cable tension is set to zero, thus simulating a cable gone slack.

The download on the slung load due to the main rotor downwash is calculated at this point. The download is

$$W_Z = \frac{1}{2} \cdot \rho \, c_w \, v_o^{\,2} f_w \quad (6)$$

where

ρ = density of air, slug/ft^3

c_w = ratio of average downwash velocity on the slung load over the average downwash velocity at the rotor disc

w_o = average downwash velocity at the rotor disc, ft/sec

f_w = equivalent flat plate area of slung load when viewed from above, ft^2

The value of f_w selected is a function of the geometry of the specific slung load which is simulated, while c_w depends on the distance the load is suspended below the main rotor. Since the pallet and container suspended by four points are both slung so near to the bottom of the helicopter, the downwash effects in these cases were ignored. It is assumed that the downwash blows back away from the slung load at forward speed. Therefore, the force on the load due to downwash is calculated only in hover. This force is assumed to act in the load direction, and no moment contributions on the load due to downwash are considered.

The additional forces and moments on the helicopter which are created by the cable tensions are given by

$$\Delta F_{x_H} = \Sigma TXi_H \quad (7)$$

$$\Delta F_{y_H} = \Sigma TYi_H \quad (8)$$

$$\Delta F_{z_H} = \Sigma TZi_H \quad (9)$$

$$\Delta \mathcal{L}_H = -\Sigma(hi_H TYi_H) + \Sigma(bi_H TZi_H) \quad (10)$$

$$\Delta M_H = \Sigma(hi_H TXi_H) - \Sigma(di_H TZi_H) \quad (11)$$

$$\Delta N_H = \Sigma(di_H TYi_H) - \Sigma(bi_H TXi_H) \quad (12)$$

where TXi_H, TYi_H, TZi_H = components of cable tension along helicopter axis directions, lb

These contributions are added to the equations of motion of the helicopter in GHSP to represent the effects of the slung load on the dynamics of the helicopter.

Returning to the slung load solution, the angle of attack, sideslip and resultant velocity of the load are computed by the equations

$$\alpha_L = \arctan\ (v_L/u_L) \quad (13)$$

$$\beta_L = \arctan\ (w_L/u_L) \quad (14)$$

$$V_{R_L} = (u_L{}^2 + v_L{}^2 + w_L{}^2)^{1/2} \quad (15)$$

where u_L, v_L, w_L = components of the slung load velocity along load axis directions, ft/sec

The aerodynamic forces and moments on the load can now be determined by scanning normalized wind tunnel data, or by representing these same data in equation form as functions of α_L and β_L. The wind tunnel data used to represent the slung loads in this particular study are given in Appendix III.

The actual equations of motion of the slung load can be solved at this point. These equations yield the components of linear and angular accelerations of the load:

$$\overset{\circ}{u}_L = v_L \cdot r_L - w_L \cdot q_L + (-m_L\ g \sin\theta_L - D_L + \Sigma TX_{i_L}) / m_L \tag{16}$$

$$\overset{\circ}{v}_L = w_L \cdot p_L - u_L \cdot r_L + (m_L\ g \cos\theta_L \sin\phi_L - Y_L + \Sigma\ TY_{i_L}) / m_L \tag{17}$$

$$\overset{\circ}{w}_L = u_L \cdot q_L - v_L \cdot p_L + (m_L g \cos\phi_L \cos\theta_L - L_L + \Sigma TZ_{i_L}) / m_L \tag{18}$$

$$\overset{\circ}{p}_L = \cdot - r_L q_L (I_{zz_L} - I_{yy_L}) + p_L\ q_L + \overset{\circ}{r}_L)\ I_{xz_L} + \mathcal{L}_L - \Sigma(h_{i_L} \cdot TY_{i_H}) + \Sigma\ (b_{i_L} \cdot TZ_{i_H}) \quad / I_{xx_L} \tag{19}$$

$$\overset{\circ}{q}_L = p_L r_L (I_{xx_L} - I_{zz_L}) + (r_1{}^2 - p_L{}^2)\ I_{xz_L} + M_L + \Sigma(h_{i_L} \cdot TX_{i_L}) + \Sigma\ (d_{i_L} \cdot TZ_{i_L}) \quad / I_{yy_L} \tag{20}$$

$$\overset{\circ}{r}_L = -p_L q_L\ (I_{yy_L} - I_{xx_L}) + (\overset{\circ}{p}_L - r_L\ q_L)\ I_{xz_L} + N_L + \Sigma\ (d_{i_L} \cdot TY_{i_L}) - \Sigma\ (b_{i_L}\ TX_{i_L}) \quad / I_{zz_L} \tag{21}$$

where p_L, q_L, r_L = roll, pitch, and yaw rates of load, rad/sec

m_L = mass of load, slug

g = acceleration of gravity, ft/sec^2

D_L, Y_L, L_L = aerodynamic drag, side force, and lift on load, lb

$\mathcal{L}_L, M_L, N_L$ = aerodynamic roll, pitch, and yaw moments on load, lb-ft

$TX_{i_L}, TY_{i_L}, TZ_{i_L}$ = components of cable tension in load axis directions, lb

$I_{xx_L}, I_{yy_Y}, I_{zz_L}, I_{xz_L}$ = moments and product of inertia of load, slug-ft^2

In these equations it is assumed that the only product of inertia of the load which is not negligible is I_{xz_L}. This is a reasonable assumption for the load types studied.

The components of angular velocity of the slung load measured along space axis directions are given by

$$\overset{\circ}{\phi}_L = p_L + q_L \sin\phi_L \tan\theta_L + r_L \cos\phi_L \tan\theta_L \quad (22)$$

$$\overset{\circ}{\theta}_L = q_L \cos\phi_L - r_L \sin\phi_L \quad (23)$$

$$\overset{\circ}{\psi}_L = (q_L \sin\phi_L + r_L \cos\phi_L) \cdot (\sec\theta_L) \quad (24)$$

A rectangular integration scheme is used to solve for velocities from accelerations and displacements from velocities. The duty cycle is the time between successive calculations and is designated by ΔT. One complete solution of the helicopter plus slung load equations must be completed within ΔT sec. The rectangular integration technique assumes a constant value of a derivative over ΔT to determine the integrated value. Once a new value of a parameter is calculated, the old value is normally discarded. The updated roll, pitch, and yaw attitudes of the load are

$$\phi_L \text{ (new)} = \overset{\circ}{\phi}_L \cdot \Delta T + \phi_L \text{ (old)} \quad (25)$$

$$\theta_L \text{ (new)} = \overset{\circ}{\theta}_L \cdot \Delta T + \theta_L \text{ (old)} \quad (26)$$

$$\psi_L \text{ (new)} = \overset{\circ}{\psi}_L \; \Delta T + \psi_L \text{ (old)} \quad (27)$$

The new components of angular velocity of the load measured along load body axis directions are

$$p_L \text{ (new)} = \overset{\circ}{p}_L \cdot \Delta T + p_L \text{ (old)} \tag{28}$$

$$q_L \text{ (new)} = \overset{\circ}{q}_L \cdot \Delta T + q_L \text{ (old)} \tag{29}$$

$$r_L \text{ (new)} = \overset{\circ}{r}_L \quad \Delta T + r_L \text{ (old)} \tag{30}$$

The new components of linear velocity of the load cg are given by

$$u_L \text{ (new)} = \overset{\circ}{u}_L \quad \Delta T + u_L \text{ (old)} \tag{31}$$

$$v_L \text{ (new)} = \overset{\circ}{v}_L \quad \Delta T + v_L \text{ (old)} \tag{32}$$

$$w_L \text{ (new)} = \overset{\circ}{w}_L \quad \Delta T + w_L \text{ (old)} \tag{33}$$

Within GHSP, the helicopter equations of motion are solved for the components of linear and angular acceleration. In a manner similar to eqs (31) to (33), the components of linear velocity of the helicopter cg are solved. Call these quantities u_H, v_H, and w_H. Then the components of relative velocity between the cg of the helicopter and the cg of the load are given by

$$\bar{u} = u_L - u_H \tag{34}$$

$$\bar{v} = v_L - v_H \tag{35}$$

$$\bar{w} = w_L - w_H \tag{36}$$

The latest values of velocity are used in eqs (34) to (36). The integration technique is used once more to determine the components of relative distance between the two cg's.

$$\bar{x} \text{ (new)} = \bar{u} \quad \Delta T + \bar{x} \text{ (old)} \tag{37}$$

$$\bar{y} \text{ (new)} = \bar{v} \quad \Delta T + \bar{y} \text{ (old)} \tag{38}$$

$$\bar{z} \text{ (new)} = \bar{w} \quad \Delta T + \bar{z} \text{ (old)} \tag{39}$$

This is the last calculation done in the cycle through the equations describing the motion of the helicopter-external load combination. The cycle is ready to be repeated again.

Similar to GHSP solution, the slung load solution contains no linearization assumptions. Neither are there any small angle or small displacement assumptions in the equations.

Single-Point Dynamic Solution

In general, the slung load equations developed for the four-point suspension may also be used to solve for the motion of a load suspended by a single cable by setting the limit on the subscript i equal to one in eqs (1) to (39). But a more accurate solution has been developed for the cases in which a bridle composed of one, three, or four nylon legs is used to attach the load to a hook on the end of a single steel cable from the helicopter. Since the spring system in the nylon bridle is much softer than the steel cable spring system, most of the load vibratory motion occurs below the hook. By making some modifications to the general four-point solution, the new set of equations more accurately describes the slung load motion relative to the steel cable, as well as relative to the helicopter itself. As the load dynamics cause changes in the tension within the legs suspending the load from the cable, these additional equations allow for the change in spring rate of the nylon legs. For very elastic members, the spring rate can change a great deal as the tension varies. The single-point suspension **solution accounts for this variation.**

The method used in the single-point suspension solution is to replace the total spring system comprised of the single steel cable and the one, three or four nylon bridle legs by an equivalent spring acting between the centers of gravity of the helicopter and load. Since the distance from the helicopter cg to helicopter hardpoint is small compared to the distance between the helicopter and the load, the location of the equivalent spring is reasonably accurate.

The tension in the cable is then solved for by the elastic method. Once the cable tension is known, the spring system is resolved to determine the correct stretch and orientation of both the steel cable and nylon bridle relative to one another and relative to the helicopter. This is basically the only difference in approach between the four-point solution and the single-point solution. The elastic cable approach is retained in the single-point solution to more accurately describe load motion and to save computation time.

Figure 12 illustrates the various parameters used in the equations of the single-point suspension system. When the load is allowed to hang freely and undisturbed in this configuration, the cg of the load will fall along the same line as the steel cable. This line, measured relative to the load body axis system by the angles λ, ζ, and ν, is referred to as line LL. The orientation of line LL relative to the load is assumed fixed and is determined by the static equilibrium

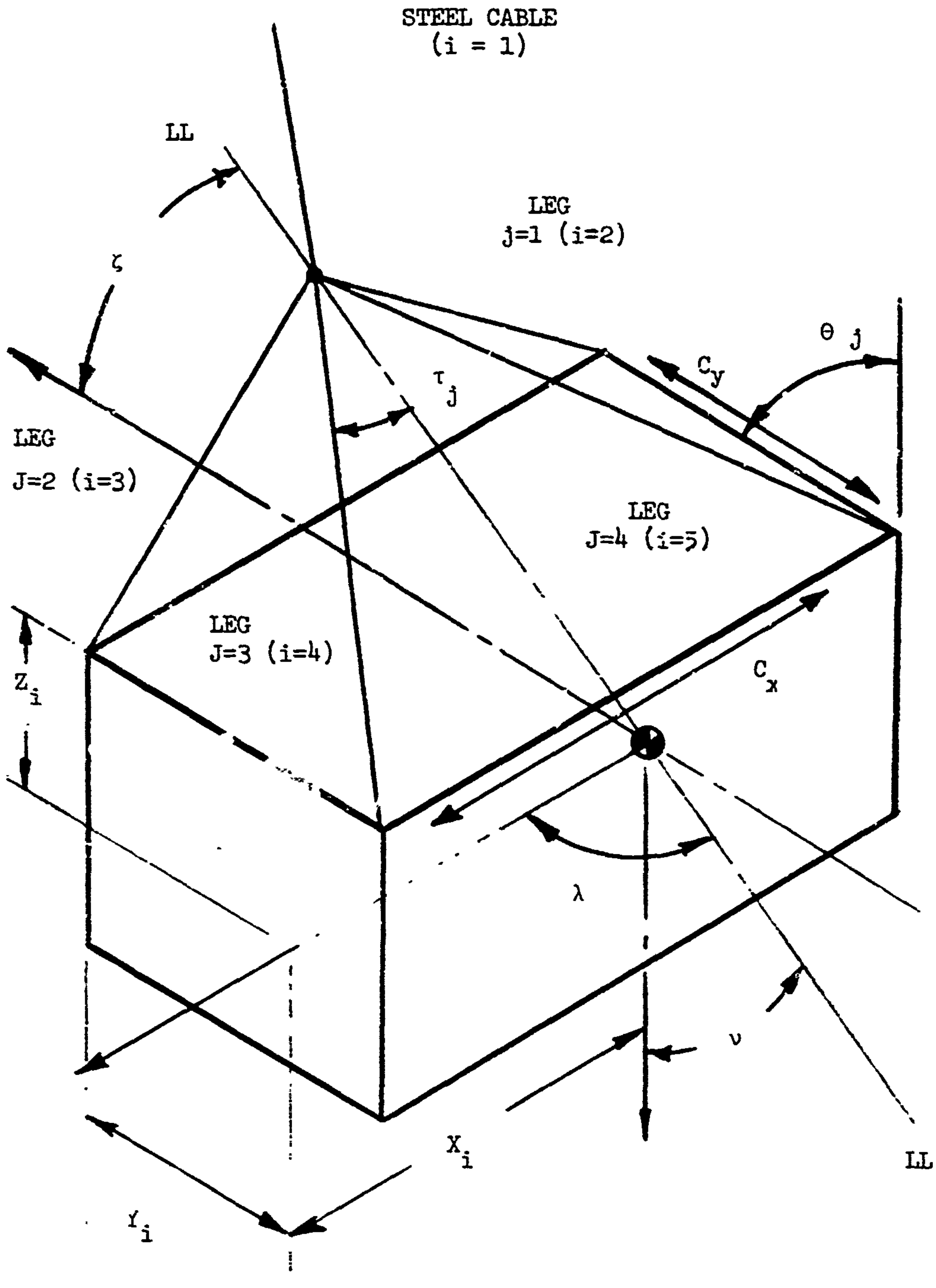

Figure 12. Single-Point Multilegged Slung Load Configuration.

position of the load. During the dynamic solution of load motion, irrespective of how line LL is oriented relative to the steel cable, it is assumed that the motion of the load cg with respect to the hook is along line LL. The orientation of the nylon legs relative to the line LL is given by the angles τ_j. These angles are also determined by the static equilibrium of the load. These angles vary so slightly with motion of the load cg relative to the hook that they can be assumed constant. The subscript j identifies individual nylon legs in the bridle. Numbering starts with $j = 2$.

The single-point solution replaces eqs (1) to (5) in the four-point solution. The distance between the helicopter cg and the load cg is

$$L_m = (\bar{x}^2 + \bar{y}^2 + \bar{z}^2)^{1/2} \tag{40}$$

The components of distance between cg's, $\bar{x}$, $\bar{y}$, and $\bar{z}$ are known either from initial conditions or from the previous pass through the solution. If L_{m_o} represents the unstretched distance between the cg's, then the change in this distance is

$$\Delta L_m = L_m - L_{m_o} \tag{41}$$

The tension in the steel cable T_1 is solved for from the change in length of an equivalent spring between helicopter cg and load cg and from the spring rate of this equivalent spring. The total equivalent spring rate is a function of the spring rate characteristics of the nylon legs as well as the spring rate of the steel cable. It is assumed that the spring rate of the steel cable K_s is constant, since this spring rate is high. But the spring rate of the nylon legs is a variable which is a function of the loads in the legs. In this study, the slung load solution was programmed for bridle legs made of MIL-W -4088F, type XXVI (1.75 in. by 0.165 in.) nylon webbing. If N_p represents the number of plys per leg, ℓ_{o_j} is the original length of each leg, and P_j is the load per ply in each leg, then the spring rate of each nylon leg made of this particular type of webbing is

$$K_j = N_p \cdot (33.5\ P_j + 30000\ \text{lb})\ /\ell_{o_j} \tag{42}$$

P_j is a function of the tension in the steel cable and is approximated by the equation

$$P_j = T_1/(N \cdot N_p \cos \tau_j) \tag{43}$$

where N = number of nylon legs

N_p = number of plys per leg

Equation (43) assumes that the components of tension in each leg in the direction of line LL are the same. This is a reasonably valid assumption for the sling configurations which were selected for this study. Each of the spring rates in the nylon legs is resolved in the direction of line LL according to the formula

$$K_{LL_j} = K_j \cos^2 \tau_j \tag{44}$$

The resultant spring rate of all the nylon legs in the direction of line LL is given by

$$K_N = \Sigma K_{LL_j} \tag{45}$$

Accounting for the effects of the steel cable, the spring rate of the total equivalent spring between the two cg's is

$$K_T = K_s \cdot K_N/(K_s + K_N) \tag{46}$$

The tension in the steel cable is

$$T_1 = K_T \; \Delta L_m \tag{47}$$

Equation (47) cannot be used alone to solve for the cable tension because from eq (43), P_j is also a function of T_1, while the value of K_T is a function of P_j. So the cable tension is found by solving eqs (42) to (47) simultaneously for T_1 once ΔL_m has been solved from eq (41). Once T_1 is known, K_N can also be solved.

The motion of the slung load relative to the hook can now be solved. The distance from the hook to the load cg at any time during the dynamic solution is

$$L_N = (T_1/K_N) + L_{N_O} \tag{48}$$

where L_{N_O} = unstretched value of L_N, ft

Although the single-point solution allows for swing of the slung load relative to the steel cable, this last equation assumes there is none; this assumption is reasonable because such swing is expected to be small for the loads studied.

Knowing the stretch in the cables in the bridle portion of the suspension system, the correct amount of stretch in the steel cable plus the proper orientation of the cable relative to the helicopter may be solved. The components of the distance from the helicopter hardpoint to the hook are

$$\begin{aligned}\bar{x}_1 &= \bar{x} + L_N \cos\lambda \cos\theta_L \cos\psi_L \\ &\quad + L_N \cos\zeta(\sin\phi_L \sin\theta_L \cos\psi_L - \cos\phi_L \sin\psi_L)\end{aligned}$$

$$+ L_N \cos\nu\,(\cos\phi_L \sin\theta_L \cos\psi_L + \sin\phi_L \sin\psi_L)$$

$$- d_{1_H} \cos\theta_H \cos\psi_H - b_{1_H} (\sin\phi_H \sin\theta_H \cos\psi_H - \cos\phi_H \sin\psi_H)$$

$$- h_{1_H} (\cos\phi_H \sin\theta_H \sin\psi_H - \sin\phi_H \cos\psi_H) \tag{49}$$

$$\bar{y}_1 = \bar{y} + L_N \cos\lambda \cos\theta_L \sin\psi_L$$

$$+ L_N \cos\zeta\,(\sin\phi_L \sin\theta_L \sin\psi_L + \cos\phi_L \cos\psi_L)$$

$$+ L_N \cos\nu\,(\cos\phi_L \sin\theta_L \sin\psi_L - \sin\phi_L \cos\psi_L)$$

$$- d_{1_H} \cos\theta_H \sin\psi_H - b_{1_H} (\sin\phi_H \sin\theta_H \sin\psi_H + \cos\phi_H \cos\psi_H)$$

$$- h_{1_H} (\cos\phi_H \sin\theta_H \cos\psi_H + \sin\phi_H \sin\psi_H) \tag{50}$$

$$\bar{z}_1 = \bar{z} - L_N \cos\lambda \sin\theta_L + L_N \cos\zeta \sin\phi_L \cos\theta_L$$

$$+ L_N \cos\nu \cos\phi_L \cos\theta_L + d_{1_H} \sin\theta_H$$

$$- b_{1_H} \sin\phi_H \cos\theta_H - h_{1_H} \cos\phi_H \cos\theta_H \tag{51}$$

Therefore, the length of the steel cable is

$$L_1 = (\bar{x}_1^2 + \bar{y}_1^2 + \bar{z}_1^2)^{1/2} \tag{52}$$

At this point the rest of the single-point suspension solution continues from eq (6) to eq (39) from the four-point solution with the limit on i equal to one.

Brooks and Perkins Pallet Dynamic Solution

The method developed for simulating a helicopter with an externally suspended load was to describe the slung load motion by a separate system of equations which were added to the already existing GHSP. The equations describing the slung load suspended from the helicopter by either four points or a single point have been discussed in the previous sections. The Brooks and Perkins pallet is one of the load types studied which falls under the four-point suspension category. The container is also slung from four points on the helicopter. However, the pallet configuration is very different because twelve cables are used to attach it to the helicopter; three cables from three different hardpoints on the pallet all go to one of the four hardpoints on the helicopter (see Figure 13). The container with the four-point suspension configuration is made up of only four cables. The arrangement of the twelve cables used to hang the Brooks and Perkins pallet from the helicopter allows for virtually no relative motion of the pallet in a fore-aft or sideways direction relative to the helicopter, whether the cables are rigid or elastic. The pallet also cannot move any appreciable distance in a vertical direction as long as weight of the payload is not small and the helicopter load factor is not near zero. For these reasons, the helicopter plus pallet combination has been assumed to act as a single rigid body. Therefore, only the GHSP alone was used for simulating the motion of the helicopter-pallet combination in real time. The gross weight, inertia, and center of gravity location of the equivalent helicopter programmed in the GHSP were adjusted for the contribution of the pallet. Solving GHSP then yielded the linear acceleration of the cg of the helicopter-pallet combination.

Since the cable arrangement used for slinging the pallet to the helicopter restricts the relative motion of the pallet, no accuracy is lost in describing the motion of the total system by using just GHSP. Since no separate slung load description is included in this case, aerodynamic forces on the pallet cannot be evaluated directly. But due to the geometry of the pallet and because this particular type of external load is slung so near to the helicopter, lift and drag contributions of the pallet are essentially zero. The elastic cable approach used in the general four-point configuration solution described previously applies best to geometries where only one cable is attached to each helicopter hardpoint. Using the same elastic cable approach with the pallet would not be incorrect, but the additional cables would make a real time solution impossible. The approach which has been used to represent the dynamics of the helicopter plus pallet in real time is shorter than the elastic cable approach would be, and is just as accurate.

Nonreal Time Runs - Fixed-Base Pilot Inputs

The helicopter-external load simulation plus the sling element and hardpoint loads computation are performed by the PDP-6 digital computer. With this digital solution, all equations are calculated during discrete time

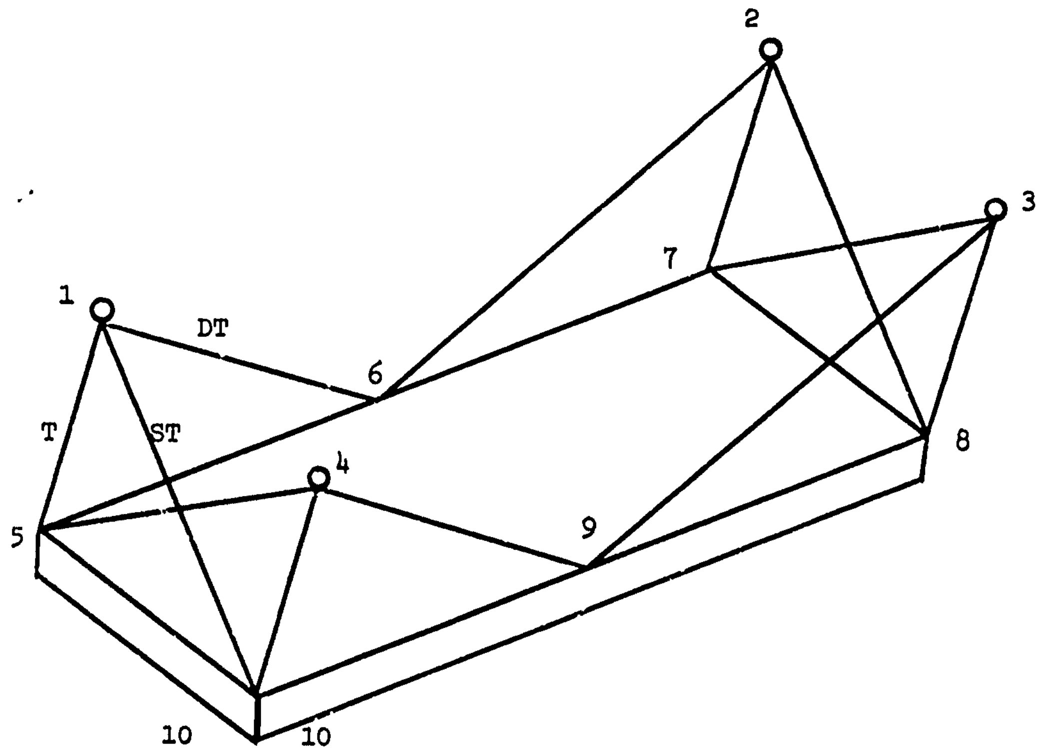

Figure 13. Brooks and Perkins Pallet.

intervals, each of which is called a pass. The time it actually takes to complete one pass may be called the computation time. If accurate and valid results are to be obtained from a real time simulation, at least 16 passes per second are needed. Thus, the computation time must be less than one-sixteenth of a second. Within the simulation model itself, the length of time used in the integration scheme which expires before updating the value of a variable is called the duty cycle. The duty cycle is the simulated time between successive passes through the solution. For the helicopter and various slung loads studied, it was necessary to have this simulated time interval to be less than one-sixth of a second. This duty cycle restriction guaranteed that the model described by the digital solution agreed with the exact mathematical description of the system. For a real time simulation, the calculation time for one pass must equal the time interval simulated within the solution during that pass. Due to the length of the helicopter-external load simulation, plus the analysis of loads developed in the sling members and at hardpoints, it was impossible for the computation time of this entire solution to be less than one-sixteenth of a second. Because the equations describing the motion of the system are independent of the component sling element and hardpoint loads analysis, a real time simulation with a pilot in the loop was done using only the solution for helicopter-external load motion. During these real time runs, the stick and pedal control motion by the pilot was monitored and recorded. Then, without the pilot, the values of the control motions were used as input to the program which now included the sling and hardpoint loads analysis as well as the equations of motion of the system. This version of the program was run in nonreal time, i.e., the computation time needed for one pass through the program could be as long as necessary to complete all the equations. Thus, the nonreal time runs created exactly the same helicopter and slung load response as were created during the same maneuvers in real time; the load factors developed in the sling members and at the hardpoints were also calculated.

The sling element and hardpoint loads are calculated by a series of equations which have been programmed with those of the slung load simulation described earlier. The latter equations are totally independent of the former, so that the sling and hardpoint equations form an ancillary package which operates on the output of the slung load simulation.

The following sling types were programmed and analyzed in this study:

1. Four-cable suspension

2. Four-cable suspension; one cable broken

3. Single-cable four-legged suspension

4. Single-cable four-legged suspension; one cable broken

5. Single-cable three-legged suspension

6. Single-cable single-legged suspension

7. Brooks and Perkins pallet

A detailed description of each of these analyses is given later. The following general assumptions have been made for all load configurations:

1. All cables and legs are weightless.
2. Aerodynamic effects on cables and legs are negligible.
3. All loads are rigid.
4. The helicopter from which the loads are suspended is rigid.
5. All cables and leg elements for any particular sling have identical diameters and properties.

Within the sling and hardpoint analyses, the tension in each cable and each nylon leg in the bridle, as well as the vertical, side, drag, and inplane components of the force at each load and helicopter hardpoint, are calculated. These values are calculated at the end of every pass through the program during the duration of the maneuver, and are expressed as load factors by nondimensionalizing each value. The cable tensions are nondimensionalized by dividing each tension by the static value of tension in that particular cable. The tensions in the legs are nondimensionalized by dividing each tension by the static value of tension in that particular leg. The vertical, side, drag, and inplane forces are all nondimensionalized by dividing each quantity by the static value of vertical force at that particular helicopter or load hardpoint.

For the real time runs, the number of blades simulated in the rotor solution was two, with the airloads analysis being done along four segments of each blade. This was necessary to reduce the entire computation time so that a real time simulation could be done. Simulating only two blades caused some inaccuracy in the helicopter load factor which was produced, giving this value an oscillatory characteristic instead of a steady value as the rotor goes through one complete revolution. The pilot could not detect this effect in real time because of the high frequency, and it did not affect the overall dynamics of the system for the same reason. Therefore, the pilot inputs and helicopter-external load motion were not affected by the two-blade rotor. But a more specific study of load factor produced over small discrete time intervals would be affected by the two-blade rotor. Therefore, the nonreal time runs were done with a rotor simulation consisting of six blades and five segments along each blade. This eliminated noise in the helicopter load factor time history, thus insuring more exact calculations of load factors in the slings and hardpoints as a function of helicopter load factor.

In addition to the sling and hardpoint loads analysis which was added to the simulation during nonreal time runs, a data acquisition file was also added. This file scans load factor data calculated in the loads analysis portion of the program, and selects any data which is pertinent to determining final design criteria. The data acquisition file is discussed in more detail in a later section.

Determination of Sling Element and Hardpoint Loads

1. Four-Cable Suspension

All of the computations for the cable tensions and hardpoint reactions at the load and at the helicopter are effectively carried out in the motion simulation portion of the program. For the load analysis, it is only necessary to set the vertical, side, drag, and inplane forces equal to

$$V_i = TX_{i_H} \tag{53}$$

$$S_i = TY_{i_H} \tag{54}$$

$$D_i = TZ_{i_H} \tag{55}$$

$$P_i = (S_i^{\,2} + D_i^{\,2})^{1/2} \tag{56}$$

$$V_k = TX_{i_L} \tag{57}$$

$$S_k = TY_{i_L} \tag{58}$$

$$D_k = TZ_{i_L} \tag{59}$$

$$P_k = (S_k^{\,2} + D_k^{\,2})^{1/2} \tag{60}$$

where i = 1 to 4; denotes individual cables or helicopter hardpoints

k = 5 to 8; denotes individual load hardpoints

These quantities are then nondimensionalized by the method described earlier. Figure 11 illustrates the numbering system used for the cables and hardpoints.

2. Four-Cable Suspension; One Cable Broken

The equations and computation scheme for this configuration are identical to the four cable suspension case with the exception that i = 1 to 3, and k = 5 to 8 (see eqs (53) through (60)). The limits on i in eqs (1) through (39) are also from 1 through 3.

3. Single-Cable Four-Legged Suspension

In the motion solution for the single-cable multileg system, the moment on the load due to the tensions in the leg is effectively evaluated by momentarily assuming a rigid structure from the hook down and computing the moment about the load cg due to the tension in the steel cable.

Any aerodynamic moment on the load will change the orientation of the slung load plus nylon bridle relative to the steel cable. Therefore, the correct effect of moments on the load is included in the motion simulation solution. The change in tension in the individual legs which results from the aerodynamic moment is included in the sling and hardpoint analysis.

In the single-cable four-legged suspension system, each leg is treated as a spring, since the structure is statistically indeterminant. The change in length from the no-load condition is calculated for each leg from known data and output of the motion simulation by

$$\Delta L_j = (L_N \cos\lambda - x_j)^2 + (L_N \cos\zeta - y_j)^2 + (L_N \cos\nu - z_j)^2 \;\; 1/2 - \ell_{o_j} \quad (61)$$

where j = 2 to 5; denotes individual legs

x_j, y_j, z_j = components of distance from load cg to load hardpoints, ft

The tension in each leg due to the external forces on the load is then calculated by rewriting eq (42) in the form

$$T_j = (30{,}000 \; N_p \; \Delta L_j) \; / \; (\ell_{oj} - 33.5 \; \Delta L_j) \quad (62)$$

The tension in each leg due to moment balance is now calculated. Refer to Figure 12. The angle between the load z - axis and the projection of the steel cable in the xz - plane of the load is

$$\gamma_M = \arctan \left[(\cos\lambda) \; / \; (\cos\nu) \right] \quad (63)$$

The pitching moment contribution about the load cg is then given by

$$M_p = (TX_{1_L} \cos\gamma M - TZ_{1_L} \sin\gamma M) \; (L_N \cos\lambda)^2 + (L_N \cos\nu)^2 . \; (L_N \cos\nu - z_c) \; / \; (L_N \cos\nu) \quad (64)$$

where z_c = z - component of distance from the load cg to the top of the load, ft

Eq (64) allows for cg variation in the x- and z- directions. Since the four-legged case is indeterminant, an approximate method is used to determine the components of force in each leg necessary to balance the pitching moment on the load. These contributions for each leg are

$$\Delta F2_M = M_p/2c_x\cos\theta_2 \quad (65)$$

$$\Delta F3_M = -Mp/2c_x\cos\theta_3 \quad (66)$$

$$\Delta F4_M = -Mp/2c_x\cos\theta_4 \quad (67)$$

$$\Delta F5_M = Mp/2c_x\cos\theta_5 \quad (68)$$

where c_x = x - component of distance between load hardpoints, ft

$\theta_2, \theta_3, \theta_4, \theta_5$ = angle between individual legs and load z- direction, rad

Effectively, these equations lift the restriction in the motion simulation portion of the program which says that line LL is fixed with respect to the load.

In a similar manner, the components of force in each leg necessary to balance the rolling moment on the load are calculated by

$$p = (TY_{1_L} \cos\gamma - TZ_{1_L} \sin\gamma) \quad (L_N\cos\zeta)^2 \quad (69)$$

$$\gamma = \arctan \quad (\cos\zeta) / (\cos\nu)$$

$$+ (L_N\cos\nu)^{2\ 1/2}. \ (L_N\cos\nu - z_c) / (L_N\cos\nu) \quad (70)$$

$$\Delta F2 = - p/2\ cy\cos\theta_2 \quad (71)$$

$$\Delta F3 = - p/2\ cy\cos\theta_3 \quad (72)$$

$$\Delta F4 = p/2\ cy\cos\theta_4 \quad (73)$$

$$\Delta F5 = p/2\ cy\cos\theta_5 \quad (74)$$

There is no yawing moment reaction at the hook because the load is free to rotate about the hook.

The total tension in each leg due to the reaction of both forces and moments on the load is now calculated by the equation

$$T_j = T_j' + \Delta F_{jM} + \Delta F_{jL} \tag{75}$$

From the four-legged tensions which are determined by eq (75), the smallest nonnegative value is selected; the remaining three-legged tensions are discarded. The tension in all four legs might be calculated by eq (75), but small errors indigenous to any computation scheme might result in a loss of equilibrium at the hook. To insure equilibrium, the three remaining tensions are calculated directly by writing the equations of equilibrium at the hook. To do this, the direction cosines of the load axes in a fixed axis system must be calculated by

$$x\ell_L = \cos\theta_L \sin\psi_L \tag{76}$$

$$y\ell_L = \sin\phi_L \sin\theta_L \cos\psi_L - \cos\phi_L \sin\psi_L \tag{77}$$

$$z\ell_L = \cos\phi_L \sin\theta_L \cos\psi_L + \sin\phi_L \sin\psi_L \tag{78}$$

$$xm_L = \cos\theta_L \sin\psi_L \tag{79}$$

$$ym_L = \sin\phi_L \sin\theta_L \sin\psi_L + \cos\phi_L \cos\psi_L \tag{80}$$

$$zm_L = \cos\phi_L \sin\theta_L \sin\psi_L - \sin\phi_L \cos\psi_L \tag{81}$$

$$xn_L = -\sin\theta_L \tag{82}$$

$$yn_L = \sin\phi_L \cos\theta_L \tag{83}$$

$$zn_L = \cos\phi_L \cos\theta_L \tag{84}$$

The coordinates of the load hardpoints in the fixed axis system are calculated from the direction cosines and the position of the load origin relative to the helicopter by the equations

$$xj_F = x\ell_L\, xj + y\ell_L\, yj + z\ell_L\, zj + \bar{x} \tag{85}$$

$$yj_F = xm_L\, xj + ym_L\, yj + zm_L\, zj + \bar{y} \tag{86}$$

$$zj_F = xn_L\, xj + ym_L\, yj + zn_L\, zj + \bar{z} \tag{87}$$

The coordinates of the hook relative to the helicopter in the fixed axes are found from the known positions of the hook relative to the load and the load relative to the helicopter according to the equations

$$x_{D_F} = \bar{x} + x\ell_L\, L_N\cos\lambda + y\ell_L\, L_N\cos\zeta + z\ell_L\, L_N\cos\nu \tag{88}$$

$$y_{D_F} = \bar{y} + xm_L\, L_N\cos\lambda + ym_L\, L_N\cos\zeta + zm_L \cdot L_N \cos\nu \qquad (89)$$

$$z_{D_F} = \bar{z} + zn_L\, L_N\cos\lambda + yn_L\, L_N\cos\zeta + zn_L \cdot L_N \cos\nu \qquad (90)$$

Eqs (85) to (90) are used to calculate the direction cosines of the sling legs in the fixed axes by

$$\ell_j = (x_{D_F} - x_{j_F})/L_j \qquad (91)$$

$$m_j = (y_{D_F} - y_{j_F})/L_j \qquad (92)$$

$$n_j = (z_{D_F} - z_{j_F})/L_j \qquad (93)$$

where

$$L_j = \Delta L_j + \ell_{oj} \qquad (94)$$

The tension in the three unknown legs may now finally be computed by solving

$$\Sigma T_j l_j + TX1_H = 0 \qquad (95)$$

$$\Sigma T_j m_j + TY1_H = 0 \qquad (96)$$

$$\Sigma T_j n_j + TZ1_H = 0 \qquad (97)$$

In eqs (95) to (97), one of the values of T_j is already known from the smallest nonnegative value of T_j solved from eq (75). The steel cable tension components $TX1_H$, $TY1_H$, and $TZ1_H$ are output directly from the motion simulation portion of the program.

Once the tension in the four legs is known, a check is made to insure that none of the values are less than zero, which insures that none of the legs have gone slack or are in compression.

The hardpoint reactions at the helicopter and at the load are now calculated by a simple geometry analysis. These hardpoint reactions at the helicopter and load, however, must be computed in their respective body axes. For the sling elements, the direction cosines in the load axes are

$$\ell_j^L = (L_N\cos\lambda - x_j)/L_j \qquad (98)$$

$$m_j^L = (L_N \cos\zeta - y_j)/L_j \tag{99}$$

$$n_j^L = (L_N \cos\nu - z_j)/L_j \tag{100}$$

Using these direction cosines, the reactions at the load hardpoints are

$$V_j = T_j \, n_j^L \tag{101}$$

$$D_j = T_j \, m_j^L \tag{102}$$

$$S_j = T_j \, \ell_j^L \tag{103}$$

$$P_j = (S_j^2 + D_j^2)^{1/2} \tag{104}$$

The reactions at the helicopter are known from the motion simulation solution and are taken directly as

$$V_1 = TZ_{1_H} \tag{105}$$

$$D_1 = TY_{1_H} \tag{106}$$

$$S_1 = TX_{1_H} \tag{107}$$

$$P_1 = (S_1^2 + D_1^2)^{1/2} \tag{108}$$

These quantities from eqs (101) to (108) are nondimensionalized for final output.

4. Single-Cable Four-Legged Suspension; One Leg Broken

The single-cable four-legged suspension with one leg failed solution is identical to that of the single-cable four-legged suspension except for a few minor modifications. Assume leg 5 (left aft) is failed and ignore all data input to that leg

for the motion and loads analysis solutions. Thus, the subscript $j = 5$ is never used anywhere. Equation (61) is still calculated for i equal 2 to 4 so that L_j may be checked to insure that no legs have gone slack. But eqs (62) to (75) are ignored and the tensions in the legs are solved by eqs (95) to (97) alone, since this configuration is not indeterminant. The resulting tensions are checked for compressive loads.

5. Single-Cable Three-Legged Suspension

The analysis for this configuration is exactly the same as for the single-cable four-legged suspension with one leg failed. The static loads used for nondimensionalization, however, are obviously based on three bridle legs instead of four.

6. Single-Cable Single-Legged Suspension

In the single-cable single-legged suspension, all tensions and reactions are calculated within the motion simulation solution. For readout and nomenclature purposes, set

$$V_1 = TZ_{1_H} \tag{109}$$

$$S_1 = TY_{1_H} \tag{110}$$

$$D_1 = TX_{1_H} \tag{111}$$

$$P_1 = (S_1^{\,2} + D_1^{\,2})^{1/2} \tag{112}$$

$$V_2 = TZ_{1_L} \tag{113}$$

$$S_2 = TY_{1_L} \tag{114}$$

$$D_2 = TX_{1_L} \tag{115}$$

$$P_2 = (S_2^{\,2} + D_2^{\,2})^{1/2} \tag{116}$$

The subscript 2 refers to the single load hardpoint.

7. Brooks and Perkins Pallet

The Brooks and Perkins pallet is a complex and multi-redundant structure whose solution requires a rather sophisticated analysis. In an effort to keep the programming requirements uncomplicated, it was decided that influence coefficients for the structure would be precalculated by the FORTRAN program FRAN (Frame Analysis) and then used as direct input for the tension and hardpoint analysis. In the simulation program the pallet is treated as a rigid member of the helicopter.

The inertial and gravitational loads and moments generated at the load cg are calculated by

$$V_{LCG} = W_L \quad g\cos\theta\cos\phi - \dot{v}_z - \dot{p}\,(y_L - y_{cg}) + \dot{q}\,(x_L - x_{cg}) \quad /g \tag{117}$$

$$S_{LCG} = W_L \quad g\cos\theta\sin\phi - \dot{v}_y + \dot{p}\,(z_L - z_{cg}) - \dot{r}\,(x_L - x_{cg}) \; /g \tag{118}$$

$$D_{LCG} = W_L \quad -g\sin\theta - \dot{v}_x - \dot{q}\,(z_L - z_{cg}) + \dot{r}\,(y_L - y_{cg}) \; / \; g \tag{119}$$

$$M_{X_{LCG}} = -I_{xx}\dot{p} \tag{120}$$

$$M_{Y_{LCG}} = -I_{yy}\dot{q} \tag{121}$$

$$M_{Z_{LCG}} = -I_{zz}\dot{r} \tag{122}$$

where $(x_L - x_{cg})$, $(y_L - y_{cg})$, $(z_L - z_{cg})$ = components of distance between the load cg and the combined cg of the load and helicopter, ft

W_L = weight of the load, lb

I_{xx}, I_{yy}, I_{zz} = moments of inertia of the combined helicopter and load, slug-ft^2

The accelerations and attitudes used in eqs (117) through (122) have been solved for in GHSP for the combined helicopter and load.

The influence coefficients are written for loads applied at a point in the center of the pallet and in the plane of the pallet. Consequently, the loads and moments solved for in eqs (117) through (122) must be transferred from the center of gravity to the center point. This transfer is

$$V_{LP} = V_{LCG} \tag{123}$$

$$S_{LP} = S_{LCG} \tag{124}$$

$$D_{LP} = D_{LCG} \tag{125}$$

$$M_{XLP} = M_{XCG} + h\ S_{LCG} \tag{126}$$

$$M_{YLP} = M_{YCG} - h\ D_{LCG} - dV_{LCG} \tag{127}$$

$$M_{ZLP} = M_{ZCG} + d\ S_{LCG} \tag{128}$$

where d = component of distance from pallet center to load center of gravity in load x - direction, ft

h = component of distance from pallet center to load center of gravity in load z - direction, ft

It is assumed that the load is laterally symmetric with the pallet. The tension in the twelve cables can be directly calculated using the loads from eqs (123) to (128) and the given influence coefficients from the FRAN program. For the standard Brooks and Perkins pallet shown in Figure 13, the influence coefficients equations in matrix form are

$$\begin{bmatrix} T_1 \\ DT_1 \\ ST_1 \\ T_2 \\ DT_2 \\ ST_2 \\ T_3 \\ DT_3 \\ ST_3 \\ T_4 \\ DT_4 \\ ST_4 \end{bmatrix} = \frac{1}{1000} \begin{bmatrix} 0 & -154.70 & 109.33 & 38.08 & -19.18 & -16.86 \\ -371.89 & -79.36 & 147.20 & 30.05 & -9.57 & 11.51 \\ 0 & -301.24 & 55.90 & -14.50 & -9.80 & -27.62 \\ 0 & -154.70 & 109.33 & 38.08 & 19.18 & 16.86 \\ -371.89 & -79.36 & 147.20 & 30.05 & 9.57 & -11.51 \\ 0 & -301.24 & 55.90 & -14.50 & 9.80 & 27.62 \\ 0 & 154.70 & 109.33 & -38.08 & 19.18 & -16.82 \\ -371.89 & 79.36 & 147.20 & -30.05 & 9.57 & 11.51 \\ 0 & 301.24 & 55.90 & 14.50 & 9.80 & -27.62 \\ 0 & 154.70 & 109.33 & -38.08 & -19.15 & 16.86 \\ -371.39 & 79.36 & 147.20 & -30.05 & -9.57 & -11.51 \\ 0 & 301.24 & 55.90 & 14.50 & -9.80 & 27.62 \end{bmatrix} \begin{bmatrix} D_{LP} \\ S_{LP} \\ V_{LP} \\ M_{XLP} \\ M_{YLP} \\ M_{ZLP} \end{bmatrix} \tag{129}$$

To obtain this matrix from FRAN, unit forces and moments were applied at the pallet center to determine these influence coefficients which, effectively, are the changes in tension in each sling member for each individually applied unit force or moment. In the FRAN solution, rather flexible cables were used, while the pallet was made almost rigid by representing it by very stiff, yet flexible, beams. This matrix solution does not prohibit the cables from accepting compressive loads. Consequently, these terms are continuously checked and the program user is notified if the value of any tension is less than zero.

With the cable tensions known, the hardpoint loads at the helicopter and at the pallet are determined by a geometric analysis. The direction cosines of each sling member are calculated and are used with the tensions from eq (129) to yield the reactions at the helicopter hardpoints and at the pallet hardpoints. These reactions are referred to as V_i, D_i, S_i, and P_i with i from 1 to 10 where the individual hardpoints are identified in Figure 13. These reactions are nondimensionalized to yield the final output from the sling element and hardpoint loads analysis section.

Data Acquisition

Operation of the entire helicopter-external load simulation program yields a time history of helicopter and load motion and a time history of load factors developed in the sling elements and at the hardpoints. These values are calculated at the end of every pass through the solution. If, as a minimum, the duty cycle of the solution is one-sixteenth of a second, then every single nondimensionalized load and helicopter hardpoint reaction is calculated sixteen times for every second which is simulated. Due to the number of reactions calculated and the length of time needed to fly the maneuvers, the amount of data which results is tremendous, and an automated method for scanning and selecting only pertinent data is an absolute necessity. Such a data acquisition program was developed and added to the end of the sling and hardpoint loads analysis section of the program.

All of the maneuvers which were flown on the fixed base rig were high helicopter load factor producing maneuvers. The only data of importance toward determining some final sling and hardpoint design criteria are the maximum load factors in the slings and at the hardpoints. At the end of each pass, the data acquisition program reads the helicopter load factor N_z. If the calculated N_z is within ± 0.025 of some designed N_z, then the value of N_z which is recorded is the designated value. The designated values in the acquisition program start at N_z = 0.85 and continue to 2.50 in steps of 0.05. Thus, for example, if N_z calculated in the GHSP portion of the solution is 1.834, it is recorded as 1.85 by the data acquisition scheme.

The remaining aspects of the data monitor and acquisition program are

merely a set of logic conditions which compares, selects, and stores the sling element and hardpoint loads in their respective load factor (nondimensionalized) form. The procedure is as follows:

1. At the completion of each program pass, the program selects the largest nondimensionalized cable tension; leg tension; vertical, drag, side, and inplane hardpoint load at the helicopter; and vertical, drag, side, and inplane hardpoint load at the slung load.

2. The program reads the value of N_z and selects the appropriate band.

3. If this is the first occurrence of N_z within the band specified in paragraph 2 above, then all of the data from paragraph 1 above is stored under that particular band.

4. If data already exists within the N_z band, each load is compared to its respective previously stored load; the largest value is retained.

5. At the completion of each run, all of the saved data are output in a convenient format.

The output format from the data acquisition scheme may then be easily scanned by eye to find the largest N_z and the largest sling and hardpoint load factors developed during the maneuver.

To increase the probability of finding the exact maximum helicopter load factor and sling and hardpoint load factors developed during a maneuver, the duty cycle used for the nonreal time runs was reduced by a factor of five compared to the duty cycle used in real time. A duty cycle of $\Delta T = 0.050$ sec was used in all the real time fixed-base runs. All of the nonreal time fixed-base runs were done with $\Delta T = 0.010$ sec. This means that for every 1 second of helicopter-load motion which was simulated, the entire program was solved 100 times. The increased number of solutions per second also guarantees a more accurate simulation, since the approximate digital solution becomes more exact as the time period over which any integrations take place decreases.

<u>Moving-Base Real Time Runs</u>

The helicopter-external load simulation was done in real time to include pilot response to the interaction between the load and the helicopter. High load factor producing maneuvers were flown by the pilot on the fixed-base simulator. In the fixed-base simulator, the interaction cues are interpreted by the pilot from his readings of the instruments and cockpit display. The question arises as to how the pilot's response would be affected by the addition of actual motion cues. Any difference in pilot control inputs would eventually be reflected in the loads developed in the sling elements and at the hardpoints. To answer this question, a real time

simulation was conducted with the motion system operative.

In addition to repeating several fixed-based maneuvers to evaluate the effects of motion cues on the final output data, entirely new maneuvers were flown on the motion system. These new maneuvers were selected because they would appear to produce pilot induced oscillations. (All the maneuvers are described in a later section of this report.) Such cases would be useless to run on a fixed-base simulator since the pilot needs motion cues to induce such oscillations. The results of the new cases would indicate if any higher load factors were produced than had been recorded during the previously run maneuvers.

The method of solution of the moving-base real time simulation is exactly the same as the fixed-base real time method. The only difference is that the accelerations solved by the motion simulation go into an analog computer where a washout program calculates the needed positioning of the moving-base rig. This calculated position is relayed to a PDP-8 computer which then feeds the motion signals to the rig.

The fixed-base real time runs were done with a duty cycle of $\Delta T = 0.055$ sec. This value is still below the maximum of 0.060 second required for an accurate real time solution.

Nonreal Time Runs - Moving-Base Pilot Inputs

The moving-base nonreal time solution is similar to the fixed-base nonreal time scheme. The nonreal time moving-base motion solution adds the sling and hardpoint loads analysis and data acquisition packages to the motion simulation. Six blades and five segments per blade are simulated for the rotor in nonreal time. The duty cycle is also reduced by a factor of five to $\Delta T = 0.011$ second.

MANEUVERS

A CH-54A helicopter was used in the simulation study and flown through various maneuvers with the external loads slung beneath it. The CH-54A with a neutral cg location and a gross weight of 25,000 lb was simulated. By nondimensionalizing the results from the simulation and expressing all data in load factor form, the design criteria derived from this study are applicable to any helicopter at any appropriate weight which can fly with an externally suspended load.

Prior to conducting the helicopter-external load simulation, the CH-54A alone was simulated by GHSP. The basic simulation was checked out by comparing the response to step and pulse control inputs with flight test data recorded for similar control inputs. The response from the simulation closely matched the CH-54A flight test data, thereby indicating a reliable simulation of this particular helicopter.

Fixed-Base Maneuvers

The maneuvers selected to be flown on the fixed-base rig were maneuvers

which would produce high load factors on the helicopter, thereby producing high load factors in the slings and at the hardpoints. The maneuvers flown for the fixed-base simulation were

1. Vertical takeoff from hover (VTO)

2. Symmetrical dive and pullout (SDPO)

3. Roll reversal (RR)

It was originally intended to fly a rolling pullout, but this maneuver was replaced by the roll reversal because the latter maneuver would produce a higher load factor.

Each of the selected maneuvers was flown on the fixed-base simulator by a pilot attempting to pull as high a load as he would pull in actual flight for the CH-54A with an externally suspended load. Each of these maneuvers was flown in real time with various types of slung loads, and the most representative pilot input for each maneuver was selected and used in the nonreal time runs. Every type of sling and load combination described in the Loads section of this report was run in nonreal time for each of the three types of maneuvers, except for the pallet which was flown only for the vertical takeoff to simulate loads which would represent landing impacts.

The selected pilot inputs were also scaled down and run in nonreal time. Effectively, this simulated the same types of maneuvers being flown less violently by the pilot. Data resulting from these runs may be used in determining a trend of load factor in slings and hardpoints versus helicopter load factor.

Moving-Base Maneuvers

The load types flown on the motion system were the container suspended from four points and the single-point four legged suspension of the same container. The same three maneuvers flown on the fixed-base rig were flown on the moving-base rig. For the moving-base nonreal time runs, however, the pilot inputs were not scaled down to recreate milder maneuvers because the effect of motion cues would be absent.

In addition to repeating the high load factor producing maneuvers, some entirely new maneuvers were flown on the motion system. These maneuvers were ones in which no appreciable helicopter load factor is produced, yet high load factors in the slings or hardpoints might result. The new maneuvers also included maneuvers which might produce pilot induced oscillations. These maneuvers were

1. Yaw reversal in hover; pedal kick (PK)

2. Approach to hover (APP)

3. Longitudinal stick stroke in hover ($x_b S$)

4. Lateral stick stroke in hover ($x_a S$)

5. Rolling pullout (RPO)

None of these maneuvers could be created realistically on the fixed-base rig because of the importance of actual motion cues to the pilot when flying them. The yaw reversal was done only with the four-point suspension.

The pilot control inputs for both the fixed-base maneuvers and the moving-base maneuvers are described in detail in Appendix IV.

Gust Considerations

To evaluate the effect of gusts on the load factors produced at the slings and hardpoints during a maneuver, a modification was made to GHSP simulating a gust acting on the helicopter. The gust is generated along a direction normal to the earth and acts on only the helicopter. Therefore, the effect of the gust is greater than if it acted on both the load and helicopter. The gust was generated by a "sine squared" function with a frequency of 0.20 cycles per second and amplitude of 10 feet per second.

The gust simulation was done with the fixed-base simulation. Two load types were flown using gusts: the container suspended from four points and the concrete block with the single-point four-legged suspension system. All three fixed-base maneuvers were flown through the gust. The gust lasted during the entirety of the maneuvers.

Stability and Control Considerations

To create the highest load factors in the sling and hardpoints, the maneuvers were flown at as high a speed as possible without exceeding the limit of 115 knots for the CH-54A. Some cases in which the slung load afforded a great deal of drag were limited by power requirements. Cases which were uncontrollable were reflown at lower speeds until the pilot could satisfactorily complete the maneuver, and data were collected for the controllable case. A drogue chute had to be added to the container slung by the single-point four-legged configuration in order to obtain any usable data.

SIMULATION RESULTS AND DISCUSSION

Table I contains the maximum load factors developed in the sling members and hardpoints during the various simulation runs conducted for this study. The load factors are defined as

$$LFT_C = T_{C_{max}}/T_{C_s} \tag{130}$$

$$LFV_H = V_{H_{max}}/V_{H_s} \tag{131}$$

$$LFD_H = D_{H_{max}}/V_{H_s} \tag{132}$$

$$LFS_H = S_{H_{max}}/V_{H_s} \tag{133}$$

$$LFP_H = P_{H_{max}}/V_{H_s} \tag{134}$$

$$LFT_L = T_{L_{max}}/T_{L_s} \tag{135}$$

$$LFV_L = V_{L_{max}}/V_{L_s} \tag{136}$$

$$LFD_L = D_{L_{max}}/V_{L_s} \tag{137}$$

$$LFS_L = S_{L_{max}}/V_{L_s} \tag{138}$$

$$LFP_L = P_{L_{max}}/V_{L_s} \tag{139}$$

where the subscript s refers to the static value of the quantity indicated. Also indicated in Table I is the maximum helicopter load factor $N_{z_{max}}$ developed during the maneuver, as well as the speed at which the maneuver was performed. The center of gravity variation is given for the container and is 10% forward or aft of the neutral position. The various cases simulated are identified by run numbers. The letter S in this number indicates that the control inputs were scaled down for that run, M indicates the case was run on the motion system, and G indicates the presence of gusts during the maneuver. NA among the data columns refers to a quantity which is not applicable to the particular configuration. The abbreviations used to describe the maneuvers are given in the Maneuvers section of this report.

Table II contains data similar to that contained in Table I, with values for the trimmed cases. Thus, the load factors are steady-state values rather than maximums developed in maneuvers.

From the computerized simulation results, it was originally intended to plot load factor in sling members and hardpoints as a function of CH-54A helicopter load factor with payload category as a parameter. After studying time histories of the load factors, however, it was decided to omit these plots since they could show no useful trends and would only be misleading. For most of the maneuvers flown, it was found that the peak load factors in sling members and hardpoints did not occur at the same time at which the helicopter developed its maximum load factor. During some of the maneuvers,

TABLE I. SLING AND HARDPOINT DYNAMIC LOAD FACTORS

Run	Load - Sling Type	CG	Cable Failed	Leg Failed	Man	Speed	$N_{z_{max}}$	LFT_C	LFV_H	LFD_H	LFS_H	LFP_H	LFT_L	LFV_L
1	Container 4 Pt/0 Leg	Mid	No	NA	SDPO	110	1.90	2.17	2.18	0.71	0.83	0.98	NA	2.15
1S		Mid	No	NA	SDPO	105	1.40	1.52	1.51	0.47	0.24	0.51	NA	1.5
1M		Mid	No	NA	SDPO	110	1.60	1.67	1.68	0.41	0.26	0.48	NA	1.68
2		Fwd	No	NA	SDPO	110	1.80	1.96	1.96	0.64	0.56	0.70	NA	1.95
2S		Fwd	No	NA	SDPO	105	1.40	1.45	1.44	0.45	0.23	0.49	NA	1.44
3		Aft	No	NA	SDPO	110	2.00	2.33	2.23	0.69	1.01	1.22	NA	2.2
3S		Aft	No	NA	SDPO	105	1.45	1.63	1.61	0.50	0.26	0.55	NA	1.6
4		Mid	No	NA	RR	100	1.25	1.34	1.34	0.37	0.36	0.46	NA	1.3
4S		Mid	No	NA	RR	100	1.10	1.14	1.15	0.33	0.26	0.38	NA	1.1
4M		Mid	No	NA	RR	100	1.30	1.49	1.50	0.40	0.45	0.57	NA	1.4
5		Fwd	No	NA	RR	100	1.25	1.34	1.34	0.34	0.34	0.46	NA	1.3
5S		Fwd	No	NA	RR	100	1.10	1.14	1.15	0.30	0.26	0.38	NA	1.1
6		Aft	No	NA	RR	100	1.25	1.34	1.34	0.32	0.36	0.46	NA	1.3
6S		Aft	No	NA	RR	100	1.10	1.14	1.15	0.28	0.26	0.38	NA	1.1
7		Mid	No	NA	VTO	0	1.55	1.65	1.65	0.48	0.32	0.54	NA	1.6
7S		Mid	No	NA	VTO	0	1.30	1.36	1.36	0.39	0.25	0.45	NA	1.3
7M		Mid	No	NA	VTO	0	1.65	1.78	1.78	0.50	0.32	0.56	NA	1.7
8		Fwd	No	NA	VTO	0	1.55	1.63	1.61	0.34	0.32	0.46	NA	1.
8S		Fwd	No	NA	VTO	0	1.30	1.35	1.35	0.26	0.25	0.34	NA	1.
9		Aft	No	NA	VTO	0	1.55	1.66	1.64	0.48	0.32	0.53	NA	1.
9S		Aft	No	NA	VTO	0	1.30	1.36	1.36	0.39	0.25	0.44	NA	1.
43M		Mid	No	NA	PK	0	1.00	1.38	1.40	0.43	0.41	0.55	NA	1.
44M		Mid	No	NA	APP	0	1.10	1.14	1.14	0.32	0.21	0.38	NA	1.
45M		Mid	No	NA	X_6S	0	1.00	1.06	1.07	0.31	0.22	0.36	NA	1.
46M		Mid	No	NA	X_aS	0	1.00	1.10	1.11	0.31	0.27	0.38	NA	1.
47M		Mid	No	NA	RPO	100	1.60	1.73	1.76	0.45	0.54	0.70	NA	1.
1G	Container 4 Pt/0 Leg	Mid	No	NA	SDPO	110	2.00	2.24	2.21	0.97	0.99	1.06	NA	2.
4G		Mid	No	NA	RR	100	1.30	1.42	1.45	0.44	0.40	0.56	NA	1.

TABLE I. SLING AND HARDPOINT DYNAMIC LOAD FACTORS

$N_{z_{max}}$	LFT_C	LFV_H	LFD_H	LFS_H	LFP_H	LFT_L	LFV_L	LFD_L	LFS_L	LFP_L	T_{CS}	V_{HS}	T_{LS}	V_{LS}
1.90	2.17	2.18	0.71	0.83	0.98	NA	2.15	0.67	0.98	1.11	3909	3850	NA	3750
1.40	1.52	1.51	0.47	0.24	0.51	NA	1.51	0.45	0.25	0.49	3909	3750	NA	3750
1.60	1.67	1.68	0.41	0.26	0.48	NA	1.68	0.40	0.27	0.48	3909	3750	NA	3750
1.80	1.96	1.96	0.64	0.56	0.70	NA	1.95	0.61	0.67	0.75	4606	4485	NA	4485
1.40	1.45	1.44	0.45	0.23	0.49	NA	1.44	0.43	0.24	0.47	4606	4485	NA	4485
2.00	2.33	2.23	0.69	1.01	1.22	NA	2.21	0.69	1.21	1.39	4606	4485	NA	4485
1.45	1.63	1.61	0.50	0.26	0.55	NA	1.61	0.48	0.27	0.52	4606	4485	NA	4485
1.25	1.34	1.34	0.37	0.36	0.46	NA	1.34	0.36	0.42	0.50	3909	3750	NA	3750
1.10	1.14	1.15	0.33	0.26	0.38	NA	1.15	0.32	0.29	0.40	3909	3750	NA	3750
1.30	1.49	1.50	0.40	0.45	0.57	NA	1.49	0.39	0.53	0.62	3909	3750	NA	3750
1.25	1.34	1.34	0.34	0.34	0.46	NA	1.34	0.34	0.42	0.51	4606	4485	NA	4485
1.10	1.14	1.15	0.30	0.26	0.38	NA	1.15	0.30	0.29	0.41	4606	4485	NA	4485
1.25	1.34	1.34	0.32	0.36	0.46	NA	1.34	0.32	0.42	0.51	4606	4485	NA	4485
1.10	1.14	1.15	0.28	0.26	0.38	NA	1.15	0.28	0.29	0.41	4606	4485	NA	4485
1.55	1.65	1.65	0.48	0.32	0.54	NA	1.66	0.46	0.35	0.54	3909	3750	NA	3750
1.30	1.36	1.36	0.39	0.25	0.45	NA	1.36	0.38	0.28	0.46	3909	3750	NA	3750
1.65	1.78	1.78	0.50	0.32	0.56	NA	1.79	0.48	0.35	0.56	3909	3750	NA	3750
1.55	1.63	1.61	0.34	0.32	0.46	NA	1.61	0.37	0.34	0.50	4606	4485	NA	4485
1.30	1.35	1.35	0.28	0.25	0.34	NA	1.32	0.31	0.28	0.42	4606	4485	NA	4485
1.55	1.66	1.64	0.48	0.32	0.53	NA	1.64	0.48	0.35	0.55	4606	4485	NA	4485
1.30	1.36	1.36	0.39	0.25	0.44	NA	1.34	0.40	0.28	0.47	4606	4485	NA	4485
1.00	1.38	1.40	0.43	0.41	0.55	NA	1.40	0.42	0.47	0.58	3909	3750	NA	3750
1.10	1.14	1.14	0.32	0.21	0.38	NA	1.14	0.31	0.22	0.38	3909	3750	NA	3750
1.00	1.06	1.07	0.31	0.22	0.36	NA	1.07	0.30	0.26	0.37	3909	3750	NA	3750
1.00	1.10	1.11	0.31	0.27	0.38	NA	1.10	0.30	0.32	0.41	3909	3750	NA	3750
1.60	1.73	1.76	0.45	0.54	0.70	NA	1.75	0.45	0.63	0.76	3909	3750	NA	3750
2.00	2.24	2.21	0.97	0.99	1.06	NA	2.21	0.89	1.18	1.24	3909	3750	NA	3750
1.30	1.42	1.45	0.44	0.40	0.56	NA	1.45	0.42	0.47	0.59	3909	3750	NA	3750

TABLE I - Continued

Run	Load - Sling Type	CG	Cable Failed	Leg Failed	Man	Speed	$N_{z_{max}}$	LFT_C	LFV_H	LFD_H	LFS_H	LFP_H	LFT_L	LFV_L
4G	Container 4 Pt/0 Leg	Mid	No	NA	VTO	0	1.60	1.65	1.65	0.48	0.32	0.55	NA	1.66
10		Fwd	Left Aft	NA	SDPO	110	1.90	2.10	2.10	0.56	1.08	1.11	NA	1.91
10S		Fwd	Left Aft	NA	SDPO	105	1.45	1.55	1.55	0.39	0.54	0.77	NA	1.44
11		Fwd	Left Aft	NA	RR	100	1.25	1.33	1.36	0.25	0.31	0.36	NA	1.33
11S		Fwd	Left Aft	NA	RR	100	1.10	1.14	1.14	0.22	0.22	0.30	NA	1.14
12		Fwd	Left Aft	NA	VTO	0	1.55	1.61	1.67	0.23	0.21	0.25	NA	1.62
12S		Fwd	Left Aft	NA	VTO	0	1.30	1.35	1.37	0.17	0.16	0.18	NA	1.32
	Block													
13	1 Pt/4 Leg	NA	No	No	SDPO	115	1.75	1.91	1.87	0.10	0.39	0.40	1.96	1.96
13S		NA	No	No	SDPO	110	1.40	1.39	1.39	0.09	0.14	0.14	1.42	1.42
14		NA	No	No	RR	100	1.40	1.70	1.68	0.11	0.48	0.48	1.74	1.74
14S		NA	No	No	RR	100	1.15	1.22	1.22	0.06	0.39	0.39	1.25	1.25
15		NA	No	No	VTO	0	1.50	1.54	1.54	0.11	0.19	0.19	1.58	1.58
15S		NA	No	No	VTO	0	1.30	1.30	1.30	0.07	0.09	0.11	1.33	1.33
	Block													
13G	1 Pt/4 Leg	NA	No	No	SDPO	115	1.70	2.01	1.98	0.20	0.49	0.50	2.43	2.06
14G		NA	No	No	RR	100	1.35	1.57	1.54	0.05	0.48	0.48	1.90	1.61
15G		NA	No	No	VTO	0	1.55	1.57	1.57	0.12	0.19	0.19	1.90	1.61
	Empty													
	Container													
16	1 Pt/4 Leg	NA	No	No	SDPO	80	1.75	3.35	3.27	1.37	0.26	1.37	3.60	3.6
16S		NA	No	No	SDPO	80	1.35	2.15	2.09	0.60	0.14	0.60	2.26	2.2
17		NA	No	No	RR	80	1.30	2.20	2.15	0.54	0.96	0.99	2.27	2.2
17S		NA	No	No	RR	80	1.20	1.76	1.71	0.42	0.48	0.54	[illegible]	1.9
18		NA	No	No	VTO	0	1.75	1.91	1.90	0.34	0.21	0.38	2.00	1.9
18S		NA	No	No	VTO	0	1.40	1.53	1.53	0.16	0.12	[illegible]	1.56	1.5
	Container													
19	1 Pt/4 Leg	Mid	No	No	SDPO	100	1.60	1.55	1.51	0.39	0.24	0.42	1.63	1.6
19S		Mid	No	No	SDPO	100	1.35	1.46	1.44	0.22	0.10	0.23	1.48	1.4
19M		Mid	No	No	SDPO	100	1.45	1.54	1.53	0.24	0.06	0.24	1.56	1.5

TABLE I - Continued

LFT_C	LFV_H	LFD_H	LFS_H	LFP_H	LFT_L	LFV_L	LFD_L	LFS_L	LFP_L	T_{C_S}	V_{H_S}	T_{L_S}	V_{L_S}
1.65	1.65	0.48	0.32	0.55	NA	1.66	0.46	0.35	0.55	3909	3750	NA	3750
2.10	2.10	0.56	1.08	1.11	NA	1.91	1.08	2.15	2.18	7850	7510	NA	7510
1.55	1.55	0.39	0.54	0.77	NA	1.44	0.76	0.77	1.36	7850	7510	NA	7510
1.33	1.36	0.25	0.31	0.36	NA	1.33	0.21	0.61	0.62	7850	7510	NA	7510
1.14	1.14	0.22	0.22	0.30	NA	1.14	0.19	0.42	0.50	7850	7510	NA	7510
1.61	1.67	0.23	0.21	0.25	NA	1.62	0.31	0.46	0.47	7850	7510	NA	7510
1.35	1.37	0.17	0.16	0.18	NA	1.32	0.26	0.38	0.39	7850	7510	NA	7510
.91	1.87	0.10	0.39	0.40	1.96	1.96	0.42	0.21	0.46	15000	15000	3860	3750
.39	1.39	0.09	0.14	0.14	1.42	1.42	0.30	0.15	0.34	15000	15000	3860	3750
.70	1.68	0.11	0.48	0.48	1.74	1.74	0.37	0.18	0.41	15000	15000	3860	3750
.22	1.22	0.06	0.39	0.39	1.25	1.25	0.27	0.13	0.30	15000	15000	3860	3750
.54	1.54	0.11	0.19	0.19	1.58	1.58	0.33	0.17	0.37	15000	15000	3860	3750
.30	1.30	0.07	0.09	0.11	1.33	1.33	0.28	0.14	0.32	15000	15000	3860	3750
2.01	1.98	0.20	0.49	0.50	2.43	2.06	0.44	0.22	0.49	15000	15000	3860	3750
.57	1.54	0.05	0.48	0.48	1.90	1.61	0.34	0.17	0.38	15000	15000	3860	3750
.57	1.57	0.12	0.19	0.19	1.90	1.61	0.34	0.17	0.38	15000	15000	3860	3750
.35	3.27	1.37	0.26	1.37	3.60	3.64	2.26	0.90	2.43	4000	4000	1210	1000
.15	2.09	0.60	0.14	0.60	2.26	2.28	1.42	0.57	1.53	4000	4000	1210	1000
.20	2.15	0.54	0.96	0.99	2.27	2.29	1.42	0.57	1.53	4000	4000	1210	1000
.76	1.71	0.42	0.48	0.54	1.97	1.98	1.24	0.49	1.33	4000	4000	1210	1000
.91	1.90	0.34	0.21	0.38	2.00	1.95	1.21	0.49	1.31	4000	4000	1210	1000
.53	1.53	0.16	0.12	0.20	1.56	1.57	0.98	0.39	1.05	4000	4000	1210	1000
.55	1.51	0.39	0.24	0.42	1.63	1.65	1.02	0.41	1.10	15000	15000	4550	3750
.46	1.44	0.22	0.10	0.23	1.48	1.49	0.92	0.37	0.99	15000	15000	4550	3750
.54	1.53	0.24	0.06	0.24	1.56	1.57	0.97	0.39	1.04	15000	15000	4550	3750

B

TABLE I - Continued

Run	Load - Sling Type	CG	Cable Failed	Leg Failed	Man	Speed	$N_{z_{max}}$	LFT_C	LFV_H	LFD_H	LFS_H	LFP_H
20	Container 1 Pt/4 Leg	Fwd	No	No	SDPO	100	1.60	1.63	1.59	0.42	0.20	0.42
20S		Fwd	No	No	SDPO	100	1.35	1.49	1.49	0.25	0.06	0.25
21		Aft	No	No	SDPO	100	1.65	1.55	1.49	0.38	0.31	0.43
21S		Aft	No	No	SDPO	100	1.35	1.42	1.41	0.21	0.07	0.21
22		Mid	No	No	RR	100	1.45	1.71	1.68	0.36	0.46	0.47
22S		Mid	No	No	RR	100	1.10	1.34	1.33	0.19	0.29	0.32
22M		Mid	No	No	RR	80	1.35	1.59	1.58	0.15	0.43	0.45
23		Fwd	No	No	RR	100	1.40	1.68	1.65	0.30	0.50	0.51
23S		Fwd	No	No	RR	100	1.10	1.34	1.32	0.21	0.30	0.33
24		Aft	No	No	RR	100	1.40	1.65	1.63	0.25	0.50	0.51
24S		Aft	No	No	RR	100	1.15	1.33	1.31	0.19	0.32	0.34
25		Mid	No	No	VTO	0	1.50	1.58	1.58	0.13	0.16	0.17
25S		Mid	No	No	VTO	0	1.30	1.34	1.33	0.08	0.09	0.12
25M		Mid	No	No	VTO	0	1.55	1.61	1.61	0.09	0.15	0.15
26		Fwd	No	No	VTO	0	1.50	1.58	1.58	0.12	0.15	0.16
26S		Fwd	No	No	VTO	0	1.30	1.34	1.33	0.08	0.08	0.11
27		Aft	No	No	VTO	0	1.50	1.58	1.58	0.13	0.13	0.16
27S		Aft	No	No	VTO	0	1.30	1.34	1.33	0.08	0.09	0.12
48M		Mid	No	No	APP	0	1.05	1.05	1.04	0.15	0.15	0.17
49M		Mid	No	No	X_bS	0	1.00	1.08	1.08	0.22	0.08	0.23
50M		Mid	No	No	X_aS	0	1.00	1.32	1.32	0.07	0.45	0.45
51M		Mid	No	No	RPO	90	1.40	1.55	1.54	0.21	0.18	0.25
31	Container 1 Pt/4 Leg	Fwd	No	Left Aft	SDPO	100	1.70	1.63	1.61	0.41	0.17	0.41
31S		Fwd	No	Left Aft	SDPO	100	1.40	1.50	1.49	0.25	0.09	0.25
32		Fwd	No	Left Aft	RR	100	1.35	1.69	1.66	0.30	0.49	0.50
32S		Fwd	No	Left Aft	RR	100	1.10	1.34	1.32	0.21	0.30	0.33
33		Fwd	No	Left Aft	VTO	0	1.55	1.60	1.60	0.11	0.12	0.15
33S		Fwd	No	Left Aft	VTO	0	1.30	1.35	1.35	0.07	0.09	[illegible]

PRECEDING PAGE BLANK

I - Continued

V_H	LFD_H	LFS_H	LFP_H	LFT_L	LFV_L	LFD_L	LFS_L	LFP_L	T_{CS}	V_{HS}	T_{LS}	V_{LS}
59	0.42	0.20	0.42	1.71	1.62	1.02	0.39	1.09	15000	15000	5155	4500
49	0.25	0.06	0.25	1.55	1.47	0.92	0.36	0.99	15000	15000	5155	4500
49	0.38	0.31	0.43	1.60	1.52	0.96	0.37	1.02	15000	15000	5155	4500
41	0.21	0.07	0.21	1.44	1.37	0.86	0.33	0.93	15000	15000	5155	4500
68	0.36	0.46	0.47	1.75	1.77	1.09	0.44	1.17	15000	15000	4550	3750
33	0.19	0.29	0.32	1.38	1.39	0.86	0.34	0.93	15000	15000	4550	3750
58	0.15	0.43	0.45	1.61	1.63	1.00	0.40	1.08	15000	15000	4550	3750
65	0.30	0.50	0.51	1.76	1.67	1.06	0.41	1.13	15000	15000	5155	4500
32	0.21	0.30	0.33	1.38	1.30	0.83	0.32	0.88	15000	15000	5155	4500
63	0.25	0.50	0.51	1.68	1.59	1.01	0.39	1.07	15000	15000	5155	4500
31	0.19	0.32	0.34	1.33	1.25	0.79	0.31	0.85	15000	15000	5155	4500
58	0.13	0.16	0.17	1.59	1.61	0.99	0.40	1.07	15000	15000	4550	3750
.33	0.08	0.09	0.12	1.34	1.36	0.84	0.34	0.90	15000	15000	4550	3750
.61	0.09	0.15	0.15	1.62	1.64	1.01	0.40	1.09	15000	15000	4550	3750
.58	0.12	0.15	0.16	1.61	1.52	0.97	0.37	1.03	15000	15000	5155	4500
.33	0.08	0.08	0.11	1.35	1.28	0.80	0.31	0.87	15000	15000	5155	4500
.58	0.13	0.13	0.16	1.62	1.53	0.98	0.37	1.04	15000	15000	5155	4500
.33	0.08	0.09	0.12	1.35	1.28	0.80	0.32	0.87	15000	15000	5155	4500
.04	0.15	0.15	0.17	1.06	1.06	0.66	0.26	0.71	15000	15000	4550	3750
.08	0.22	0.08	0.23	1.09	1.10	0.68	0.27	0.73	15000	15000	4550	3750
.32	0.07	0.45	0.45	1.35	1.36	0.84	0.34	0.91	15000	15000	4550	3750
.54	0.21	0.18	0.25	1.56	1.58	0.97	0.39	1.05	15000	15000	4550	3750
.61	0.41	0.17	0.41	1.55	1.46	0.92	0.35	0.99	15000	15000	9500	8380
.49	0.25	0.09	0.25	1.42	1.34	0.84	0.33	0.91	15000	15000	9500	8380
.66	0.30	0.49	0.50	1.59	1.49	0.94	0.36	1.02	15000	15000	9500	8380
.32	0.21	0.30	0.33	1.26	1.17	0.74	0.28	0.79	15000	15000	9500	8380
.60	0.11	0.12	0.15	1.51	1.42	0.90	0.35	0.96	15000	15000	9500	8380
.35	0.07	0.09	0.11	1.28	1.20	0.76	0.29	0.81	15000	15000	9500	8380

B

TABLE I - Concluded

Run	Load - Sling Type	CG	Cable Failed	Leg Failed	Man	Speed	$N_{z_{max}}$	LFT_C	LFV_H	LFD_H	LFS_H	LFP_H	LFT_L
28	CH-47 - 1 Pt/4 Leg	NA	No	No	SDPO	115	1.30	1.80	1.79	0.16	0.24	0.24	2.37
28S	↓	NA	No	No	SDPO	110	1.45	1.62	1.62	0.10	0.30	0.13	1.90
29	↓	NA	No	No	RR	100	1.30	1.67	1.66	0.22	0.25	0.27	3.12
29S	↓	NA	No	No	RR	100	1.10	1.41	1.40	0.12	0.20	0.20	2.34
30	↓	NA	No	No	VTO	0	1.55	1.86	1.86	0.1[illegible]	0.14	0.17	1.86
30S	↓	NA	No	No	VTO	0	1.30	1.56	1.58	0.09	0.12	0.15	1.56
34	OV-1 - 1 Pt/3 Leg	NA	No	No	SDPO	115	1.90	1.34	1.34	0.15	0.20	0.23	1.50
34S	↓	NA	No	No	SDPO	110	1.40	1.15	1.15	0.08	0.11	0.12	1.27
35	↓	NA	No	No	RR	100	1.45	1.30	1.30	0.15	0.39	0.39	2.08
35S	↓	NA	No	No	RR	100	1.15	1.04	1.04	0.06	0.25	0.26	1.51
36	↓	NA	No	No	VTO	0	1.55	1.88	1.88	0.11	0.20	0.20	1.94
36S	↓	NA	No	No	VTO	0	1.30	1.61	1.61	0.07	0.11	0.12	1.63
37	Block 1 Pt/1 Leg	NA	No	No	SDPO	115	1.85	1.93	1.93	0.17	0.34	0.38	1.93
37S	↓	NA	No	No	SDPO	115	1.40	1.41	1.40	0.09	0.15	0.16	1.41
38	↓	NA	No	No	RR	100	1.35	1.46	1.45	0.06	0.23	0.23	1.46
38S	↓	NA	No	No	RR	100	1.10	1.15	1.14	0.04	0.18	0.18	1.15
39	↓	NA	No	No	VTO	0	1.55	1.58	1.58	0.07	0.11	0.12	1.58
39S	↓	NA	No	No	VTO	0	1.30	1.32	1.32	0.05	0.09	0.09	1.32
40	Brooks & Perkins Pallet	Mid	NA	No	VTO	0	1.55	NA	1.64	0.42	0.54	0.66	1.60
40S	↓	Mid	NA	No	VTO	0	1.30	NA	1.39	0.35	0.46	0.56	1.34
41	↓	Fwd	NA	No	VTO	0	1.55	NA	1.58	0.38	0.54	0.59	1.42
41S	↓	Fwd	NA	No	VTO	0	1.30	NA	1.35	0.30	0.46	0.50	1.20
42	↓	Aft	NA	No	VTO	0	1.55	NA	1.58	0.37	0.53	0.59	1.41
42S	↓	Aft	NA	No	VTO	0	1.30	NA	1.32	0.32	0.46	0.45	1.19

PRECEDING PAGE BLANK

TABLE I - Concluded

z_{max}	LFT_C	LFV_H	LFD_H	LFS_H	LFP_H	LFT_L	LFV_L	LFD_L	LFS_L	LFP_L	T_{C_S}	V_{H_S}	T_{L_S}	V_{L_S}
1.80	1.80	1.79	0.16	0.24	0.24	2.37	2.02	3.00	0.26	3.01	12990	12990	5790	3840
1.45	1.62	1.62	0.10	0.10	0.13	1.90	1.54	2.42	0.21	2.43	12990	12990	5790	3840
1.30	1.67	1.66	0.22	0.25	0.27	3.12	2.52	3.95	0.34	3.96	12990	12990	5790	3840
1.10	1.41	1.40	0.12	0.20	0.20	2.24	1.80	2.83	0.25	2.84	12990	12990	5790	3840
1.55	1.86	1.86	0.1[illegible]	0.14	0.17	1.86	1.93	2.04	0.18	2.04	12990	12990	5790	3840
1.30	1.56	1.58	0.09	0.12	0.15	1.56	1.64	1.73	0.15	1.73	12990	12990	5790	3840
1.90	1.34	1.34	0.15	0.20	0.23	1.50	1.50	0.59	0.24	0.59	11520	11520	4920	4750
1.40	1.15	1.15	0.08	0.11	0.12	1.27	1.26	0.49	0.20	0.49	11520	11520	4920	4750
1.45	1.30	1.30	0.15	0.39	0.39	2.08	2.07	0.51	0.33	0.55	11520	11520	4920	4750
1.15	1.04	1.04	0.06	0.25	0.26	1.51	1.51	0.43	0.24	0.43	11520	11520	4920	4750
1.55	1.88	1.88	0.11	0.20	0.20	1.94	1.93	0.82	0.31	0.82	11520	11520	4920	4750
1.30	1.61	1.61	0.07	0.11	0.12	1.63	1.63	0.69	0.26	0.69	11520	11520	4920	4750
1.85	1.93	1.93	0.17	0.3[illegible]	0.38	1.93	1.93	0.04	0.02	0.04	15000	15000	15000	15000
1.40	1.41	1.40	0.09	0.15	0.16	1.41	1.41	0.01	0.01	0.01	15000	15000	15000	15000
1.35	1.46	1.45	0.06	0.23	0.23	1.46	1.47	0.04	0.04	0.05	15000	15000	15000	15000
1.10	1.15	1.14	0.04	0.18	0.18	1.15	1.15	0.01	0.02	0.02	15000	15000	15000	15000
1.55	1.58	1.58	0.07	0.11	0.12	1.58	1.58	0.02	0	0.02	15000	15000	15000	15000
1.30	1.32	1.32	0.05	0.09	0.09	1.32	1.32	0.01	0	0.01	15000	15000	15000	15000
1.55	NA	1.64	0.42	0.54	0.66	1.60	1.56	0.27	0.28	0.35	NA	3750	2250	3264
1.30	NA	1.39	0.35	0.46	0.56	1.34	1.30	0.23	0.23	0.29	NA	3750	2250	3264
1.55	NA	1.58	0.38	0.54	0.59	1.42	1.56	0.37	0.29	0.47	NA	4701	2537	3260
1.30	NA	1.35	0.30	0.46	0.50	1.20	1.31	0.31	0.25	0.39	NA	4701	2537	3260
1.55	NA	1.58	0.37	0.53	0.59	1.44	1.56	0.36	0.28	0.45	NA	4701	2537	3260
1.30	NA	1.32	0.32	0.46	0.49	1.19	1.31	0.31	0.24	0.38	NA	4701	2537	3260

B

TABLE II. SLING AND HARDPOINT STATIC TRIM LOAD FACTORS

Load - Sling Type	CG	Speed	LFT_C	LFV_H	LFD_H	LFS_H	LFP_H	LFT_L	LFV_L	LFD_L	LFS_L
ner - 4 Pt/0 Leg	Mid	0	1.02	1.02	0.30	0.19	0.35	NA	1.02	0.30	0.19
	Fwd	0	1.01	1.02	0.21	0.18	0.27	NA	1.02	0.21	0.18
	Aft	0	1.03	1.02	0.28	0.18	0.33	NA	1.02	0.28	0.18
	Mid	115	1.03	1.02	0.33	0.16	0.36	NA	1.02	0.33	0.16
	Fwd	115	1.05	1.03	0.32	0.15	0.34	NA	1.03	0.32	0.15
	Aft	115	1.01	1.01	0.23	0.16	0.25	NA	1.01	0.23	0.16
ner - 0 Leg; 1 cable failed	Fwd	0	1.00	1.04	0.16	0.08	0.16	NA	1.04	0.16	0.08
	Fwd	115	1.15	1.15	0.20	0.26	0.32	NA	1.15	0.20	0.26
- 1 Pt/4 Leg	NA	0	1.01	1.01	0.03	0.05	0.06	1.02	1.02	0.22	0.11
	NA	115	1.00	1.00	0.05	0.03	0.06	1.02	1.02	0.22	0.11
Container - 1 Pt/4 Leg	NA	0	1.11	1.11	0.04	0.06	0.07	1.14	1.14	0.68	0.2
	NA	80	1.60	1.57	0.33	0.05	0.34	1.70	1.69	1.06	0.4
ner - 1 Pt/4 Leg	Mid	0	1.04	1.04	0.03	0.06	0.06	1.05	1.06	0.65	0.2
	Fwd	0	1.04	1.04	0.03	0.06	0.07	1.03	0.99	0.62	0.2
	Aft	0	1.04	1.04	0.03	0.05	0.06	1.03	0.99	0.62	0.2
	Mid	100	1.21	1.20	0.17	0.05	0.17	[illegible]	1.27	0.80	0.3
	Fwd	100	1.16	1.14	0.18	0.05	0.19	1.22	1.15	0.73	0.2
	Aft	100	1.18	1.17	0.17	0.03	0.17	1.17	1.11	0.70	0.2
ner - 1 Pt/4 Leg; 1 Leg failed	Fwd	0	1.04	1.04	0.03	0.06	0.07	0.99	0.93	0.59	0.
	Fwd	100	1.16	1.14	0.18	0.05	0.19	1.05	0.98	0.62	0.
- 1 Pt/4 Leg	NA	0	1.25	1.25	0.04	0.07	0.08	1.23	1.27	1.35	0.
	NA	115	1.29	1.28	0.14	0.04	0.14	1.51	1.17	1.95	0.

PRECEDING PAGE BLANK

II. SLING AND HARDPOINT STATIC TRIM LOAD FACTORS

CG	Speed	LFT_C	LFV_H	LFD_H	LFS_H	LFP_H	LFT_L	LFV_L	LFD_L	LFS_L	LFP_L
Mid	0	1.02	1.02	0.30	0.19	0.35	NA	1.02	0.30	0.19	0.35
Fwd	0	1.01	1.02	0.21	0.18	0.27	NA	1.02	0.21	0.18	0.27
Aft	0	1.03	1.02	0.28	0.18	0.33	NA	1.02	0.28	0.18	0.34
Mid	115	1.03	1.02	0.33	0.16	0.36	NA	1.02	0.33	0.16	0.36
Fwd	115	1.05	1.03	0.32	0.15	0.34	NA	1.03	0.32	0.15	0.34
Aft	115	1.01	1.01	0.23	0.16	0.25	NA	1.01	0.23	0.16	0.25
Fwd	0	1.00	1.04	0.16	0.08	0.16	NA	1.04	0.16	0.08	0.16
Fwd	115	1.15	1.15	0.20	0.26	0.32	NA	1.15	0.20	0.26	0.32
A	0	1.01	1.01	0.03	0.05	0.06	1.02	1.02	0.22	0.11	0.24
A	115	1.00	1.00	0.05	0.03	0.06	1.02	1.02	0.22	0.11	0.24
A	0	1.11	1.11	0.04	0.06	0.07	1.14	1.14	0.68	0.28	0.77
A	80	1.60	1.57	0.33	0.03	0.34	1.70	1.69	1.06	0.42	1.14
Mid	0	1.04	1.04	0.03	0.06	0.06	1.05	[illegible]	0.65	0.26	0.70
Fwd	0	1.04	1.04	0.03	0.06	0.07	1.03	0.99	0.62	0.24	0.67
Aft	0	1.04	1.04	0.03	0.05	0.06	1.03	0.99	0.62	0.24	0.67
Mid	100	1.21	1.20	0.17	0.05	0.17	[illegible]	1.27	0.80	0.31	0.85
Fwd	100	1.16	1.14	0.18	0.05	0.19	1.22	1.15	0.73	0.28	0.78
Aft	100	1.18	1.17	0.17	0.03	0.17	1.17	1.11	0.70	0.27	0.75
Fwd	0	1.04	1.04	0.03	0.06	0.07	0.99	0.93	0.59	0.23	0.63
Fwd	100	1.16	1.14	0.18	0.05	0.19	1.05	0.98	0.62	0.24	0.67
A	0	1.25	1.25	0.04	0.07	0.08	1.23	1.27	1.35	0.12	1.36
A	115	1.29	1.28	0.14	0.04	0.14	1.51	1.17	1.95	0.17	1.96

B

TABLE II - Concluded

Load - Sling Type	CG	Speed	LFT_C	LFV_H	LFD_H	LFS_H	LFP_H	LFT_L	LFV_L	LFD_L
OV-1 - 1 Pt/3 Leg	NA	0	1.28	1.27	0.04	0.07	0.08	1.28	1.28	0.53
	NA	115	0.95	0.94	0.07	0.03	0.07	0.97	0.97	0.41
Block - 1 Pt/1 Leg	NA	0	1.01	1.01	0.03	0.05	0.06	1.01	1.01	0
	NA	115	1.00	1.00	0.05	0.03	0.06	1.00	1.00	0
Brooks & Perkins Pallet	Mid	0	NA	1.08	0.28	0.35	0.44	1.05	1.00	0.18
	Fwd	0	NA	1.05	0.21	0.35	0.39	0.96	1.00	0.23
	Aft	0	NA	1.05	0.21	0.34	0.39	0.96	1.00	0.23
	Mid	115	NA	1.09	0.31	0.34	0.45	1.14	0.99	0.18
	Fwd	115	NA	1.05	0.21	0.35	0.39	0.96	1.00	0.23
	Aft	115	NA	1.04	0.21	0.35	0.39	0.96	1.00	0.23

PRECEDING PAGE BLANK

TABLE II - Concluded

CG	Speed	LFT_C	LFV_H	LFD_H	LFS_H	LFP_H	LFT_L	LFV_L	LFD_L	LFS_L	LFP_L
NA	0	1.28	1.27	0.04	0.07	0.08	1.28	1.28	0.53	0.20	0.53
NA	115	0.95	0.94	0.07	0.03	0.07	0.97	0.97	0.41	0.15	0.41
NA	0	1.01	1.01	0.03	0.05	0.06	1.01	1.01	0	0	0
NA	115	1.00	1.00	0.05	0.03	0.06	1.00	1.00	0	0.01	0.01
Mid	0	NA	1.08	0.28	0.35	0.44	1.05	1.00	0.18	0.18	0.22
Fwd	0	NA	1.05	0.21	0.35	0.39	0.96	1.00	0.23	0.18	0.30
Aft	0	NA	1.05	0.21	0.34	0.39	0.96	1.00	0.23	0.18	0.30
Mid	115	NA	1.09	0.31	0.34	0.45	1.14	0.99	0.18	0.18	0.22
Fwd	115	NA	1.05	0.21	0.35	0.39	0.96	1.00	0.23	0.18	0.30
Aft	115	NA	1.04	0.21	0.35	0.39	0.96	1.00	0.23	0.18	0.30

sling load factor would decrease as N_z increased, after which the sling load factor would decrease as N_z continued increasing toward its maximum value. Such a plot would be useless, and therefore the load factor data are presented in tabular form.

During the study, time histories were evaluated before final reduction to the data in Table I. It was found that for the maneuvers and load configurations studied, the maximum value of tension during the dynamic solution always occurred in the leg or cable which had the highest static value of tension.

The data in Table I indicate very little change in load factor with a change in cg location of the load in the container.

The pallet runs contained a check to indicate if any of the sling legs carried compressive loads due to the nature of the FRAN method incorporated in this solution. Results from the pallet cases which were solved showed that no legs carried compressive loads; therefore the pallet solution was valid.

Table I includes the maximum speed at which each maneuver was flown for a given load type. This speed was based on pilot opinion and overall controllability of the helicopter-load system, plus the capability of the CH-54A. The data from run numbers 10 and 10s are questionable because it appeared that the container motion during the dive and pullout was great enough to permit the container to strike the helicopter. This broken cable configuration appeared to be rather unstable.

Table I shows that the load factors developed in sling members and hardpoints often exceeded the helicopter load factor which was pulled during a maneuver. The design load factor $N_z = 2.5$ for the CH-54A was never obtained in any of the cases simulated, yet this number was exceeded at hardpoints or in sling members during runs 16, 28, 29, and 29s.

While the pilot was able to distinguish the presence of an externally suspended load by interpreting the response of the helicopter as indicated by the cockpit instruments in the fixed-base rig, he had difficulty recognizing the inertial properties or sling geometries of different types of loads. With the addition of actual motion cues on the moving-base rig, the pilot was able to easily recognize the inertial characteristics of the load as well as distinguish the difference between methods of suspending the load from the helicopter. Therefore, the addition of motion cues increased the pilot's awareness of the response of the slung load beneath him; and therefore, he would respond in a more realistic manner.

The results of the same maneuvers flown on both the fixed-base rig and the moving-base rig show in general that for the roll reversal and the vertical takeoff, the moving-base runs yield slightly higher load factors than the fixed-base runs. The differences here are small and may be due to any random difference the pilot may make in flying the same maneuver at two different times. These runs do show correlation between the two types of

PRECEDING PAGE BLANK

simulations, indicating that the motion cues which the washout program calculates for the rig are valid.

Comparing the results obtained for the fixed-base and the moving-base runs of the symmetrical dive and pullout indicates that higher load factors were pulled during the fixed-base runs. This can be explained after studying the time histories of the pilot control input for these runs. (See Figures 23 and 24 in Appendix IV.) It was found that during the fixed-base runs, the amount of longitudinal cyclic stick applied by the pilot was twice as much as the amount he applied during the moving-base runs to begin the pullout. This is the primary reason that the fixed-base load factors are higher than the moving-base results. The fixed-base maneuver was much more severe than the moving-base maneuver in terms of load factors developed. With the addition of motion cues, the pilot was reluctant to pull back on the stick as much as he did during the fixed-base runs. This reluctance is probably due in some part to the pilot's sense of restriction in the moving-base simulation, as well as to his reaction to the motion cues he receives from the load.

The fixed-base results in this case are possibly more meaningful because they represent the actual capability of the helicopter, while the moving-base runs do not approach the load factors which can be produced by the CH-54A.

The pilot was particularly pleased with the motion cues he received from the load in hover maneuvers such as the control stick strokes and approach to hover. The pilot was able to handle the loads in the approach over a point. He did produce satisfactory pilot induced oscillations in the stick stroke maneuvers.

Tables I and II present raw load factor data from the simulation. A rational interpretation of these raw data is needed to convert them into useful sling and hardpoint design criteria. The logic and mechanics of this interpretation are presented in Appendix V. Appendix V also contains preliminary plots of the modified sling and hardpoint load factor data versus helicopter design load factor. Figures 31 through 44 were used as working plots in eventually determining the design criteria.

SLING AND HARDPOINT DESIGN CRITERIA

The data presented in Appendix V have been developed into sling and hardpoint design criteria, (Figures 14 through 21). These figures are plots of sling and hardpoint design load factors versus helicopter design load factor, as a function of slung load type. The specific loads studied in the simulation are classified under more general slung load type categories, and the notation used to denote the general types is:

TYPE I, B	=	Type I, bridle = block - 1 pt/4 leg
TYPE I, P	=	Type I, pendant = block - 1 pt/1 leg
TYPE II, B	=	Type II, bridle = container - 1 pt/4 leg
TYPE II, 4 PT	=	Type II, 4 point = container - 4 pt/0 leg
TYPE III	=	Type III = empty container - 1 pt/4 leg
FWAC	=	fixed wing aircraft = OV-1 Mohawk - 1 pt/3 leg
HELO	=	helicopter = CH-47 Chinook - 1 pt/4 leg
TYPE II, B - 1MF	=	Type II, bridle, 1 member failed = container - 1 pt/4 leg; 1 leg failed
TYPE II, 4 PT - 1MF	=	Type II, 4 point, 1 member failed = container - 4 pt/0 leg, 1 cable failed

The method for using the design criteria plots is outlined as follows:

1. For a given helicopter design load factor and slung load type, select the corresponding sling and/or hardpoint load factors of interest as indicated by the design criteria plots.

2. For a given slung load weight and cg location, calculate the values of static forces which have been used to normalize the data collected in step (1). A method for determining these static values is presented in Appendix VI.

3. The actual absolute values of the maximum force developed dynamically in the sling members and/or hardpoints being investigated are then found from the data collected in steps (1) and (2) according to the formulas

$$S_{H_{max}} = V_{H_S} \cdot LFS_{H_{max}} \tag{143}$$

$$V_{L_{max}} = V_{L_{max}} \cdot LFV_{L_{max}} \tag{144}$$

$$D_{L_{max}} = V_{L_{max}} \cdot LFD_{L_{max}} \tag{145}$$

$$S_{L_{max}} = V_{L_{max}} \cdot LFS_{L_{max}} \tag{146}$$

$$T_{L_{max}} = T_{L_{max}} \cdot LFT_{L_{max}} \tag{147}$$

The strength of the sling members or hardpoints should be based on these absolute values of forces solved for from eqs (140) through (147). The drag force D, side force S, and vertical force V are the components of force along the appropriate helicopter or slung load body axis X-, Y-, and Z- directions respectively.

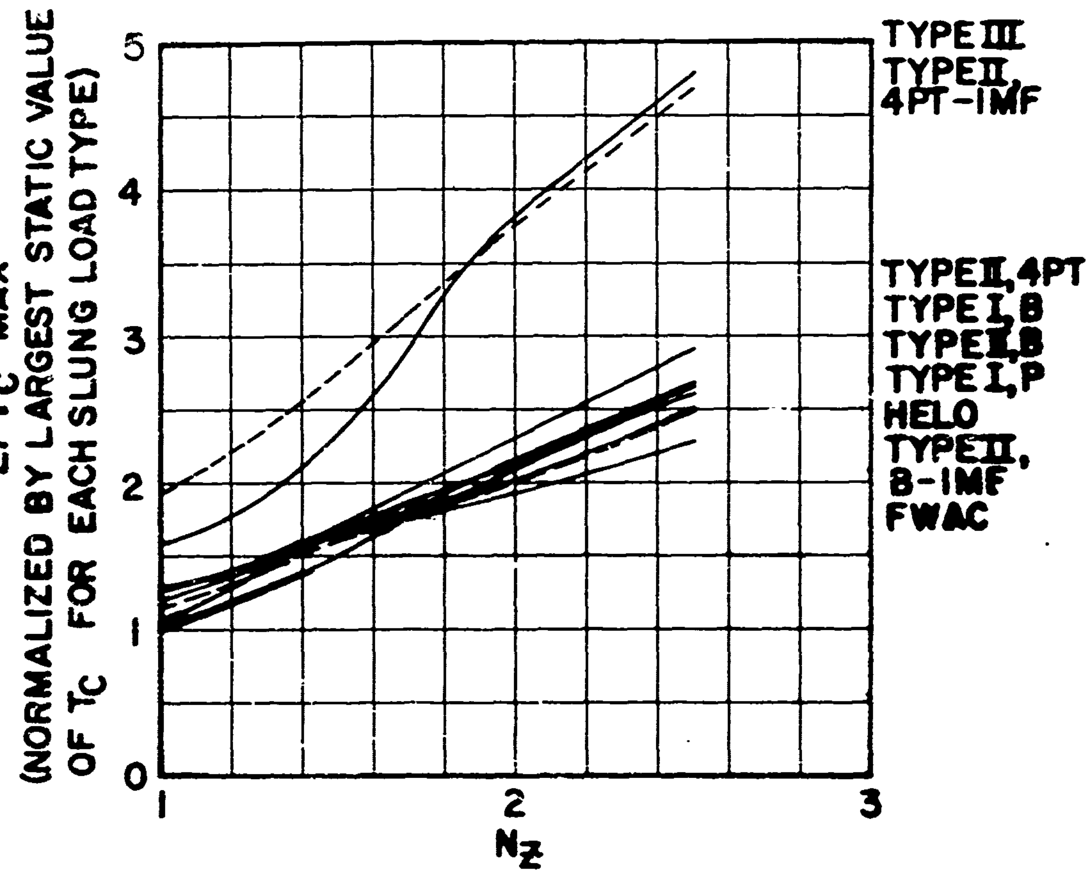

Figure 14. Maximum Dynamic Cable (Pendant) Tension Load Factor vs Helicopter Design Load Factor.

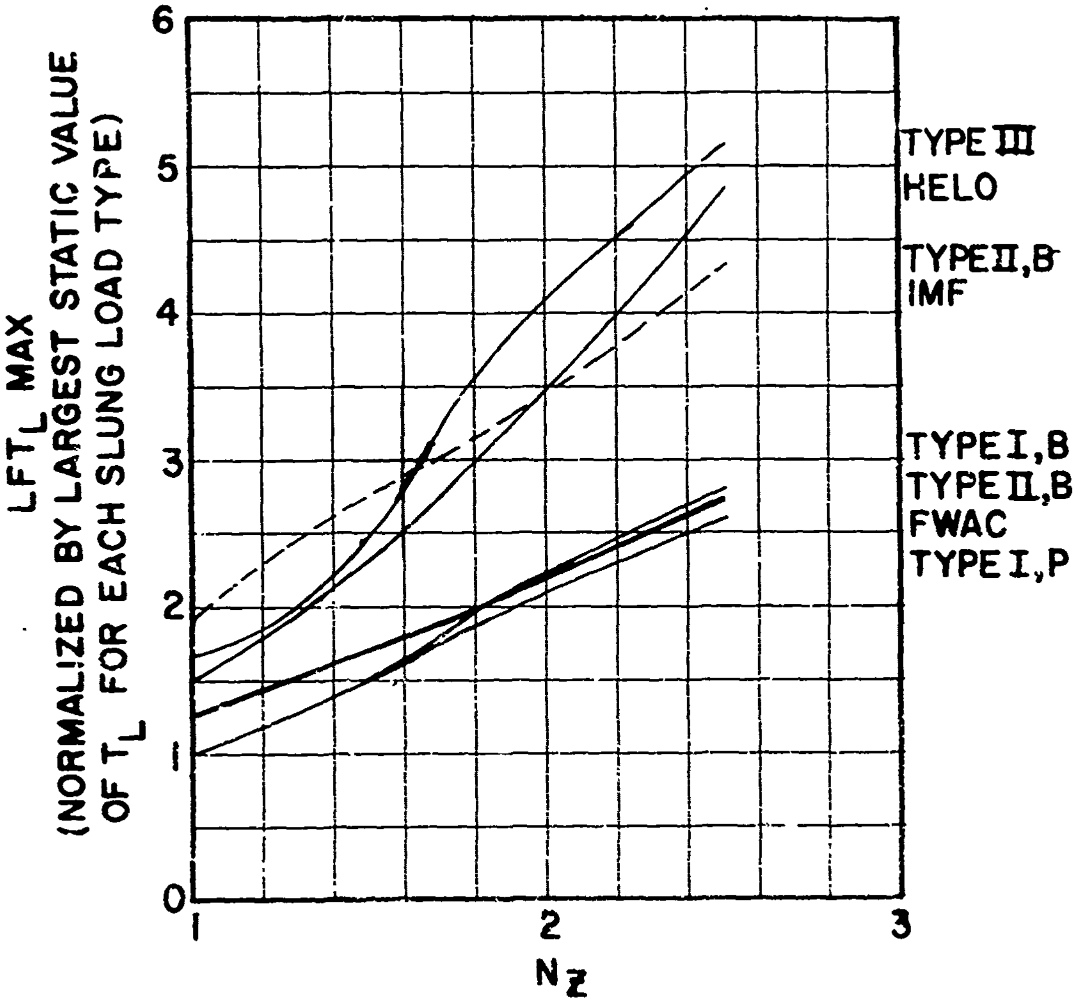

Figure 15. Maximum Dynamic Leg (Bridle) Tension Load Factor vs Helicopter Design Load Factor.

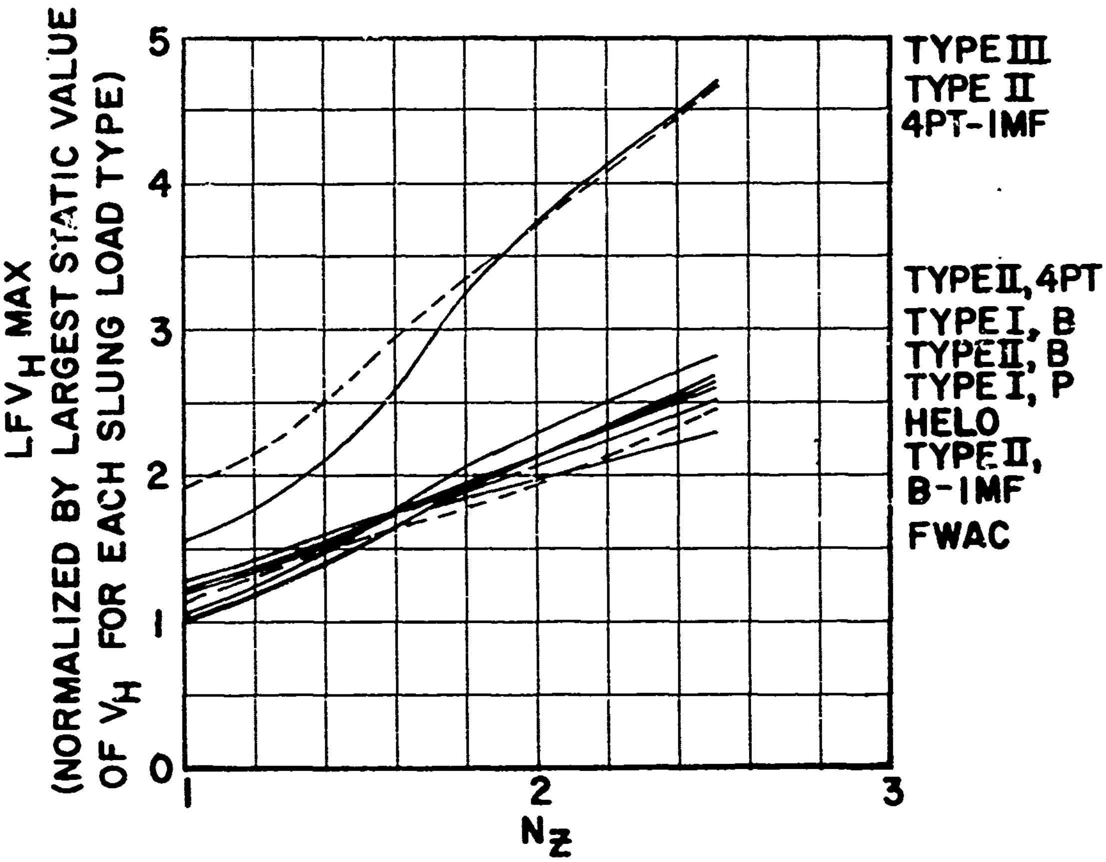

Figure 16. Maximum Dynamic Helicopter Hardpoint Vertical Force Load Factor vs Helicopter Design Load Factor.

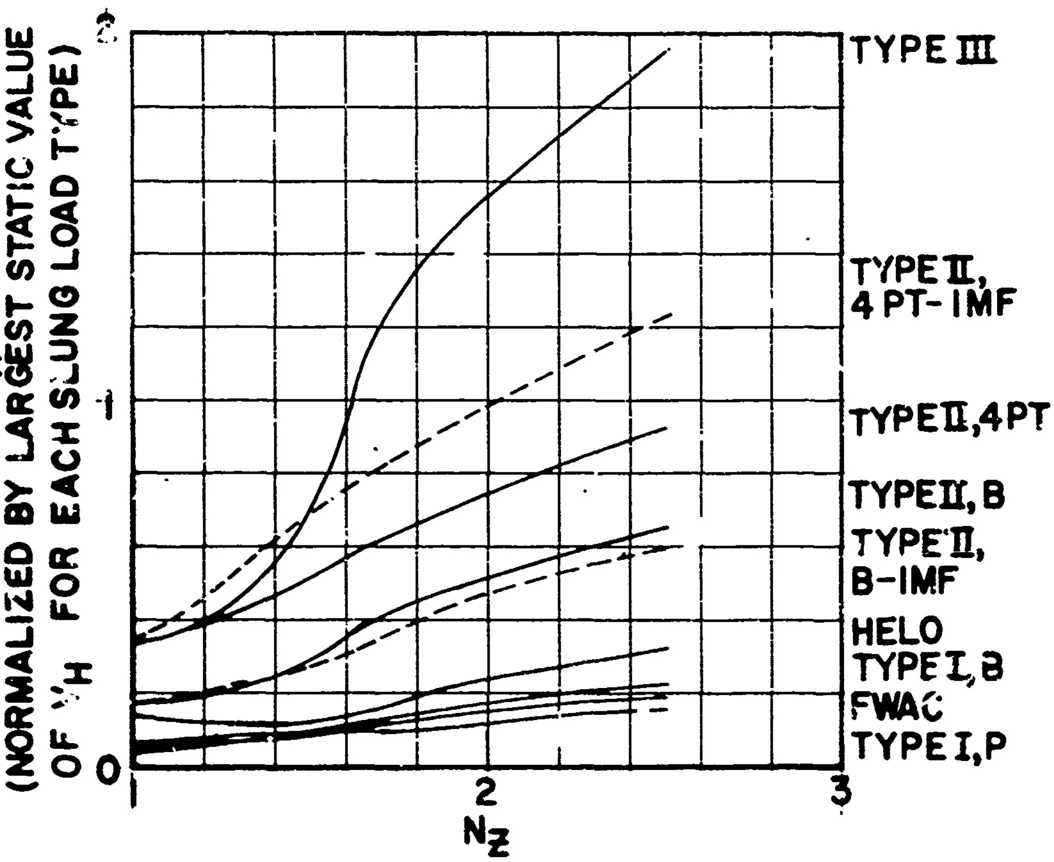

Figure 17. Maximum Dynamic Helicopter Hardpoint Drag Force Load Factor vs Helicopter Design Load Factor.

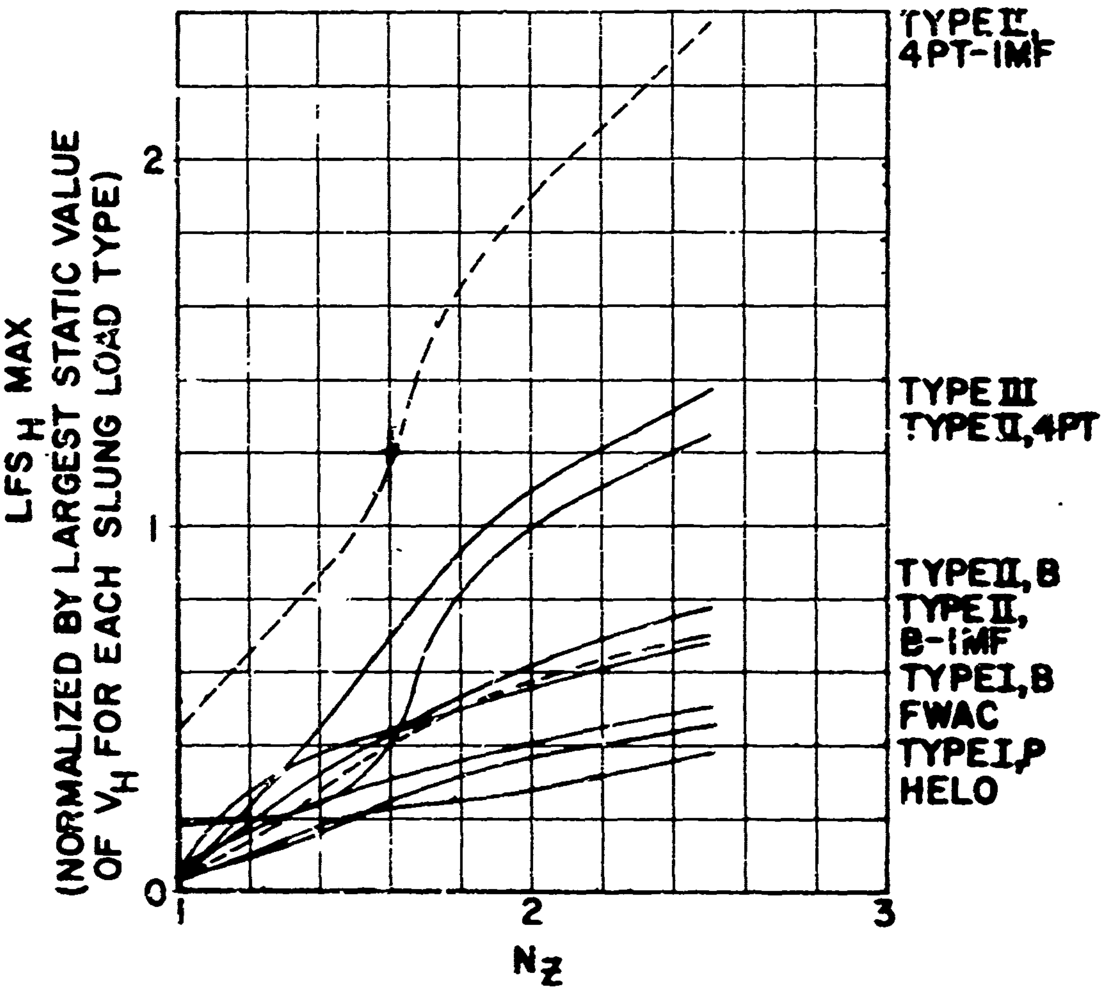

Figure 18. Maximum Dynamic Helicopter Hardpoint Side Force Load Factor vs Helicopter Design Load Factor.

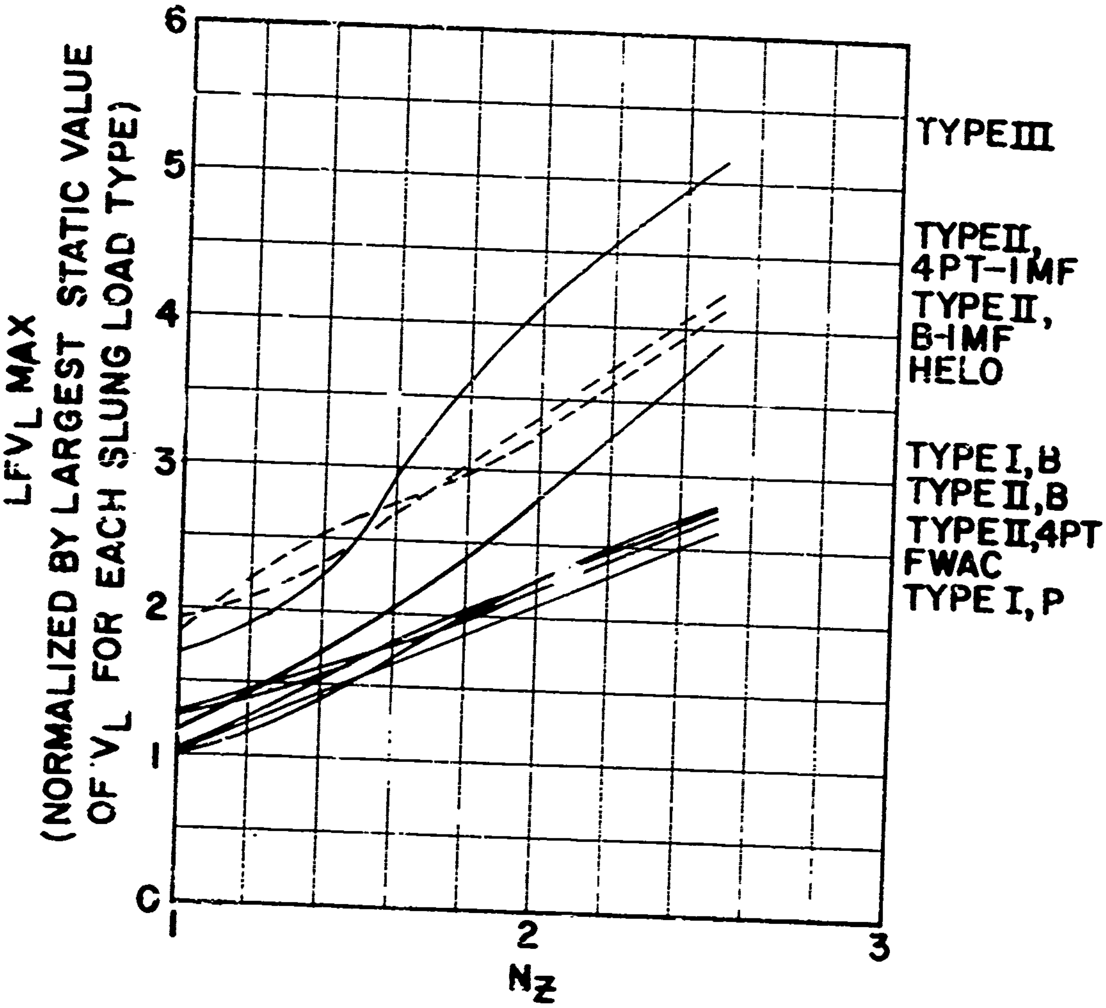

Figure 39. Maximum Dynamic Slung Load Hardpoint Vertical Force Load Factor vs Helicopter Design Load Factor.

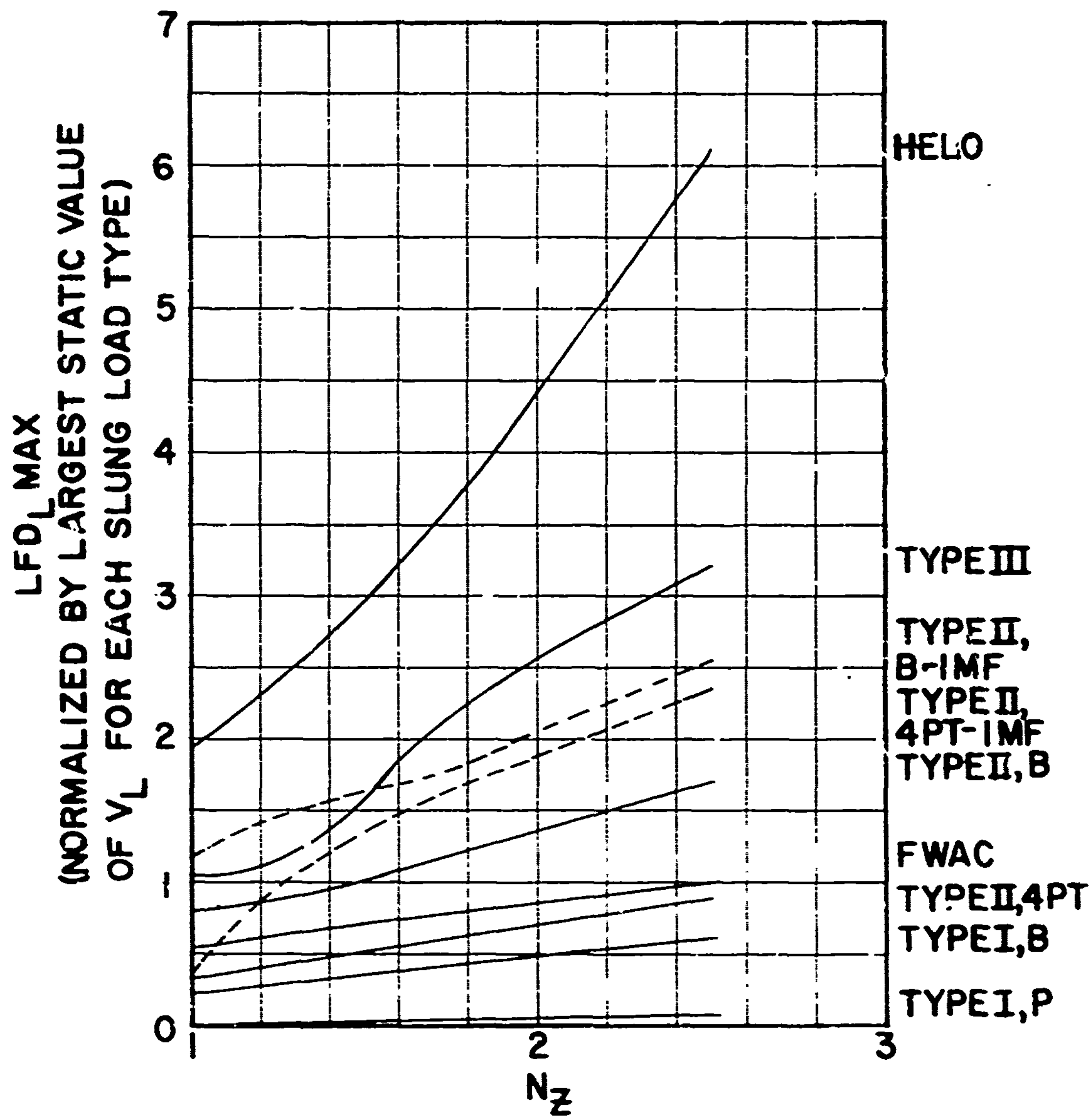

Figure 20. Maximum Dynamic Slung Load Hardpoint Drag Force Load Factor vs Helicopter Design Load Factor.

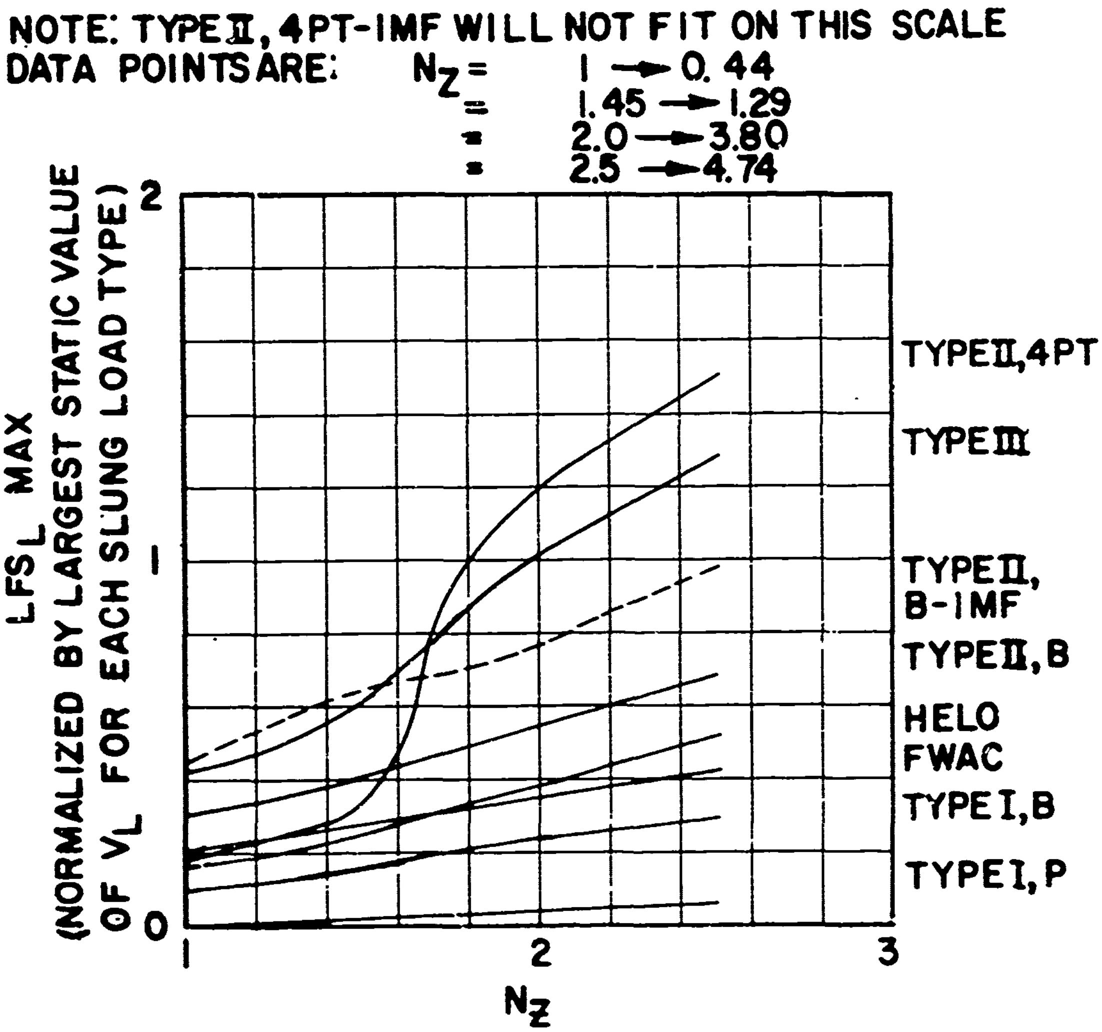

Figure 21. Maximum Dynamic Slung Load Hardpoint Side Force Load Factor vs Helicopter Design Load Factor.

DISCUSSION OF DESIGN CRITERIA

The sling and hardpoint design criteria presented in Figures 14 through 21 were created from pertinent data selected from the preliminary plots appearing in Appendix V. The design criteria plots are the highest load factor data points found for each of the corresponding slung load types in the figures in Appendix V. Some of the slung load types are separated as a function of the slinging arrangement because different load factors are developed for the same slung load for different sling arrangements. In-plane force data at hardpoints have been omitted from the design criteria plots.

None of the data from cases run with gusts are incorporated into the design criteria plots. Two slung load types were simulated with gusts, and the data from these cases do not indicate the existence of any standard correction by which the load factor data for all the slung load types can be adjusted to account for gusts. Also, the change in sling and hardpoint load factors due to gusts is a function of the magnitude, frequency, and shape of the gust. Therefore, to avoid confusion and misinterpretation of any design criteria, the gust data collected for this study have been omitted from Figures 14 through 21.

Load fa tor data obtained for the two slung load types simulated on the moving-base rig were not incorporated into the design criteria plots, since the moving-base values were usually not critical. In a few instances in which the moving-base load factor values exceeded the fixed-base values, the difference was small enough to be attributed to variations in pilot reaction between two executions of the same maneuver. The maneuvers simulated on the motion system which were not high load factor producing maneuvers did not produce critical values of forces in slings and hardpoints. However, in some cases these maneuvers did produce higher values of forces than were produced during some of the high load factor maneuver cases.

Load factors obtained for the pallet have not been incorporated into the design criteria plots. The purpose for simulating the pallet cases was to gather data which would represent landing impact loads, anticipating the possibility that these loads might be larger than the loads developed during any of the runs with the container slung from four helicopter hardpoints (this was the only slung load type which would allow the helicopter to land). In almost all instances, the container - four-point data had higher values than the pallet data. The few instances in which the pallet load factor data values were higher are attributed to the difference in sling geometry between the pallet and container configurations. Therefore, the pallet data were not included to avoid confusion and misinterpretation and also because the pallet load factor values were not critical when compared to the container - four-point data.

The dotted line plots in Figures 14 through 21 represent slung load types with broken sling members. In the load factor working plots included in Appendix VI, the failed sling member data were nondimensionalized by the static values of the failed configurations as indicated in Table I. However, the failed member data presented in final form were

nondimensionalized by the appropriate nonfailed static values (for the forward cg location) for the dotted line design criteria plots, since this method does not require an additional calculation of static values for the failed configurations. The failed sling member data should be used to design for fail-safe cases only.

Some restrictions in the use of the design criteria plots should be noted here. The data presented in Figures 14 through 21 should be used directly only for the specific sling and hardpoint geometries simulated for each slung load type in this study. The dynamic load factors represented in these figures are superimposed upon the static load factors carried in sling members and at hardpoints, and the static load factors are a function of the specific geometry of the slinging configuration and hardpoint locations. A method for applying the design criteria data determined by this study to any sling geometry for a given slung load type is being developed under contract with the Army. The method being developed under this contract will be applicable to any slung load type and sling geometry except for slung load types which are characterized by relatively large aerodynamic moments - specifically, the fixed-wing aircraft and helicopter. In these cases the interaction between the aerodynamic moment and the restoring moment provided by the sling members cannot be accounted for by only a geometry correction applied to the design criteria data developed in this study.

The method outlined here and in Appendix VI for using the design criteria data plots implies the generalization that all cables, legs, helicopter hardpoints, or slung load hardpoints for a specific slung load and sling geometry are designed to the same strength regardless of any difference in the static values of forces these members may carry. This generalization is necessary because during the study it was found that for a maneuver with a given slung load, the forces developed in different slings and hardpoints did not increase in the same proportion. The design criteria data reflect only the maximum forces developed. Thus, some sling members or hardpoints may be overdesigned.

This approach was adopted, since the alternative would be to match the hardpoint on a load with the rated strength of a specific leg of a sling assembly. The sling would thus be oriented in a specific manner with respect to the load. Since slings are used for a variety of cargo, this approach is obviously impractical.

CONCLUSIONS

1. The simulation indicated that the load factors developed in slings and hardpoints often exceeded the basic helicopter load factor developed for many of the maneuvers and slung load configurations which were simulated. Occasionally, the sling and hardpoint load factors were two or three times as great as the basic helicopter load factor. In some instances the sling and hardpoint load factors exceeded the design limit load factor of the helicopter, although the helicopter normal load factor never reached this value for any of the simulated runs.

2. In almost all cases, the symmetrical dive and pullout maneuver provided the critical load factor values which were used as a basis for the design criteria.

3. At different hardpoints on the slung load, the forces do not necessarily vary in the same proportion at all locations during a maneuver. For example, during the symmetrical dive and pullout with the CH-47 as the slung load type, the maximum vertical force developed at the rear hardpoints on the slung load was 280 percent of the static value at the same hardpoints, while the maximum vertical force at the front hardpoints was over 400 percent of the static value at these hardpoints.

4. The density of the slung load is an important parameter in determining slung load type general categories because load factors vary a great deal with density. The empty container and full container slung load types illustrate the effect of density; the load factors for the empty container were nearly 200 percent greater than they were for the fully loaded container.

5. Results from the simulation indicated the importance of representing all the major aerodynamic loads on individual slung load configurations.

6. The failed member data indicate a substantial increase in loading compared to the nonfailed configurations. Typically, the failed configuration load factor data were about 170 percent greater than the nonfailed data, although this difference was as high as 310 percent in some instances. However, the failed configuration data do not indicate any universal change in load factor values which could be applied to all sling and hardpoint load factor parameters or to all slung load types to account for the possibility of failure of sling members.

7. Results from the moving base simulation showed that motion cues are most important in maneuvers where the pilot response is primarily a function of load motion. Some of the nonload factor producing maneuvers actually created larger sling and hardpoint load factors than were produced by some of the high load factor producing maneuvers, but none of these were critical values.

8. The data from the fixed-base simulation runs were used for formulating the design criteria. The data gathered from the moving-base runs indicate some conservatism in the fixed base data. The limited selection of maneuvers simulated with the motion system were not identical to the same maneuvers done on the fixed-base rig (particularly the symmetrical dive and pullout) on which the majority of the information was gathered.

9. The slinging geometry (bridle or cable acuteness) used for attaching the external load to the helicopter is an important parameter in determining the maximum forces developed in sling members and hardpoints.

10. The simulation approach for determining dynamic load factors in slings and hardpoints as a function of helicopter normal load factor proved to be an adequate and easily usable method, yielding valid results.

11. A two-phase approach to the problem of collecting load factor data from the simulation proved desirable in obtaining pertinent data. A real time solution was needed to obtain pilot response, while a non-real time solution was used to solve for load factors in all slings and hardpoints.

12. Since the sling and hardpoint load factors for a given slung load type appear to be functions of the slinging arrangement, particularly the number of legs used in forming the bridle, sling geometry parameters should be investigated more closely with regard to their effect on load factor values.

13. Additional slung load types with failed sling members should be investigated by the simulation program. A more thorough design criteria study would be beneficial to investigate other slung load types which are less stable than those already studied and which can create oscillations while suspended due to sensitivity of the orientation of the slung load.

14. A detailed study is recommended to establish the gust parameters that affect load factors; these parameters should be varied through a selected range during the simulation. All slung load types of interest should then be simulated with the selected gusts added to the program, thereby producing proper information for determining any change in design criteria as a function of gust type.

APPENDIX I

MILITARY VEHICLES AND EQUIPMENT AS EXTERNAL HELICOPTER LOADS

SMALL TRAILERS AND TRAILER MOUNTED EQUIPMENT

Description	Weight(lb)	Load Type
High Power Illuminator, Hawk w/trlr AN/MPQ-39	9300	II
Radar, Pulse Acquisition, Hawk w/trlr AN/MPQ-35(XO-5)	8800	I, II
Radar CW Acquisition, Hawk AN/MPQ-34	4900	II
Range Only Radar, Hawk AN/MPQ-37	5005	II
Launcher, Zero Length XM-78E3 Hawk	4380	II
Chassis Trlr, 2 ton, 2 whl, M390C w/missile pallet, w/o missiles	4800	II
Shop Equipment, GM, Organizational Maint. AN/MSM-43	5500	I
Battery Control Central, Trlr Mtd. AN/MSW-9(XO-1)	8170	II
Generator Set, DED, Trlr Mtd. PU 239 D/G	4250	II
Generator Set, 20 Kw Diesel PU 239	4450	II
Generator Set, 45 Kw PU 648/M	4700	II
Lubricating & Servicing Unit, Trlr, Mtd. PWR Operated	5150	II
Trailer, Water Tank, 1 1/2 ton, 2 whl, M107A2	2380	II
Trailer, Water Tank, 400 Gals. M149	2550	II
Compressor, Rotary, 315 COH w/trlr	9550	I, II
Trailer, Floodlight 5 Kw Type MC-2	2600	II
Generator Set, Diesel Engine, Trlr Mtd. PU-482M	4900	II
Generator Set, DED, PU-239 E/G	4200	II
Welding Machine, ARC, DED	5250	II
Generator Set, DED, 20 Kw Trlr Mtd. PU-344G	5650	II
Generator Set, DED, 30 Kw Trlr Mtd. PU-482M	5000	II
Engine, Diesel for Sawmill Model 3029-C 95 H.P.	4320	II
Bath Unit, Trlr Mtd., 24 Head, EC8B-57, EC8B-61	6220	I
Central Office, Telephone AN/MTC-1 Generator Set PU-619/M 10 Kw Trlr Mtd.	4090	II
Floodlight Set, Trlr Mtd. 5 Kw.	2820	II
Weapons Loader - SATS M12 A/S 32K-1	5440	I, II
Trailer, Tank Lox 150 Gallon, 4 wheel	3180	II
Trailer, Air or Nitrogen Servicing	2400	I, II
Dolly, Trailer Converter, 6 ton, 2 whl. M197A1	2880	II
Trailer, Tank, Liquid Oxygen, 500 Gal.	7210	II
Trailer, Tank, Liquid Nitrogen, 500 Gal.	7019	II
Generator Set, DED, Trlr Mtd. PU-587/M	2282	I, II
Laundry Unit, Trlr Mtd.	9000	II
Dolly, Trailer Converter, 18 ton, M199	7700	I
Cryptographic Center, Mobile AN/MSQ-42S-222	3200	II, III
Trailer, Cargo 1 1/2 ton, 2 shl. M105A2	2750	II
Water Purification Unit 600 Gph Trlr Mtd Model A-800011	3000	II
AN/TSC-15 Communications Central in M105 Trlr	4750	II
Generator Set DED, PU-463/MRC Mtd. in M101A1	2350	II

Generator Set, PU-670G on M101A1 Trlr (PWR ACC. GP) A-8439/TRC-97C	2,640	II
Generator Set, PU/357 Trlr Mtd.	2,510	II
Radio Set V334/TRC-97 in M101 (Gen. & Ant. only)	3,590	II

2-1/2-TON TRUCK MOUNTED EQUIPMENT

Truck, Cargo, 2 1/2 ton, 6 x 6 M35A1 w/winch	13,530	II
Truck, Cargo Dropside, 2 1/2 ton, M35A2C w/o winch	13,000	II
Truck, Tank, Fuel Servicing, 1200 gal. 2-1/2 ton, 6 x 6 M49A2C	14,470	II
Truck, Cargo, 2 1/2 ton, 6 x 6 w/winch M36	15,240	II
Truck, Van, 2 1/2 ton, 6 x 6, M109A3, w/o winch	15,881	II

1-1/4-TON TRUCK MOUNTED EQUIPMENT

Truck, Ambulance, 1-1/4 ton, 4 x 4, M725 w/o winch	6,400	II
Truck, Cargo, 1-1/4 ton, 4 x 4, M715 w/winch	5,500	II

LARGE ENGINEER EQUIPMENT

Crane, Anthony, M65 (Sectionalized Boom)	20,700	I, II
Mixer, Concrete, 6 cu ft., Trlr Mtd, GED	3,225	II
Grader, Road, Towed 125-M61	12,100	II
Mixer, Concrete, Trlr Mtd., 16 cu ft., Model 16S-2A	6,200	I
Tractor, Compressor, Wheeled, 125 CFM	5,810	II
Loader, Scoop Type, Sectionalized TL-16SMD-G.M.	19,000	I
Compressor, Reciprocating, Power Driven, COH 105 CFM	6,000	II
Roller, Road, Towed, 13 Wheel, Pneumatic R-13	4,120	I
Mat, Beaching, Woven Wire 33 Joined Section		I
Electric Power Plant NC-5	6,200	II
Bridge Fixed Span M4T6 #1 35 ft. Section	12,390	I
Bridge Fixed Span M4T6 #2 35 ft. Section	12,390	I
Boat Bridge 27 ft. A-27 Bow Half	1,300	III
Boat Bridge 27 ft. A-27 Stern Half	5,000	II

3/4-TON TRUCK MOUNTED EQUIPMENT

Radio Terminal AN/MRC-62 TRK Mtd in M37	7,400	II
Truck, Cargo, 3/4 ton, 4 x 4, M37, w/winch	5,917	II
AN/TSC-15 Communications Central in M36 Truck	8,500	II
Radio Terminal AN/MRC-62A MTD in M37	7,500	II
Radio Set AN/TRC-97 MTD in M37	7,700	II
Radio Terminal AN/MRC-63 MTD in M37	7,400	II
Radio Set V334/TRC-97 MTD in M37	7,640	II
Radio Set AN/MRC-60 TRK MTD in M37	7,200	II

1/4-TON TRUCK MOUNTED EQUIPMENT

Radio Set AN/MRC-83 Mounted in M38A1	3,190	II
AN/MRC-110 Radio	2,605	II
Radio Set Central AN/MRC-87 M170	3,489	II

Truck, Utility, 1/4 ton, M151	2,400	II
Truck, Ambulance, Front Line, 1/4 ton, 4 x 4, M718	2,780	II
Truck, Firefighting, 1/4 ton, Model 3088-1	3,450	II

LARGE TRAILERS

Semitrailer, Cargo, 12 ton, 4 whl, M127A2C	14,240	I
Semitrailer, Low Bed, 25 ton, M172A1	14,860	I
Low Pressure Generating Plant, Mobile, Liquid Oxygen/Nitrogen	15,100	II
Semitrailer, Van, Expansible, 6 ton, M313	14,700	II
Weapons Trailer AN-32U-13, Airborne Armament Maint.	6,000	II

FORKLIFT TRUCKS

Truck, Forklift, RT-ART-30	3,375	II, III
Truck, Forklift, DED, RT-RUF-060	18,000	I
Truck, Forklift, Gas, 6000 lb cap	9,620	I

MISSILE CAN

Guided Missile, Canned, MTM-23A IN XM430	3,245	II, III

AIRCRAFT TOWING TRACTORS

Tractor, Aircraft Towing, Garwood	5,800	I

TRACKED VEHICLES

Carrier, Cargo, Amphibious, Tracked M116A1		II, III
Carrier, Cargo, Amphibious, Tracked XM733 (Armored)		I
Loader, Transporter, Hawk XM501BZ	5,365	II

SHOP VAN BOXES

Battery Control Central, Hawk AN/TWS-2	5,400	II, III
AN/GRM-48A Shelter, Electronic Maint. Support	3,660	III
Field Maintenance Shop Equip. Shop 2 AN/TSM-41	6,800	II
Field Maintenance Shop Equip. 1 Shop 3 AN/TSM-42	6,400	II
Field Maintenance Shop Equip. Shop 4 AN/TSM-43	5,800	II, III
Field Maintenance Shop Equip. Shop 5 XM/2E2	5,900	II, III
Field Maintenance Shop Equip. Shop 6 AN/TSM-45	5,900	II, III
Field Maintenance Shop Equip. Shop 7 AN/TSM-40	5,900	II, III
Operations Central AN/TSQ-39	5,010	II, III
Operations Central AN/TSQ-39	8,110	II
Shelter, Crypto S-126/G	2,660	III
Communications Central AN/TSC-15 Skid Mtd.	2,100	III
AN/UPS-1 Radar Set, Shelter S-269 & Basket	4,450	III
Shop, Electronic AN/GRM-38A	4,750	II, III
AN/TPQ-10 Radar, Course Directing Control	6,864	II
Communications Central Group AN/TYA-11	4,650	II, III
Shelter, Elect. Equip. AN/TYA-19 Prt. of AN/TYQ-3	4,754	II, III

Maint./Trans. Group AN/TYA-24 Prt. of AN/TYQ-3	4,531	II, III
Data Terminal Group AN/TYA-17 Prt. of AN/TYQ-3	4,914	II, III
Computer Group Comp. AN/TYA-20 Prt. of AN/TYQ-3	4,810	II, III
Hut, Operator Group AN/TYA-9A Prt. of AN/TYQ-2	5,215	II, III
Hut, Comm. Group AN/TYA-12A Prt. of AN/TYQ-2	4,475	II, III
Hut, Central Comp. Group AN/TYA-5 Prt. of AN/TYQ-2	5,000	II, III
Hut, Transport Data 2D/3D Radar AN/TYA-18 Prt. of AN/TYQ-2	4,215	III
Hut, Transport Data 2D/3D Radar AN/TYA-18 Prt. of AN/TYQ-2	4,215	III
Hut, Transport Data Ancillary Group AN/TYA-26 Part of AN/TYQ-2	3,785	III
Hut, Transport Data Geog. Display AN/TYA-7 Part of AN/TYQ-2	5,000	II, III
Hut, Photographic Transport Group AN/TYA-25 Part of AN/TYQ-2	2,900	III
Hut, Unit Test Group AN/TYA-23 Prt. of AN/TYQ-2	3,450	III
Hut, Maint. Group Export Data AN/TYA-27 Part of AN/TYQ-2	3,900	III
Electronic Shop AN/GRM-32A	5,495	II, III
Central Office, Telephone, Manual AN/MTC-1 S-179A	4,200	III
Central Office, Telephone, Manual AN/MTC-1 S-18A	4,400	III
Tower - A/C Control Group AN/TSA-13	2,190	III
S-142 Shelter AN/TSA-13	3,680	III
Landing Control Central OA-8391/TSQ-18A	7,200	II
AN/TSM-98 Van	7,220	II
AN/TSM-98 Spare Parts Van	7,220	II
AN/TSQ-68 Transcriber, Translator Facility	2,975	III
AN/TSQ-46 Van	5,600	II, III
AN/TSQ-64 Van Signal Analysis Facility	5,000	II, III
AN/GRM-82 Electronics Shop	6,140	II, III
AN/TSQ-86 (V) Light Signal Monitor Facility	2,037	III
AN/GRM-48 Shelter, Electr., Maint., Support	4,700	II, III
AN/TSQ-52	2,825	III
AN/TSQ-54	2,800	III
AN/MSC-43 Special Comm., Central	5,850	II, III
Distribution Box J-2573/TYQ-2 Part of AN/TYQ-2	1,300	III

LARGE TRUCKS

Truck, Dump, 5 ton, 6 x 6, w/winch, M51	14,460	II
Truck, Crash, Fire, Oshkosh, Model A1111-41927MB-5	20,000	II

PALLETS

Test Equipment Pallet AN/TSM-44	1,195	II, III
AN/UPS-1 Radar Set Pallets		III
AN/TRQ-10 Radar Course Directing Control - Pallet Antenna AS-1310/TYQ-3 TD CC System	2,520	II
MX-7852/TYA Pallet-Air Cond. Cable Reel - Prt. of AN/TYQ-3	1,130	III
AN/TYQ-2 Cable & Air Cond. Pallet No. 1	3,496	II

AN/TYQ-2 Cable & Air Cond. Pallet No. 2	4,021	II
Pallet No. 2	4,021	II
Pallet No. 3	3,991	II
Pallet No. 4	3,751	II
Pallet No. 5	4,106	II
Pallet No. 6	4,271	II
Pallet No. 7	3,441	II
Pallet No. 8	3,881	II
Pallet No. 9	3,851	II
Pallet No. 10	3,831	II
Pallet No. 11	2,981	II
Reeling Machine RL-26-C with 2 reels of wire	834	II
<u>GUNS</u>		
Howitzer, Towed, 155 mm M114A1	12,700	I
Howitzer, Towed, 105 mm M101A1	5,500	II

APPENDIX II

VERTICAL BOUNCE CRITERIA

The following is a reprint of Appendix 4 from Technical Report 68-2 entitled, Aerial Recovery Kit, Concept Formulation Study; U. S. Army Aviation Materiel Command, St. Louis, Missouri, June 1968, AD 673102.

2.1.4.1 APPENDIX 4

TITLE: Design Criteria and Analysis for the Prevention of Vertical Bounce

4.1 Summary

A dynamic analysis was performed to generate Universal Sling Kit Design criteria for the prevention of "vertical bounce", which is a condition of excessive helicopter vibration at a frequency of 1 x main rotor speed resulting from normal, inherent, main rotor forces amplified by the tuned response of an aircraft and its suspended load. Further, the system's tuning characteristics are primarily controlled by the spring rate of the suspension system between the two masses.

Design criteria, or limitations on the spring rate of the Universal Sling, were established for the UH-1D and CH-47 aircraft. These criteria were based on Sikorsky Aircraft's experience and data obained during the development of the CH-54A aircraft. No limitations were imposed on the sling for use on the CH-54A aircraft since a dynamic decoupler has already been incorporated into this aircraft's cargo handling system.

An analysis of the actual Universal Sling design is presented to justify that it meets the design criteria requirements. It was shown that the Universal Sling Kit, for use with either prime mover aircraft, or for any suspended load configuration, meets and exceeds the design criteria requirements.

4.2 Symbols

1p	1 x main rotor
f1p	frequency of 1p or system excitation frequency (cpm)
f_{RBM}	coupled aircraft - load rigid body mode natural frequency (cpm)
$f1p/f_{RBM}$	proximity ratio (cpm/cpm)
Wsl	weight of slung load (lb)
$W_{A/C}$	weight of aircraft (lb)
μ	$Wsl/W_{A/C}$ = mass ratio (lb/lb)
Ks	spring rate of suspension system (lb/in.)
g	gravitational constant (in./sec^2)
f_{VBM}	aircraft uncoupled first vertical bending mode natural frequency (cpm)
$f1p/f_{VBM}$	proximity ratio (cpm/cpm)

4.3 Background

During the early stages of the CH-54A development program, a vibration phenomenon was sometimes encountered when heavy loads were lifted by a cable suspension system. The incidence of these events was infrequent. However, when encountered, it was evident that the response could build up and become serious enough to cause the pilot to jettison the load. It was also noted that the frequency of the response was at or near 1p.

This phenomenon was explained as a resonance of the aircraft and suspended load system, excited by the main rotor head 1p forces. The aircraft behaved basically as a rigid body mass, the suspension system constituted the spring, and the suspended load was the second mass in the total dynamic system.

High response could most easily be achieved by slowly varying the cable length while in-flight. Since this varied the cable spring rate, this was a convenient means of experimentally tuning the system. Significantly, the response curve exhibited a narrow "Q" characteristic, meaning that significant response only occurred within a narrow proximity margin. This is defined as the proximity ratio $f1p/f_{RBM}$.

High response was also most evident to the pilot when heavy loads were carried. As the suspended load to prime mover aircraft mass ratio increased, the system's mode shape was altered resulting in increased aircraft or cockpit participation. This mass ratio is defined as $\mu = W_{sl}/W_{A/C}$.

For design purposes, vibration acceptability levels are based on pilot comfort criteria rather than structural integrity criteria. These oscillations are characterized by large displacement excursions and low acceleration amplitudes. In this region, inertial forces are low, but human susceptibility is high.

As part of the CH-54A development program, a dynamic decoupler was incorporated into the single point cargo handling system. This provision is basically a soft spring which is compatible with any impendance, or suspended load characteristic, keeping the system always well within acceptable limits of vibration. It only functions for suspended loads having mass ratios of approximately 0.5 or higher. This parameter, and its proximity ratio parameter, have been fully evaluated and substantiated by flight test measurements.

4.4 Parametric Considerations

The "background" introduced each of the pertinent parameters necessary to consider in establishing design criteria. Each is discussed below:

Proximity Ratio of Fuselage First Vertical Bending Mode (f_{1p}/f_{VBM})

Investigation of the vertical bounce phenomenon at Sikorsky Aircraft has shown that cockpit response is the summation of the rigid body response and some first fuselage bending mode response. However, the model below is a close analog representation of the phenomenon capable of extrapolating the CH-54A experience to other aircraft, if the following proximity margin relationship is observed.

$$f_{1p}/f_{VBM} \leq \frac{185\ \text{cpm}}{235\ \text{cpm}} = 0.79 \tag{54}$$

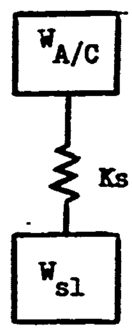

Proximity Ratio (f_{1p}/f_{RBM})

Experience with the CH-54A aircraft has substantiated the following proximity ratio with the heaviest suspended load:

$$f_{1p}/f_{RBM} \geq \left.\frac{185\ \text{cpm}}{105\ \text{cpm}}\right|_{\text{CH-54A}} = 1.76 \tag{55}$$

Mass Ratio $\mu = W_{sl}/W_{A/C}$

Experience with the CH-53A aircraft has shown that the suspended load is significant only for mass ratios:

$$\mu = W_{sl}/W_{A/C} \geq \left.\frac{10{,}000\ \text{lb}}{22{,}000\ \text{lb}}\right|_{\text{CH-54A}} = 0.45 \tag{56}$$

Spring Rate (K_s)

The non-trivial natural frequency of the rigid body system shown above is:

$$f = \frac{60}{2\pi}\left[\frac{K_s\,(W_{A/C} + W_{sl})\,g}{(W_{A/C})(W_{sl})}\right]^{1/2} \tag{57}$$

We now have the significant parameters defined and are prepared to determine the dynamic design criteria for the prevention of vertical bounce.

4.5 Design Criteria

Dynamic criteria for the Universal Sling Kit will be generated by defining limitations and latitude of the stiffness of the sling. By controlling the sling stiffness the frequency of the rigid body mode is controlled thereby providing suitable isolation from the 1p forces. Using the parameters developed above, stiffness criteria for the sling were developed for use of the kit with the UH-1D and CH-47. Characteristics of slings used on the CH-54A are not restricted because load isolation is incorporated in its cargo handling system.

The 1p frequencies and fuselage first vertical bending mode frequencies are tabulated below.

MODEL	f_{1p}	f_{VBM}	f_{1p}/f_{VBM}
CH-54A	185 cpm	235 cpm	0.79
UH-1D	310 cpm	395 cpm	0.79
CH-47	230 cpm	470 cpm	0.49

As shown in the table the UH-1D and CH-47 meet or exceed the requirements of equation (54).

The required rigid body mode frequency is found by rearranging equation (55).

$$f_{RBM} \leq 0.57 \, f_{1p} \tag{58}$$

and substituting the appropriate 1p frequency for the UH-1D and CH-47. With the maximum rigid body mode frequency defined, the sling stiffness may be evaluated. Algebraic manipulation of equation (57) to solve for sling stiffness gives

$$Ks = \left(\frac{2 \, f\pi}{60}\right)^2 \frac{(W_{A/C})(W_{sl})}{(W_{A/C} + W_{sl}) \, g} \tag{59}$$

by solving equation (59) using the rigid body mode frequency determined from equation (58) and the maximum slung load weight, the sling stiffness for the UH-1D and CH-47 is determined. This spring rate represents the upper limit.

For the purpose of this analysis the slung load weight was defined as the maximum payload, and aircraft weight was defined as the difference between the maximum gross weight and the maximum payload. These values are tabulated below.

MODEL	G.W. (MAX.)	W_{sl}	$W_{A/C}$
CH-54A	42,000 lb	20,000 lb	22,000 lb
UH1D	9,500 lb	4,000 lb	5,000 lb
CH-47	33,000 lb	17,000 lb	16,000 lb

Rearrangement of equation (55) gives

$$W_{sl} \text{ (Min.)} = 0.45\, W_{A/C} \qquad (60)$$

Substituting the respective aircraft weights as defined above permits evaluation of the minimum sling load weight for which isolation is required. Results of the dynamic design criteria determinations are shown graphically in Figure (84).

FIGURE 84

UNIVERSAL SLING KIT
TOTAL SLING STIFFNESS VS. SLUNG LOAD WEIGHT
RESTRICTIONS APPLICABLE TO UH-1D & CH-47 A/C.

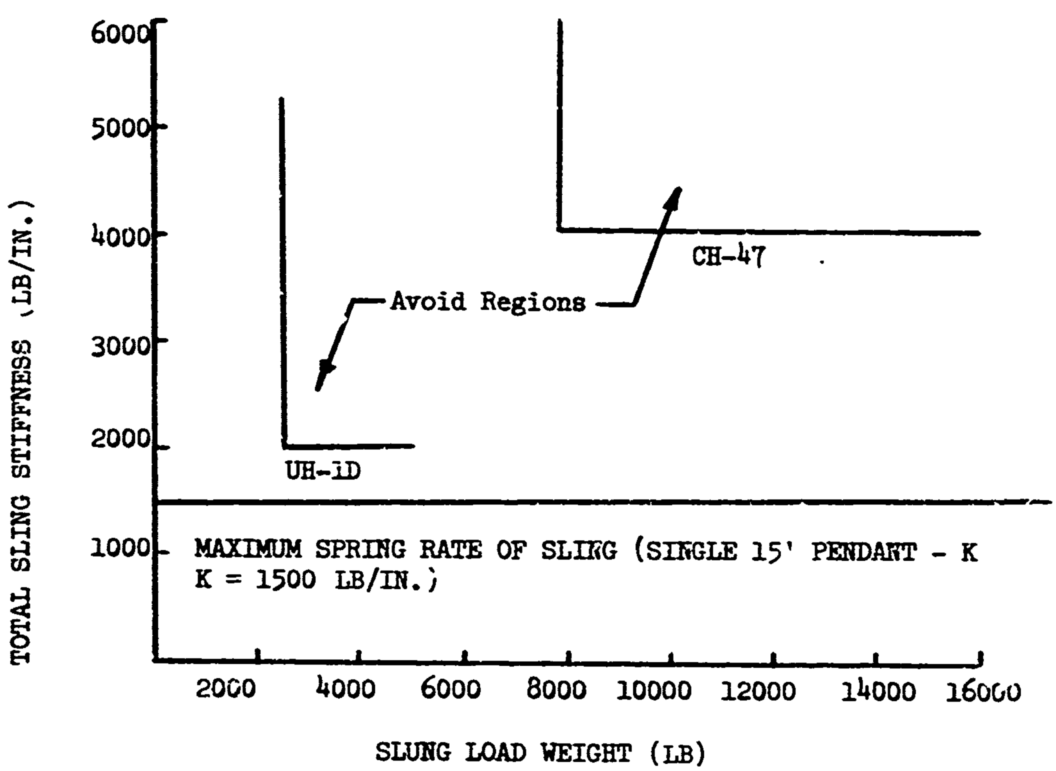

NOTES:
Upper weight boundaries defined by maximum sling load capacity.
Lower weight boundaries defined by the ratio of mass of slung load to mass of prime mover.

DESIGN JUSTIFICATION

Upon determination of the general design configuration of the Universal Sling Kit it is necessary to evaluate the equivalent stiffness of specific sling configurations. The stiffness criteria developed represents the total sling stiffness whereas the kit may logically be thought of as consisting of three separate and distinct sections, the pendant, bridle, and belly bands, which contribute to the kit's total stiffness. Techniques for evaluating the stiffness of the individual sections, and then the total stiffness of configuration are shown in Figure (85).

Review of all the sling arrangements showed that the stiffest sling configuration was the single 15' pendant used to carry a downed UH-1D by attachment to the rotor head. Analysis of this configuration indicated that its spring rate is 1,500 lb/in.. Referring to the criteria, shown in Figure (84) shows that this stiffness, for the stiffest possible sling configuration, is well below that required. Consequently the universal sling kit design will provide greater isolation than that required for the prevention of vertical bounce.

The kit will also provide isolation from the Np forces. This is shown by recalling that $f_{np} = N f_{1p}$

and therefore $f_{np} > f_{1p}$

substituting in equation (58) shows $f_{RBM} \ll f_{np}$

indicating an even greater isolation from Np forces.

FIGURE 85

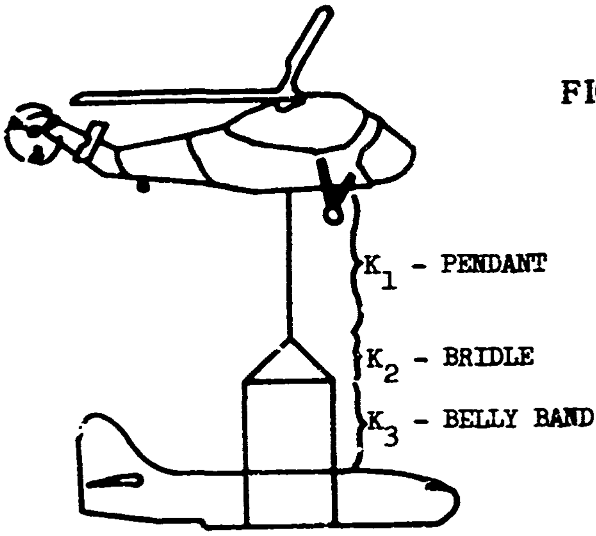

$$K_T = \frac{K_1K_2K_3}{K_1K_2 + K_1K_3 + K_2K_3}$$

PENDANT

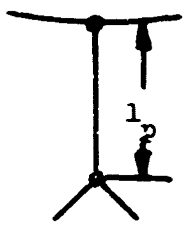

$$K_1 = \frac{k_p}{l_p}$$

k_p = Spring Rate of Pendant Material per Unit Length

BRIDLE

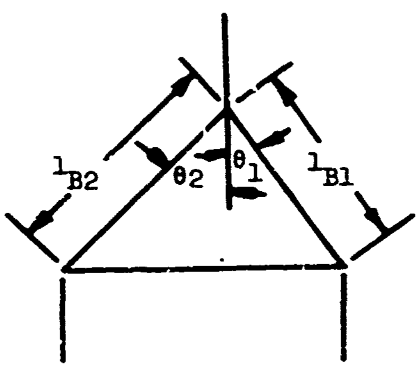

$$K_2 = K_B \left[\frac{1}{l_{B1}} \cos^2 \theta_1 + \frac{1}{l_{B2}} \cos^2 \theta_2\right]$$

k_B = Spring Rate of Bridle Material per Unit Length

BELLY BAND

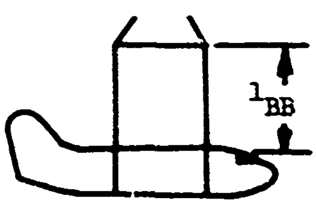

$$K_3 = N \frac{k_{BB}}{l_{BB}}$$

k_{BB} = Spring Rate of Belly Band per Unit Length

APPENDIX III

SLUNG LOADS AERODYNAMIC DATA

The normalized aerodynamic wind tunnel data for each of the slung loads which were simulated are given as a function of angle of attack α_L and sideslip β_L in Tables III to VI. These data have been normalized by the dynamic pressure q. The forces and moments of the CH-47B are along body axis directions; the forces and moments on the remaining three load types are along wind axis directions. The drag, side force, lift, and rolling, pitching, and yawing moments may be converted from wind axes to body axes according to the formulas

$$D_L = D_w \cos\beta_L \cos\alpha_L + Y_w \sin\beta_L \cos\alpha_L - L_w \sin\alpha_L \quad (148)$$

$$Y_L = D_w \sin\beta_L + Y_w \cos\beta_L \quad (149)$$

$$L_L = D_w \cos\beta_L \sin\alpha_L + Y_w \sin\beta_L \sin\alpha_L + L_w \cos\alpha_L \quad (150)$$

$$\mathcal{L}_L = \mathcal{L}_w \cos\beta_L \cos\alpha_L - M_w \sin\beta_L \cos\alpha_L - N_w \sin\alpha_L \quad (151)$$

$$M_L = \mathcal{L}_w \sin\beta_L + M_w \cos\beta_L \quad (152)$$

$$N_L = \mathcal{L}_w \cos\beta_L \sin\alpha_L - M_w \sin\beta_L \sin\alpha_L + N_w \cos\alpha_L \quad (153)$$

where the subscripts w refers to wind axes and L refers to body axes.

Because the container exhibited unstable yaw characteristics when suspended by the single-point four-legged sling arrangement, the effects of a drogue chute were added to the aerodynamic data of this load. The additional drag and yawing moment contributions on the container which are due to the chute are given by

$$\Delta D/q = 100 \cos\beta_L \quad (154)$$

$$\Delta N/q = 1000 \sin\beta_L \quad (155)$$

This represents a chute of 6.5 feet diameter attached to the rear end of the container. These two contributions due to the chute are in body axis directions and should be added to the basic container wind tunnel data once it has been converted to body axis directions.

TABLE III. CONTAINER AERODYNAMIC DATA ALONG WIND AXIS DIRECTIONS

LIFT/q(ft^2)

α_L(deg)	β_L(deg)								
	-20	-15	-10	-5	0	5	10	15	20
-20	-85	-90	-94	-99	-100	-99	-94	-90	-85
-15	-28	-52	-66	-72	-75	-72	-66	-52	-28
-10	9	-18	-38	-45	-50	-45	-38	-18	9
- 5	36	10	-10	-20	-25	-20	-10	10	36
- 0	55	35	15	5	0	5	15	35	55
- 5	68	54	39	29	25	29	39	54	68
10	78	70	60	53	50	53	60	70	78
15	84	82	79	77	75	77	79	82	84
20	85	90	95	100	100	100	95	90	85

DRAG/q(ft^2)

α_L(deg)	β_L(deg)								
	-20	-15	-10	-5	0	5	10	15	20
-20	108	105	100	97	95	97	100	105	108
-15	103	98	93	90	87	90	93	93	103
-10	98	93	87	84	81	84	87	93	98
- 5	96	89	83	80	76	80	83	89	96
0	94	87	82	77	75	77	83	87	94
5	96	89	83	80	76	80	83	89	96
10	98	93	87	84	81	84	87	93	98
15	103	98	93	90	87	90	93	98	103
20	108	105	100	97	95	97	100	105	108

TABLE III - Continued

SIDE FORCE/q(ft^2)

α_L(deg)	β_L(deg)								
	-20	-15	-10	-5	0	5	10	15	20
-20	65	50	35	15	0	-15	-35	-50	-65
-15	82	64	44	22	0	-22	-44	-64	-82
-10	93	73	51	26	0	-26	-51	-73	-93
- 5	99	79	55	29	0	-29	-55	-79	-99
0	100	80	55	30	0	-30	-55	-80	-100
5	93	73	49	28	0	-28	-49	-73	-93
10	73	54	34	20	0	-20	-34	-54	-73
15	34	20	7	6	0	- 6	- 7	-20	-34
20	-65	-50	-35	-15	0	15	35	50	65

ROLLING MOMENT/q(ft^3)

α_L(deg)	β_L(deg)								
	-20	-15	-10	- 5	0	5	10	15	20
-20	46.8	35.1	23.4	11.7	0	-11.7	-23.4	-35.1	-46.8
-15	35.1	26.1	17.5	8.7	0	- 8.7	-17.5	-26.1	-35.1
-10	23.4	17.4	11.7	5.8	0	- 5.8	-11.7	-17.4	-23.4
- 5	11.7	8.7	5.8	2.9	0	- 2.9	- 5.8	- 8.7	-11.7
0	0	0	0	0	0	0	0	0	0
5	-11.7	- 8.7	- 5.8	- 2.9	0	- 2.9	5.8	11.7	11.7
10	-23.4	-17.4	-11.7	- 5.8	0	5.8	11.7	17.5	23.4
15	-35.1	-26.1	-17.5	- 8.7	0	8.7	17.5	26.1	35.1
20	-46.8	-35.1	-23.4	-11.7	0	11.7	23.4	35.1	46.8

TABLE III - Concluded

PITCHING MOMENT/q(ft^3)

α_L(deg)	β_L(deg) -20	-15	-10	-5	0	5	10	15	20
-20	-300	-275	-250	-225	-200	-175	-150	-125	-100
-15	-250	-225	-200	-175	-150	-125	-100	-75	-50
-10	-200	-175	-150	-125	-100	-75	-50	-25	0
-5	-150	-125	-100	-75	-50	-25	0	25	50
0	-100	-75	-50	-25	0	25	50	75	100
5	-50	-25	0	25	50	75	100	125	150
10	0	25	50	75	100	125	150	175	200
15	50	75	100	125	150	175	200	225	250
20	100	125	150	175	200	225	250	275	300

YAWING MOMENT/q(ft^3)

α_L(deg)	β_L(deg) -20	-15	-10	-5	0	5	10	15	20
-20	300	260	200	100	20	-90	-200	-360	-470
-15	250	210	160	80	15	-70	-160	-260	-350
-10	220	180	130	60	10	-60	-130	-190	-270
-5	200	160	110	50	5	-50	-110	-160	-220
0	200	150	100	50	0	-50	-100	-150	-200
5	220	160	110	50	-5	-50	-110	-160	-200
10	270	190	130	60	-10	-60	-130	-180	-220
15	350	260	160	70	-15	-80	-160	-210	-250
20	470	360	200	90	-20	-100	-200	-260	-300

TABLE IV. BLOCK AERODYNAMIC DATA ALONG WIND AXIS DIRECTIONS

LIFT/q (ft^2)

α_L (deg) \ β_L (deg)	-20	-15	-10	-5	0	5	10	15	20
-20	0	0	0	0	0	0	0	0	0
-15	0	0	0	0	0	0	0	0	0
-10	0	0	0	0	0	0	0	0	0
- 5	0	0	0	0	0	0	0	0	0
0	0	0	0	0	0	0	0	0	0
5	0	0	0	0	0	0	0	0	0
10	0	0	0	0	0	0	0	0	0
15	0	0	0	0	0	0	0	0	0
20	0	0	0	0	0	0	0	0	0

DRAG/q (ft^2)

α_L (deg) \ β_L (deg)	-20	-15	-10	-5	0	5	10	15	20
-20	27	26	25	24	24	24	25	26	27
-15	26	24	23	22	22	22	23	24	26
-10	24	23	22	21	20	21	22	23	24
- 5	24	22	21	20	19	20	21	22	24
0	23	21	20	19	18	19	20	21	23
5	24	22	21	20	19	20	21	22	24
10	24	23	22	21	20	21	22	23	24
15	26	24	23	22	22	22	23	24	26
20	27	26	25	24	24	24	25	26	27

TABLE IV - Continued

SIDE FORCE/q (ft^2)

α_L(deg)	β_L(deg)								
	-20	-15	-10	-5	0	5	10	15	20
-20	16	12	9	4	0	-4	-9	-12	-16
-15	20	16	11	6	0	-4	-11	-16	-20
-10	23	18	13	7	0	-7	-13	-18	-23
- 5	25	20	14	7	0	-7	-14	-20	-25
0	25	20	14	8	0	-8	-14	-20	-25
5	23	18	12	7	0	-7	-12	-18	-23
10	18	14	9	5	0	-5	- 9	-14	-18
15	9	5	2	1	0	-1	- 2	- 5	- 9
20	-16	-12	- 9	-4	0	4	9	12	16

ROLLING MOMENT/q (ft^3)

α_L(deg)	β_L(deg)								
	-20	-15	-10	-5	0	5	10	15	20
-20	0	0	0	0	0	0	0	0	0
-15	0	0	0	0	0	0	0	0	0
-10	0	0	0	0	0	0	0	0	0
- 5	0	0	0	0	0	0	0	0	0
0	0	0	0	0	0	0	0	0	0
5	0	0	0	0	0	0	0	0	0
10	0	0	0	0	0	0	0	0	0
15	0	0	0	0	0	0	00	0	0
20	0	0	0	0	0	0	0	0	0

TABLE IV - Concluded

PITCHING MOMENT/q (ft^3)

α_L (deg)	β_L (deg)								
	-20	-15	-10	-5	0	5	10	15	20
-20	0	0	0	0	0	0	0	0	0
-15	0	0	0	0	0	0	0	0	0
-10	0	0	0	0	0	0	0	0	0
- 5	0	0	0	0	0	0	0	0	0
0	0	0	0	0	0	0	0	0	0
5	0	0	0	0	0	0	0	0	0
10	0	0	0	0	0	0	0	0	0
15	0	0	0	0	0	0	0	0	0
20	0	0	0	0	0	0	0	0	0

YAWING MOMENT/q (ft^3)

α_L (deg)	β_L (deg)								
	-20	-15	-10	-5	0	5	10	15	20
-20	38	32	25	12	3	-11	-25	-45	-59
-15	31	26	20	10	2	- 9	-20	-32	-44
-10	28	22	16	7	1	- 7	-16	-24	-34
- 5	25	20	13	6	1	- 6	-13	-20	-27
0	25	19	12	6	0	- 6	-12	-19	-25
5	27	20	13	6	-1	- 6	-13	-20	-25
10	34	24	16	7	-1	- 7	-16	-22	-28
15	44	32	20	9	-2	-10	-20	-26	-31
20	59	45	25	11	-3	-12	-25	-32	-38

TABLE V. CH-47B CHINOOK AERODYNAMIC DATA ALONG BODY AXIS DIRECTIONS

LIFT/q(ft^2)

α_L(deg)	β_L(deg) -20	-15	-10	-5	0	5	10	15	20
-20	-125	-128	-135	-133	-133	-134	-139	-138	-127
-15	- 60	- 80	- 90	-100	-100	-100	-100	- 95	- 85
-10	- 34	- 50	- 56	- 60	- 60	- 60	- 55	- 47	- 33
- 5	2	- 12	- 24	- 31	- 35	- 29	- 22	- 10	0
0	35	19	7	- 10	- 12	- 5	8	20	35
5	65	48	33	15	10	20	34	51	68
10	100	81	58	40	30	45	60	85	101
15	150	125	95	70	70	80	95	115	135
20	185	160	126	100	85	104	130	159	185

DRAG/q (ft^2)

α_L(deg)	-20	-15	-10	-5	0	5	10	15	20
-20	29.4	36.5	40.3	41.2	39.8	40.9	40.1	36.6	27.5
-15	35.5	39.7	43.4	42.9	41.3	42.3	42.5	40.4	34.4
-10	37.6	41.5	44.7	44.6	42.0	43.8	44.0	42.3	37.0
- 5	38.3	42.2	45.3	45.3	42.4	44.4	44.8	43.1	38.0
0	37.8	41.9	45.3	45.1	42.0	44.4	45.0	43.0	37.0
5	35.3	40.2	43.7	43.8	40.7	42.9	43.7	41.4	36.4
10	31.4	37.6	41.4	41.7	38.5	40.7	41.4	39.0	33.7
15	25.5	33.5	37.9	38.3	35.1	37.2	38.0	35.2	29.4
20	13.3	22.5	27.5	28.0	25.5	26.5	26.9	23.8	15.8

SIDE FORCE/q(ft^2)

α_L(deg)	-20	-15	-10	-5	0	5	10	15	20
-20	200	145	95	50	2	-48	-100	-150	-207
-15	185	140	90	50	0	-45	-90	-140	-185
-10	175	134	84	44	0	-45	- 85	-134	-178
- 5	165	124	80	40	0	-45	- 80	-130	-170
0	158	121	75	34	0	-40	-80	-119	-158
5	150	115	70	35	0	-35	-75	-115	-150
10	145	110	65	30	-2	-34	-80	-107	-145
15	140	105	60	30	0	-30	-60	-125	-140
20	135	96	58	26	9	-25	-60	-100	-135

TABLE V - Concluded

ROLLING MOMENT/q(ft^3)

α_L(deg) \ β_L(deg)	-20	-15	-10	-5	0	5	10	15	20
-20	54	52	42	34	-10	-3	-40	-77	-85
-15	58	45	35	27	0	-8	-34	-70	-90
-10	62	35	26	24	- 5	-2	-32	-64	-95
- 5	62	32	22	22	0	-5	-32	-62	-95
0	60	28	16	20	- 3	-6	-32	-60	-98
5	55	25	20	15	- 7	-15	-35	-58	-95
10	50	21	12	22	-18	-22	-46	-57	-91
15	15	8	0	-5	-25	-30	-50	-58	-85
20	-38	-21	-13	-27	-49	-43	-65	-59	-72

PITCHING MOMENT/q(ft^3)

α_L(deg) \ β_L(deg)	-20	-15	-10	-5	0	5	10	15	20
-20	-1100	-1040	-1150	-1260	-1360	-1260	-1160	-1120	-1200
-15	- 880	- 840	- 860	- 950	-1000	- 950	- 900	- 880	- 880
-10	- 650	- 580	- 600	- 600	- 760	- 680	- 640	- 660	- 750
- 5	- 380	- 320	- 300	- 350	- 420	- 360	- 330	- 380	- 480
0	- 130	- 40	20	0	- 20	- 40	- 20	- 100	- 240
5	140	270	390	410	440	340	310	170	40
10	420	590	760	820	860	750	670	480	300
15	680	900	1020	1120	1200	1200	1130	950	700
20	940	1290	1540	1600	1590	1520	1420	1240	830

YAWING MOMENT/q(ft^3)

α_L(deg) \ β_L(deg)	-20	-15	-10	-5	0	5	10	15	20
-20	-220	-10	-20	-60	-40	-65	15	92	325
-15	- 85	40	30	0	-38	-65	-45	10	200
-10	25	85	80	45	-33	-64	-90	-50	77
- 5	125	135	120	78	-25	-62	-124	-100	-27
0	220	183	151	45	-15	-58	-145	-141	-140
5	305	225	165	95	15	-45	-148	-170	-230
10	385	270	170	90	49	-15	-130	-200	-330
15	475	310	165	75	100	20	- 95	-225	-420
20	565	350	155	0	145	78	- 24	-250	-510

TABLE VI. OV-1 MOHAWK AERODYNAMIC DATA ALONG WIND AXIS DIRECTIONS

LIFT/q(ft^2)

α_L(deg) \ β_L(deg)	-20	-15	-10	-5	0	5	10	15	20
-20	-250	-250	-250	-250	-250	-250	-250	-250	-250
-15	-320	-320	-320	-320	-320	-320	-320	-320	-320
-10	-198	-198	-198	-198	-198	-198	-198	-198	-198
- 5	- 75	- 75	- 75	- 75	- 75	- 75	- 75	- 75	- 75
0	66	66	66	66	66	66	66	66	66
5	165	165	165	165	165	165	165	165	165
10	297	297	297	297	297	297	297	297	297
15	440	440	440	440	440	440	440	440	440
20	480	480	480	480	480	480	480	480	480

DRAG/q(ft^2)

α_L(deg) \ β_L(deg)	-20	-15	-10	-5	0	5	10	15	20
-20	33	33	33	33	33	33	33	33	33
-15	15	15	15	15	15	15	15	15	15
-10	13	13	13	13	13	13	13	13	13
- 5	12	12	12	12	12	12	12	12	12
0	13	13	13	13	13	13	13	13	13
5	15	15	15	15	15	15	15	15	15
10	33	33	33	33	33	33	33	33	33
15	58	58	58	58	58	58	58	58	58
20	67	67	67	67	67	67	67	67	67

SIDE FORCE/q(ft^2)

α_L(deg) \ β_L(deg)	-20	-15	-10	-5	0	5	10	15	20
-20	63	48	31	17	0	-17	-31	-48	-63
-15	72	55	36	19	0	-19	-36	-55	-72
-10	78	59	39	20	0	-22	-39	-59	-78
- 5	86	65	43	22	0	-22	-43	-65	-86
0	92	69	46	23	0	-23	-46	-69	-92
5	98	74	49	24	0	-24	-49	-74	-98
10	98	74	49	24	0	-24	-49	-74	-98
15	92	69	46	23	0	-23	-46	-69	-92
20	86	65	43	22	0	-22	-43	-65	-86

TABLE VI - Concluded

ROLLING MOMENT/q(ft^3)

α_L(deg)	β_L(deg) -20	-15	-10	-5	0	5	10	15	20
-20	463	348	232	115	0	-115	-232	-348	-463
-15	472	354	236	118	0	-118	-236	-354	-472
-10	477	358	238	119	0	-119	-238	-358	-477
- 5	482	362	241	120	0	-120	-241	-362	-482
0	482	362	241	120	0	-120	-241	-362	-482
5	468	350	234	117	0	-117	-234	-350	-468
10	432	324	216	108	0	-108	-216	-324	-432
15	384	288	192	96	0	- 96	-192	-288	-384
20	362	262	181	90	0	- 90	-181	-262	-362

PITCHING MOMENT/q(ft^3)

α_L(deg)	-20	-15	-10	-5	0	5	10	15	20
-20	244	244	244	244	244	244	244	244	244
-15	332	332	332	332	332	332	332	332	332
-10	192	192	192	192	192	192	192	192	192
- 5	62	62	62	62	62	62	62	62	62
0	0	0	0	0	0	0	0	0	0
5	-75	-75	-75	-75	-75	-75	-75	-75	-75
10	-224	-224	-244	-244	-244	-244	-244	-244	-244
15	-424	-424	-424	-424	-424	-424	-424	-424	-424
20	-500	-500	-500	-500	-500	-500	-500	-500	-500

YAWING MOMENT/q(ft^3)

α_L(deg)	-20	-15	-10	-5	0	5	10	15	20
-20	-1330	-990	-663	-332	0	332	663	990	1330
-15	-1330	-990	-663	-332	0	332	663	990	1330
-10	-1330	-990	-663	-332	0	332	663	990	1330
- 5	-1330	-990	-663	-322	0	332	663	990	1330
0	-1330	-990	-663	-322	0	332	663	990	1330
5	-1330	-990	-663	-322	0	332	663	990	1330
10	-1330	-990	-663	-322	0	332	663	990	1330
15	-1330	-990	-663	-322	0	332	663	990	1330
20	-1330	-990	-663	-322	0	332	663	990	1330

APPENDIX IV

PILOT CONTROL INPUTS FOR THE SIMULATED MANEUVERS

Figures 22 through 30 illustrate the control inputs used by the pilots to simulate the various maneuvers in the study. A typical set of input examples is shown for each of the different types of maneuvers. The pilot inputs for the symmetrical dive and pullout done during the moving-base simulation were considerably different from the inputs for the same maneuver during the fixed-base simulation. For this reason, these resulting maneuvers were not really the same; therefore, example sets of input are shown for both the fixed-base and moving-base version of this maneuver.

Figures 22 through 30 are time histories of cyclic control stick, collective control stick, and/or pedal position deviation away from the trim position of these controls, as applied by the pilot. Since these values are stick readings, they do not show any contribution due to control coupling or from any automatic stabilization equipment. For each maneuver, only the pilot control inputs which are considered important in describing the manner in which the maneuver was simulated are shown.

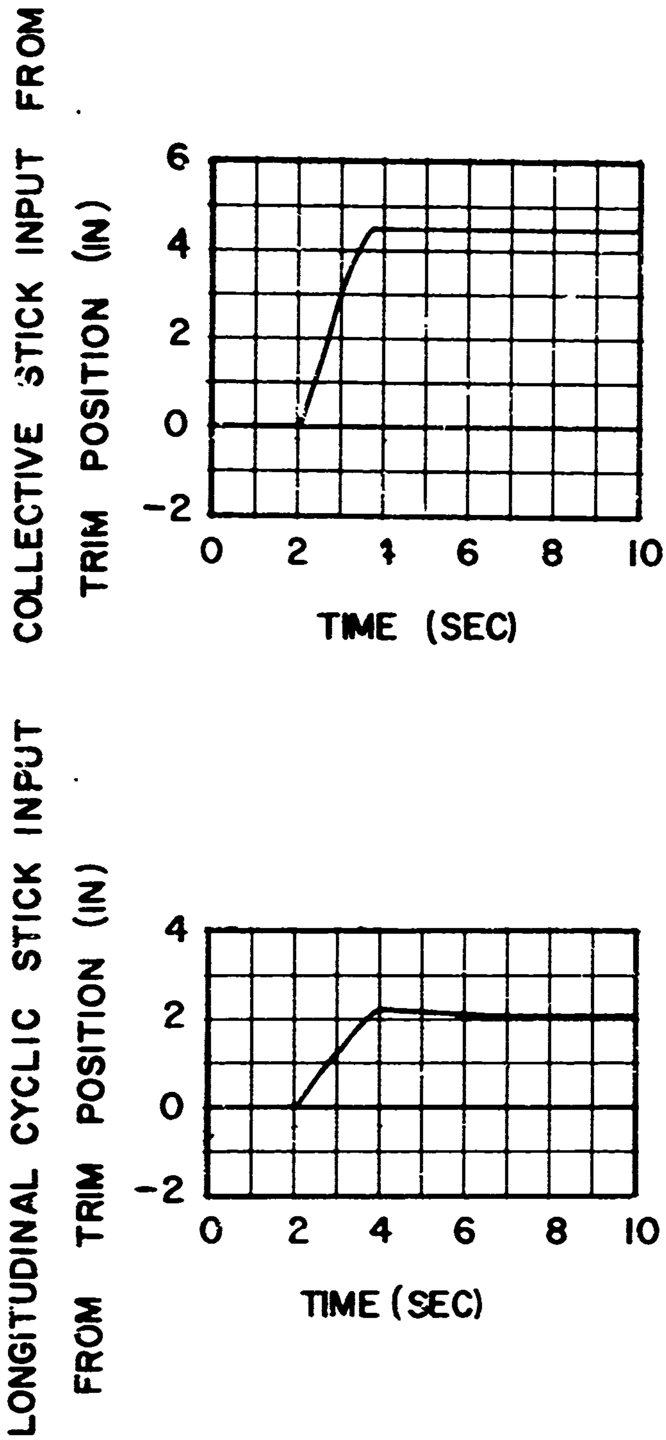

Figure 22. Pilot Control Input for the Simulated Vertical Takeoff Maneuver.

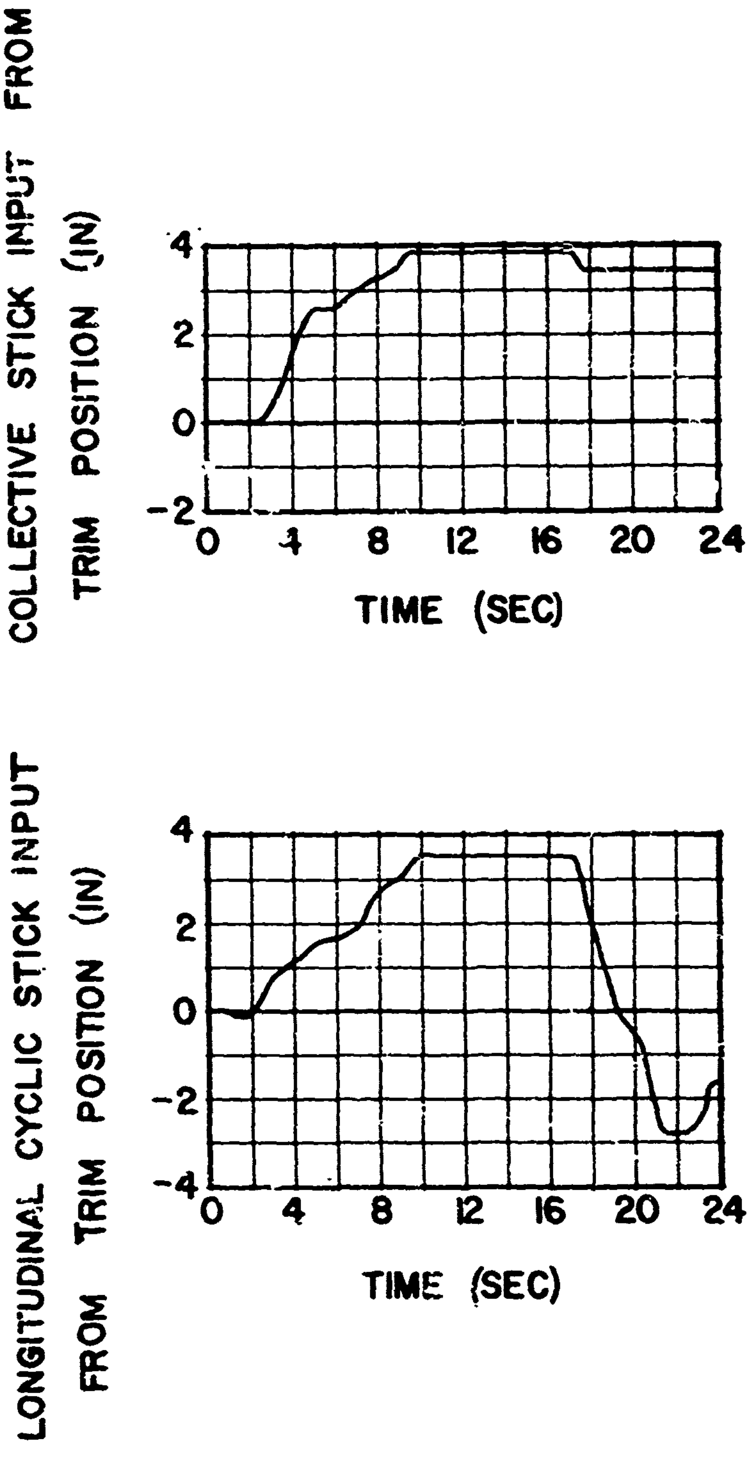

Figure 23. Pilot Control Input for the Simulated Symmetrical Dive and Pullout (on Fixed-Base Simulator) Maneuver.

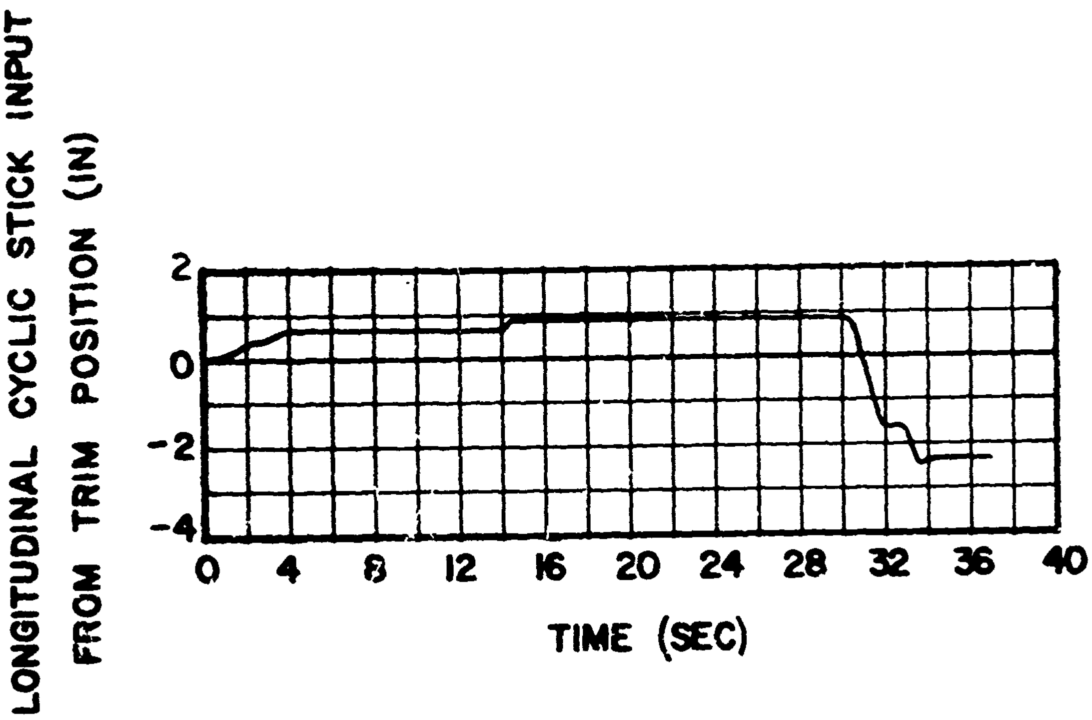

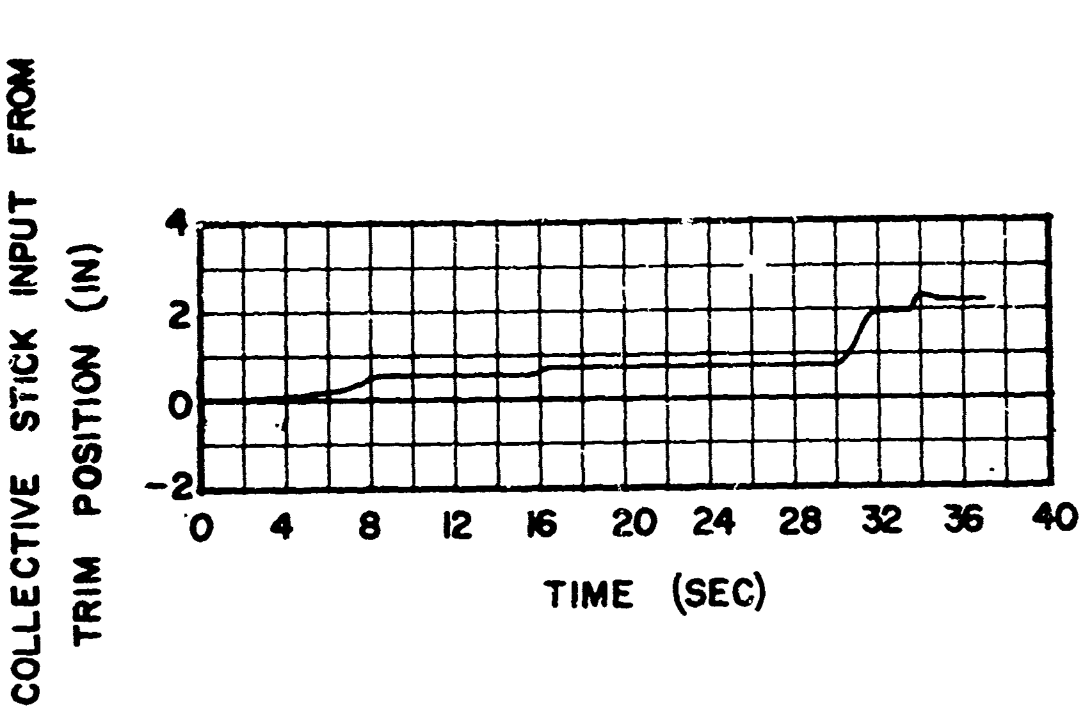

Figure 24. Pilot Control Input for the Simulated Symmetrical Dive and Pullout (on Moving-Base Simulator) Maneuver.

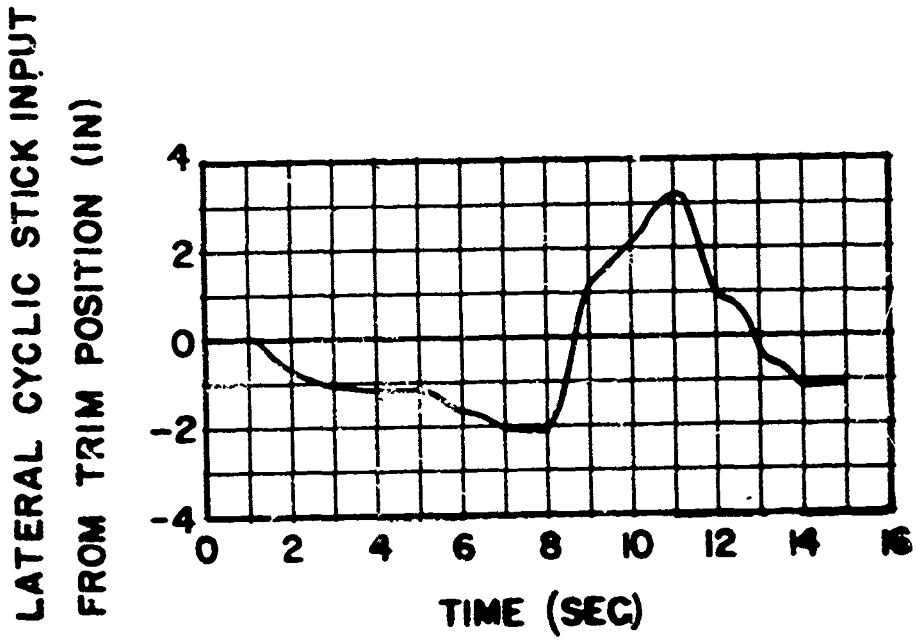

Figure 25. Pilot Control Input for the Simulated Roll Reversal Maneuver

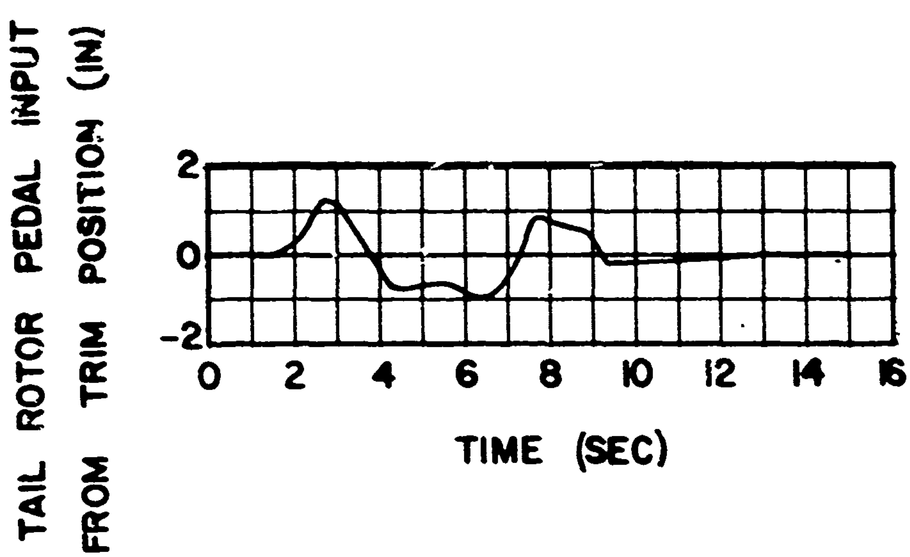

Figure 26. Pilot Control Input for the Simulated Pedal Kick Maneuver.

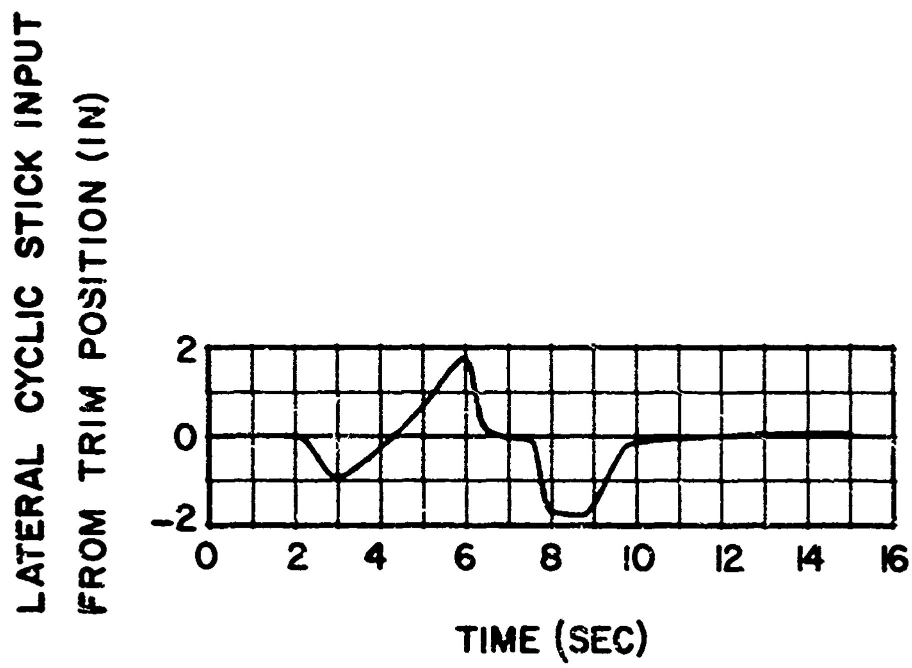

Figure 27. Pilot Control Input for the Simulated Lateral Stick Stroke Maneuver.

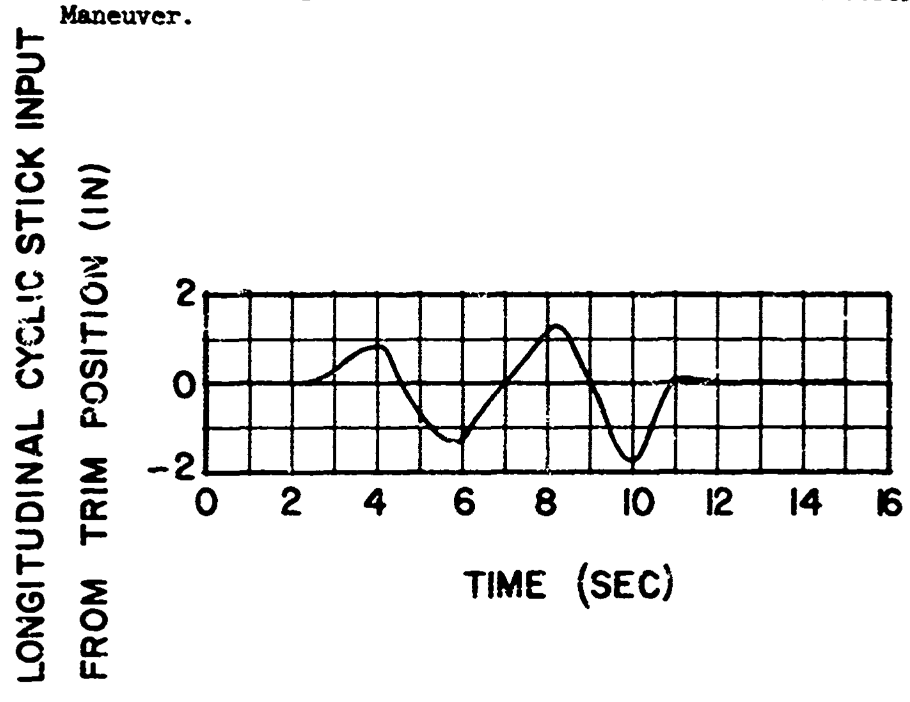

Figure 28. Pilot Control Input for the Simulated Longitudinal Stick Stroke Maneuver.

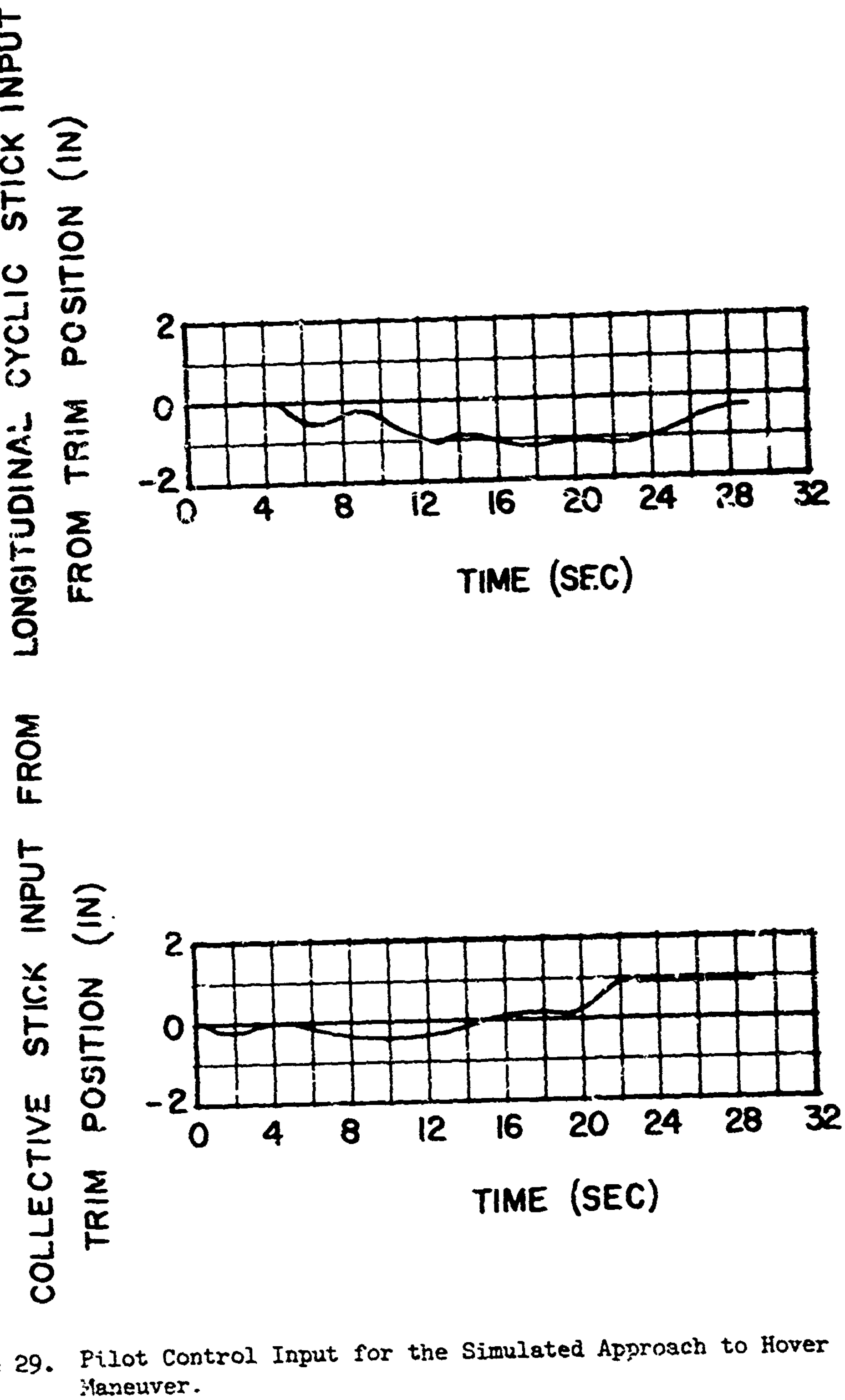

Figure 29. Pilot Control Input for the Simulated Approach to Hover Maneuver.

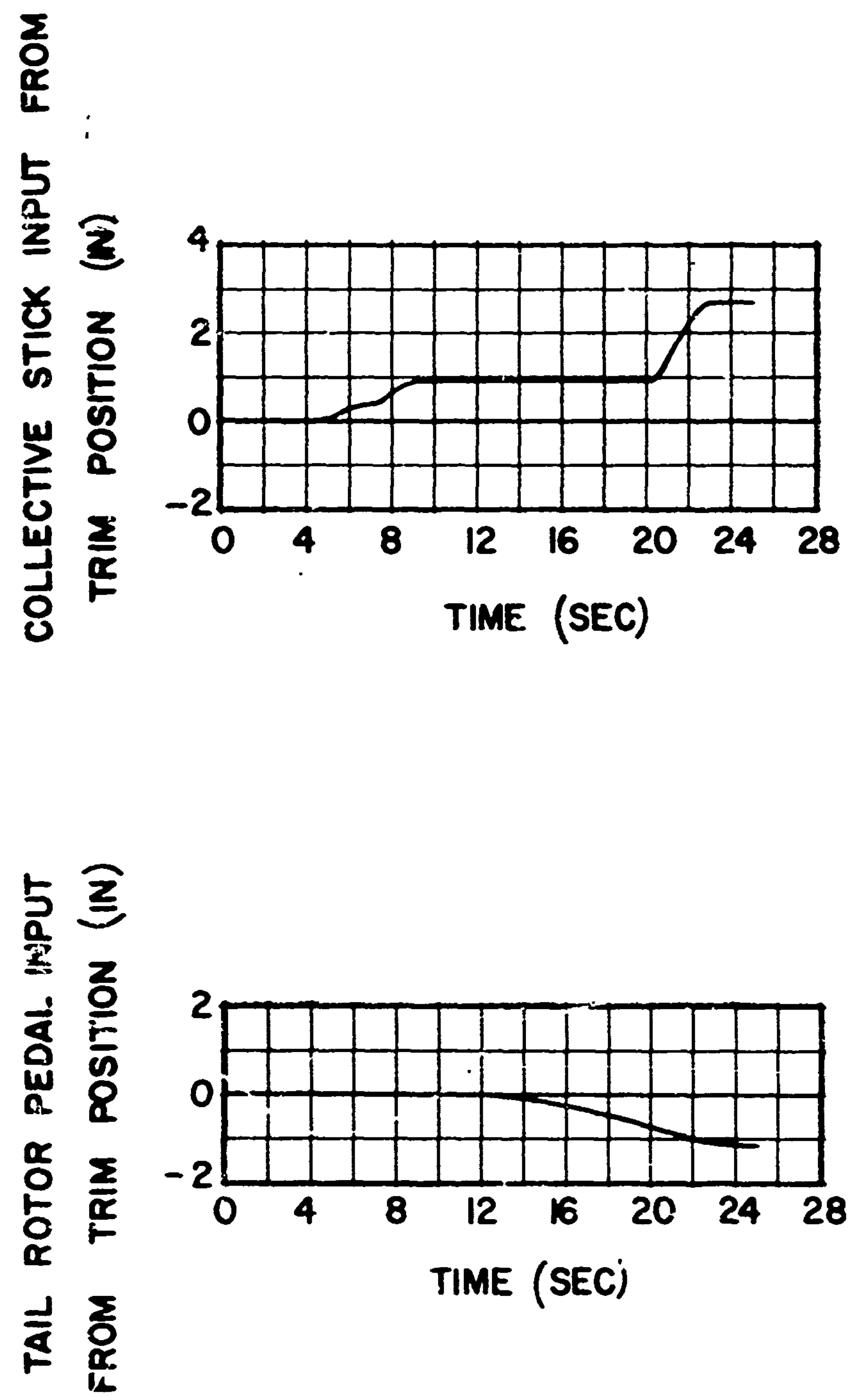

Figure 30. Pilot Control Input for the Simulated Rolling Pullout Maneuver.

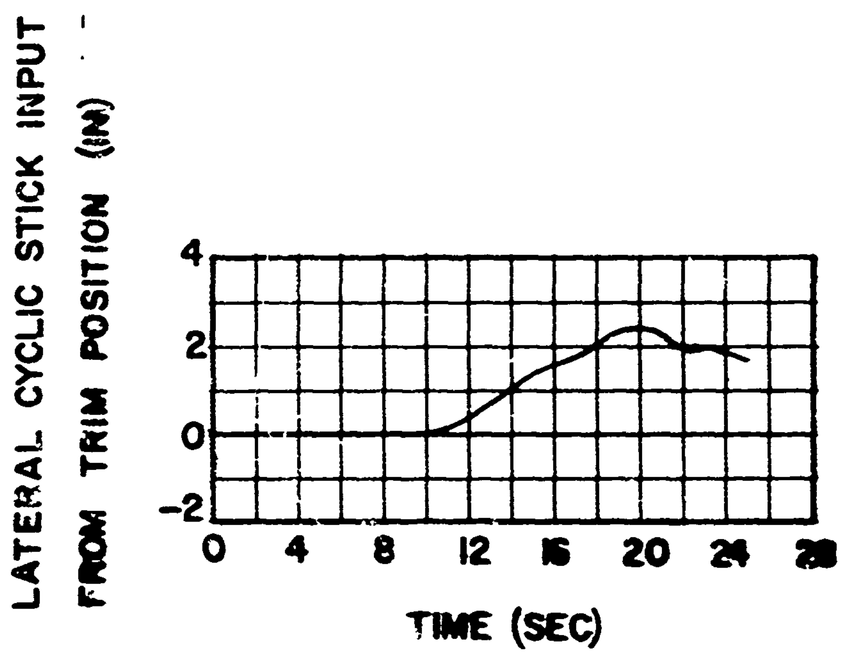

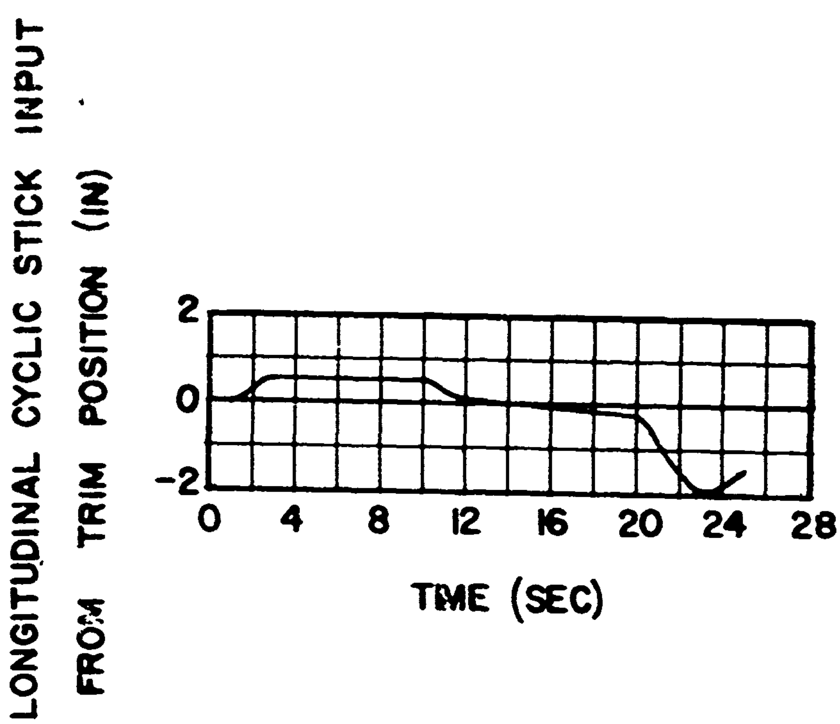

Figure 30. Concluded.

APPENDIX V

SLING AND HARDPOINT LOAD FACTOR DATA UTILIZATION TECHNIQUES

To establish useful design criteria for external suspension system components with slung load type as a parameter, two assumptions must be made. First, it must be assumed that the helicopter can attain its design load factor with an externally suspended load. Second, it must be assumed that the helicopter can attain its design load factor with every type of slung load. Table I indicates that the maximum helicopter load factor attained varied with external load type. Table I also indicates that the design load factor of 2.5 for the CH-54A was never achieved during any of the maneuvers. Therefore, a method for adjusting the load factor data is necessary in determining useful design criteria.

Within a given slung load type, the maximum load factor pulled at the helicopter always occurred during the symmetrical dive and pullout. The $N_{Z_{max}}$ data in Table I have been corrected for any unexact variation in value which may have occurred as the main rotor approached stall during any of the more severe maneuvers. Table I indicates that the maximum load factor pulled at the helicopter over the entire field of slung load types was 2.0. Therefore, it is assumed that the maximum capability of the helicopter used in the simulation was 2.0.

The highest values of $N_{Z_{max}}$ attained over all the cases simulated occurred during runs 3 and 1G, where, in both cases, $N_{Z_{max}}$ is 2.0. Assuming that this value is the load factor capability of the helicopter, N_Z equal to 2.0 was attained only with the container slung by four points from the helicopter. But all the slung load types for each cg location must be adjusted to this same helicopter capability. All the dynamic load factor data which was collected for runs with pilot inputs which were not scaled down is used in determining design criteria for a helicopter with a design load factor of 2.0.

For all the cases which were run using scaled pilot inputs, the highest $N_{Z_{max}}$ ever attained was 1.45 during run 3s. The scaled input cases were conducted with the intention of gathering data to be used as design criteria for a helicopter with a lower design load factor. Thus, all scaled input data in Table I is used for determining design criteria for a helicopter with a design load factor of 1.45.

The method used to adjust the load factor data for a helicopter capable of pulling a normal load factor of 2.0 with each of the slung loads types attached is as follows:

1. For a particular slung load type (and a particular cg location when applicable), the ratio of 2.0 over the highest value of $N_{Z_{max}}$

within the particular slung load type is determined. (The gust, moving base, and scaled input cases are excluded. The data adjustment methods for these cases are explained subsequently.)

2. The hardpoint and sling member load factor data within the particular slung load type (and the particular cg location when applicable) are then either multiplied by the ratio ($2.0/N_{Z_{max}}$) determined in step (1) if the data are from a roll reversal or symmetric dive and pullout maneuver, or multiplied by this ratio raised to the 0.714 power if the data are from a vertical takeoff maneuver. The resultant sling and hardpoint load factor data then represent the values these various load factors would take if the helicopter were capable of a normal load factor of 2.0 with the particular slung load type and cg location.

The adjustment method described above can be explained as follows. The vertical takeoff, symmetrical dive and pullout, and roll reversal maneuvers all produce high load factors. A high normal load factor N_Z at the helicopter can be expected to create high load factors at slings and hardpoints. Let N_s represent any of the sling or hardpoint load factors. This study is based on the relation

$$N_s = (\text{constant})\,(N_Z) \tag{156}$$

Therefore, the same helicopter - external load flown through the same type of maneuver. where N_Z varies between two cases a and b (because the maneuver is flown more severely in one case than the other), the variation in N_s is given by

$$\frac{N_s(\text{case b})}{N_s(\text{case a})} = \frac{N_Z(\text{case b})}{N_Z(\text{case a})} \tag{157}$$

For a given helicopter, the variation of N_Z during a vertical takeoff is not the same as it would be during a symmetrical dive and pullout or roll reversal. For either the pullout or reversal maneuver, N_Z is proportional to control power, while for the vertical takeoff, N_Z is proportional to thrust. The maneuver which produced the highest value of $N_{Z_{max}}$ within each set of runs for a particular slung load type was the symmetrical dive and pullout. Within a particular slung load type set of runs, assume that the full control power capability of the helicopter corresponds to the control power which was utilized during the maneuver which yielded this highest value of $N_{Z_{max}}$ For two different pullout cases, the relation between N_Z and control power would be

$$\frac{N_Z(\text{case b})}{N_Z(\text{case a})} = \frac{\text{control power (case b)}}{\text{control power (case a)}} \tag{158}$$

If eq (158) is applied to two specific cases of interest - the simulated case which produced the highest $N_{Z_{max}}$ for a particular slung load type, and the desired case which would represent the same type maneuver executed severely enough for $N_{Z_{max}}$ to equal 2.0 - the control power needed to attain the desired value of $N_Z = 2.0$ can be obtained from the relation

$$\frac{\text{control power (needed)}}{\text{control power (maximum simulated)}} = \frac{2.0}{N_{Z_{max}}} \tag{159}$$

If the helicopter now had this increased capability, then, from eq (157), the N_s data taken from the actual simulation is adjusted according to the equation

$$N_s(\text{adjusted}) = \frac{2.0}{N_{Z_{max}}} \cdot N_s(\text{simulated}) \tag{160}$$

Eq (160) applies to N_s data taken from symmetric dive and pullout or roll reversal maneuvers.

The vertical takeoff data must be handled differently because N_Z is proportional to thrust rather than control power during this maneuver. For most helicopters, irregardless of size, the relation between thrust and control power can be approximated by saying thrust is proportional to the control power raised to the 0.714 power. For two different vertical takeoff cases the relations between N_Z and control power can then be expressed as

$$\frac{N_Z(\text{case b})}{N_Z(\text{case a})} = \left[\frac{\text{control power (case b)}}{\text{control power (case a)}}\right]^{0.714} \tag{161}$$

But the control power has been adjusted to allow an N_Z capability of 0.2, so substituting eq (159) into eq (161) yields

$$\frac{N_Z(\text{case b})}{N_Z(\text{case a})} \quad \left[\frac{2.0}{N_{Z_{max}}}\right]^{0.714} \tag{162}$$

Substituting this relation into eq (157) thus indicates that the value of N_s taken from vertical takeoff maneuvers should be adjusted by the relation

$$N_s(\text{adjusted}) = \left[\frac{2.0}{N_{Z_{max}}}\right]^{0.714} N_s(\text{simulated}) \qquad (163)$$

The adjusted values of sling and hardpoint load factor data determined from either eq (160) or eq (163) represent the values these quantities would take if the helicopter were capable of a load factor of $N_Z = 2.0$ with specific slung load type attached.

All of the data from runs using scaled inputs is adjusted in a similar manner to represent sling and hardpoint load factor values attained for the slung load attached to a helicopter with a capability of $N_Z = 1.45$. This is the highest value of $N_{Z_{max}}$ ever attained during all of scaled input runs. Therefore, the ratios by which N_s values are adjusted for these cases are $(1.45/N_{Z_{max}})$ and $(1.45/N_{Z_{max}})^{0.714}$, depending on the type of maneuver, where $N_{Z_{max}}$ is the highest value this parameter takes within all the scaled input runs for the particular slung load type (and cg location) being investigated at the moment.

To determine data points for a helicopter capable of $N_Z = 2.5$ with an externally suspended load, the data which were adjusted for $N_Z = 2.0$ are extrapolated to the highest design load factor. The extrapolation is done linearly by multiplying the N_s values which were adjusted for $N_Z = 2.5$ by either the ratio (2.5/2.0 or $(2.5/2.0)$,$^{0.714}$ depending on whether the data being extrapolated are from a pullout or reversal maneuver or from a vertical takeoff maneuver.

In addition to the sling and hardpoint load factor data which have been modified to represent data from a helicopter with an N_Z capability of 1.45, 2.0, and 2.5, the data from Table II are used to specify the values these load factor parameters assume during trim ($N_Z = 1.0$).

Figures 31 through 40 show the various manipulated sling and hardpoint load factor data plotted at the appropriate helicopter design load factor for which the data were adjusted or extrapolated. Only the largest extrapolated value of any N_s parameter is shown on the plots at $N_Z = 2.5$, since only maximum values are of importance in determining design criteria. Trim values of N_s are plotted at $N_Z = 1.0$. The data were modified separately for each slung load type and are grouped this way in the figures. The data were also modified separately for each cg location within slung load types (where applicable), but all of these varying cg location data points have been placed on a single plot, identified only by the slung load type.

A key is given which defines the type of maneuver represented by each datum point which has been plotted. This key is applicable to every figure contained in this appendix.

Key to Symbols Describing Maneuvers in Figures 31 to 44	
▲	Vertical takeoff
⊙	Symmetrical dive and pullout
⊟	Roll reversal
▼	Pedal kick
⬟	Approach to hover
◪	Longitudinal stick stroke
⊙	Lateral stick stroke
▽	Rolling pullout

Symbols with single flags denote data from moving base runs.
Symbols with double flags denote data from runs with gusts.

The data obtained from runs which included gusts are used in a slightly different manner. Since any gust contribution to N_s values should be an addition to the contribution due to the basic maneuver, the method used to obtain the gust data is to find the change in each N_s value between the gust run and the corresponding case without gusts. This change in each N_s value is then added to the N_s value from the run without gusts. The resultant values of N_s are then adjusted in the manner described previously to obtain data for a design load factor of 2.0, and these data are then extrapolated to a design load factor of 2.5. No gust data were calculated for $N_Z = 1.45$ because none of the gust runs were done with scaled pilot inputs. Figures 41 and 42 contain the gust data points as well as the corresponding points which do not include the gust effects. These nongust points are taken from Figures 31 and 33, and are reproduced on the gust data plots for easy comparison. Only the neutral cg data points are taken from Figure 31 and appear on Figure 41 because only the neutral cg configuration of the container slung from four points on the helicopter was simulated with gusts.

The method of utilizing the moving-base data is similar to the method previously described for the fixed-base runs. The ratios $(2.0/N_{Z_{max}})$ and $(2.0/N_{Z_{max}})^{0.714}$ for adjusting the moving base data for a particular slung load type is found by using the highest value of $N_{Z_{max}}$ from among all the moving-base runs for that particular slung load type. Since the rolling pullout is a high load factor producing maneuver, the data from this maneuver are adjusted in the same manner as the roll reversal and symmetrical dive and pullout data. The moving-base data from the maneuvers which are not considered high load factor producing maneuvers (such as the approach to hover) are not adjusted at all, and are plotted directly at

$N_Z = 2.0$. The extrapolation method to $N_Z = 2.5$ is the same as outlined earlier. Figures 43 and 44 are plots of the moving-base data. Also included in these figures for comparison are the corresponding data points for the same slung load type cases from the fixed-base simulation. These additional data points are taken from Figures 31 and 35, but only the neutral cg points are shown on the moving-base plots. No data are shown at $N_Z = 1.45$ because the moving-base runs could not be resimulated with scaled pilot inputs.

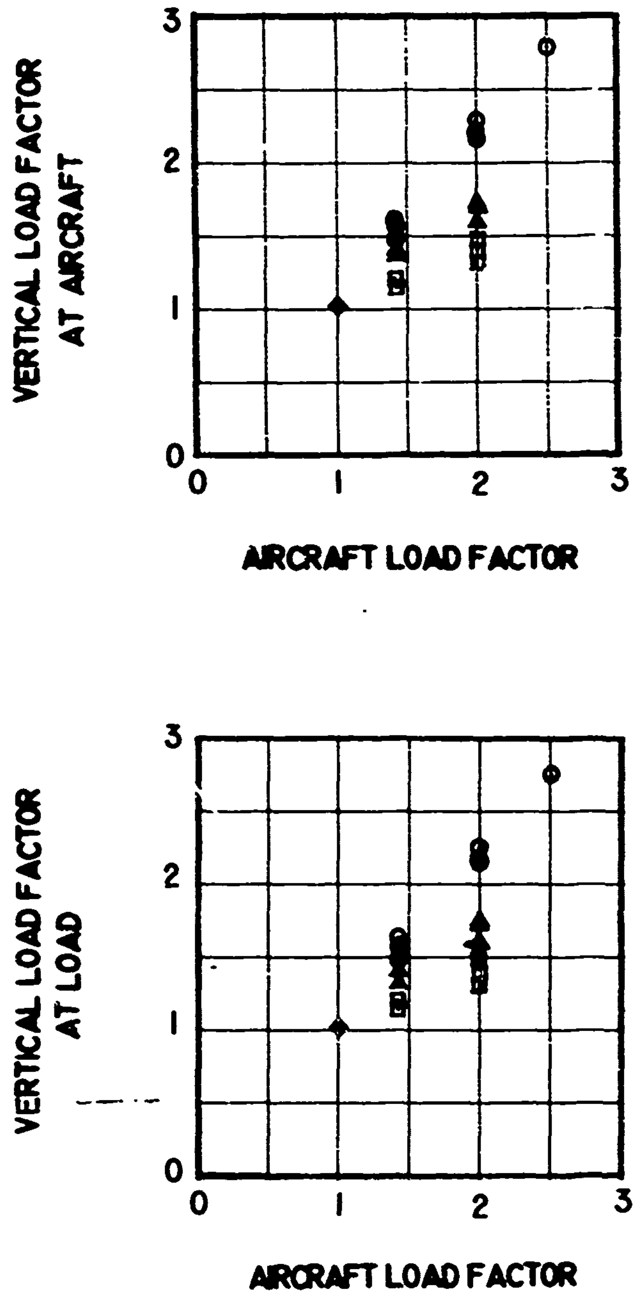

Figure 31. Adjusted Sling and Hardpoint Load Factor Data for the Container - 4 Pt/ 0 Leg Load.

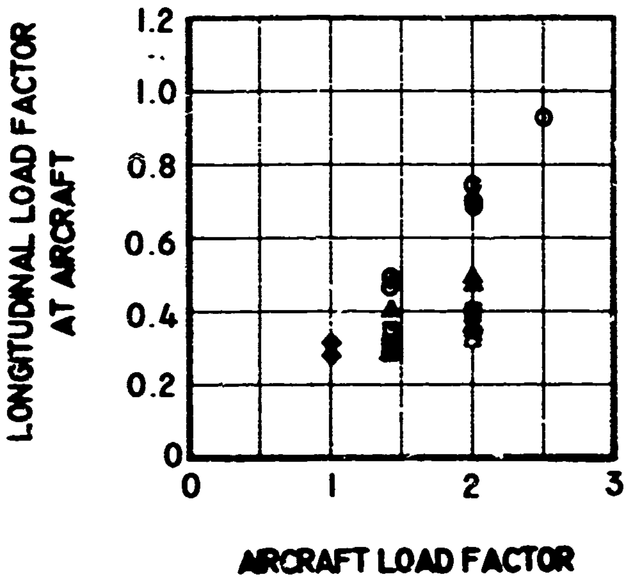

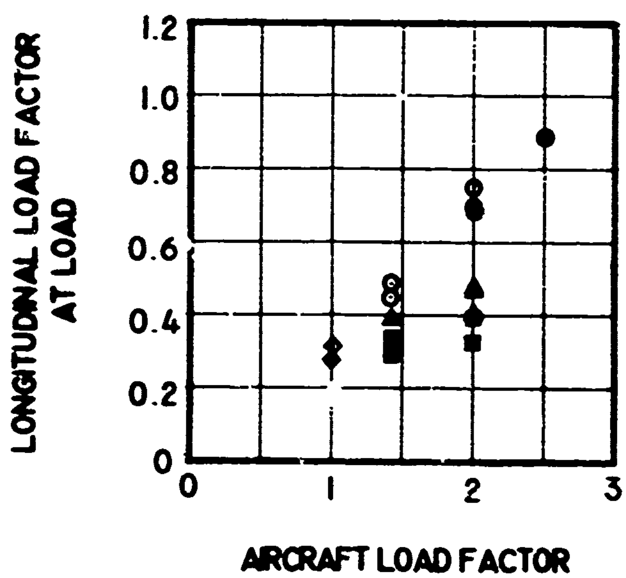

Figure 31. Continued.

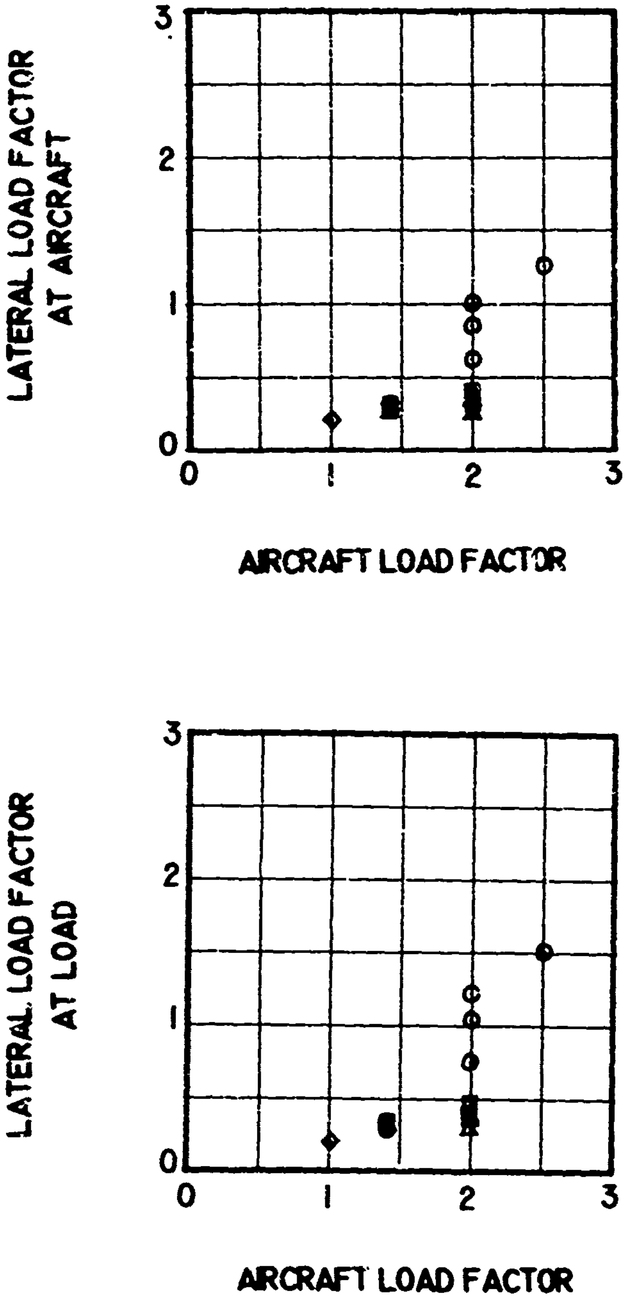

Figure 31. Continued.

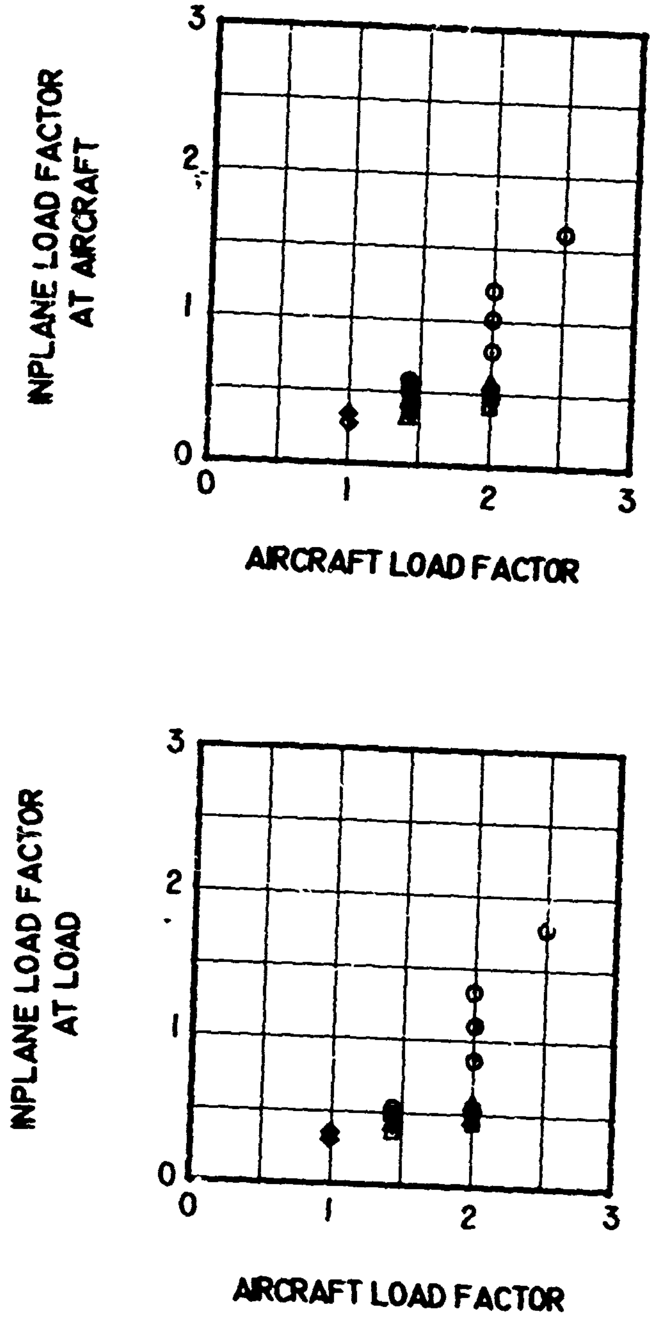

Figure 31. Continued.

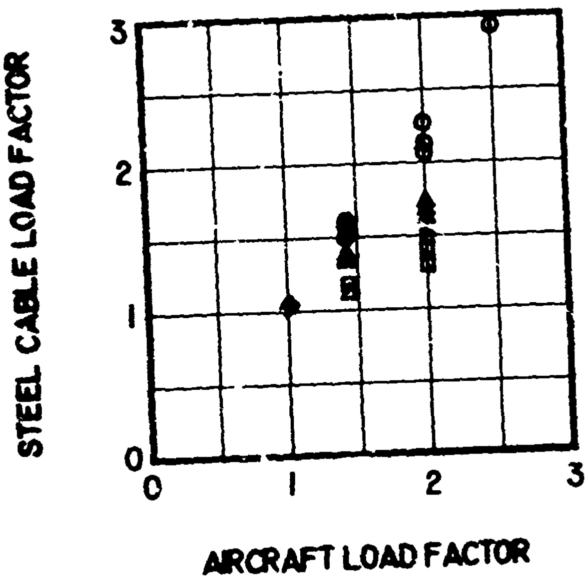

Figure 31. Concluded.

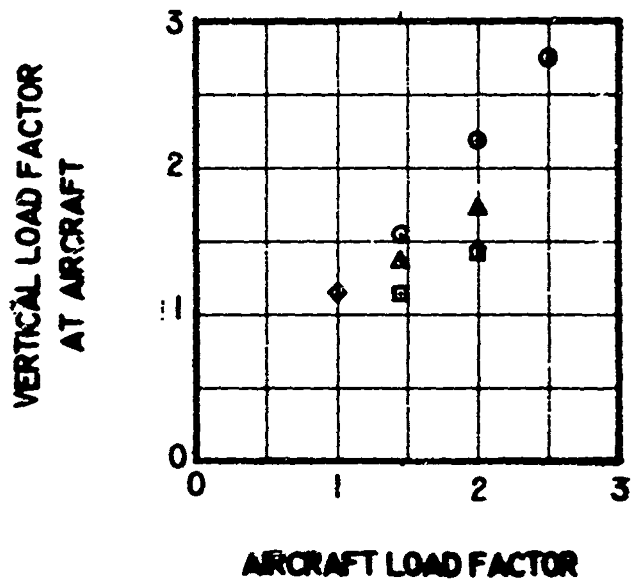

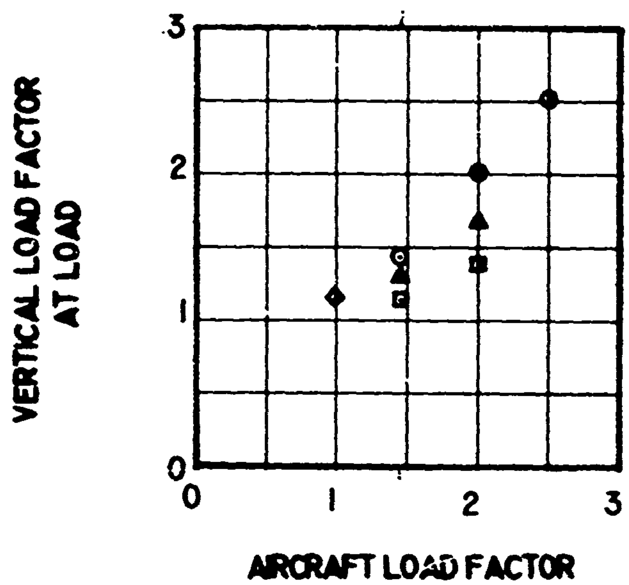

Figure 32. Adjusted Sling and Hardpoint Load Factor Data for the Container - 4 Pt/ 0 Leg, 1 Cable Failed Load.

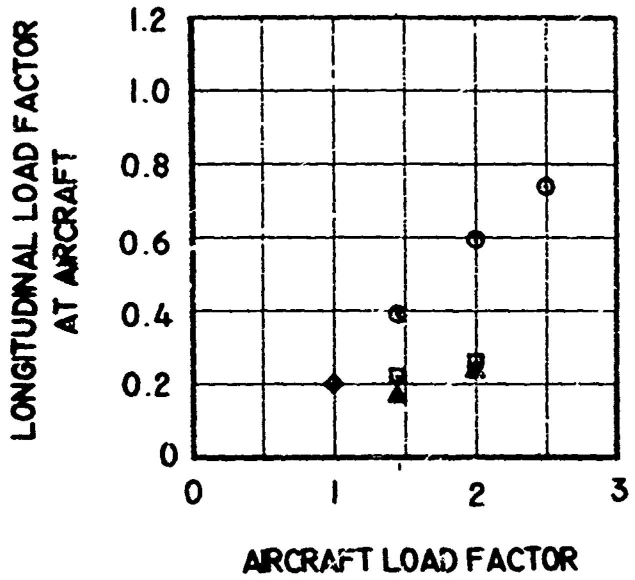

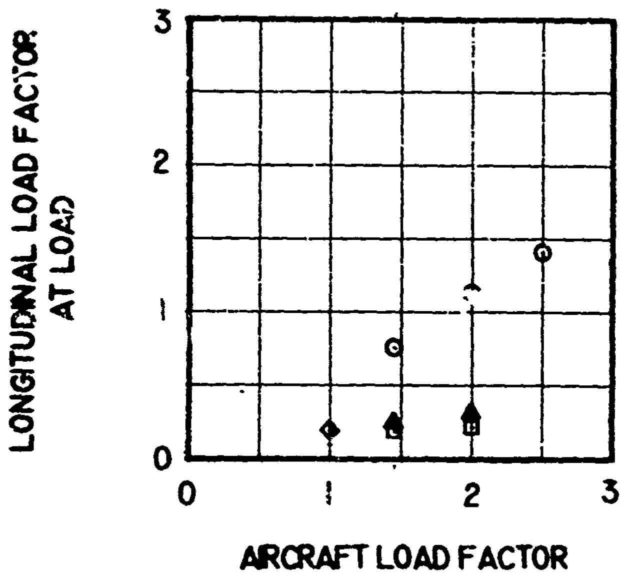

Figure 32. Continued.

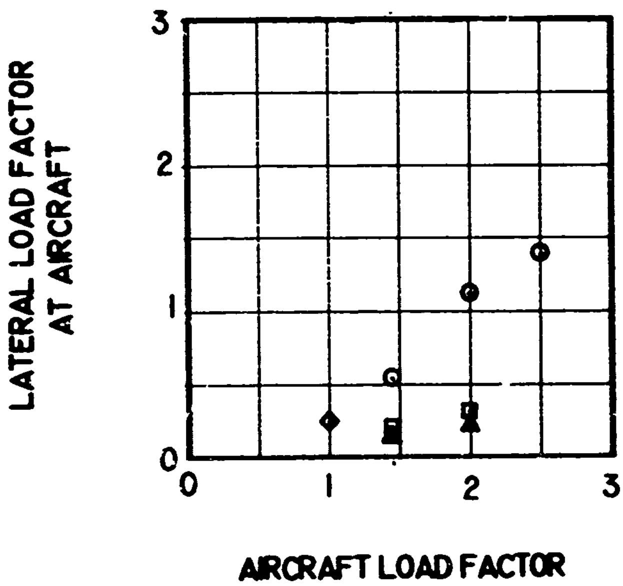

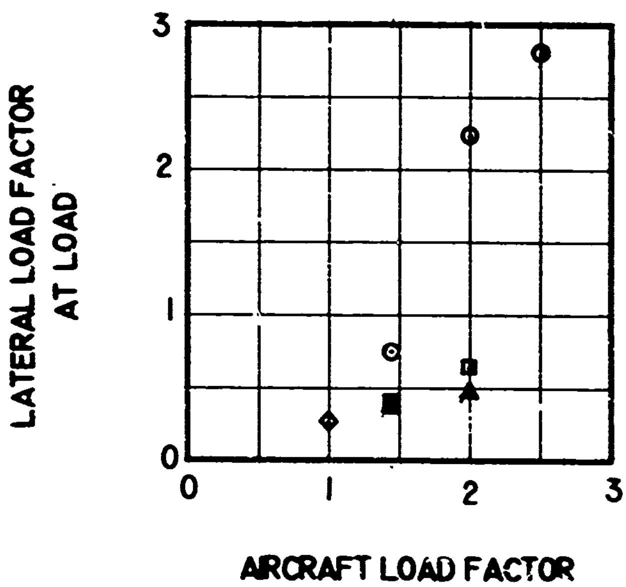

Figure 32. Continued.

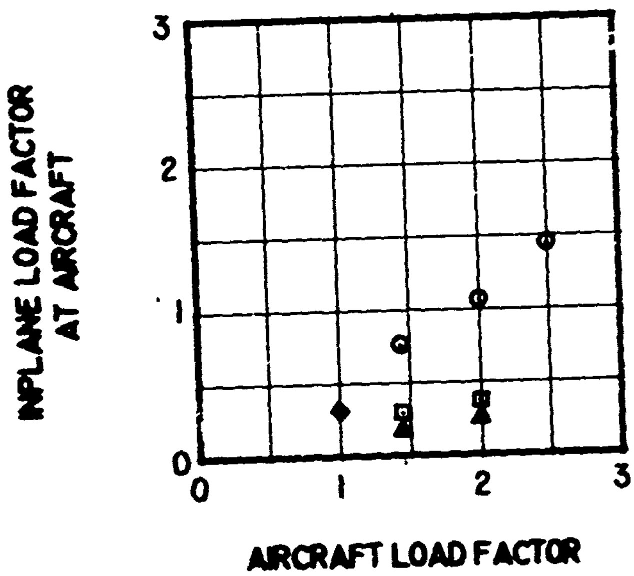

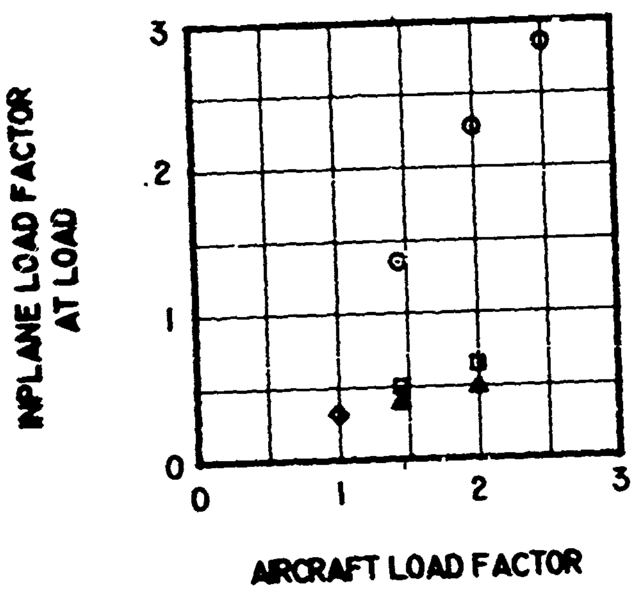

Figure 32. Continued.

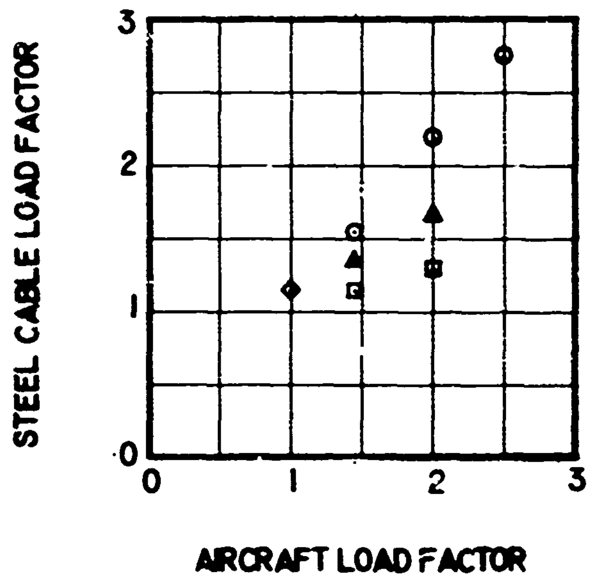

Figure 32. Concluded.

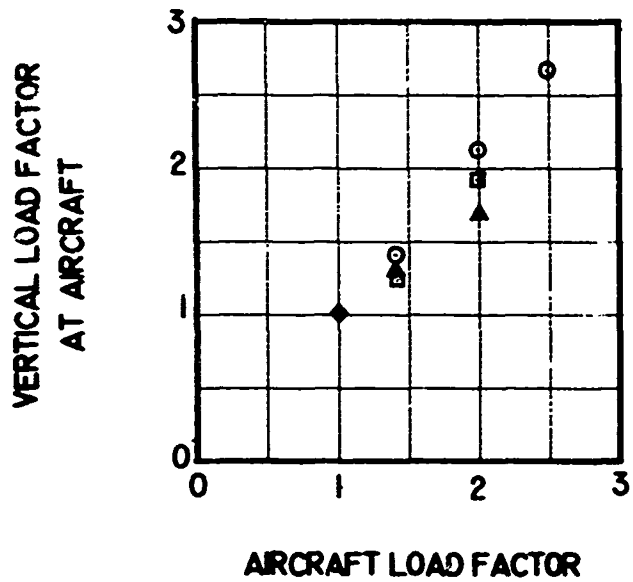

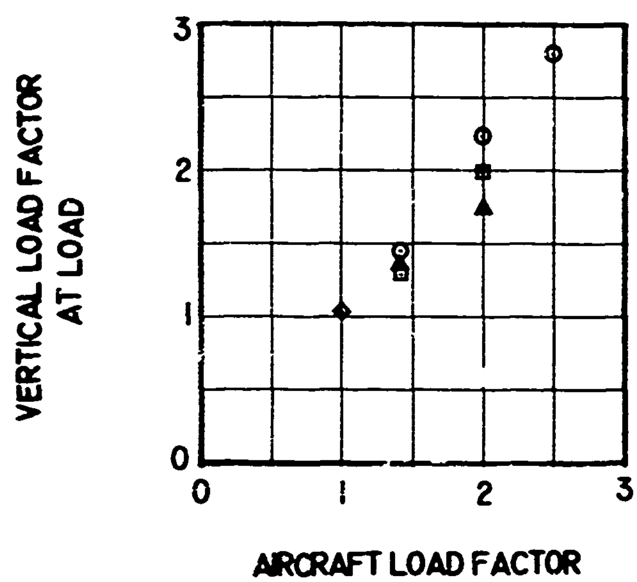

Figure 33. Adjusted Sling and Hardpoint Load Factor Data for the Block - 1 Pt/ 4 Leg Load.

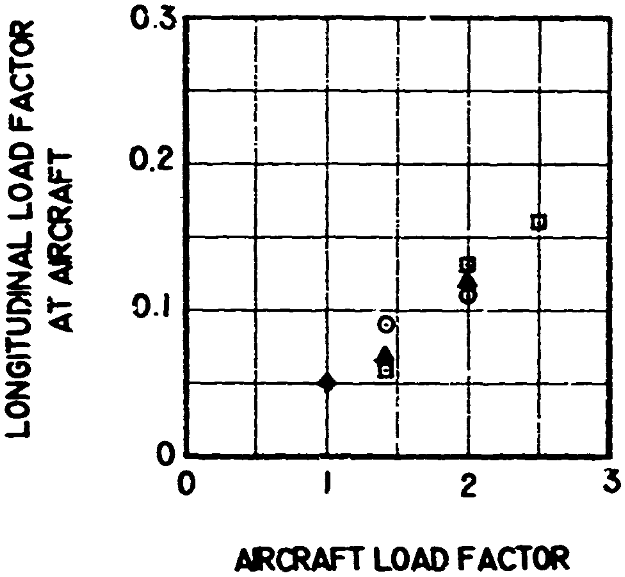

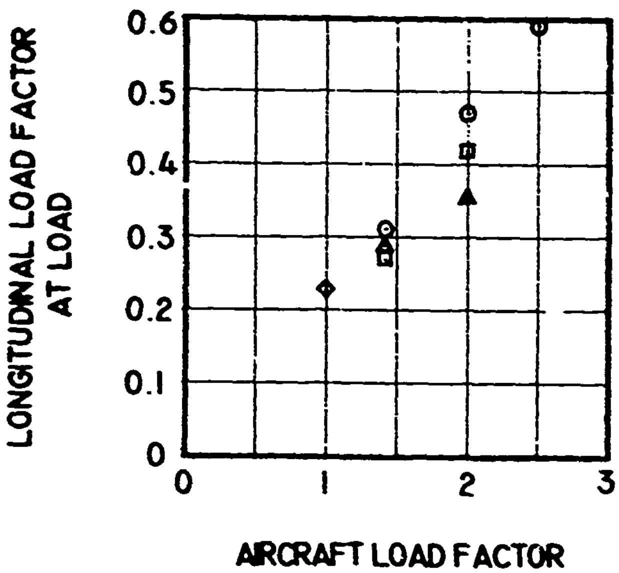

Figure 33, Continued.

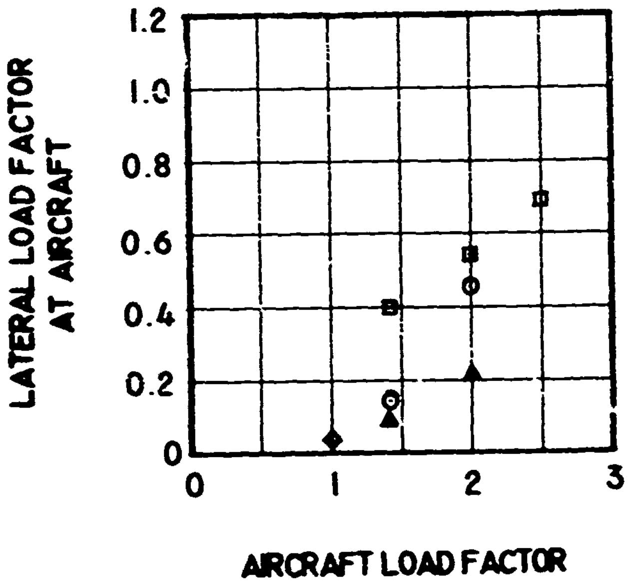

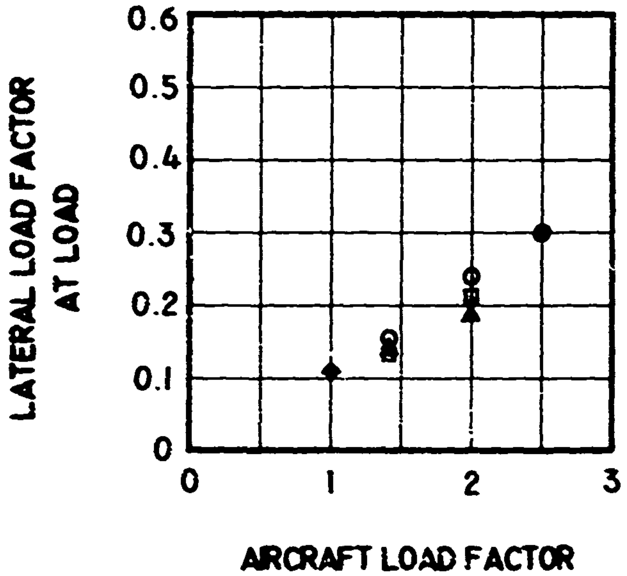

Figure 33. Continued.

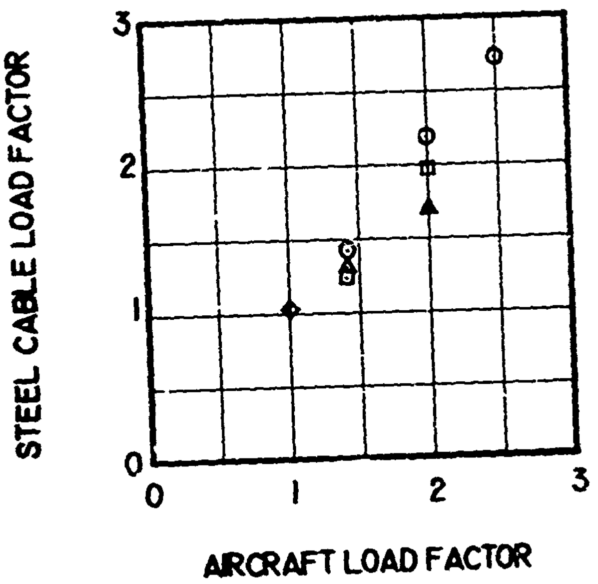

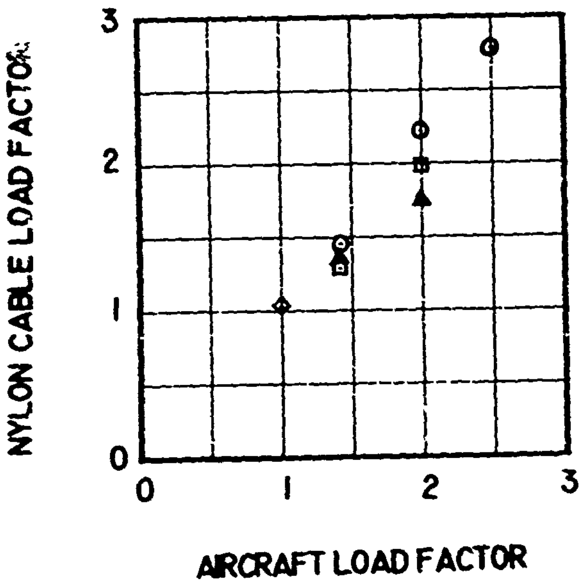

Figure 33. Concluded.

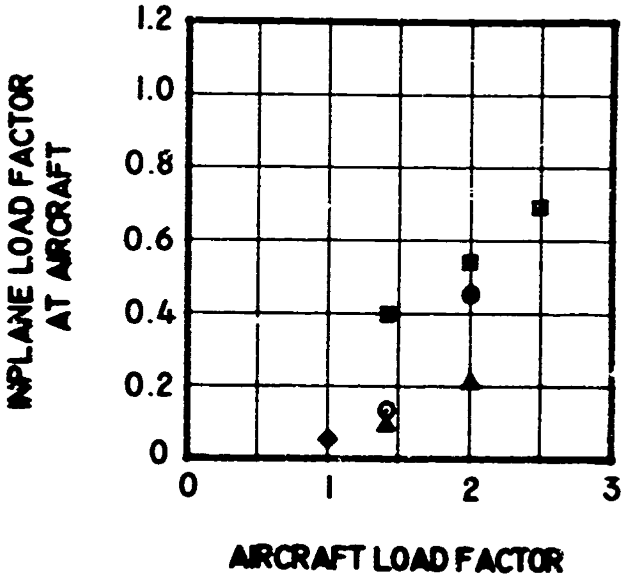

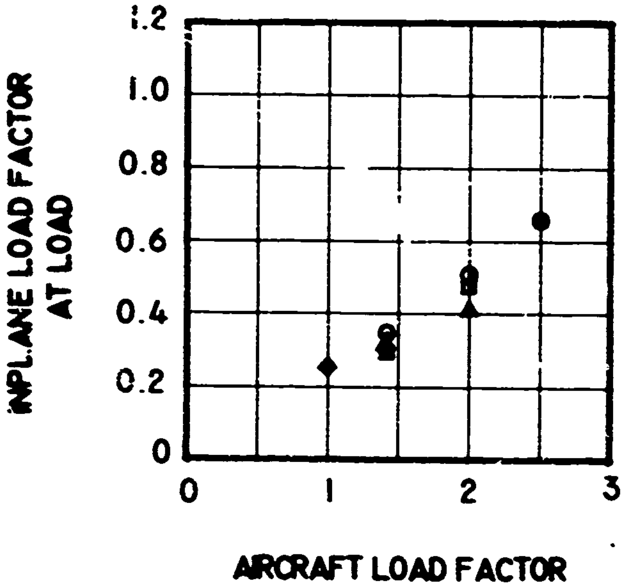

Figure 33. Continued.

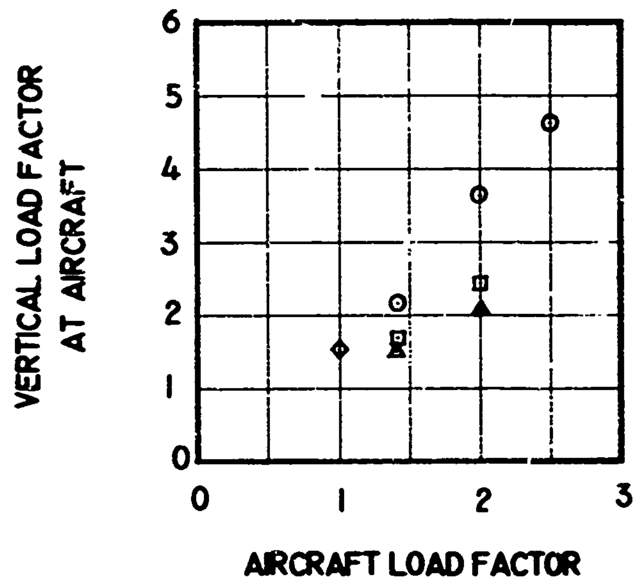

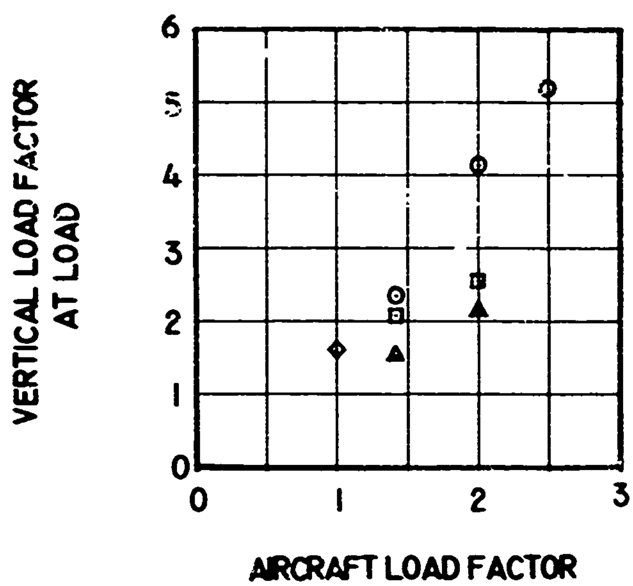

Figure 34. Adjusted Sling and Hardpoint Load Factor Data for the Empty Container - 1 Pt/ 4 Leg Load.

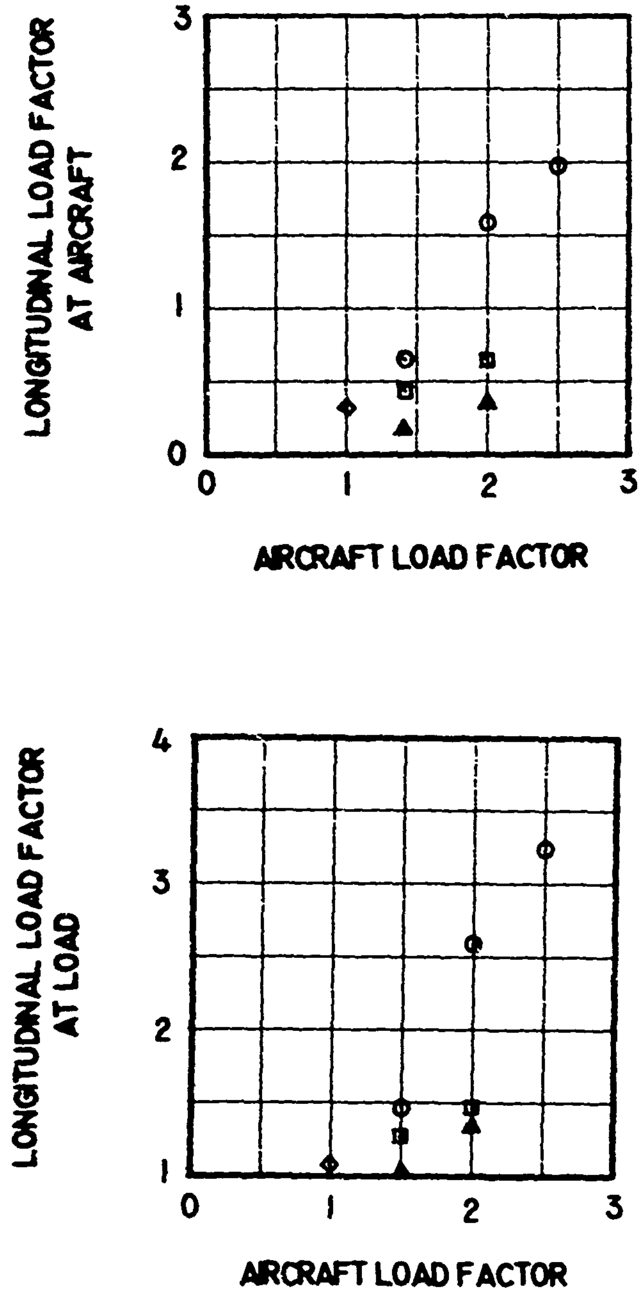

Figure 34. Continued.

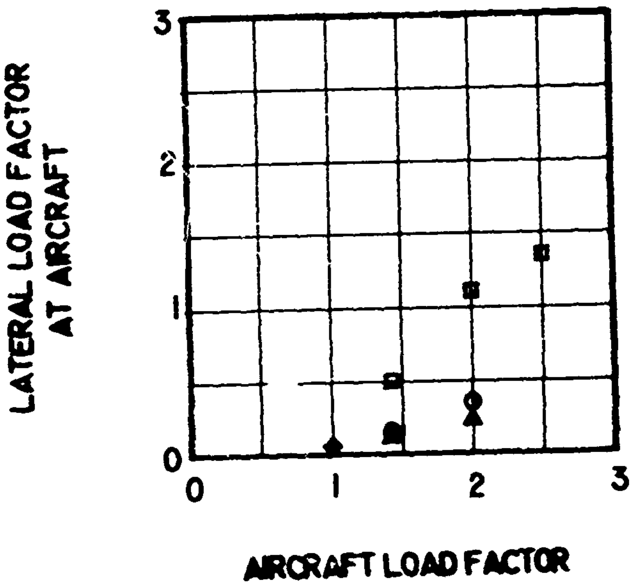

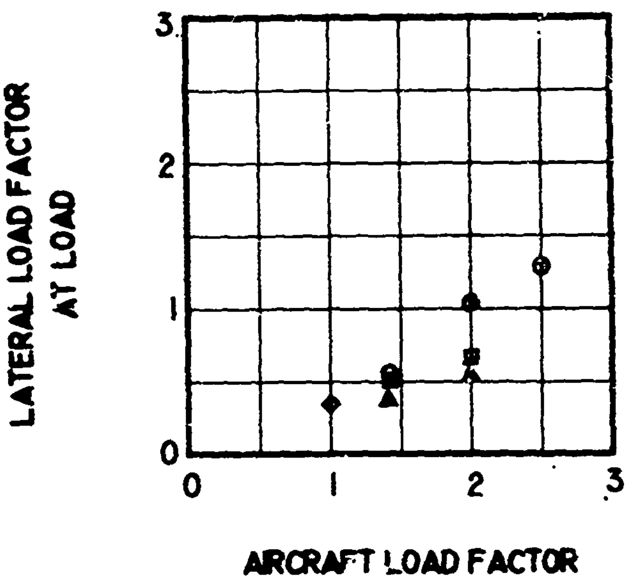

Figure 34. Continued.

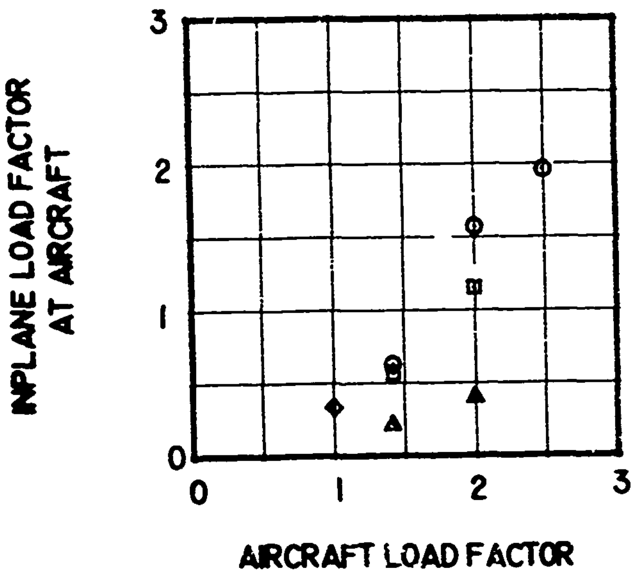

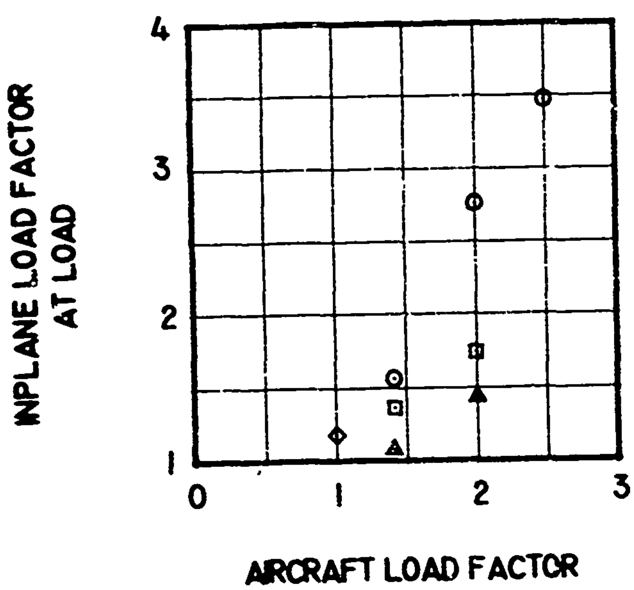

Figure 34. Continued.

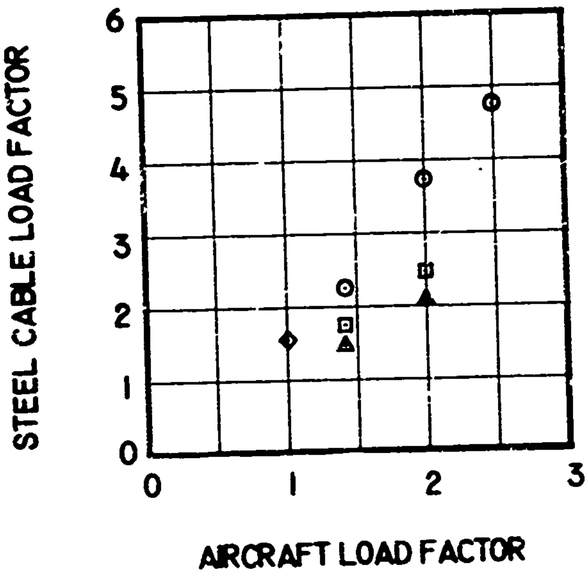

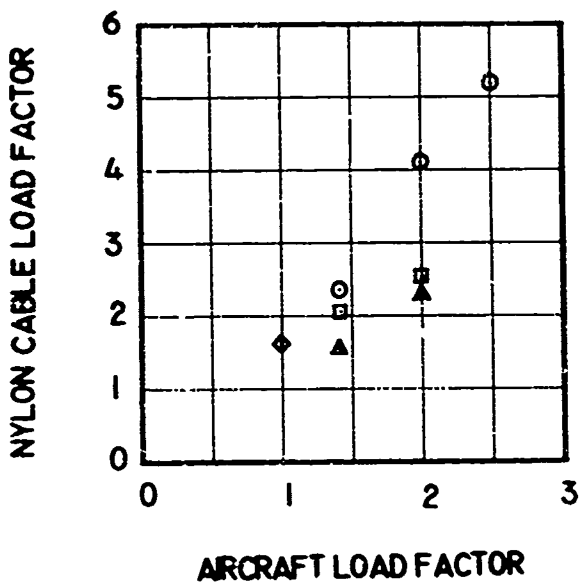

Figure 34. Concluded.

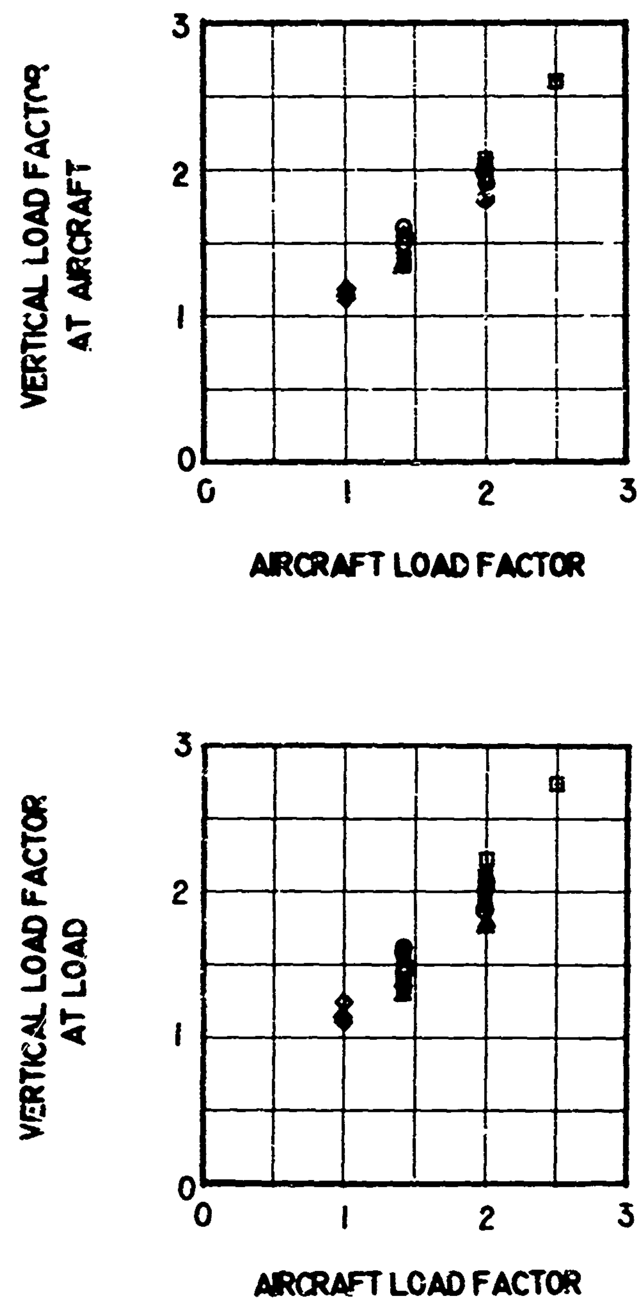

Figure 35. Adjusted Sling and Hardpoint Load Factor Data for the Container - 1 Pt/ 4 Leg Load.

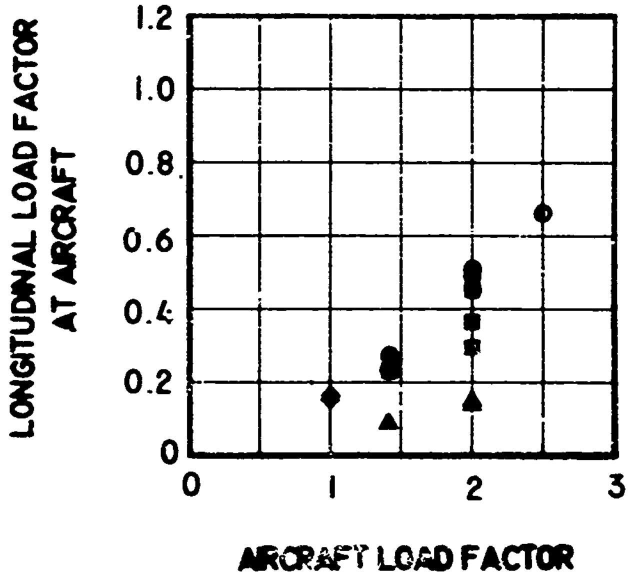

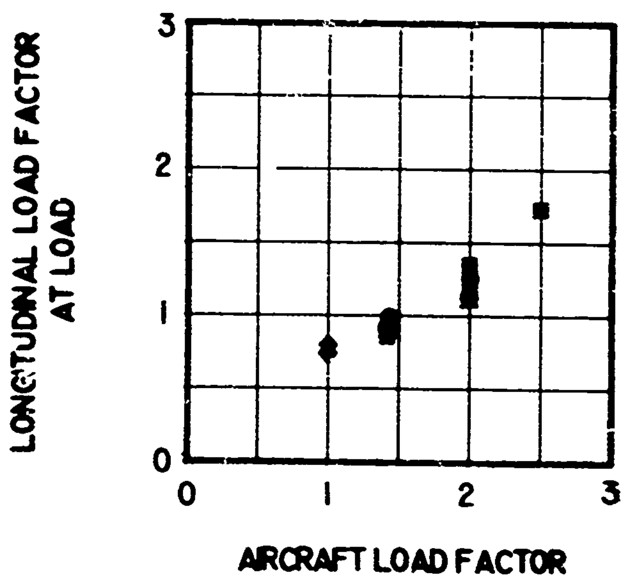

Figure 35. Continued.

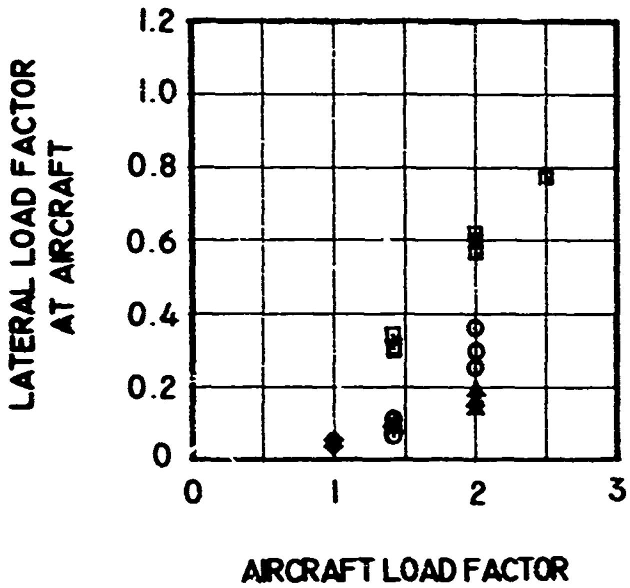

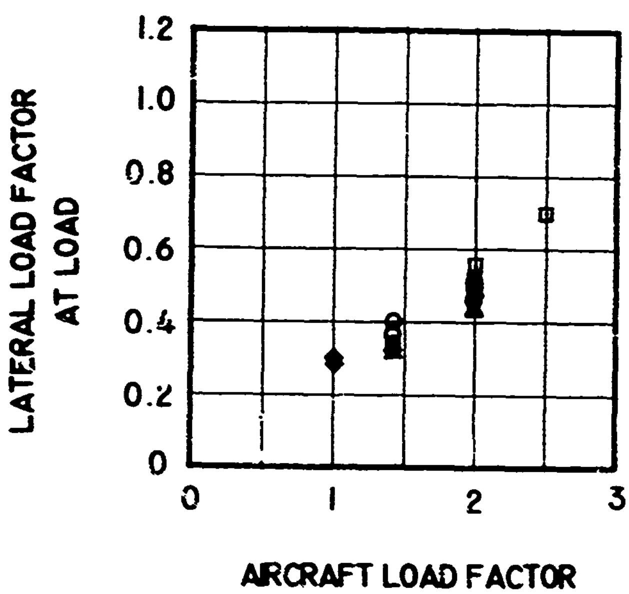

Figure 35. Continued.

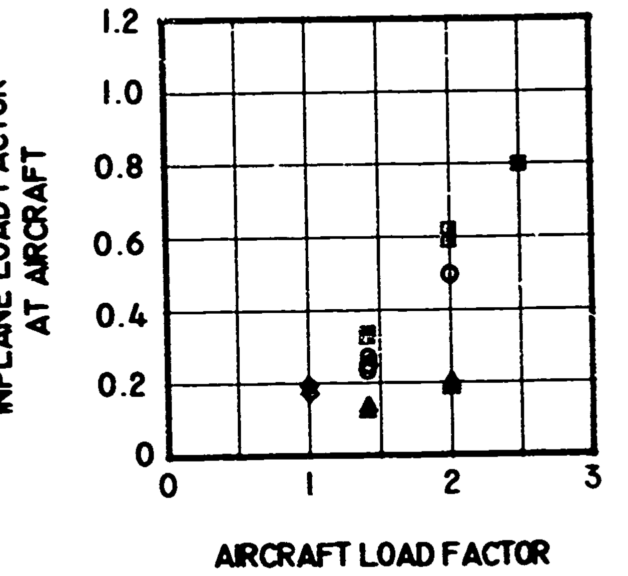

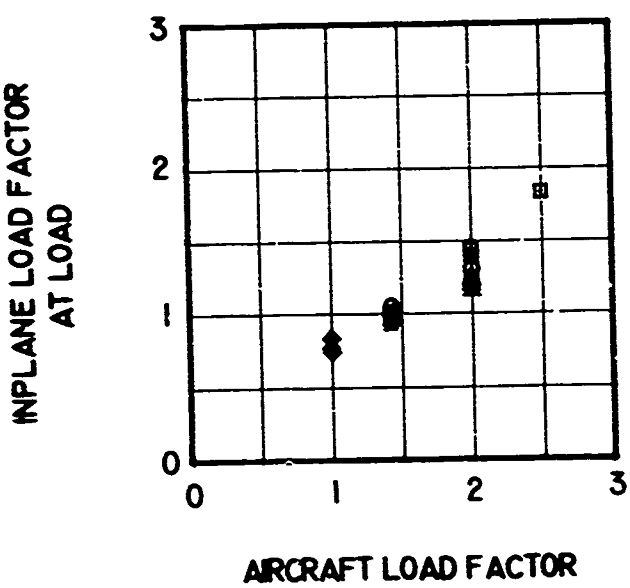

Figure 35. Continued.

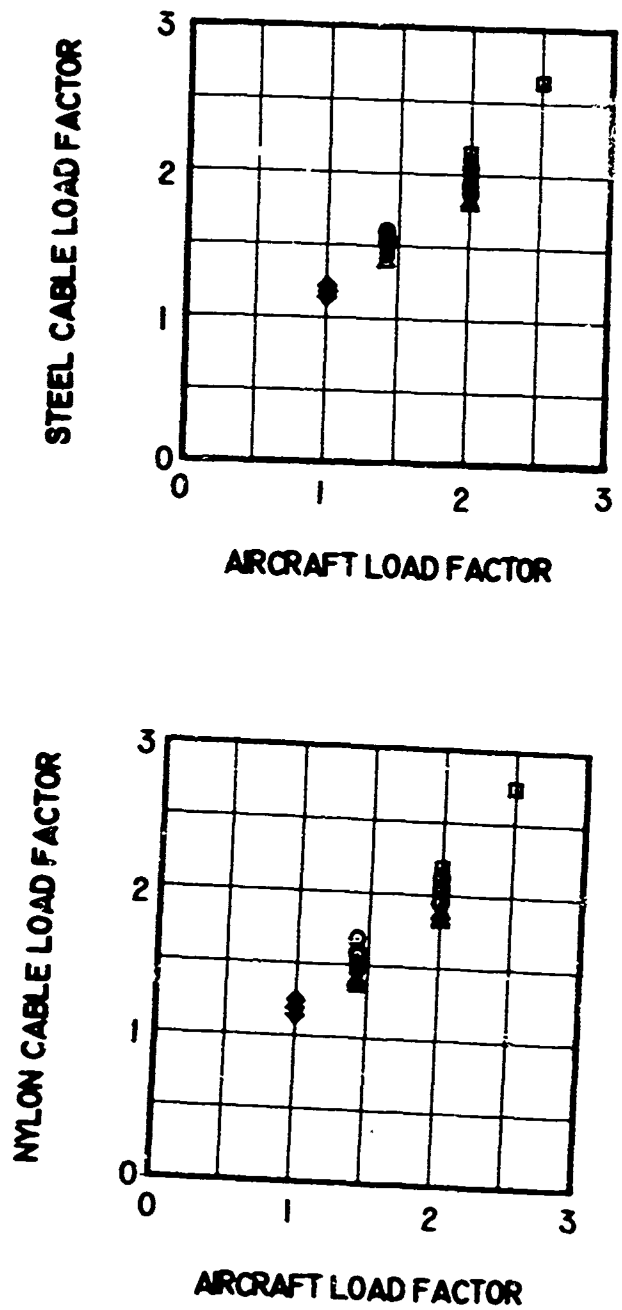

Figure 35. Concluded.

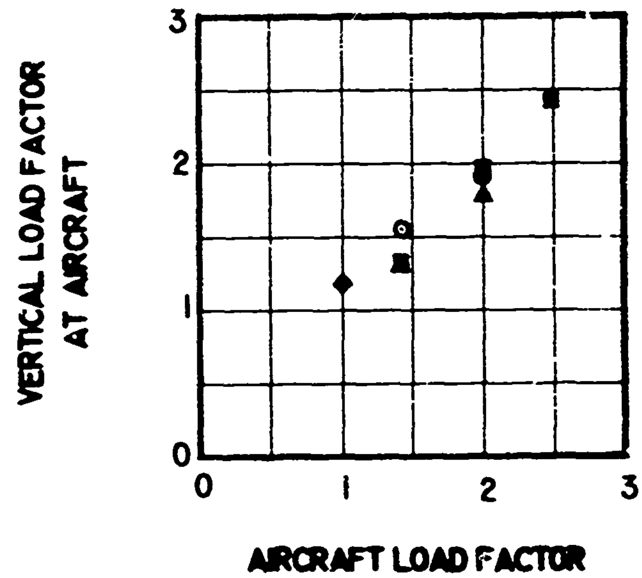

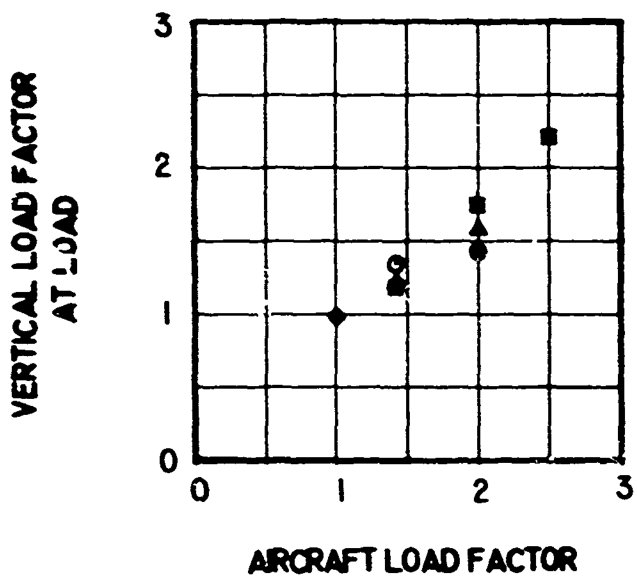

Figure 36. Adjusted Sling and Hardpoint Load Factor Data for the Container - 1 Pt/ 4 Leg, 1 Leg Failed Load.

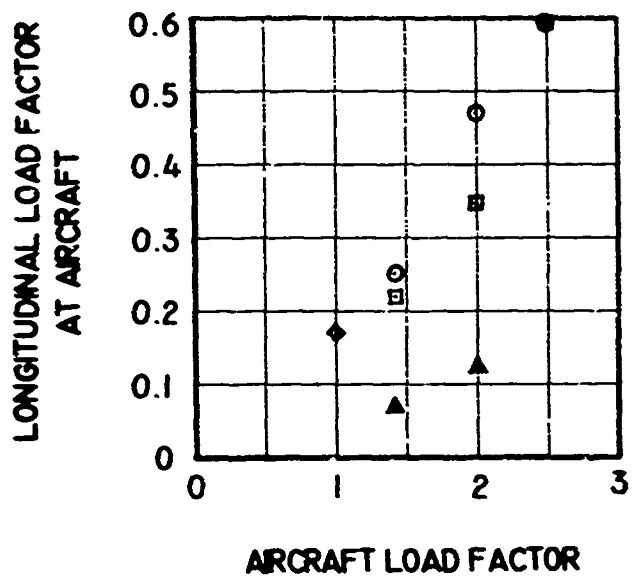

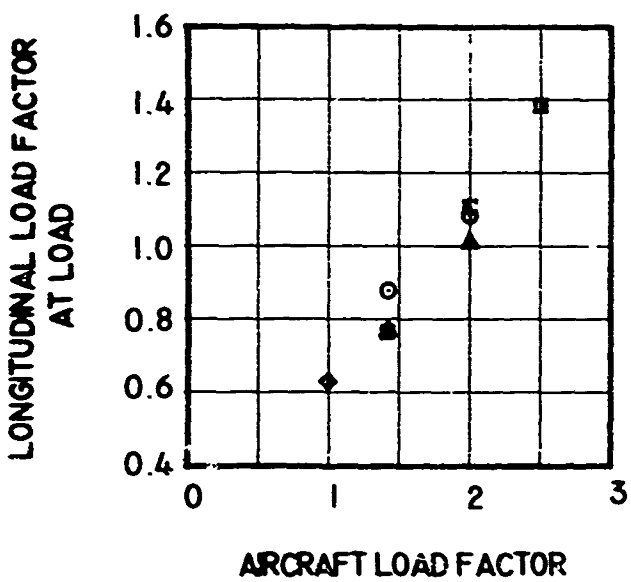

Figure 36. Continued.

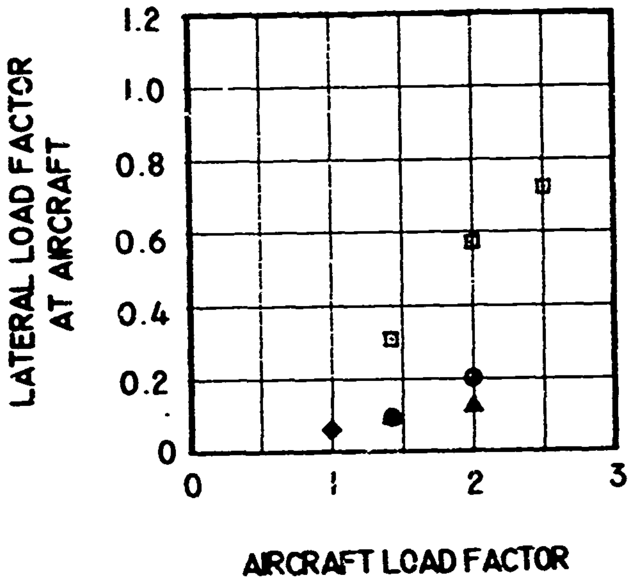

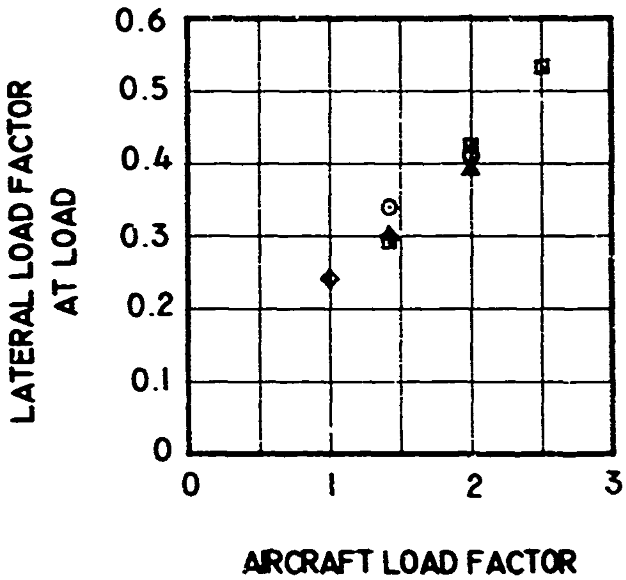

Figure 36. Continued.

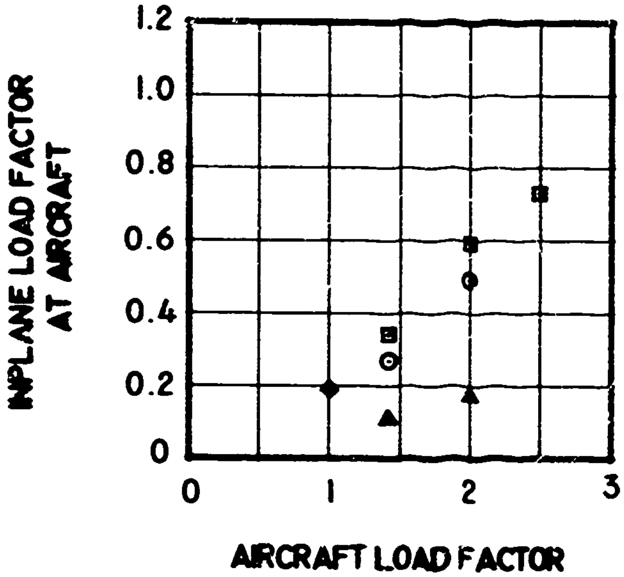

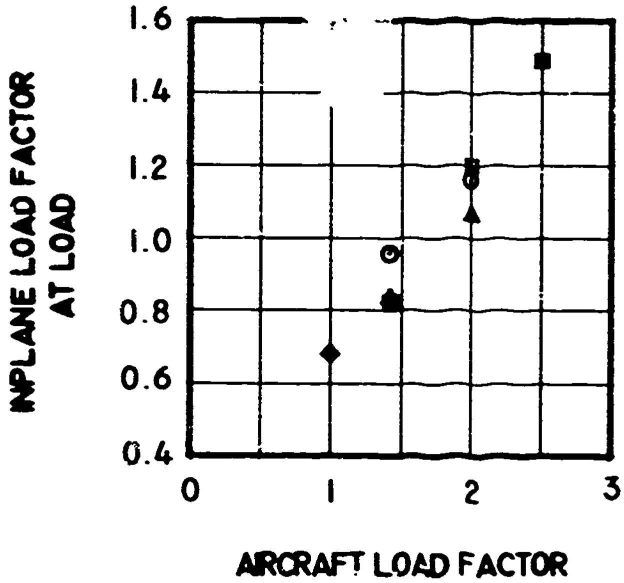

Figure 36. Continued.

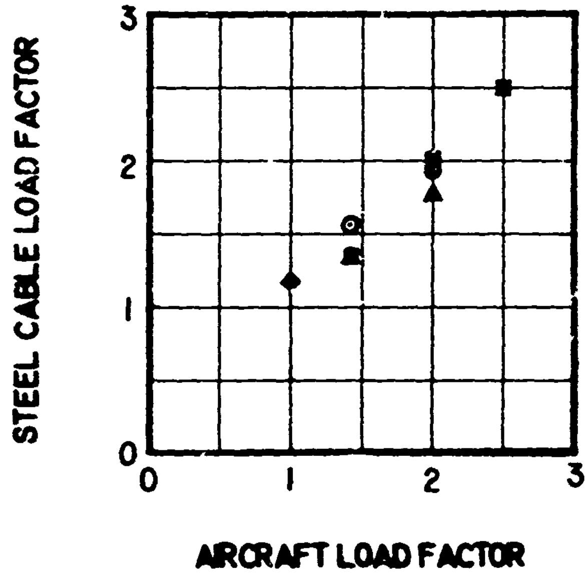

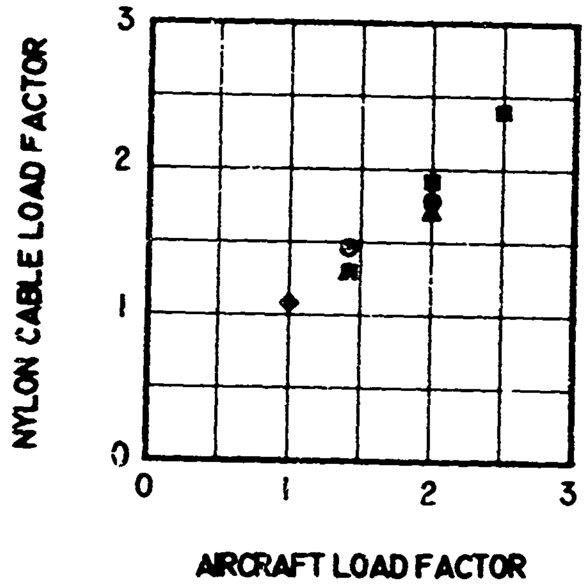

Figure 36. Concluded.

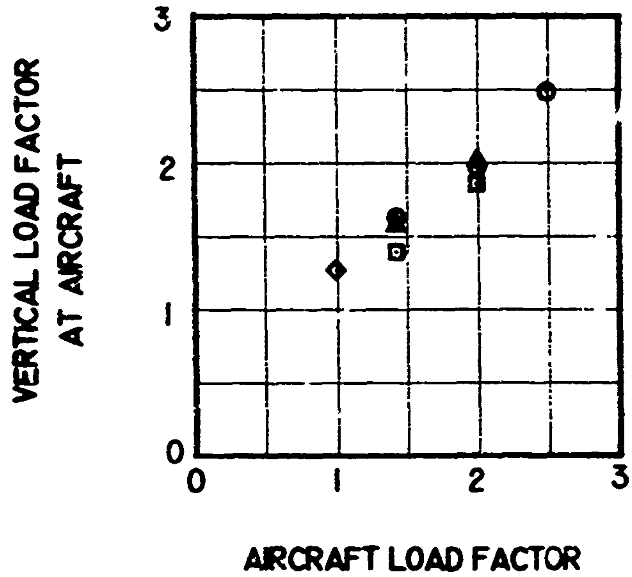

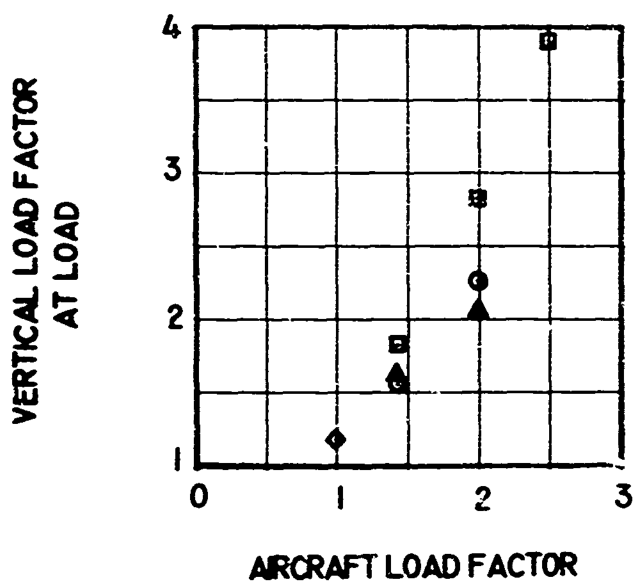

Figure 37. Adjusted Sling and Hardpoint Load Factor Data for the CH-47 - 1 Pt/ 4 Leg Load.

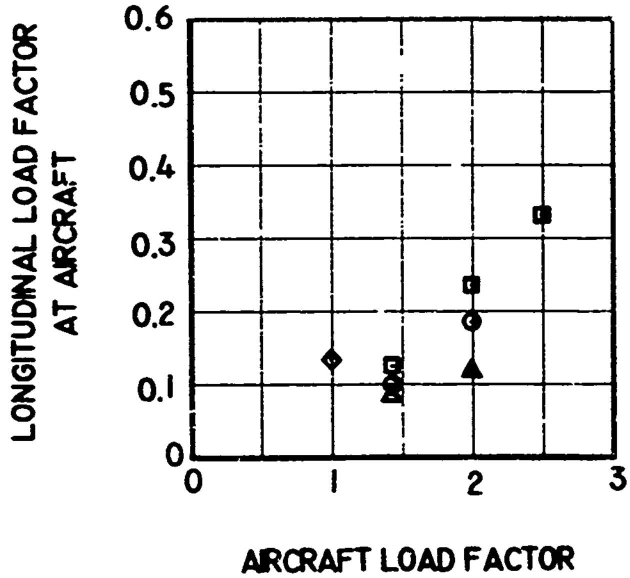

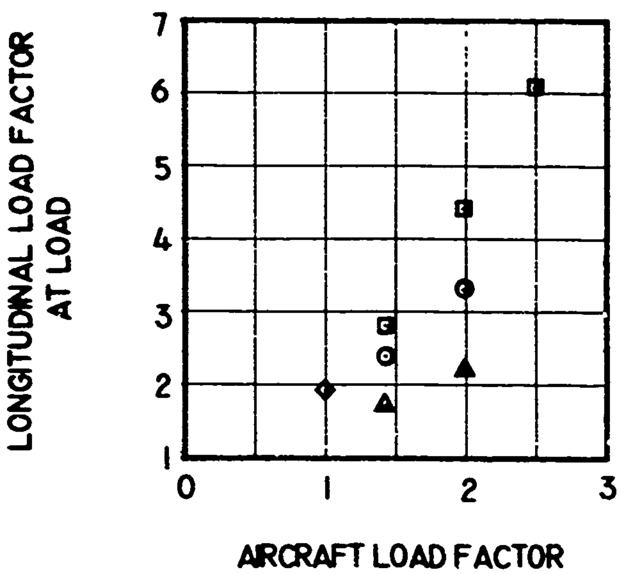

Figure 37. Continued.

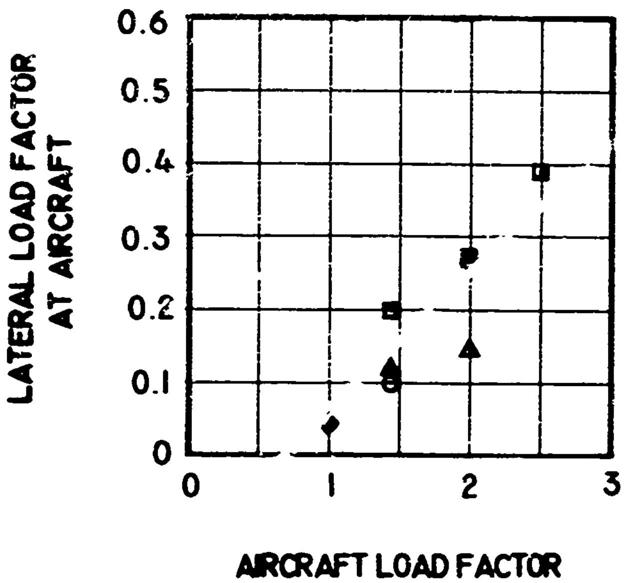

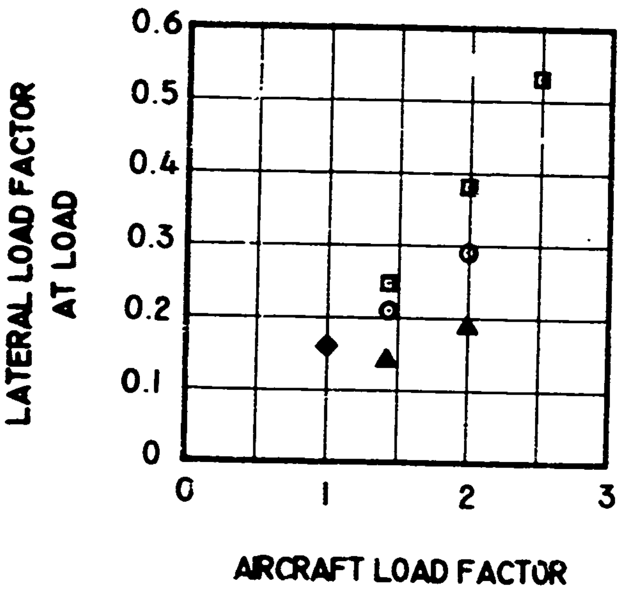

Figure 37. Continued.

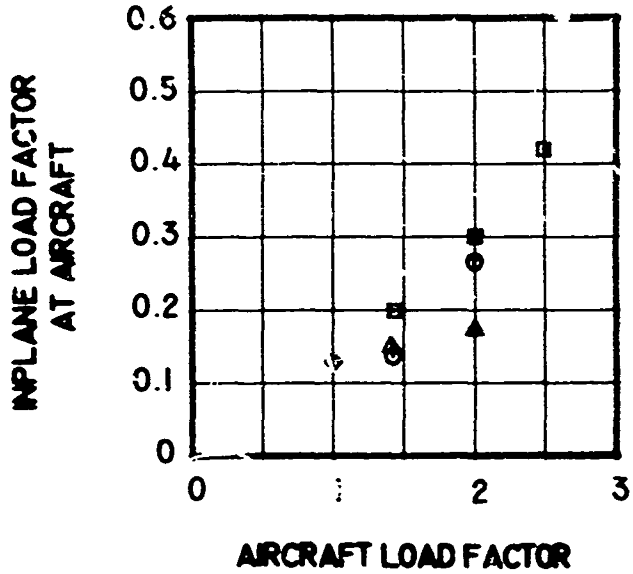

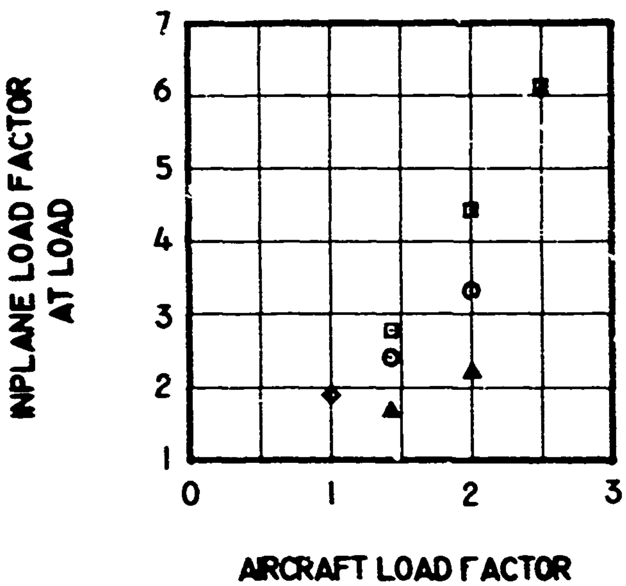

Figure 37. Continued.

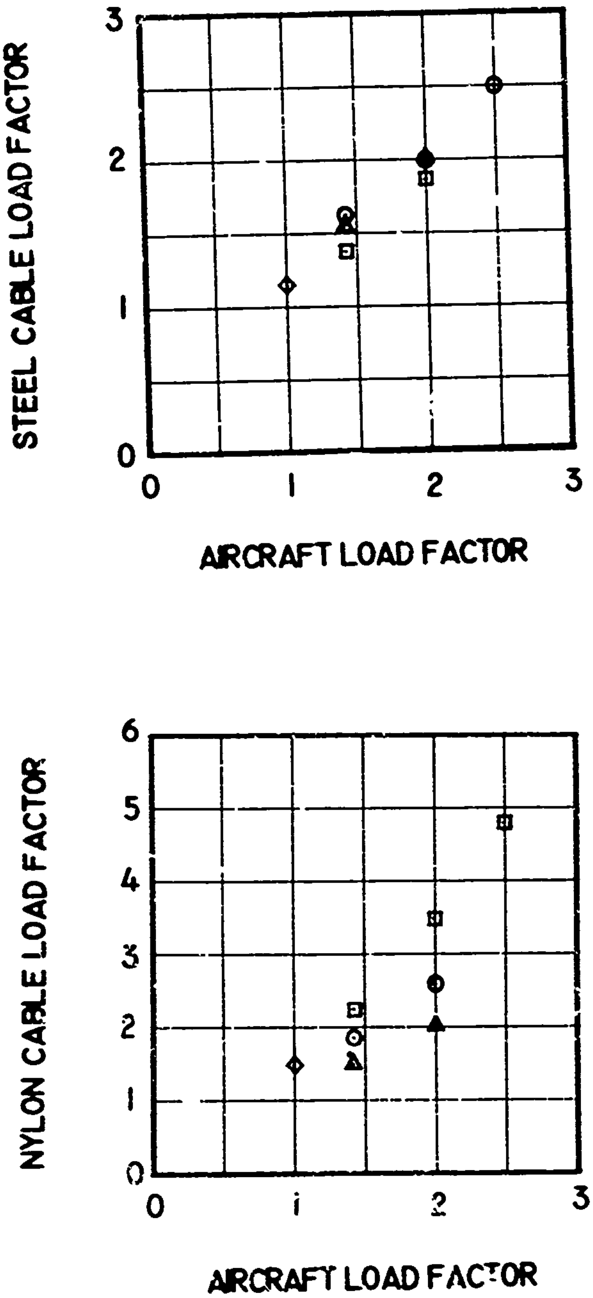

Figure 37. Concluded.

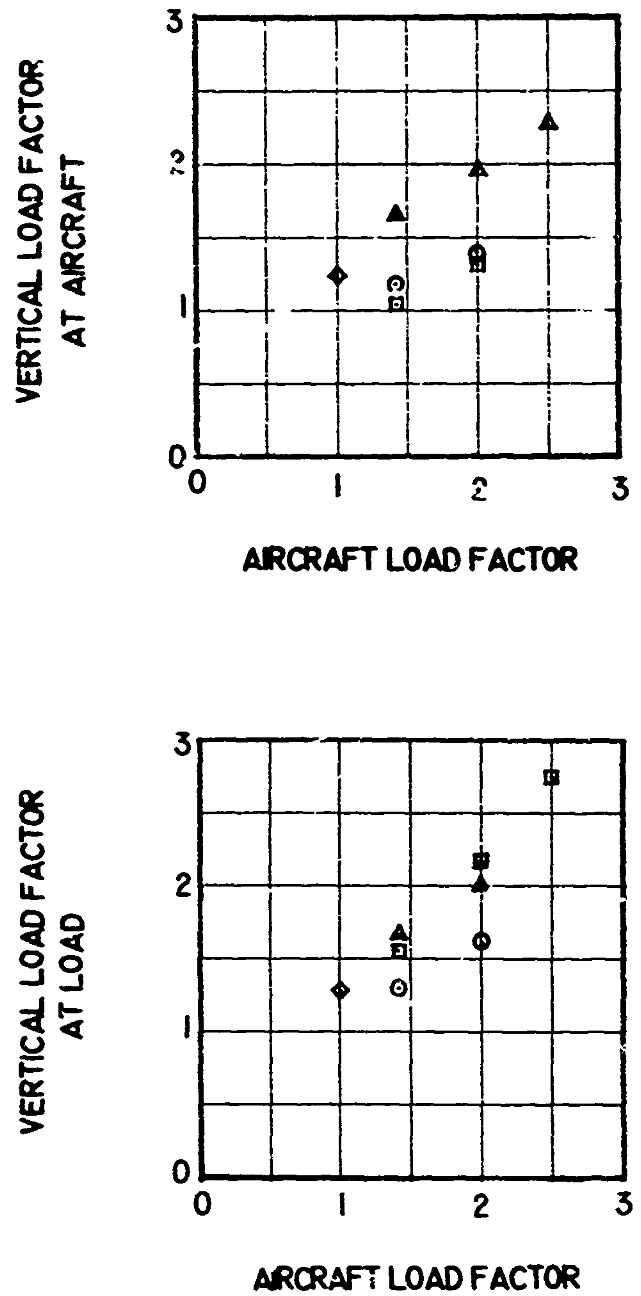

Figure 38. Adjusted Sling and Hardpoint Load Factor Data for the OV-1 - 1 Pt/ 3 Leg Load.

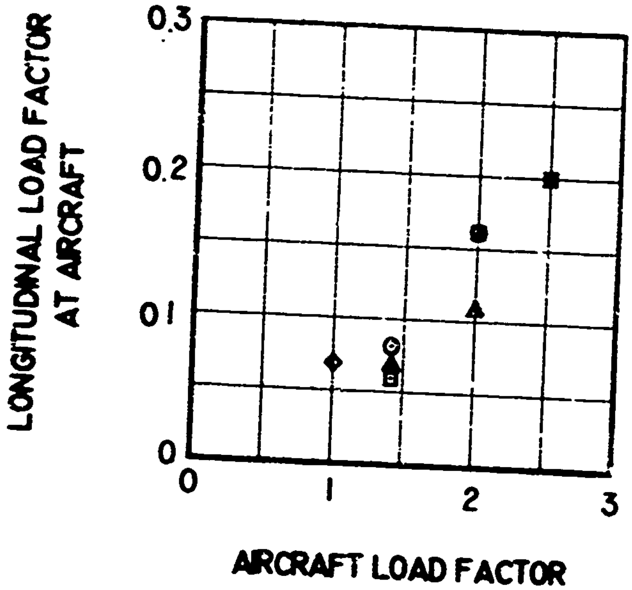

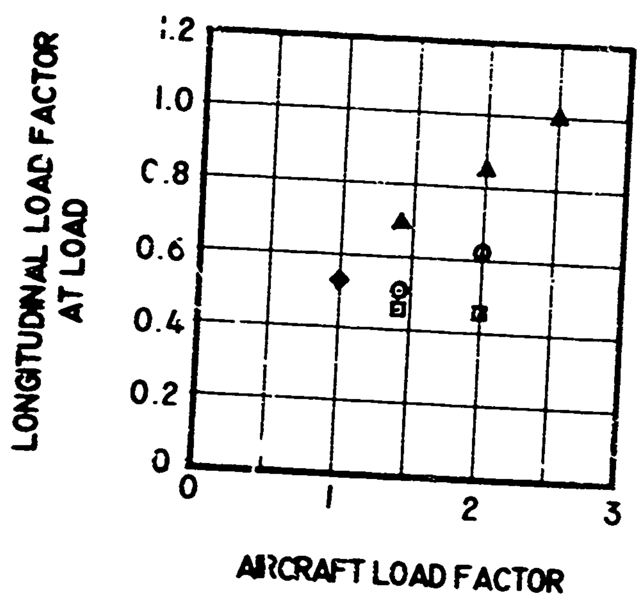

Figure 38. Continued.

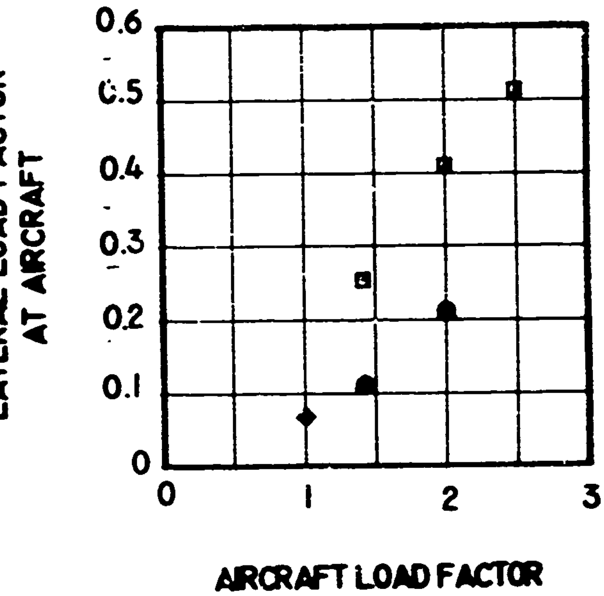

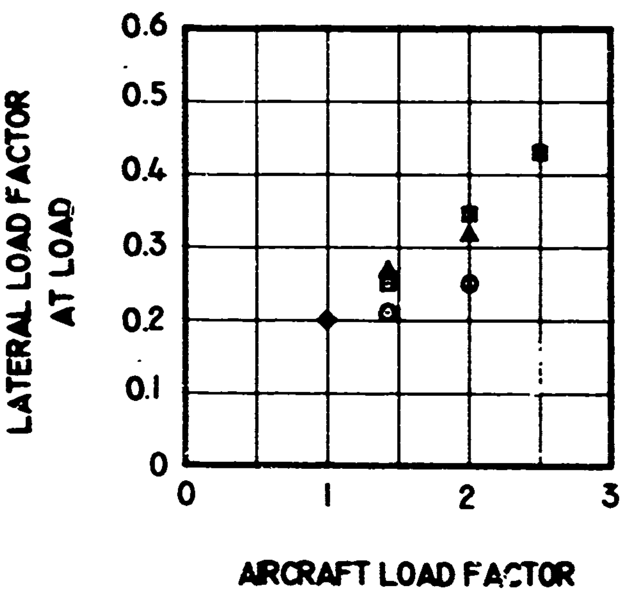

Figure 38. Continued.

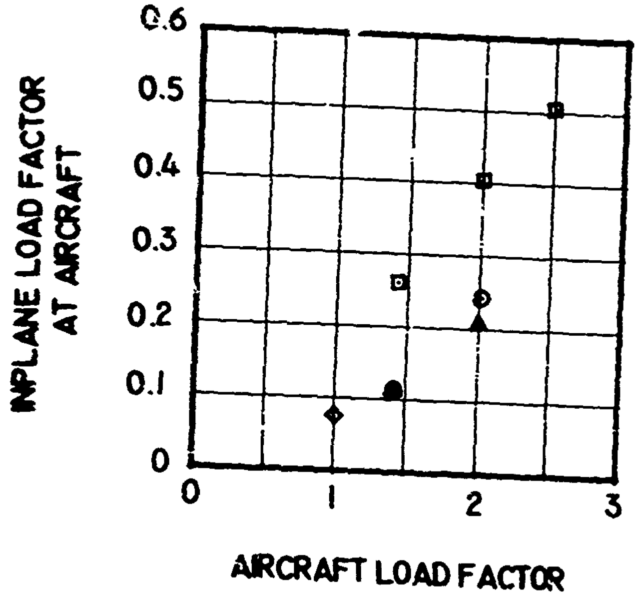

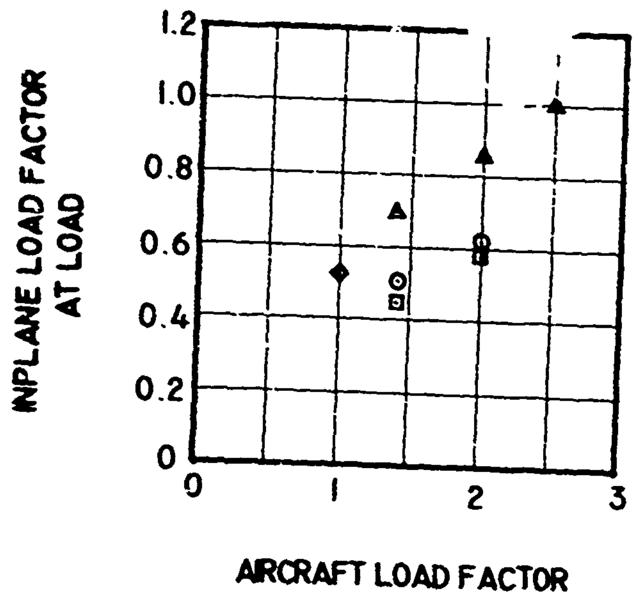

Figure 38. Continued.

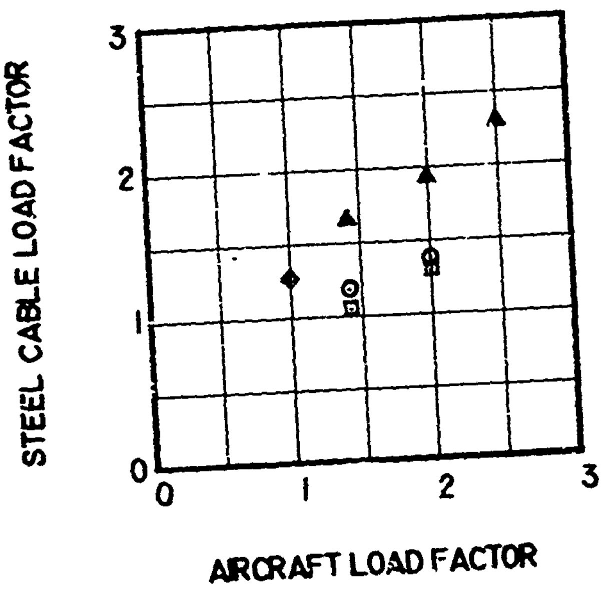

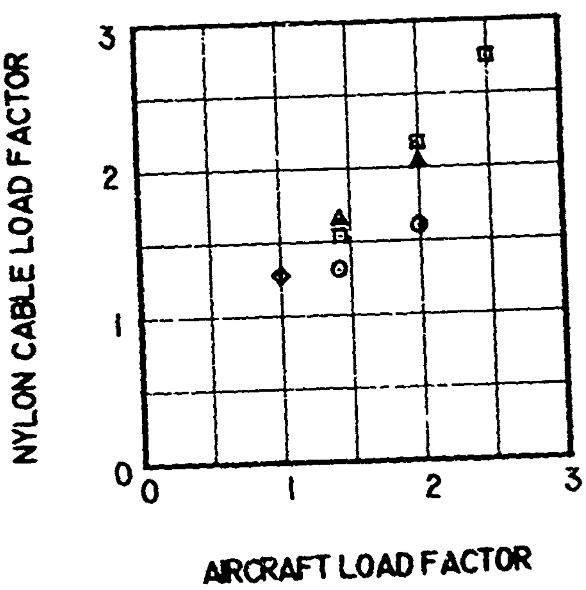

Figure 38. Concluded.

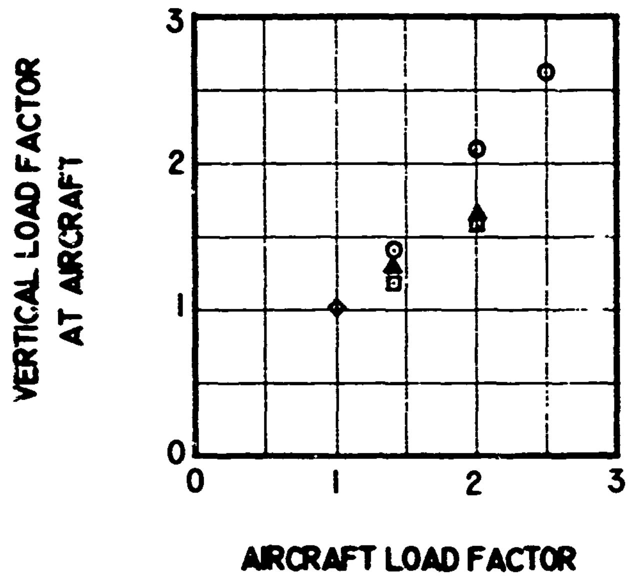

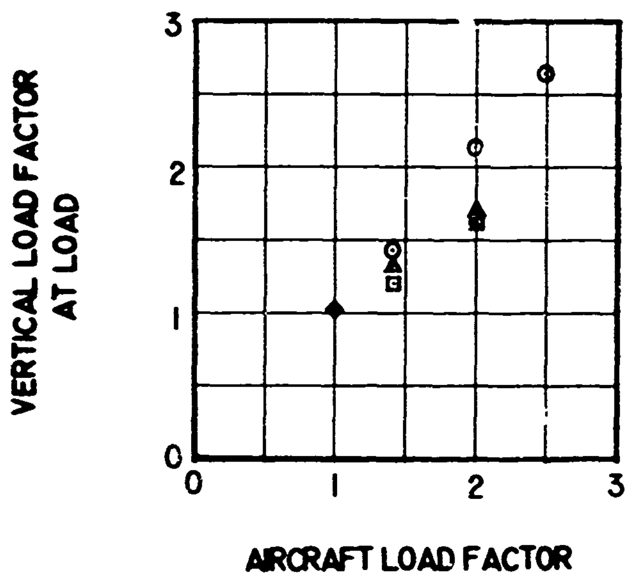

Figure 39. Adjusted Sling and Hardpoint Load Factor Data for the Block - 1 Pt/ 1 Leg Load.

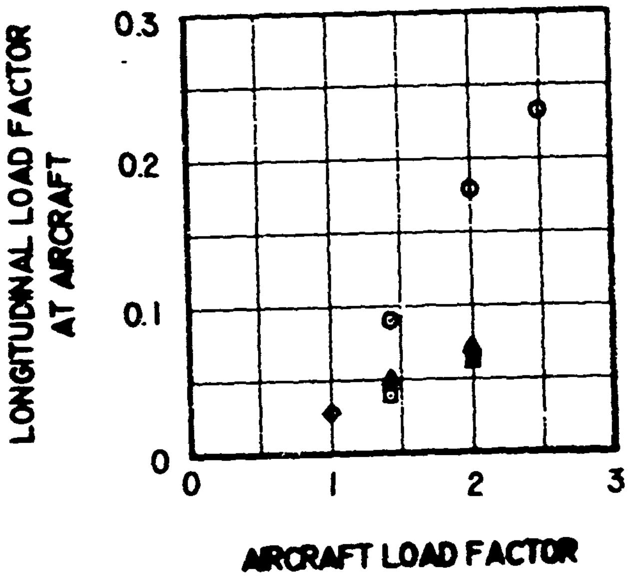

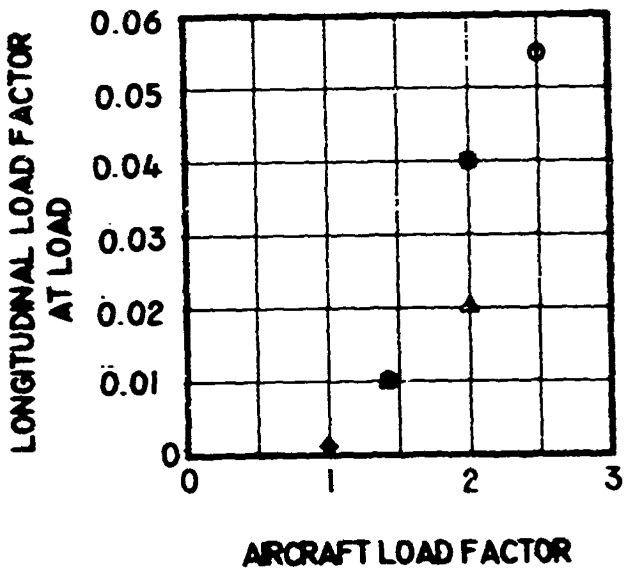

Figure 39. Continued.

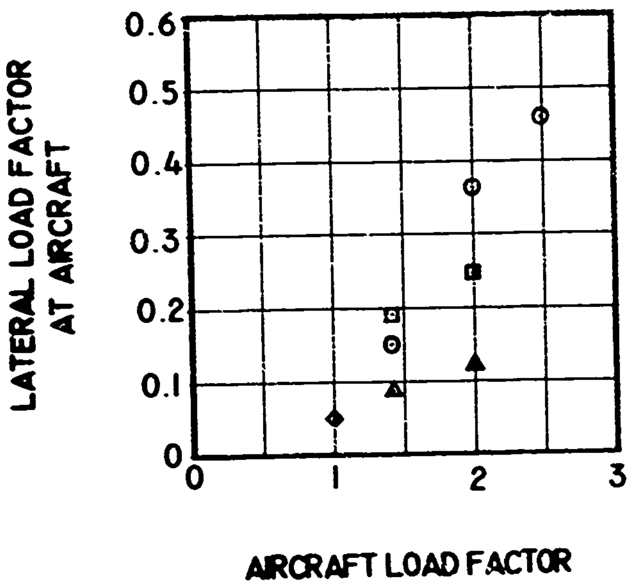

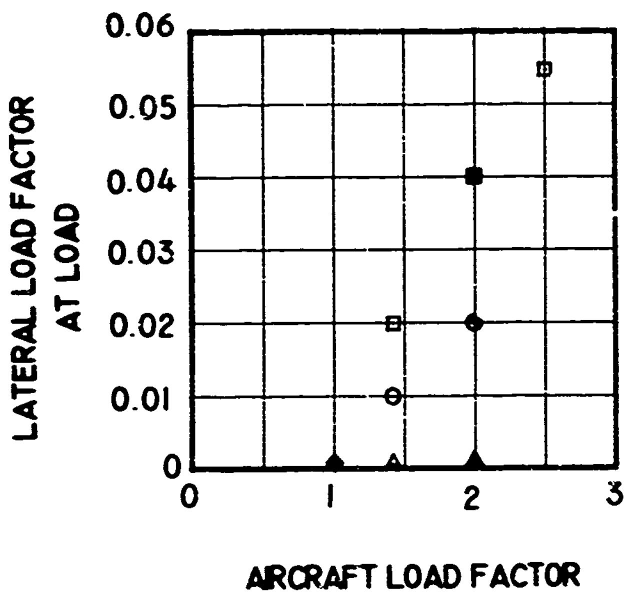

Figure 39. Continued.

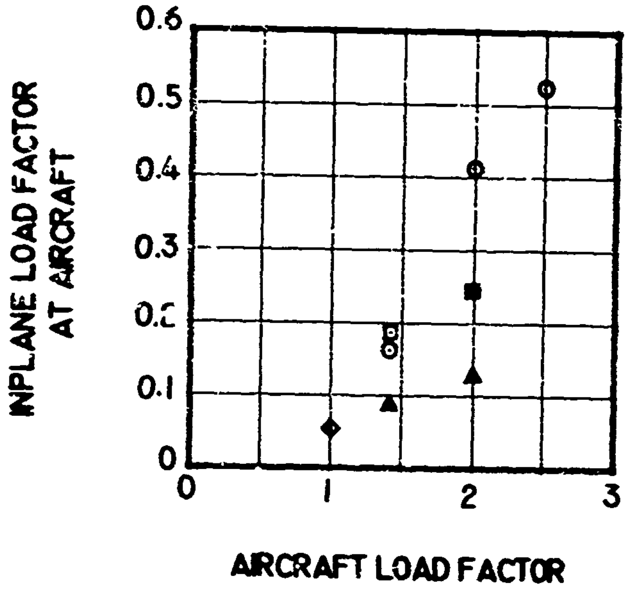

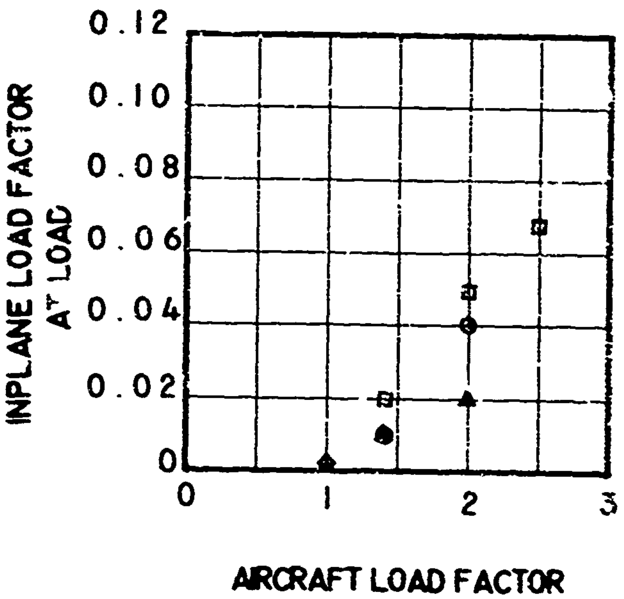

Figure 39. Continued.

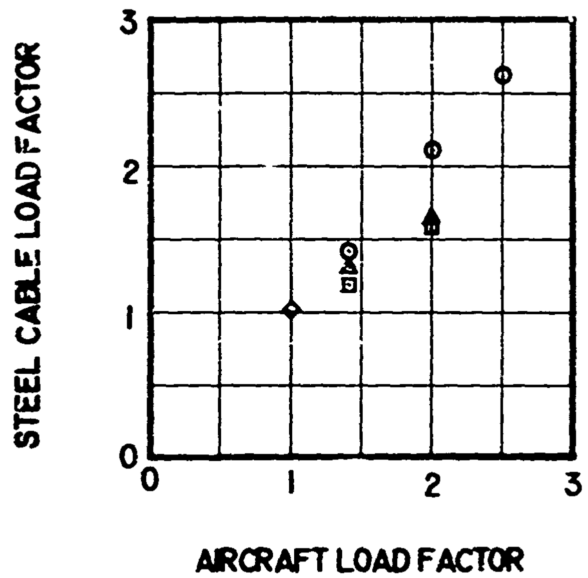

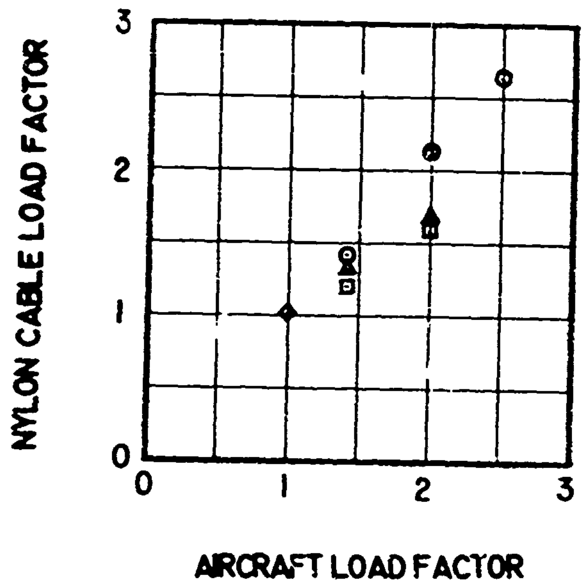

Figure 39. Concluded.

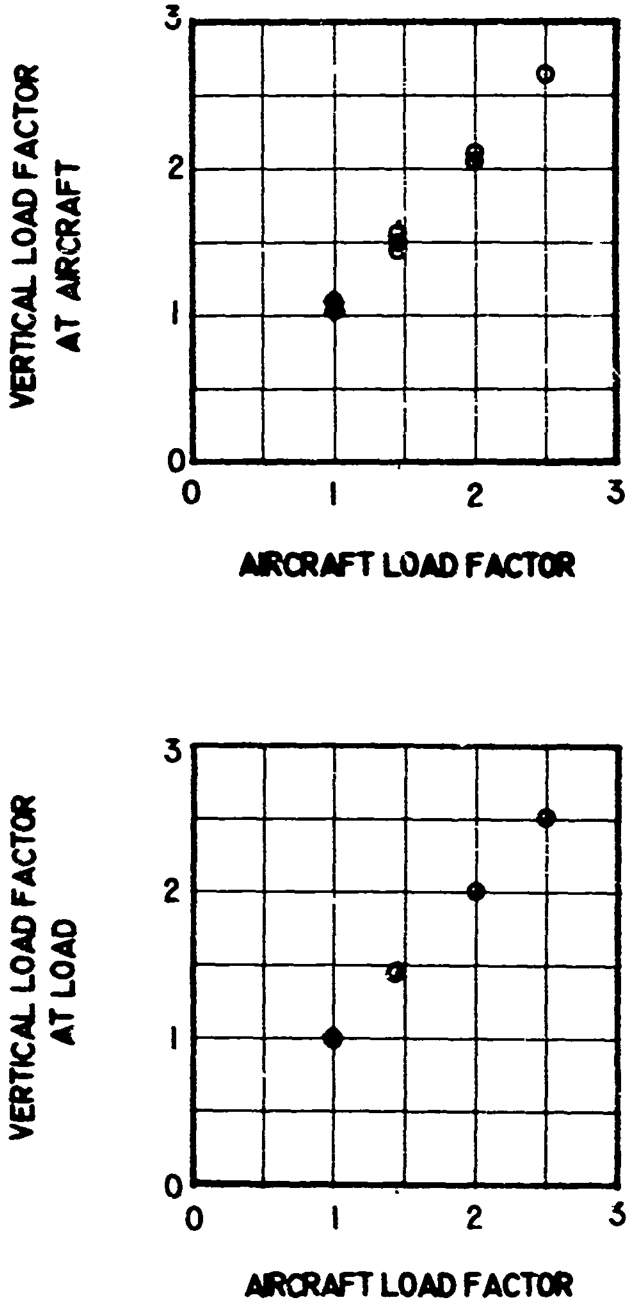

Figure 40. Adjusted Sling and Hardpoint Load Factor Data for the Brooks and Perkins Pallet Load.

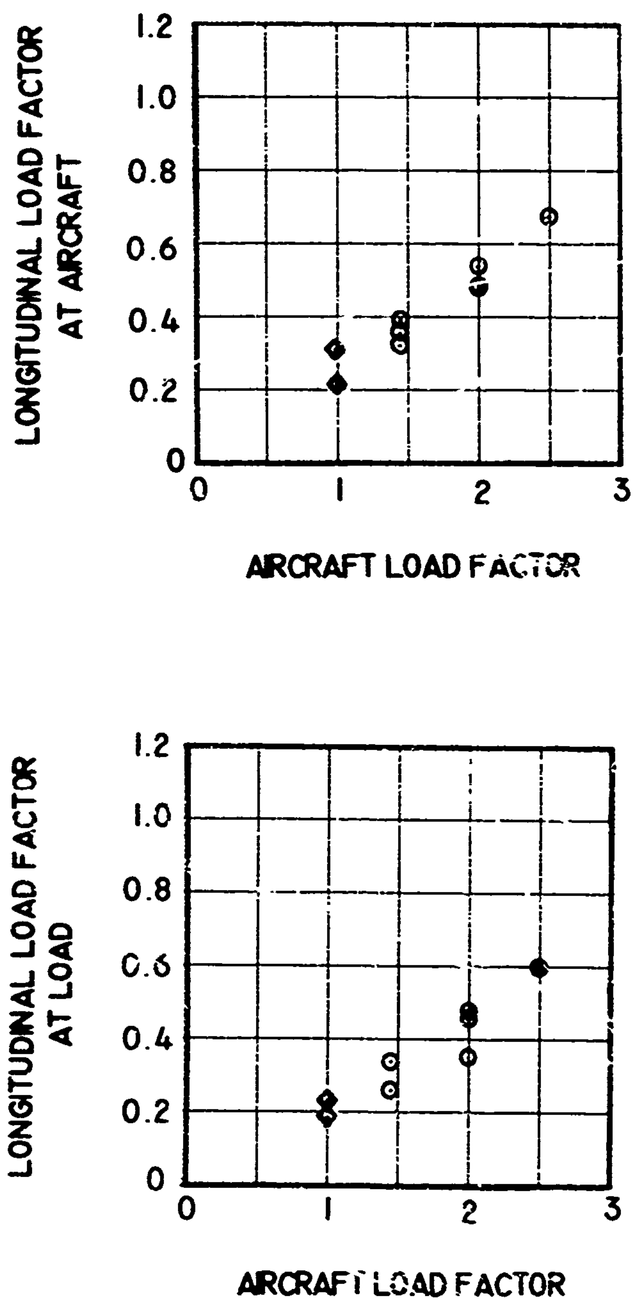

Figure 40. Continued.

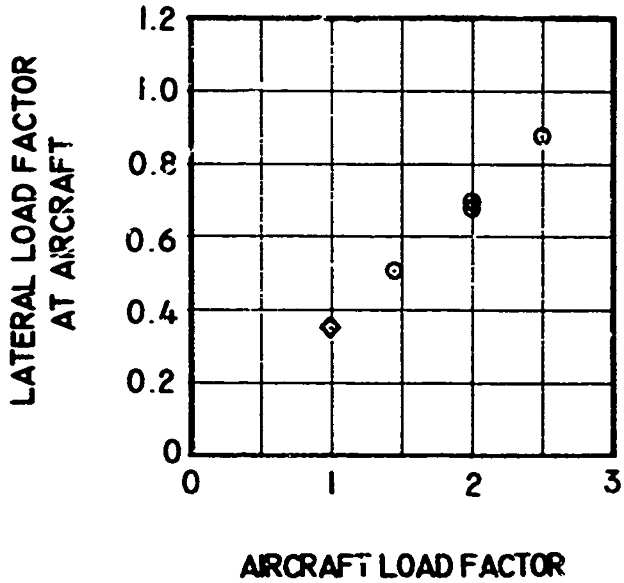

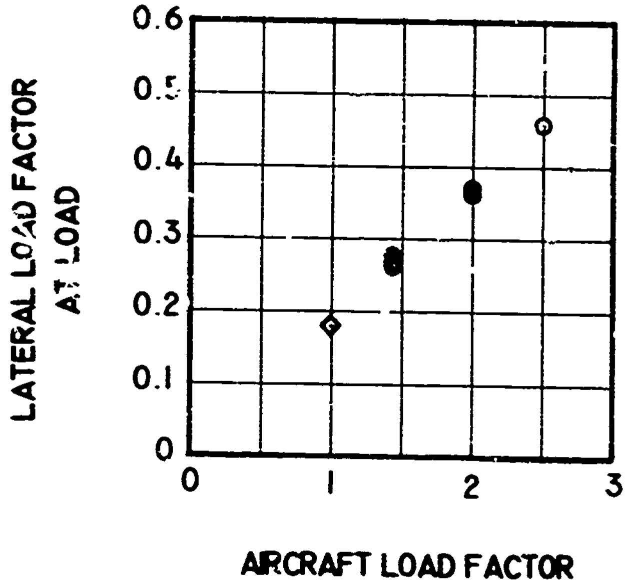

Figure 40. Continued.

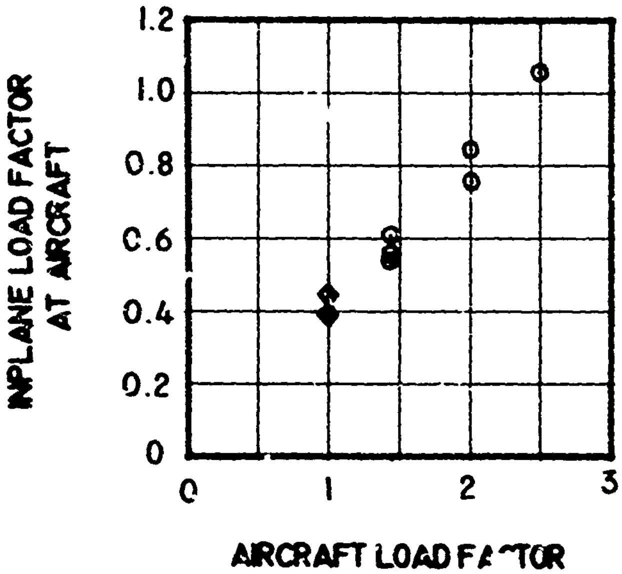

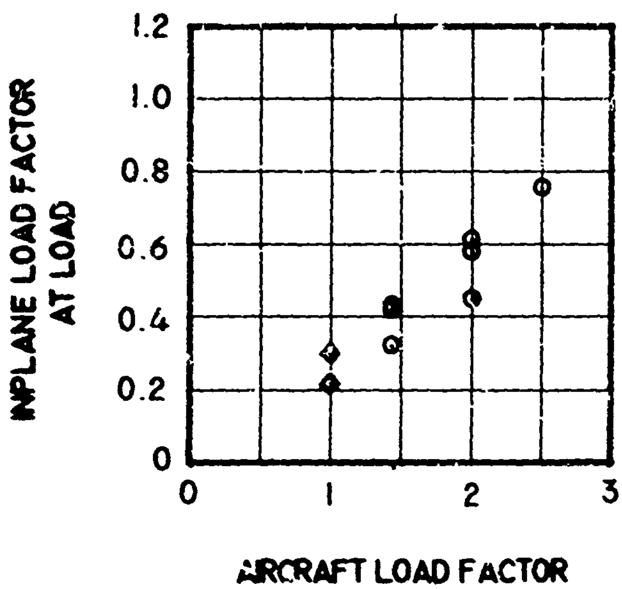

Figure 40. Continued.

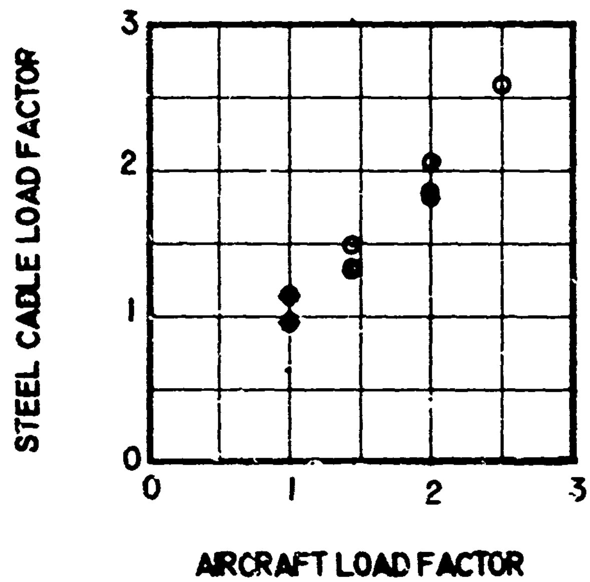

Figure 40. Concluded.

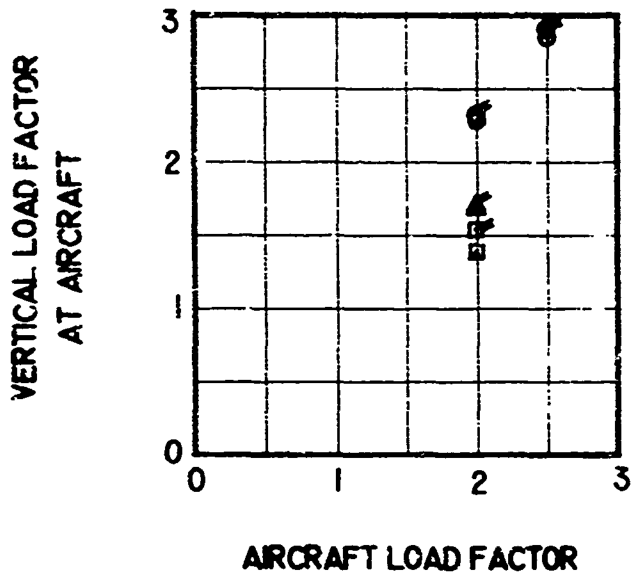

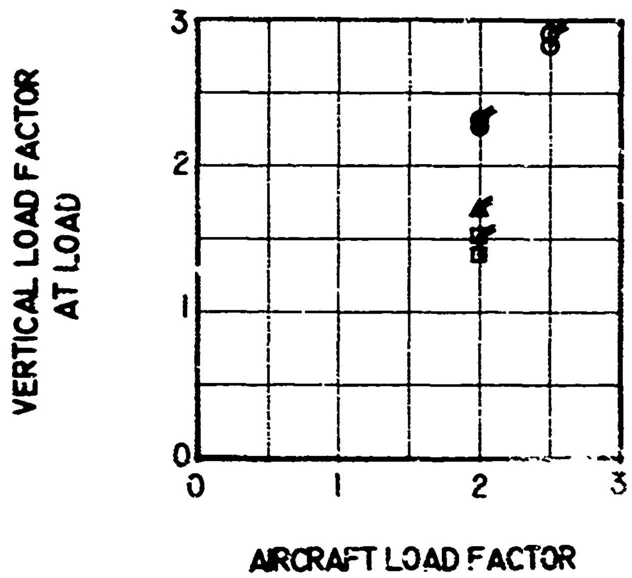

Figure 41. Adjusted Sling and Hardpoint Load Factor Data for the Container - 4 Pt/ 0 Leg, Mid cg Only Load, Including Gust Cases Data.

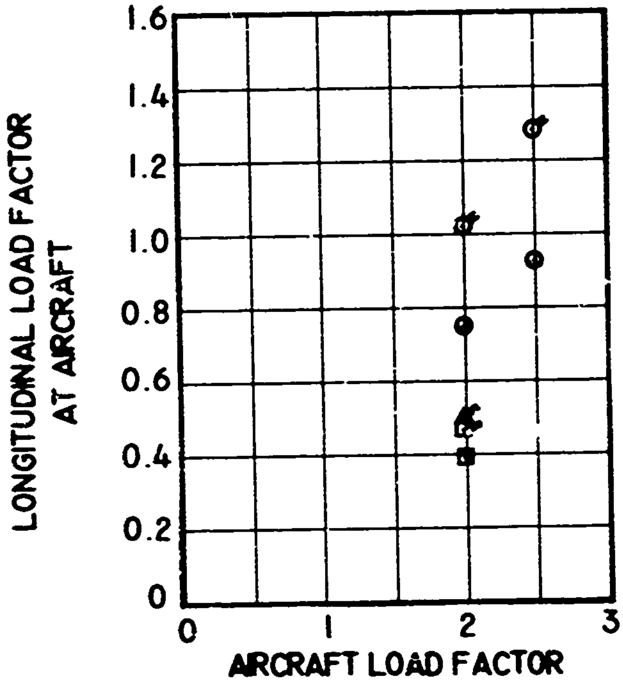

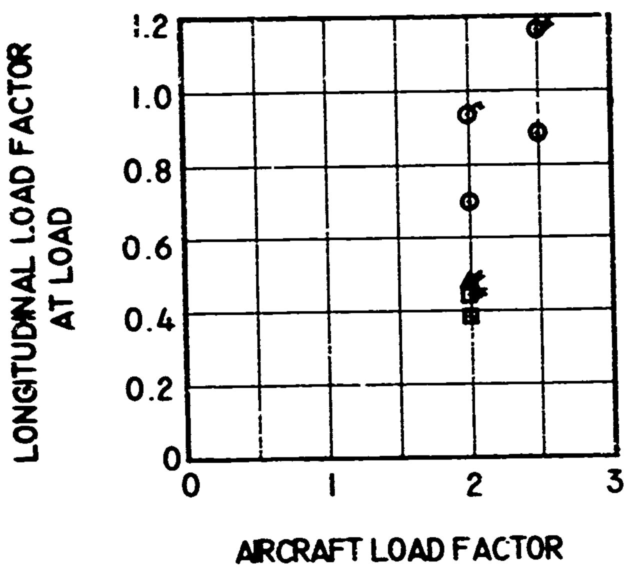

Figure 41. Continued.

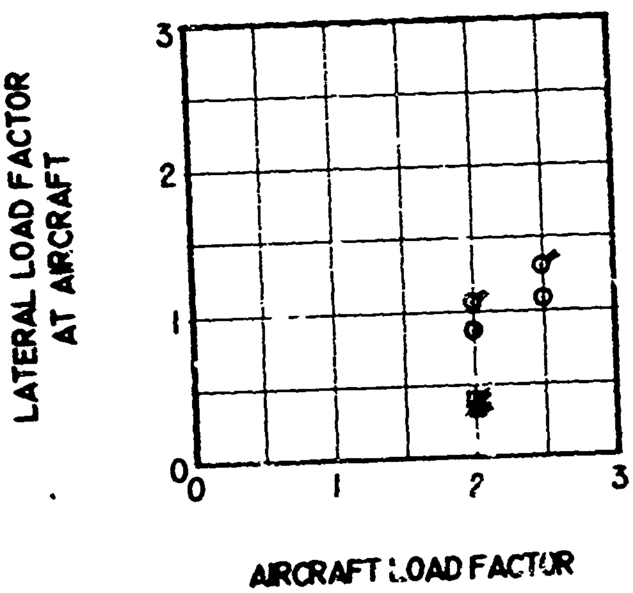

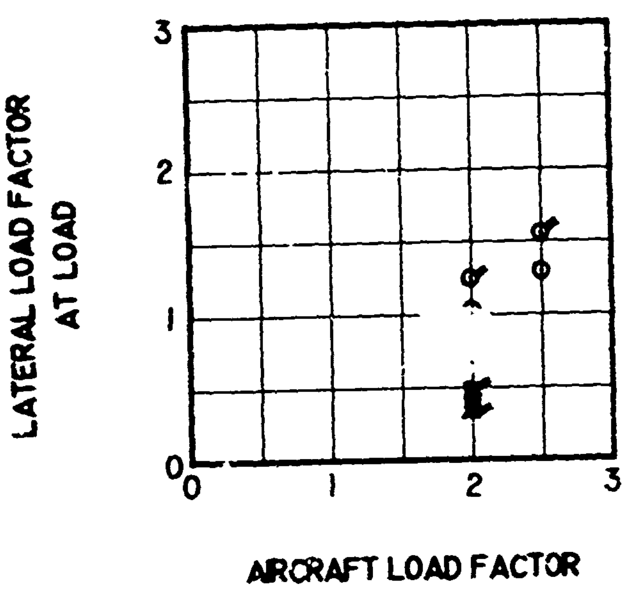

Figure 41. Continued.

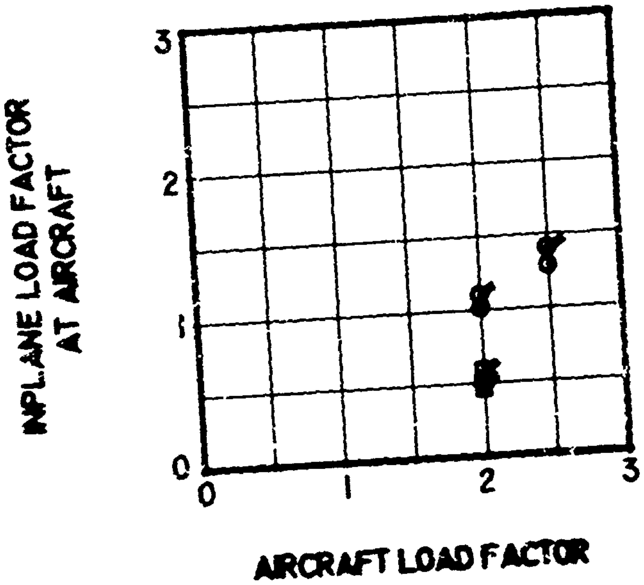

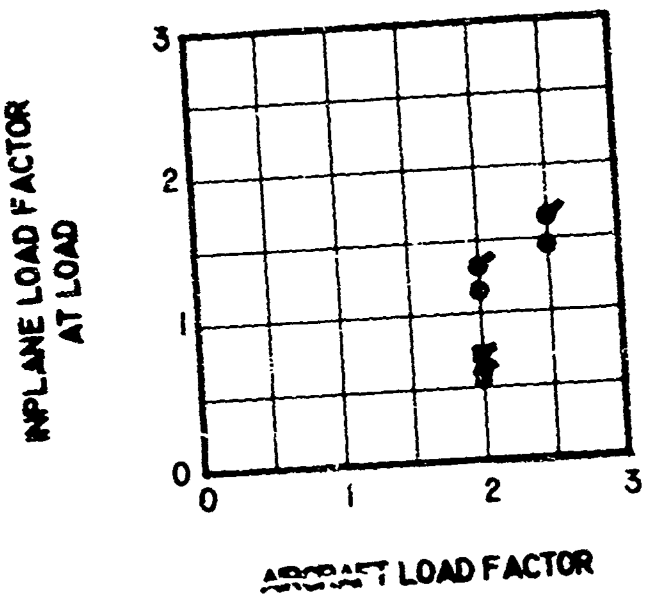

Figure 41. Continued.

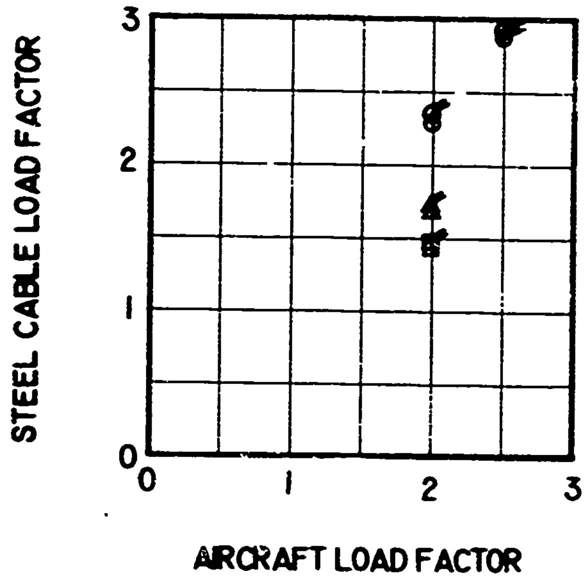

Figure 41. Concluded.

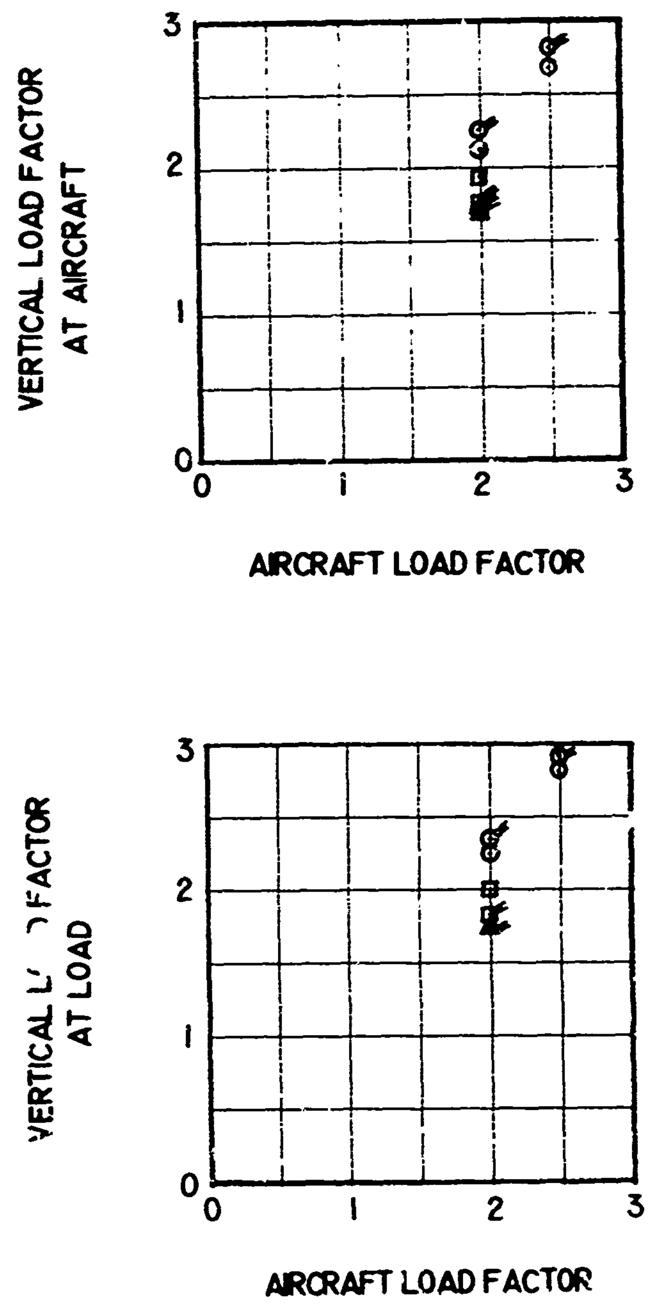

Figure 42. Adjusted Sling and Hardpoint Load Factor Data for the Block - 1 Pt/ 4 Leg Load, Including Gust Cases Data.

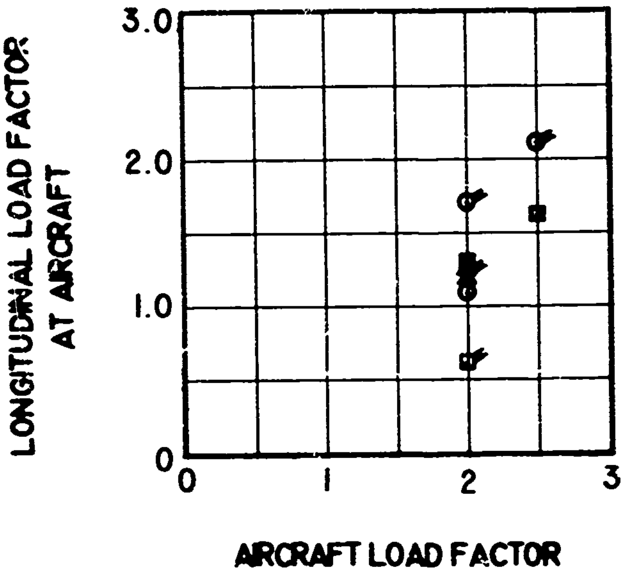

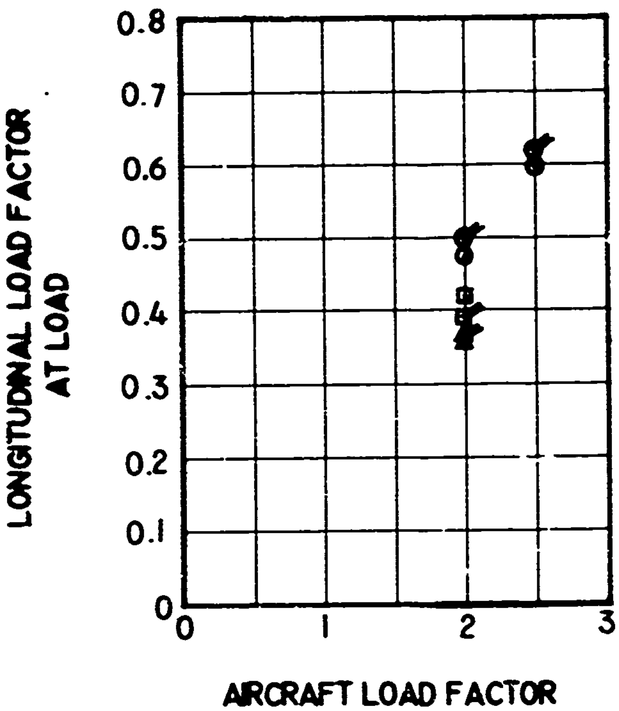

Figure 42. Continued.

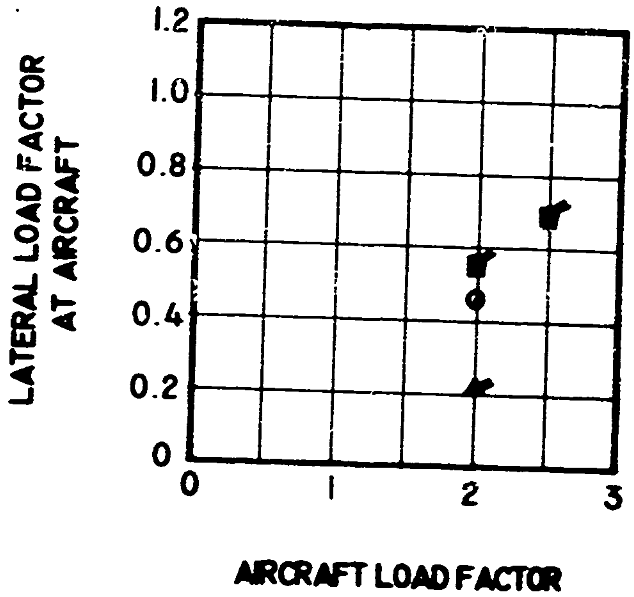

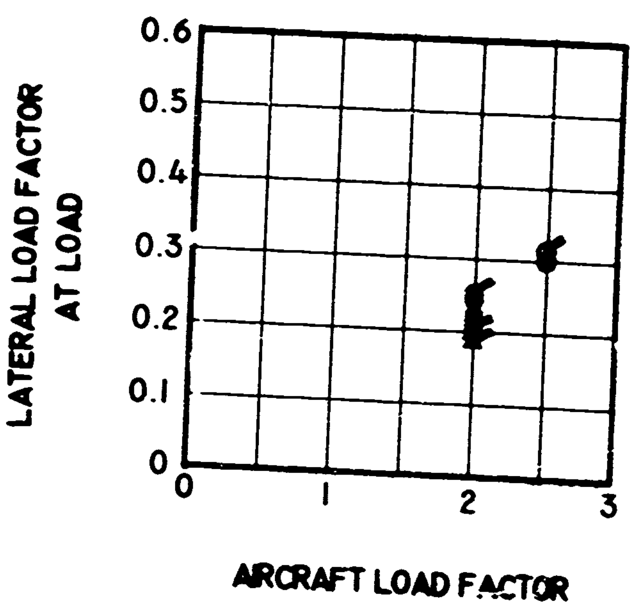

Figure 42. Continued.

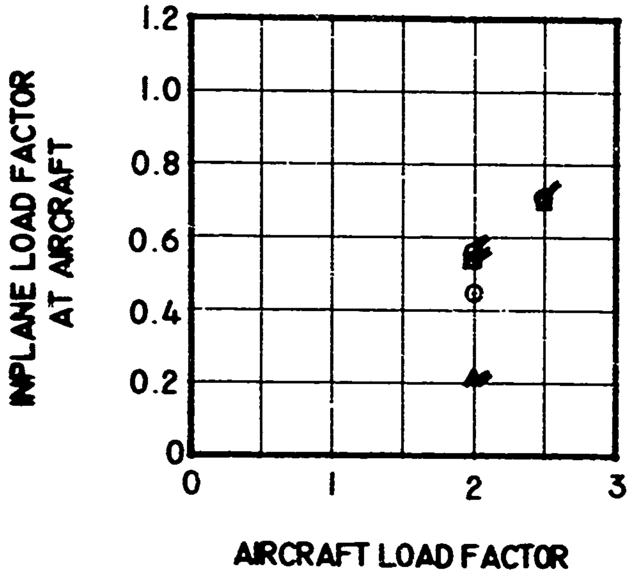

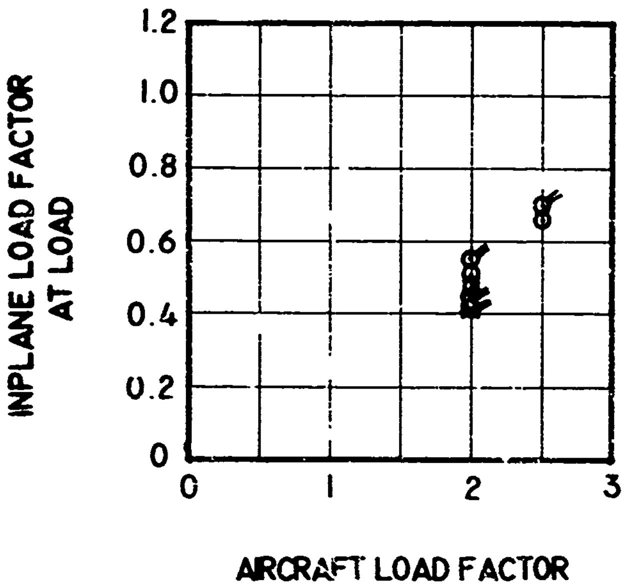

Figure 42. Continued.

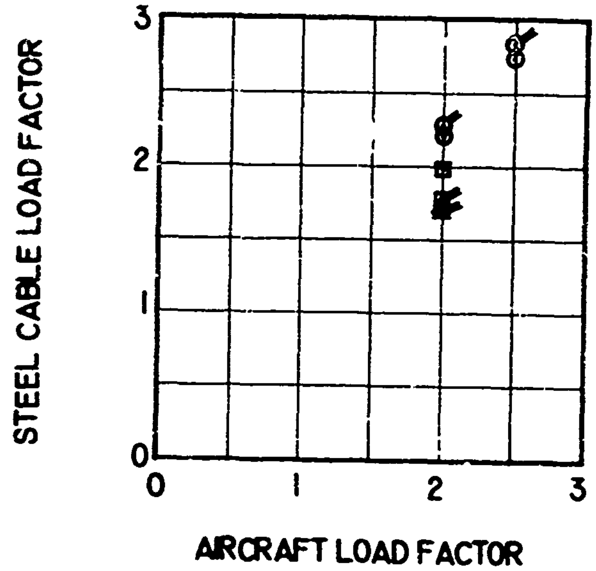

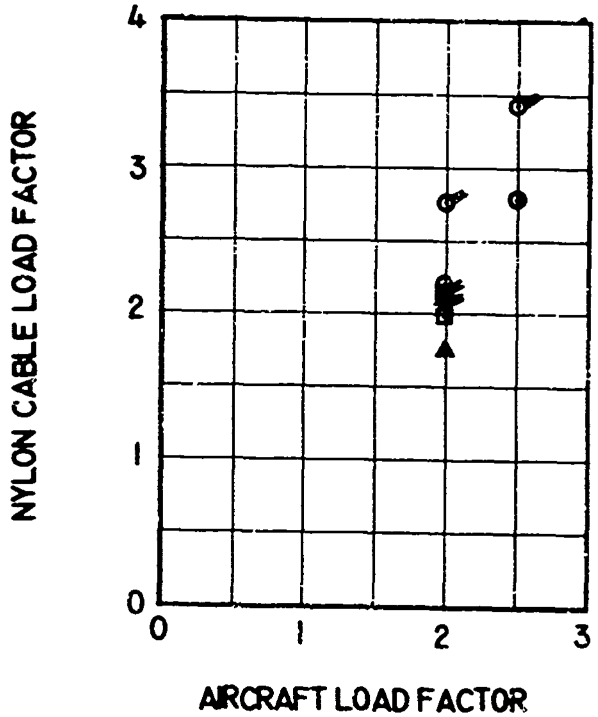

Figure 42. Concluded.

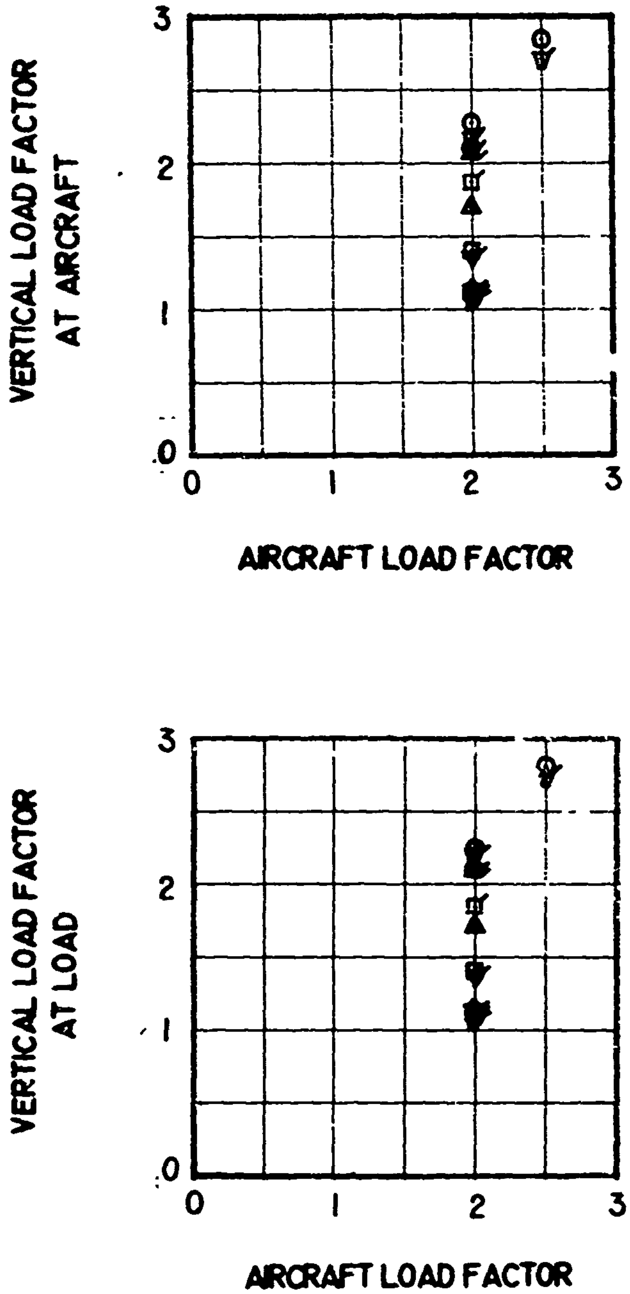

Figure 43. Adjusted Sling and Hardpoint Load Factor Data for the Container - 4 Pt/ 0 Leg, Mid cg Only Load, Including Moving-Base Data.

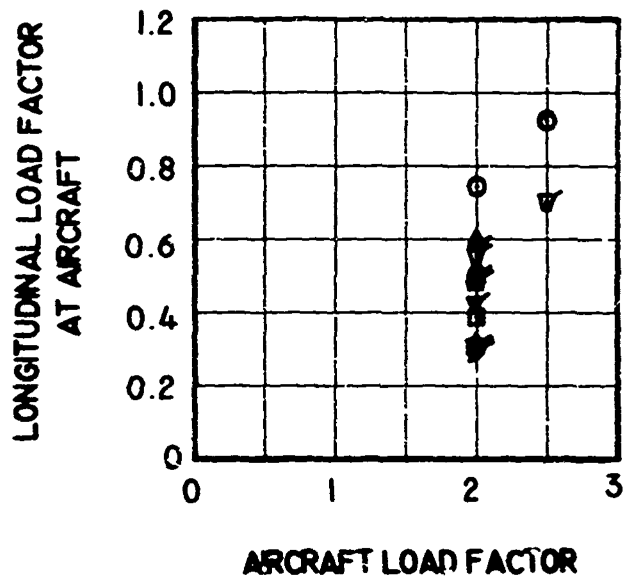

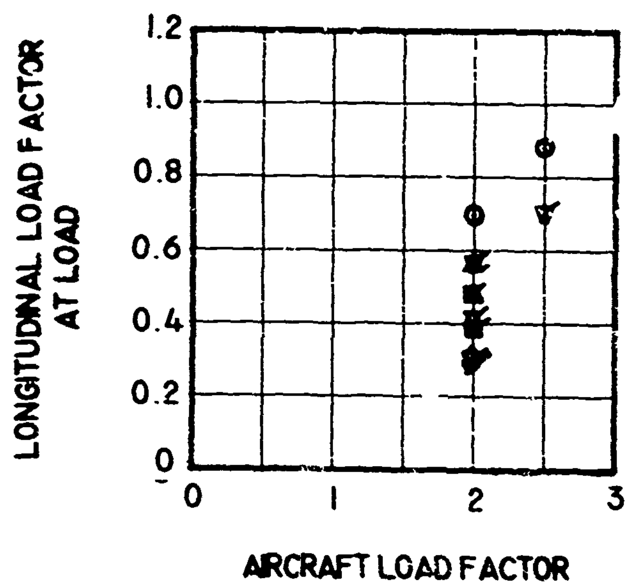

Figure 43. Continued.

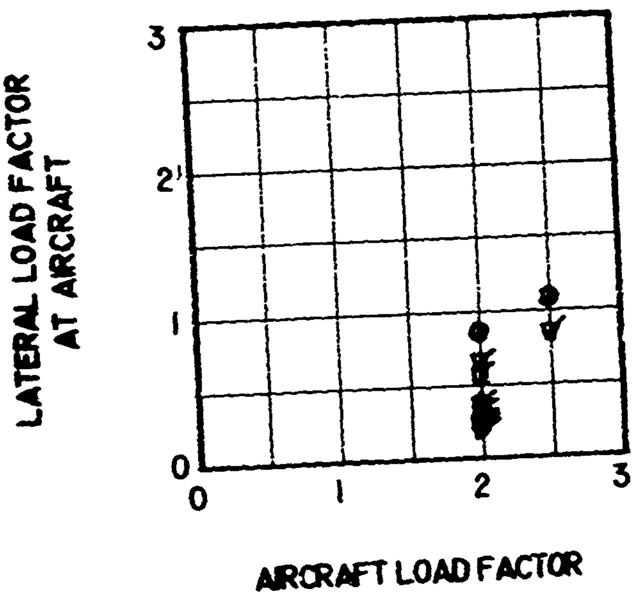

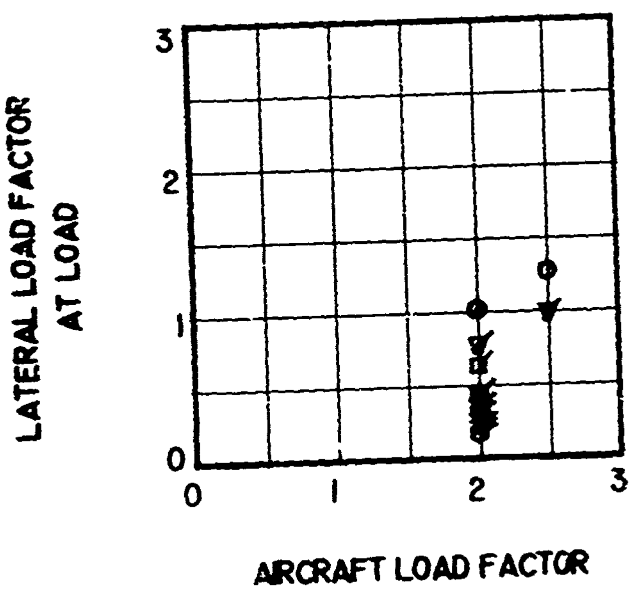

Figure 43. Continued.

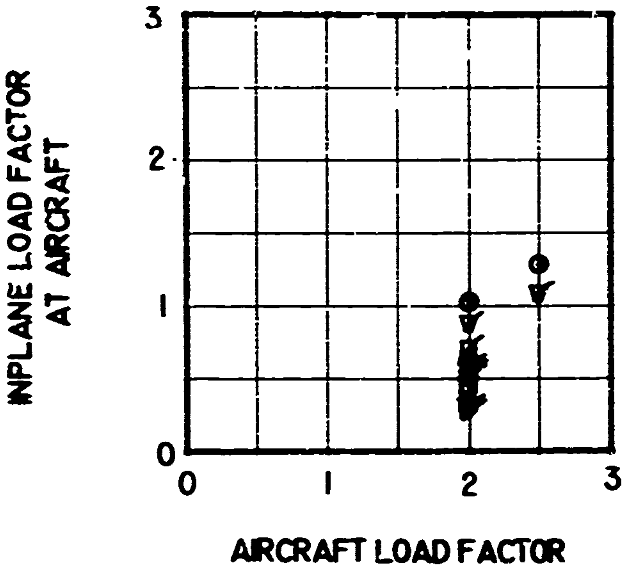

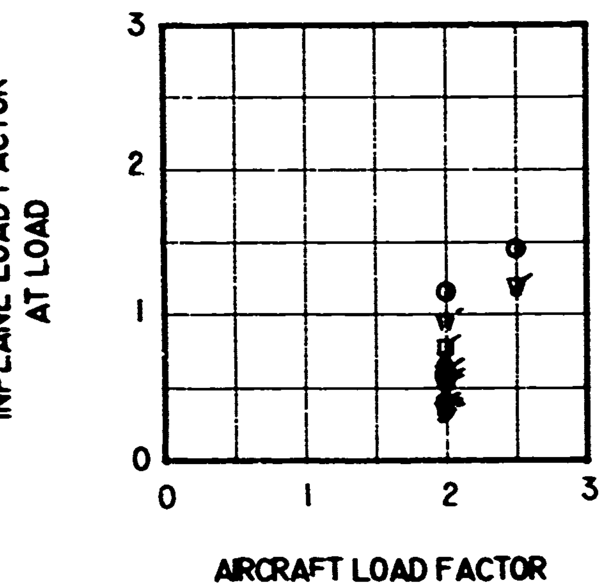

Figure 43. Continued.

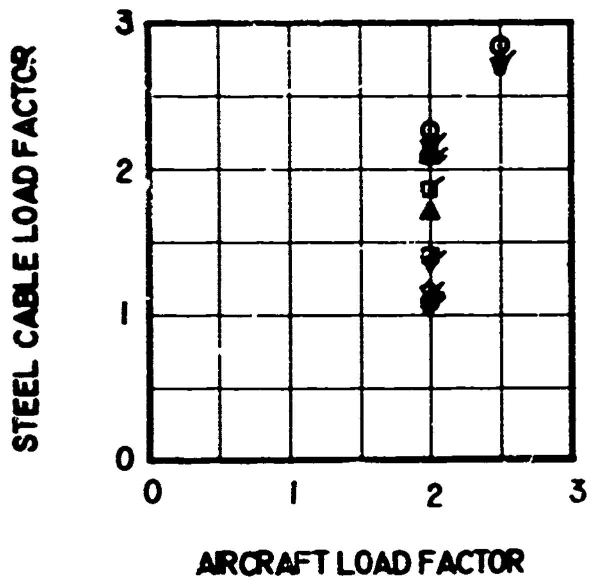

Figure 43. Concluded.

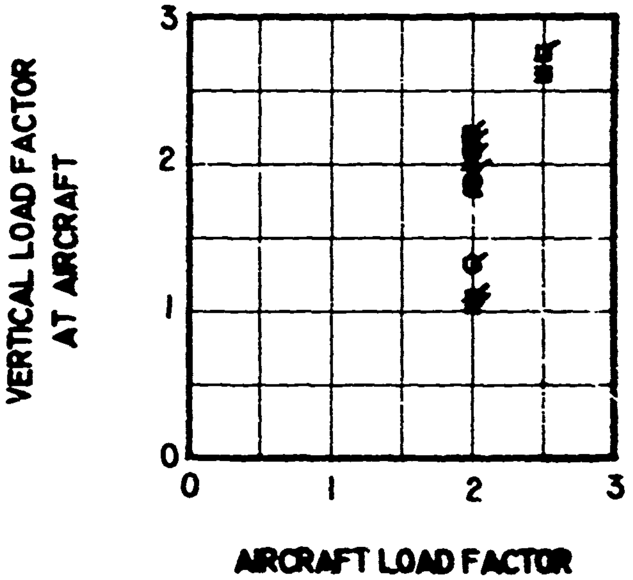

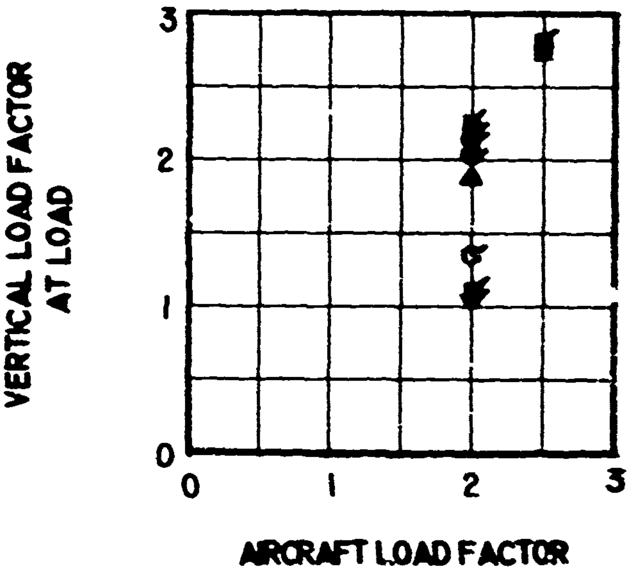

Figure 44. Adjusted Sling and Hardpoint Load Factor Data For the Container - 1 Pt/ 4 Leg, Mid cg Only Load, Including Moving-Base Data.

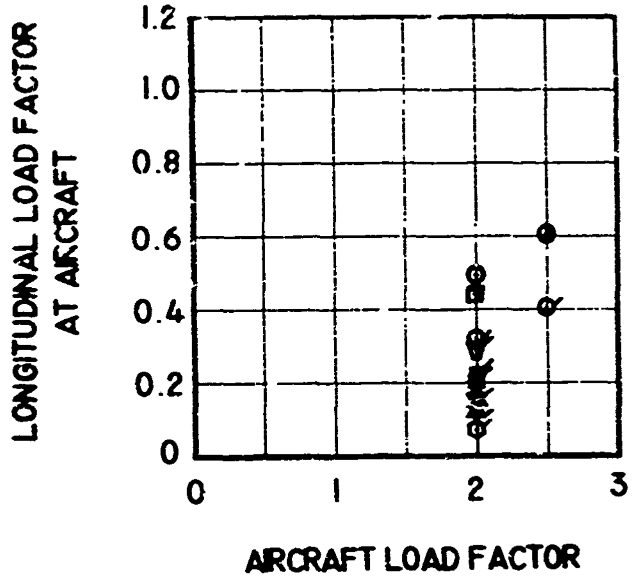

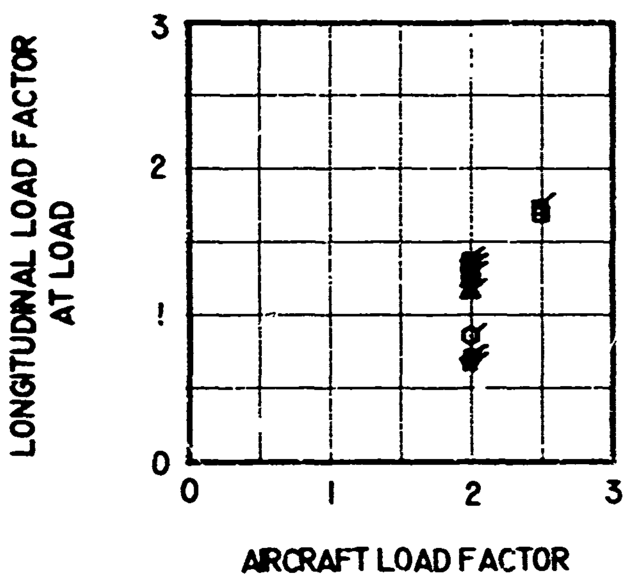

Figure 44. Continued.

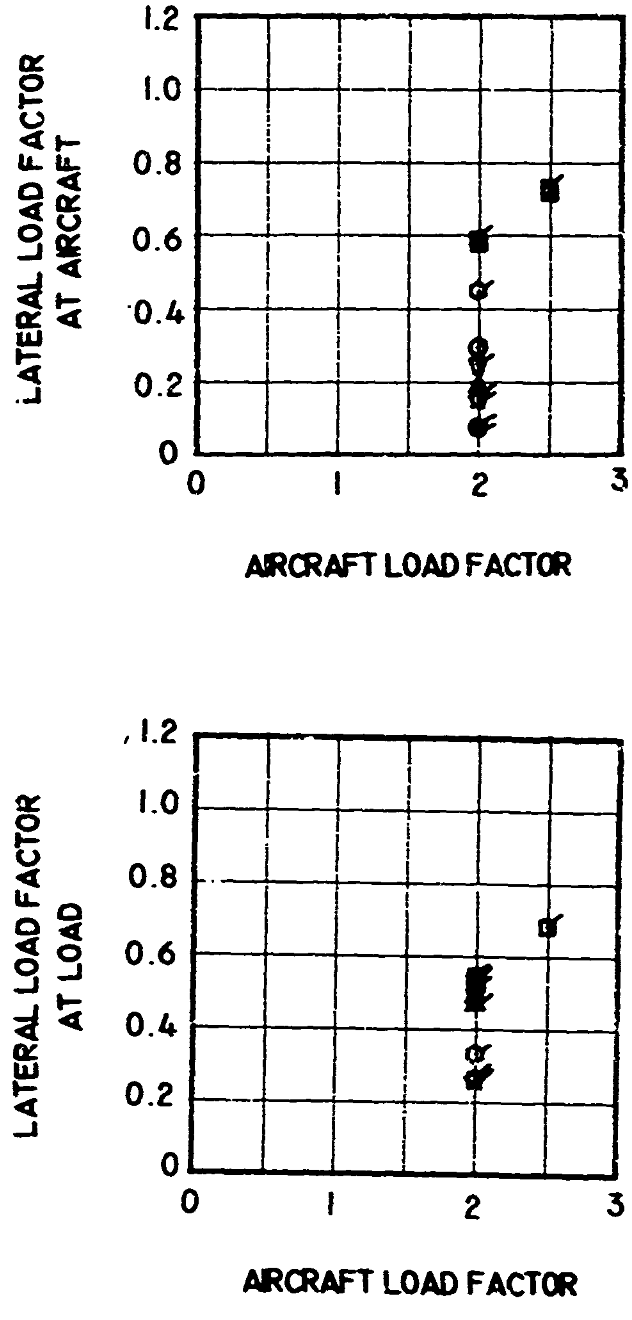

Figure 44. Continued.

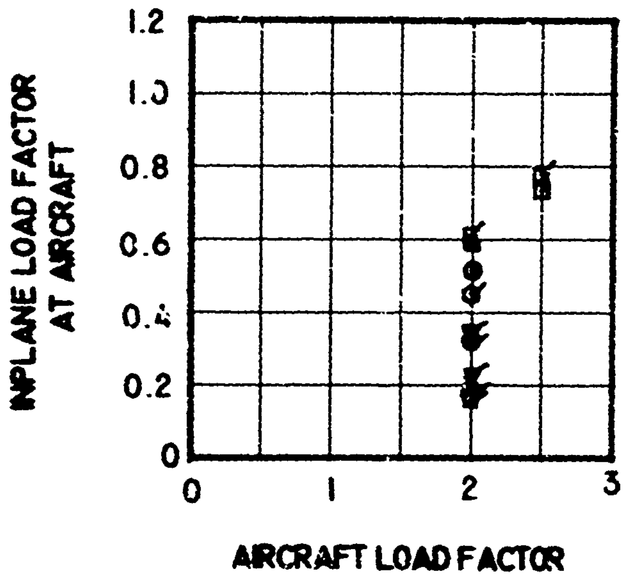

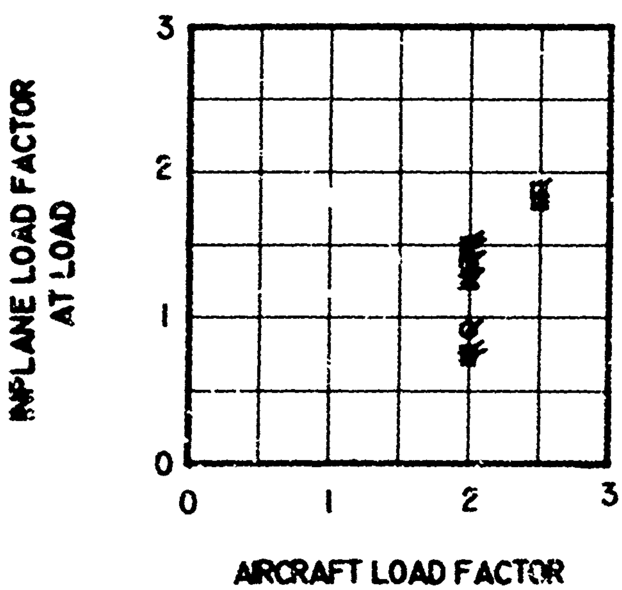

Figure 44. Continued.

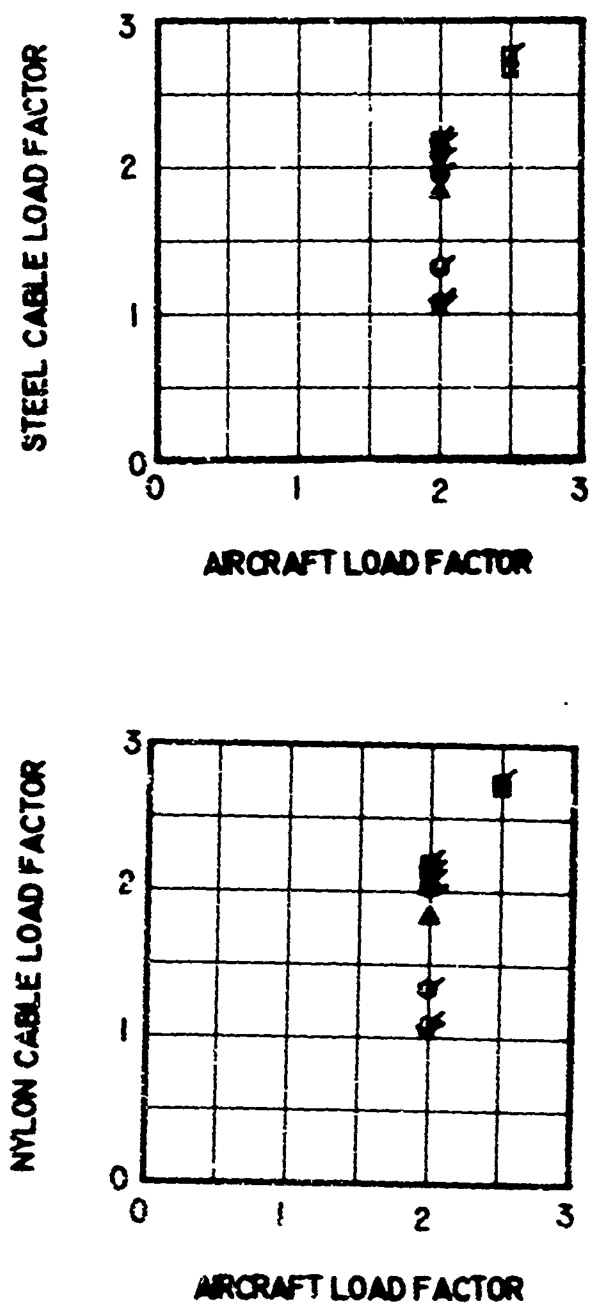

Figure 44. Concluded.

APPENDIX VI

DETERMINATION OF STATIC LOADS USED IN THE NONDIMENSIONALIZATION OF LOAD FACTOR DATA

The manner for determining the values of the static loads T_{c_s}, T_{L_S} and V_{H_S} used to nondimensionalize the sling and hardpoint load factor data is presented here for the single-point and four-point sling configurations. For either configuration, these static forces are found by equating forces and moments acting on the slung load to zero. Any body axis system with the origin at the slung load cg may be selected which satisfies the condition that the sling configuration be symmetrical with respect to the xz-plane. Once selected, this axis system remains fixed in the slung load at all times. The method illustrated is used for solving the static loads of an indeterminant system which has four cables or four [illegible].

SINGLE-POINT CONFIGURATION

Figure 45 illustrates the parameters used in the solution. The subscripts f and r refer to front and rear sling members, and the subscript h refers to the hook. The distances d and h are measured along the slung load body axes directions and specify the location of hardpoints or hook (donut) from the slung load cg. The angles θ_f and θ_r are the true angles between the sling members and the body axis vertical direction. The projection of these angles in the xz-plane are referenced as $\theta_{f_{xz}}$ and $\theta_{r_{xz}}$. These geometric quantities plus the slung load weight W_l should all be known quantities.

The summation of static forces in the z-direction yields the equation

$$W_l \cos\theta_h = V'_{L_{S_f}} + V'_{L_{S_r}} \tag{164}$$

while equating moments about the slung load cg to zero yields the equation

$$(V'_{L_{S_f}})(d_f) + (V'_{L_{S_r}})(d_r) = (D'_{L_{S_f}})(h_f) + (D'_{L_{S_r}})(h_r) \tag{165}$$

where

$$\theta_h = \arctan\left[\frac{(d_h)}{(h_h)}\right] \tag{166}$$

$$D'_{L_{S_f}} = V'_{L_{S_f}} \tan\theta_{f_{xz}} \tag{167}$$

$$D'_{L_{S_r}} = V'_{L_{S_r}} \tan\theta_{r_{xz}} \tag{168}$$

Equations (164) to (168) are solved simultaneously for $V'_{L_{S_f}}$ and $V'_{L_{S_r}}$.

For any slung load geometry the following sign convention should be used when substituting values into eqs (164) to (168):

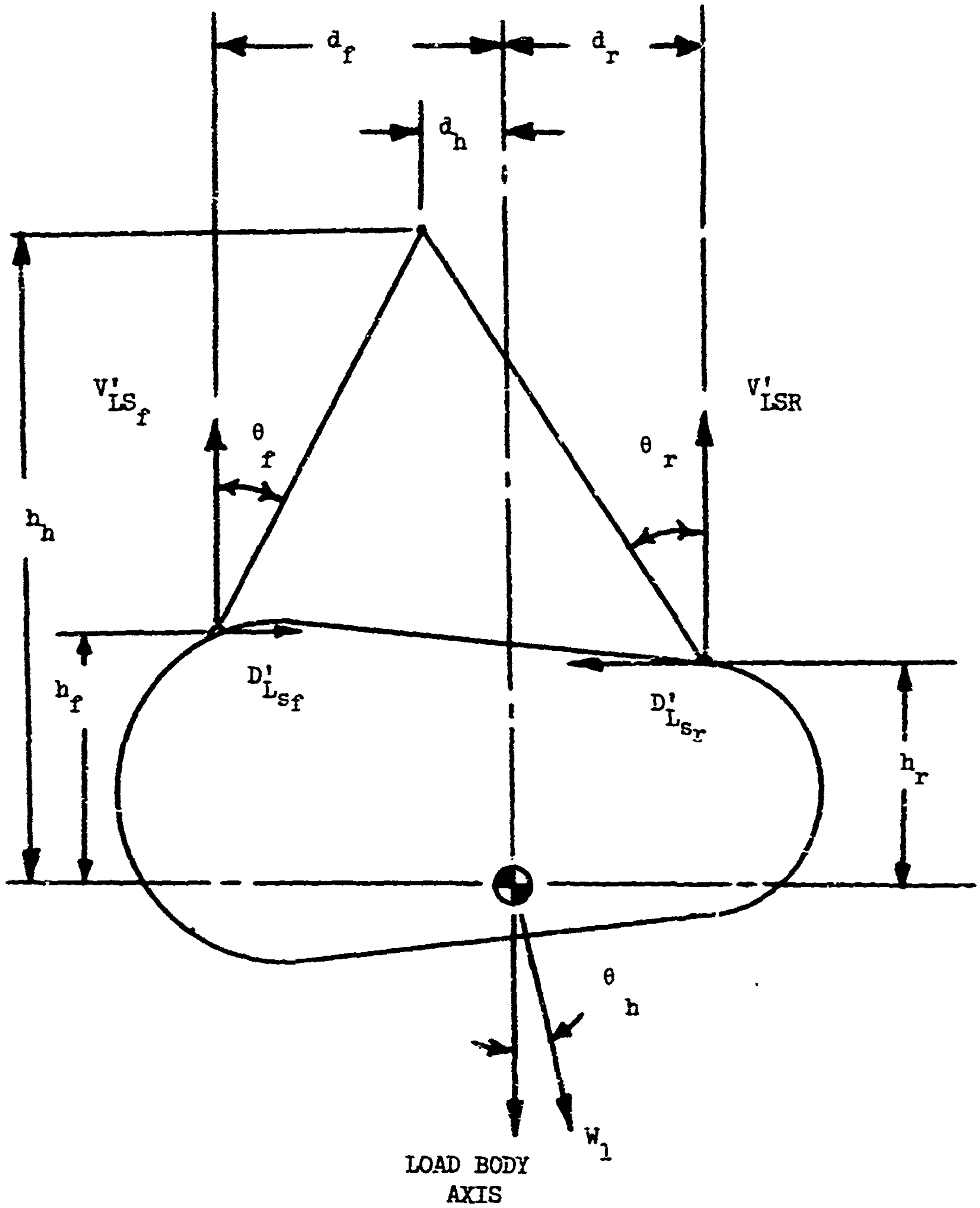

Figure 45. Static Loads Calculation Parameters.

$V'_{L_{s_f}}$, $V'_{L_{s_r}}$ are positive along the negative z body direction

$D'_{L_{s_f}}$, $D'_{L_{s_r}}$ are positive along the negative X_{body} direction

h_h, h_f, h_r are positive for hook or hardpoint below the cg

d_h, d_f, d_r are positive for hook or hardpoint forward of the cg

The primes in the preceding equations are used to specify that these values are not in themselves the values of static drag or vertical force. Once $V'_{L_{s_r}}$ and $V'_{L_{s_f}}$ have been solved, the method for finding the value of V_{L_s} used for normalizing the load factor data for the particular slung load under investigation is outlined as follows:

(1) If the sling has two front legs, then

$$V_{L_{s_f}} = (V'_{L_{s_f}})/2 \tag{169}$$

If the sling has one front leg, then

$$V_{L_{s_f}} = V'_{L_{s_f}} \tag{170}$$

(2) If the sling has two rear legs, then

$$V_{L_{s_r}} = (V'_{L_{s_r}})/2 \tag{171}$$

If the sling has one rear leg, then

$$V_{L_{s_r}} = V'_{L_{s_r}} \tag{172}$$

(3) If $V_{L_{s_f}}$ is greater than $V_{L_{s_r}}$, then $V_{L_s} = V_{L_{s_f}}$ (173)

If $V_{L_{s_r}}$ is greater than $V_{L_{s_f}}$, then $V_{L_s} = V_{L_{s_r}}$ (174)

The value of V_{L_s} from either equation (173) or (174) has been used to normalize the design criteria data in Figures (19) through (21).

The value of T_{L_s} used to nondimensionalize the design criteria data is found from V_{L_s} according to the equation:

$$T_{L_{s_f}} = (V_{L_{s_f}})/\cos\theta_f \tag{175}$$

$$T_{L_{s_r}} = (V_{L_{s_r}})/\cos\theta_r \tag{176}$$

$$T_{L_s} = T_{L_{s_f}} \;(\text{ if } T_{L_{s_f}} > T_{L_{s_r}}) \tag{177}$$

$$T_{L_s} = T_{L_{s_r}} \quad (\text{if } T_{L_{s_r}} > T_{L_{s_f}}) \tag{178}$$

The value of V_{H_s} used for normalization of the data for the single point configurations is given by

$$V_{H_s} = W_1 \tag{179}$$

The value of T_{C_s} used for normalization of the data for single point configurations is given by

$$T_{C_s} = W_1 \tag{180}$$

Only absolute values of both static and dynamic forces are considered in this design criteria study.

FOUR-POINT CONFIGURATION

The calculation of V_{L_s} for the four point sling configuration is similar to the same single point calculation. Figure 45 may be referenced for the four-point calculation, with the exception that the sling members do not all come to a common point. Also, the angle θ_h for the four-point arrangement is zero for the configurations studied. The equations and method specified for solving V_{L_s} for the single-point configuration may then be used to solve for V_{L_s} for the four-point configuration.

Once V_{L_s} is known, T_{C_s} for the four point arrangement may be solved for in the same manner as T_{L_s} for the single-point arrangement. The sling members which are referred to as legs for the single point configuration are equivalent to the cables in the four point configuration.

V_{H_s} for the four point configuration is found by first determining the static values for vertical force at the front and rear helicopter hardpoints according to the equations

$$V_{H_{s_f}} = T_{c_{s_f}} \cos \gamma_f \tag{181}$$

$$V_{H_{s_r}} = T_{c_{s_r}} \cos \gamma_r \tag{182}$$

In equations (181) and (182), γ_f and γ_r represent the true angles between the sling members and the helicopter body axis vertical direction. Once $V_{H_{s_f}}$ and $V_{H_{s_r}}$ are found, then V_{H_s} is selected according to the relations

$$V_{H_s} = V_{H_{s_f}} \quad (\text{if } V_{H_{s_f}} > V_{H_{s_r}}) \tag{183}$$

$$V_{H_s} = V_{H_{s_r}} \quad (\text{if } V_{H_{s_r}} > V_{H_{s_f}}) \tag{184}$$

Examples of the Application of the Sling and Hardpoint Design Criteria

Example 1.

CH-47 Chinook - 1 Pt/4 Leg slung from a helicopter with a Design Load Factor of N_z = 2.5.

For N_z = 2.5 the following data is available from Figures (14) to (21) for the helicopter type load:

$$LFT_{C\ max} = 2.50$$

$$LFT_{L\ max} = 4.81$$

$$LFV_{H\ max} = 2.50$$

$$LFD_{H\ max} = 0.33$$

$$LFS_{H\ max} = 0.39$$

$$LFV_{L\ max} = 3.89$$

$$LFD_{L\ max} = 6.10$$

$$LFS_{L\ max} = 0.53$$

The static forces are now calculated with the following known load and sling geometrics and properties (see Figure 46):

$$W_L = 12{,}990 \text{ lb}$$

$$\theta_f = 59.3 \text{ deg}$$

$$\theta_{f_{xz}} = 59.1 \text{ deg}$$

$$\theta_r = 48.5 \text{ deg}$$

$$\theta_{r_{xz}} = 48.2 \text{ deg}$$

$$d_f = 17.4 \text{ ft}$$

$$d_r = -12.0 \text{ ft}$$

$$h_f = 0.04 \text{ ft}$$

$$h_r = 0.3 \text{ ft}$$

$$d_n = 0 \text{ ft}$$

$$h_h = 10.4 \text{ ft}$$

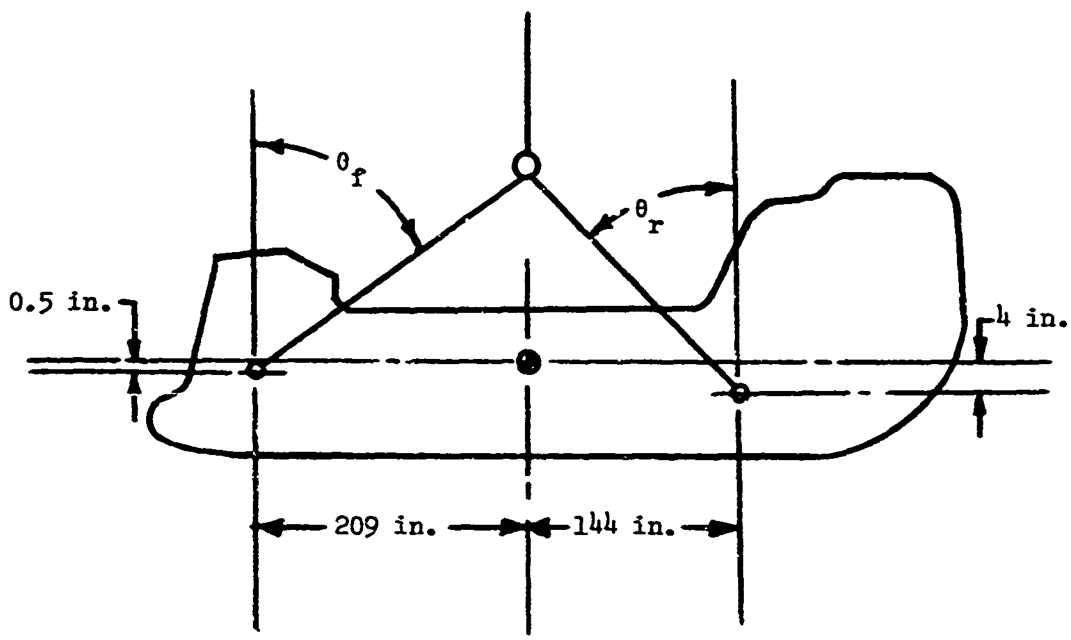

Figure 46. Sling Geomet'y of CH-47 Chinook -
1 Pt/ 4 Leg Load.

substituting these values into eqs (164) through (168) yields,

$$(12990) \cos \theta_h = V_{L_{s_f}}' + V_{L_{s_r}}'$$

$$(V_{L_{s_f}}') (17.4) + (V_{L_{s_r}}') (-12.0) = (D_{L_{s_f}}) (0.04) + (D_{L_{s_r}}') (0.3)$$

$$\theta_h = \arctan (0)/(10.4)$$

$$D_{L_f}' = V_{L_{s_f}}' \tan (59.1^\circ$$

$$D_{L_{s_r}}' = V_{L_{s_r}}' \tan (48.2^\circ)$$

solving simultaneously for $V_{L_{s_p}}'$ and $V_{L_{s_r}}'$ yields,

$$V_{L_{s_f}}' = 5310$$

$$V_{L_{s_r}}' = 7680$$

since the sling configuration has two forward legs and two rear legs, eqs (169) and (171) are used to find

$$V_{L_{s_f}} = (5310)/2 = 2655 \text{ lb}$$

$$V_{L_{s_r}} = (7680)/2 = 3840 \text{ lb}$$

$V_{L_{s_r}}$ $V_{L_{s_f}}$, therefore

$$V_{L_s} = 3840 \text{ lb}$$

From eqs (175) and (176);

$$T_{L_{s_f}} = 2655/\cos (59.3^\circ) = 5160 \text{ lb}$$

$$T_{L_{s_r}} = 3840/\cos (48.5^\circ) = 5790 \text{ lb}$$

Therefore

$$T_{L_s} = 5790 \text{ lb}$$

For any single point configuration eqs (179) and (180) yield

$$V_{H_s} = W_L = 12990 \text{ lb}$$

$$T_{C_s} = W_L = 12990 \text{ lb}$$

Eqs (140) to (147) are now used to solve for the values

$$T_{C_{max}} = (12990)\ (2.50) = 32{,}400\ \text{lb}$$

$$V_{H_{max}} = (12990)\ (2.50) = 32{,}400\ \text{lb}$$

$$D_{H_{max}} = (12990)\ (0.33) = 4{,}280\ \text{lb}$$

$$S_{H_{max}} = (12990)\ (0.39) = 5{,}070\ \text{lb}$$

$$V_{L_{max}} = (3840)\ (3.89) = 14{,}940\ \text{lb}$$

$$D_{L_{max}} = (3840)\ (6.10) = 23{,}400\ \text{lb}$$

$$S_{L_{max}} = (3840)\ (0.53) = 2{,}040\ \text{lb}$$

$$T_{L_{max}} = (5790)\ (4.81) = 27{,}800\ \text{lb}$$

These are the maximum forces which can be developed dynamically for this slung load type and sling arrangement when suspended from a helicopter capable of attaining a normal load factor of 2.5.

Example 2.

Container - 4 Pt/0 Leg (fwd cg) slung from a helicopter with a Design Load Factor of $N_z = 2.0$.

For $N_z = 2.0$ the following data is available from Figures (14) to (21) for the Type II, 4 Pt load:

$$LFT_{C_{max}} = 2.33$$

$$LFV_{H_{max}} = 2.29$$

$$LFD_{H_{max}} = 0.75$$

$$LFS_{H_{max}} = 1.01$$

$$LFV_{L_{max}} = 2.26$$

$$LFD_{L_{max}} = 0.70$$

$$LFS_{L_{max}} = 1.21$$

The slung load and slinging geometry is illustrated in Figure 47.

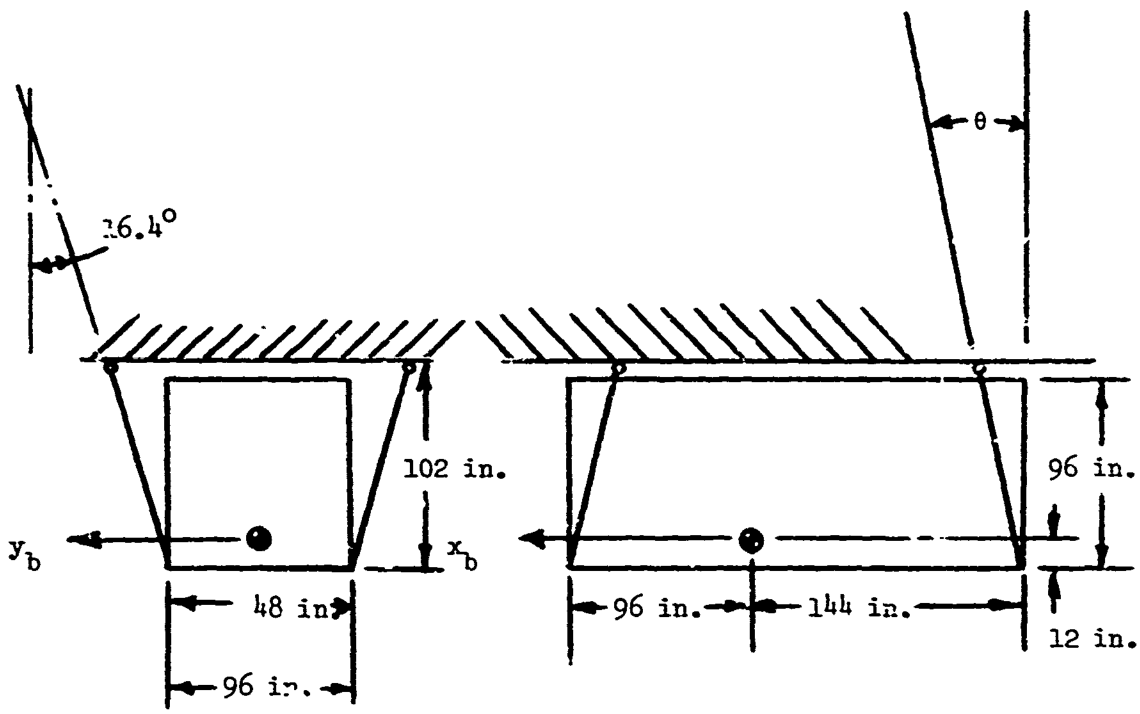

Figure 47. Sling Geometry of Container -
4 Pt/ 0 Leg (fwd cg) Load.

From the geometry, the following quantities are known:

$$W_L = 15{,}000 \text{ lb}$$

$$\theta_f = 16.4 \text{ deg}$$

$$\theta_{f_{xz}} = 14.5 \text{ deg}$$

$$\theta_r = 16.4 \text{ deg}$$

$$\theta_{r_{xz}} = 14.5 \text{ deg}$$

$$d_f = 8.0 \text{ ft}$$

$$d_r = -12.0 \text{ ft}$$

$$h_f = 1.0 \text{ ft}$$

$$h_r = 1.0 \text{ ft}$$

$$\theta_h = 0 \text{ deg (for the 4 Pt configuration)}$$

Eqs (164) to (168 then yield

$$(15000)\cos\theta_h = V'_{L_{s_f}} + V'_{L_{s_r}}$$

$$V'_{L_{s_f}}(8) + V'_{L_{s_r}}(-12) = D'_{L_{s_f}}(1) + D'_{L_{s_r}}(1)$$

$$\theta_h = 0$$

$$D'_{L_{s_f}} = V'_{L_{s_f}} \tan(14.5^\circ)$$

$$D'_{L_{s_r}} = -V'_{L_{s_r}} \tan(14.5^\circ)$$

Solving these eqs simultaneously for $V'_{L_{s_f}}$ and $V'_{L_{s_r}}$ yields

$$V_{L_{s_f}} = 8960$$

$$V_{L_{s_r}} = 6040$$

Since the sling configuration has two forward legs and two rear legs, eqs (169) and (171) are used to find

$$V_{L_{s_f}} = (8960)/2 = 4480$$

$$V_{L_{s_r}} = (6040)/2 = 3020$$

$V_{L_{S_f}} > V_{L_{S_r}}$, therefore

$$V_{L_S} = 4480 \text{ lb}$$

From eqs (175) and (176);

$$T_{C_{S_f}} = 4480/\cos(16.3^\circ) = 4610$$

$$T_{C_{S_r}} = 3020/\cos(16.3^\circ) = 3140$$

Therefore

$$T_{C_S} = 4610 \text{ lb}$$

V_{H_S} can be solved from eqs (181) to (184) accordingly:

$$V_{H_{S_f}} = (4610)\cos(16.3^\circ) = 4480$$

$$V_{H_{S_r}} = (3140)\cos(16.3^\circ) = 3020$$

$V_{H_{S_f}} > V_{H_{S_r}}$, therefore

$$V_{H_S} = 4480 \text{ lb}$$

Eqs (140) to (147) are now used to solve for the values

$$T_{C_{max}} = (4610)(2.23) = 10{,}300 \text{ lb}$$

$$V_{H_{max}} = (4480)(2.29) = 10{,}250 \text{ lb}$$

$$D_{H_{max}} = (4480)(0.75) = 3{,}360 \text{ lb}$$

$$S_{H_{max}} = (4480)(1.01) = 4{,}530 \text{ lb}$$

$$V_{L_{max}} = (4480)(2.26) = 10{,}100 \text{ lb}$$

$$D_{L_{max}} = (4480)(0.70) = 3{,}140 \text{ lb}$$

$$S_{L_{max}} = (4480)(1.21) = 5{,}420 \text{ lb}$$

These are the maximum forces which can be developed dynamically for this slung load type and sling arrangement when suspended from a helicopter capable of attaining a normal load factor of 2.0.